FACULTY OF ENGINEERING
AND ARCHITECTURE

Adaptive Solutions with Predictive Control for Salient-Pole Permanent-Magnet Synchronous Machine Drives

Chenwei Ma

Doctoral dissertation submitted to obtain the academic degree of
Doctor of Electromechanical Engineering

Supervisors

Prof. Frederik De Belie, PhD* - Prof. Xuliang Yao, PhD**

* Department of Electromechanical, Systems and Metal Engineering
Faculty of Engineering and Architecture, Ghent University

** Institute of Electrical Engineering
College of Intelligent Systems Science and Engineering, Harbin Engineering University, China

August 2021

GHENT
UNIVERSITY

FACULTY OF ENGINEERING AND ARCHITECTURE

Adaptive Solutions with Predictive Control for Salient-Pole Permanent-Magnet Synchronous Machine Drives

Chenwei Ma

Doctoral dissertation submitted to obtain the academic degree of
Doctor of Electromechanical Engineering

Supervisors
Prof. Frederik De Belie, PhD* - Prof. Xuliang Yao, PhD**

* Department of Electromechanical, Systems and Metal Engineering
Faculty of Engineering and Architecture, Ghent University

** Institute of Electrical Engineering
College of Intelligent Systems Science and Engineering, Harbin Engineering University, China

August 2021

GHENT UNIVERSITY

ISBN 978-94-6355-509-8
NUR 959
Wettelijk depot: D/2021/10.500/57

Members of the Examination Board

Chair

Prof. Patrick De Baets, PhD, Ghent University

Other members entitled to vote

Arne De Keyser, PhD, Ghent University
Prof. Jeroen De Kooning, PhD, Ghent University
Prof. José Rodríguez, PhD, Universidad Andrés Bello, Chile
Prof. Giacomo Scelba, PhD, Università degli Studi di Catania, Italy
Prof. Zhenbin Zhang, PhD, Shandong University, China

Supervisors

Prof. Frederik De Belie, PhD, Ghent University
Prof. Xuliang Yao, PhD, Harbin Engineering University, China

Acknowledgment

After three years' study at Ghent University, this PhD thesis was finally accomplished. Without the help of many people, it could never be completed, thus I would like to express my sincere gratitude towards them.

First and foremost, I would like to express my sincere gratitude to my promoter Prof. dr. ir. Frederik. De. Belie, who influenced me with his insightful ideas and meaningful inspirations, guided me with practical academic advice and feasible instructions. I owe my heartfelt thanks to Frederik for his continuous support and encouragement during this work and for his great effort on discussion, thinking and review of all my work. Frederik is always supportive, patient and willing to share his ideas with me. I will never forget the invaluable suggestions that he gave me during the past years. I do believe we will have great cooperation and do a lot of interesting things together in the future.

I would like to thank my second supervisor Prof. dr. Yao for his continuous support and concern during my PhD study.

My faithful appreciation goes to all the members of the examination board: Prof. dr. ir. Patrick De Baets, Prof. dr. Zhenbin Zhang, Prof. dr.-ing Jose Rodriguez, Prof. dr. ir. Giacomo Scelba, Prof. dr. ir. Jeroen De Kooning and Dr. ir. Arne De Keyser for their effort to review my work and the positive evaluation.

I am very grateful of all my colleagues which I was sharing the same office with them. Dr. Huayu Li, Dr. Tom Lefebvre, Dr. Florian Verbelen, Dr. Hendrik Vansompel, Jordi Van Damme and Khalid Javed. Thank them for the nice working atmosphere, interesting talks, help and support. I wish to thank Lynn Verkroost, Jordi Van Damme, Dr. Pieter Nguyen Phuc and Matthias Vandeputte for the interesting abroad conference experiences with them. I would like to thank Mrs.

Marilyn Van den Bossche for her essential administrative work. Many thanks to Jordi Van Damme, Vincent Gevaert and Tony Boone for helping me a lot during my experimental tests. Jordi helped me to repair the experimental setup for more than one time. It was difficult without his help.

I would like to express my gratitude to Prof. dr. Zhenbin Zhang and Prof. dr.-ing Jose Rodriguez for the good cooperation in publishing papers and for their valuable support and suggestions on my research and career.

Finally, I would like to thank my parents, whose care and support motivate me to move on. I would like to give my special thanks to my lovely wife, Yang Cao, for her unconditional patience, support, encouragement and sacrifice.

Gent, July 2021

Chenwei Ma

Contents

Acknowledgment ..... **i**

Contents ..... **iii**

Summary ..... **vii**

Samenvatting ..... **xiii**

List of Abbreviations ..... **xix**

1 Introduction **1**

1.1 Application of PMSM 1

1.1.1 Electric Vehicle 2

1.1.2 PMSM for EVs 3

1.2 Control Strategies for Motor Drives 4

1.3 Conventional Control Schemes of PMSM 5

1.4 Challenges for Control Schemes 6

1.5 MPC in Power Electronics and Drives 7

1.5.1 Development of MPC 7

1.5.2 Advantages of MPC for Power Electronics and Drives 9

1.5.3 Challenges for MPC 10

1.6 Research Questions 11

1.7 Outline 15

1.8 Scientific Publications 17

2 PMSM Drive and Conventional Control Strategies **19**

2.1 Dynamic Model of Salient-Pole PMSM 19

2.2 Conventional Control Strategies for PMSM 23

2.2.1 Field Oriented Control 23

2.2.2 Direct Torque Control 26

2.3 Characteristics and Discussions 31

2.4 Conclusions 33

3 Model Predictive Control for Power Electronic and Drives 35
3.1 Classification of Predictive Control Strategies 35
3.2 Basic Principles of Model Predictive Control 39
3.2.1 Control Problem 39
3.2.2 Control Principle 40
3.3 Model Predictive Torque Control of PMSM 46
3.3.1 Structure of Conventional MPTC 47
3.3.2 State Estimation 48
3.3.3 Behavior Prediction 49
3.3.4 Objective Function Optimization 49
3.4 Research Questions Related to Model Predictive PMSM Control 51
3.5 Conclusions 53

4 Optimization of FCS-MPC for PMSM to Improve Steady-State Performance 55
4.1 Introduction 55
4.2 Effects of Different Optimization Solutions on the Steady-State Performance 57
4.2.1 Control Structure of a Two-Vectors MPTC 58
4.2.2 Torque and Flux Estimation 60
4.2.3 Calculation of Flux and Torque Slope 61
4.2.4 Duty Ratio Optimization 63
4.2.5 Prediction and Objective Function Evaluation 65
4.2.6 Comparative Results and Discussions 65
4.3 A Boundary-Based MPTC with Consideration of Optimization Problems 70
4.3.1 Structure of the Proposed Boundary Based MPTC 74
4.3.2 Construction of Candidate Inputs 74
4.3.3 Prediction and Objective Function Minimization 81
4.4 Experimental Verifications 84
4.4.1 Effects of Fixed Torque Boundary Settings 86
4.4.2 Validation of the Torque Boundary Self-Adjustment 88
4.4.3 Steady-State Performance 89
4.4.4 Dynamic Performance 95
4.4.5 Simulation Results of Torque Reversal Operation from Regenerative Mode to Motoring Mode 98
4.4.6 Computation Burden Analysis 99
4.4.7 Analysis of Parameter Sensitivity 99

4.5 Conclusions 101

5 Simplification and Control Flexibility of FCS-MPC 105

5.1 Introduction 105
5.2 Reference Voltage Vector based MPTC 108
5.2.1 Control Principle 108
5.2.2 Reference Voltage Vector Generation 111
5.2.3 Optimal Voltage Vector Determination 112
5.2.4 Duty Ratio Optimization 114
5.2.5 Objective Function Evaluation 114
5.2.6 Simulation Results 115
5.3 Improvement of RVV-MPC with Setting Adaptive Reference Variants 117
5.3.1 Control Structure of Reference-Variant-Based MPC 118
5.3.2 Calculation of Reference Current under MTPA Control 119
5.3.3 Setting Up of Current Reference Variants 121
5.3.4 Mapping of Reference Voltage 123
5.3.5 Candidate Solutions Construction 125
5.3.6 Objective Function Evaluation 126
5.4 Simulation Results 130
5.4.1 Current Boundary 131
5.4.2 Comparison with RVV-MPC 132
5.4.3 Parameter Sensitivity 135
5.5 Experimental Verification 138
5.5.1 Steady-State Performance 138
5.5.2 Dynamic Performance 143
5.6 Discussions on Characteristics of Different Control Schemes 145
5.7 Conclusions 146

6 Current-Difference Sample Based Predictive Current Control 149

6.1 Introduction 149
6.2 Parameter Sensitivity Analysis for Model Predictive Current Control 152
6.3 Current Difference Sample Based Predictive Current Control 155
6.3.1 Basic Principle 155
6.3.2 Current Difference Construction in Conventional Methods 156
6.3.3 Proposed Current Difference Updating Mechanism 158
6.4 Experimental Verifications 165

6.4.1 Current Difference Update 166
6.4.2 Steady-State Performance 169
6.4.3 Low Load Test 177
6.4.4 Torque Step Test 178
6.4.5 Speed Reversal Test 179
6.4.6 Computational Time 180
6.4.7 Simulation Results of Stability Test 181
6.5 Conclusions 182

7 Concluding Remarks and Future Research 185
7.1 Conclusions 185
7.2 Future Research 188

Bibliography 191

Summary

Electrical machine is widely used in various industrial areas, such as aerospace, shipping, transport, industrial automation and automotive. With excellent advantages such as high energy efficiency and no emissions of gases or liquids, these machines have become an important option for the current development of a more energy-efficient and green automotive industry to meet today's demand for sustainable energy use and long-term livable environment. Permanent Magnet Synchronous Machine (PMSM) is an interesting choice as an electric drive motor in the drive system of Electric Vehicles (EVs). Due to its considerable advantages, such as very high energy efficiency and high energy density, these motors are used in modern applications in which space or weight is often a limiting factor. Since the electric drive system is an important component for EVs, it is useful to further study the control of PMSM to improve the performance of EVs.

Field Oriented Control (FOC), and Direct Torque Control (DTC), are established control strategies widely used in electric drive systems. In addition, in recent years, Model Predictive Control (MPC), with a more intuitive effect of control, has also received more and more attention from academia and industry. MPC has a customizable property and is currently considered a promising alternative to the more rigid FOC and DTC. MPC in electric drives regularly predicts the system behavior for the various possible control actions based on a system model, and requires an objective function that contains all the objectives. On the basis of an appropriate evaluation of this objective function on a, often very limited, number of possible control actions, the most suitable control actions are obtained. An important advantage of MPC is that it works with a simple and intuitive structure without internal control loops as in FOC, thus allowing for a fast dynamic torque response. In addition, MPC offers the possibility to explicitly take into account additional system limitations. To support the use of MPC in

PMSM drive systems, MPC can be further improved in a number of aspects compared to the current strategies as described in the international scientific literature: better steady-state performance with lower torque ripples, simplification in execution with as high flexibility in control as possible, and robust control against system variations. The focus of this thesis is to provide a number of adaptive solutions with predictive control for PMSM drives with recessed magnets in the rotor. With the latter machine, in addition to the distinguished synchronous torque due to the permanent magnetic field, a cooperating reluctance torque can be also created.

The MPC strategies used in power electronics and electric drives can often be classified into Finite Control Set MPC (FCS-MPC) and Continuous Control Set-MPC (CCS-MPC). The first strategy, FCS-MPC, is based on the limited number of switching states of the power converter, and is most often discussed in the international scientific literature. As in DTC, FCS-MPC may suffer from low steady-state performance with significant torque ripple due to the lack of a deeper control action modulation strategy. The FCS-MPC strategy places the power converter in only one of the switching states for an entire control period, resulting in large ripples in the torque. In addition, in inverters, the number of the switching states is often low, limited by the demand for a simple switching topology, which makes ripples inevitable. In order to achieve good steady-state performance, the switching frequency can be increased so that the control period decreases and more variation occurs in the control actions. However, this solution results in an increased switching loss in the inverter. To tackle this, previous MPC strategies have been put in place that allow two consecutive switching states during a single control period. Such strategies avoid the higher switching losses during conventional modulation techniques and optimize the switching moment between two states to improve the steady-state performance. This switching moment optimization is therefore a major setting factor of these MPC schemes. The deadbeat solution can be used to calculate the switching moment for each control period. However, the focus of the latter technique is on reducing the torque deviation at a single specific moment within the control period, and therefore means that the torque deviation is not considered at other moments. In order to further improve the overall steady-state performance, additional efforts must therefore be made in which the objective function plays a role.

In conventional strategies, weighting factors are often applied in the objective function of an MPC strategy. In a Model Predictive Torque Control (MPTC) there are two variables to be controlled, namely the torque and the stator flux. Because of the different dimensions of these two variables, a weighting factor is required to maintain a correct balance between these variables. Since there is no theoretical guideline to determine this weighting factor, and an experimental setting is not always possible or requires a lot of resources, avoiding a weighting factor during the design of a controller is often desirable. That is why this thesis proposes an MPTC strategy without weighting factor. The proposed MPTC strategy uses two states of the power converter in each control period, and aims to keep the torque ripple within torque boundaries throughout the control period. The torque boundaries are automatically adjusted to look for the minimum possible ripple, so that the steady-state performance can be improved as well as possible. The weighting factor in the objective function is thus avoided with the introduction of these control boundaries for torque, thus achieving a new and more intuitive MPTC strategy. The improvements of the proposed MPTC strategy over conventional MPC strategies are verified through various experimental tests conducted on a PMSM setup in the Electrical Energy Laboratory (EELAB).

With an FCS-MPC for PMSMs, the currents under all possible voltage inputs must be predicted to determine an optimal input. However, in each control period, most switching states are far from optimal. Evaluating the machine model for all states during each control period can therefore reduce the computational efficiency of MPC. In particular, following the introduction of two states per control period, the problem of computational efficiency may be more serious, as more candidate solutions are involved, and therefore more calculations are required. A quick calculation of the optimal input is then highly desirable. To address this issue, a Reference Voltage Vector Based MPC (RVV-MPC) is introduced. Such a scheme converts the main control objectives, such as torque reference and stator flux reference, into a single reference voltage, based on the machine model. On the basis of this reference, an optimal solution can then be obtained in a simple way, with a reduction in the calculation time compared to conventional strategies in which the model is evaluated for every possible input. However, additional studies are needed to support additional restraints, such as limiting currents within set boundaries in this RVV-MPC.

In order to achieve a structurally flexible MPC that also fulfils system limitations, a reference variant FCS-MPC is proposed in this thesis. In the proposed strategy, the original reference is considered under an optimal control such as the Maximum Torque Per Ampere (MTPA) scheme. Because additional limitations cannot be supported in RVV-MPC, it is proposed to look for the optimal reference that is feasible under the set limitations. Therefore, instead of capturing the reference, a well-considered group of MTPA reference variants are introduced and these variants are processed, resulting in a series of optimal control candidates. As multiple, but still finite, optimal solutions are possible, additional efforts can be made within the objective function to include additional system limitations. The size of the reference space can be adjusted automatically to generate sufficient reference variants that are consistent with the constraints. In this way, an improved MPC with flexible structure that supports the development of control performance is achieved. The effectiveness of the proposed strategy is evaluated by simulations as well as by experimental results on the above-mentioned setup.

The MPC strategy performs on the basis of a system model, which means that it depends heavily on the quality of the model. Any inaccuracies in the model and uncertainties in its identification may affect the accuracy of the predictions and thus impact the control performance. In a PMSM drive system, the machine parameters are difficult to determine precisely due to measurement errors. In addition, some parameters are variable during the operation of the motor. For example, the resistance is sensitive to temperature, and the induction values can be affected by a variable magnetic state of the iron. Such parameter uncertainties can greatly affect the system performance. Therefore, a robust predictive control scheme is desirable. Previously, some MPC schemes with parameter observers have been proposed in the international scientific literature. Such diagrams use an observer to identify the machine parameters used in the MPC algorithm during operation of the machine. The robustness of the parameter is improved with such schemes, however at the expense of higher system complexity and more calculations. In addition, observers may include additional parameters to be tuned and convergence problems may also arise.

By applying the switching states during a control period, a current difference can be measured. Such current information can later be used to replace the machine model to achieve predictions for a given state of

the power converter. That is why a Current-Difference Sample Based Predictive Current Control (CDSPCC) is introduced in this dissertation. This scheme does not include parameter observers and instead collects data on current difference due to each switching state. Since no machine parameters are used in the proposed CDSPCC, the influence of any parameter uncertainties or system variations can be greatly reduced. In addition, to ensure the reliability of current predictions, an advanced data update mechanism is introduced to refresh current information in each control period. As a result, the proposed CDSPCC can achieve a similar performance to the model-based approach based on the correct parameters. Compared to the observer-based MPC schemes, the proposed CDSPCC achieves an improvement in robustness against parameter variations in a simple and intuitive way without complex formulations. The performance of the proposed CDSPCC is demonstrated by various experimental tests performed on the setup abovementioned.

Samenvatting

Elektrische machines worden regelmatig aangewend in verscheidene industriële sectoren, zoals in lucht- en ruimtevaart, scheepvaart, transportsector, bij industriële automatisatie en in de automobiel industrie. Met uitstekende voordelen zoals een hoge energie-efficiëntie en geen uitstoot van gassen of vloeistoffen zijn deze machines een belangrijke optie geworden voor de huidige ontwikkeling van een meer energiezuinige en groene auto-industrie, nodig om de hedendaagse vraag naar een duurzaam energiegebruik en langdurig leefbaar milieu te beantwoorden. De permanente-magneet synchrone machine of kortweg PMSM is als elektrische aandrijfmotor in het aandrijfsysteem van elektrische voertuigen of EVs een interessante keuze. Vanwege de aanzienlijke voordelen, zoals een zeer hoog energierendement en hoge energiedichtheid, past men deze motoren toe in moderne toepassingen waarin ruimte of gewicht vaak een beperkende factor zijn. Daar het elektrische aandrijfsysteem een belangrijk onderdeel is voor EV's, is het nuttig de regeling van PMSM verder te bestuderen om de prestaties van EV's te verbeteren.

Veldoriëntatie, “Field Oriented Control” of FOC, en directe koppelcontrole, “Direct Torque Control” of DTC, zijn gevestigde stuurstrategieën die op grote schaal gebruikt worden in elektrische aandrijfsystemen. Daarnaast heeft tijdens de afgelopen jaren ook modelvoorspellende controle, “Model Predictive Control” of MPC, met een meer intuïtieve werking van sturing, steeds meer aandacht gekregen door de academische wereld en de industrie. De MPC heeft een aanpasbare eigenschap en wordt momenteel beschouwd als een veelbelovend alternatief voor de meer starre FOC en DTC. De MPC in elektrische aandrijvingen voorspelt zeer regelmatig het systeemgedrag voor de verscheidene mogelijk stuuracties op basis van een systeemmodel, en vergt een objectieve functie die alle doelen bevat. Op basis van een geschikte evaluatie van deze objectieve functie over het,

vaak zeer beperkt, aantal mogelijke stuuracties, worden de meest geschikte stuuracties verkregen. Een groot voordeel van MPC is dat het met een eenvoudige en intuïtieve structuur werkt, zonder interne stuurlussen zoals in DTC, en steunt op een model zoals in FOC waardoor een snel dynamisch koppelantwoord kan worden bekomen. Bovendien biedt MPC de mogelijkheid om expliciet rekening te houden met extra systeembeperkingen. Om het gebruik van MPC in PMSM-aandrijfsystemen te ondersteunen, kan MPC in een aantal aspecten verder verbeterd worden ten opzichte van de huidige stand zoals beschreven in de internationale wetenschappelijke literatuur: een betere regimeprestatie met lagere koppelrimpels, een vereenvoudiging in uitvoering met zoveel mogelijk flexibiliteit in sturing, en een robuuste sturing ten opzichte van systeemvariaties. De focus van dit proefschrift ligt in het aanreiken van een aantal adaptieve oplossingen via het aanwenden van voorspellende controle, en dit voor PMSM-aandrijvingen met verzonken magneten in de rotor. Bij deze laatste machine kan, naast het voorname synchrone koppel als gevolg van het permanente magneetveld, bijkomend een meewerkend reluctantiekoppel gegeneerd worden.

De MPC strategieën die worden toegepast bij vermogenselektronische voedingen, of vermogensomvormers, in elektrische aandrijvingen kunnen vaak geclassificeerd worden als hetzij Finite Control Set MPC (FCS-MPC) of als Continuous Control Set-MPC (CCS-MPC). De eerste strategie, FCS-MPC, steunt op het heel beperkt aantal toestanden waartussen de vermogensomvormer aan een hoge frequentie kan schakelen, een voordeel voor schakelverlies in de convertor, en wordt het vaakst besproken in de internationale wetenschappelijke literatuur. Net als in DTC kan FCS-MPC lijden aan een lage prestatie tijdens regime met een significante koppelrimpel als gevolg van het ontbreken van een diepere modulatiestrategie van de stuursignalen. De FCS-MPC strategie plaatst de vermogensomvormer in slechts één van de schakeltoestanden gedurende een hele controleperiode met grote rimpels in het koppel tot gevolg. Bovendien is in omvormers het aantal toestanden vaak laag, beperkt door de vraag naar een eenvoudige schakeltopologie, waardoor rimpels onvermijdelijk zijn. Om toch een goede regimeprestatie te bereiken, kan de schakelfrequentie verhoogd worden zodat de controleperiode verkleint en meer variatie optreedt in de stuuracties. Deze oplossing resulteert echter in een verhoogd schakelverlies in de omvormer. Om hierop een antwoord te geven, zijn voorheen MPC-strategieën

vooropgesteld die twee opeenvolgende schakeltoestanden toelaten tijdens een enkele controleperiode. Dergelijke strategieën vermijden de hogere schakelverliezen tijdens conventionele modulatietechnieken en optimaliseren het schakelmoment tussen twee toestanden om de regimeprestatie te verbeteren. Deze optimalisatie is dus een voorname instelfactor van deze MPC regelingen. Alternatief kan de deadbeat-oplossing, gebruikt worden om het schakelmoment voor iedere controleperiode te berekenen. De focus van deze laatste techniek ligt echter op het reduceren van de koppelafwijking op een enkel welbepaald moment binnen de controleperiode, en betekent dus dat de koppelafwijking op andere momenten niet wordt beschouwd. Om de globale regimeprestatie verder te verbeteren moeten dus extra inspanningen geleverd worden waarbij de objectieve functie een rol speelt.

In conventionele uitvoeringen worden wegingsfactoren toegepast in de objectieve functie van een MPC strategie. In de koppelregeling "Model Predictive Torque Control" of MPTC zijn twee te sturen variabelen aanwezig, namelijk het koppel en de bekrachtiging of flux. Vanwege de verschillende dimensies van deze twee variabelen is een wegingsfactor vereist om een juist evenwicht tussen deze variabelen te behouden. Aangezien geen theoretische richtlijn bestaat om deze wegingsfactor te bepalen, en een experimentele instelling niet steeds mogelijk is of veel middelen vergt, is het vermijden van een wegingsfactor tijdens het ontwerp van een regelaar vaak wenselijk. Daarom wordt in dit proefschrift een MPTC strategie zonder wegingsfactor voorgesteld. De voorgestelde MPTC strategie gebruikt twee toestanden van de vermogensomvormer per controleperiode, en heeft als doel de koppelrimpel binnen koppelgrenzen te houden gedurende de hele controleperiode. De koppelgrenzen worden daarbij automatisch aangepast om te zoeken naar een zo minimaal mogelijke rimpel, zodat de regimeprestaties zo goed als het kan worden verbeterd. De wegingsfactor in de objectieve functie wordt dus vermeden met de introductie van deze controlegrenzen voor het koppel waardoor een nieuw en meer intuïtieve MPTC-strategie bereikt wordt. De verbeteringen van de voorgestelde MPTC strategie ten opzichte van de conventionele MPC strategieën worden geverifieerd via verschillende experimentele testen uitgevoerd op een PMSM opstelling in het Laboratorium voor Elektrische Energie (EELAB).

Bij een FCS-MPC voor PMSMS moeten de fasestromen onder alle mogelijke spanningsingangen worden voorspeld om een optimale

schakeling te bepalen. In elke controleperiode zijn de meeste schakeltoestanden echter verre van optimaal. Het evalueren van het machinemodel voor alle toestanden tijdens iedere controleperiode kan hierdoor de computationele efficiëntie van MPC verminderen. Met name na de invoering van twee toestanden per controleperiode kan het probleem van de computationele efficiëntie meer problematisch zijn, daar meer kandidaat-oplossingen betrokken zijn, en dus meer berekeningen. Een snelle berekening van de optimale input is zeer wenselijk. Om dit probleem aan te pakken, wordt een Reference Voltage Vector Based MPC (RVV-MPC) geïntroduceerd. Een dergelijk schema zet de belangrijkste stuurdoelstellingen, zoals referentiewaarden voor koppel en statorflux, om in een enkele referentiespanning, op basis van het machinemodel. Vervolgens kan op basis van deze referentie op een eenvoudige manier een optimale oplossing verkregen worden omtrent de schakeltoestanden en schakeltijd, met een vermindering van de rekentijd tov conventionele uitvoeringen waarbij het model geëvalueerd wordt voor iedere mogelijk ingang. Bijkomede studies zijn echter nodig om aanvullende beperkingen, zoals het beperken van de stromen binnen gestelde grenzen, in deze RVV-MPC te ondersteunen.

Om een structureel flexibele MPC te bereiken die ook systeembeperkingen vervult, wordt in dit proefschrift een referentievariant FCS-MPC voorgesteld. In de voorgestelde strategie wordt de originele referentie beschouwd onder een optimale regeling zoals de MPTA-regeling (Maximum Torque Per Ampere). Omdat extra beperkingen niet kunnen worden ondersteund in RVV-MPC, wordt voorgesteld om te zoeken naar de optimale referentie die haalbaar is onder de gestelde beperkingen. Daarom wordt, in plaats van de referentie vast te leggen, een weloverwogen omgeving van de MTPA-referentie geïntroduceerd en worden deze varianten verwerkt, wat resulteert in een reeks optimale stuurkandidaten. Naarmate meerdere, maar nog steeds eindig aantal, optimale oplossingen mogelijk zijn, kunnen binnen de objectieve functie extra inspanningen geleverd worden om extra systeembeperkingen op te nemen. De grootte van de referentieruimte kan automatisch worden aangepast om voldoende referentievarianten te genereren die in overeenstemming zijn met de beperkingen. Op deze wijze wordt een verbeterde MPC met flexibele structuur bereikt die de ontwikkeling van de stuurprestaties ondersteunt. De doeltreffendheid van de voorgestelde strategie wordt

geëvalueerd door simulaties alsook door middel van experimentele resultaten op de eerder vermelde opstelling.

De MPC strategie presteert op basis van een systeemmodel, wat betekent dat het sterk afhankelijk is van de kwaliteit van het model. Eventuele onnauwkeurigheden in het model en onzekerheden in de identificatie ervan kunnen de juistheid van de voorspellingen beïnvloeden en zo de stuurprestaties benadelen. In een PMSM-aandrijfsysteem zijn de motorparameters echter moeilijk precies te bepalen vanwege meetfouten. Bovendien zijn sommige parameters variabel tijdens de werking van de motor, zo is de weerstand gevoelig voor temperatuur en de inductiewaarden worden beïnvloed door een veranderlijke magnetische toestand van het ijzer. Dergelijke parameteronzekerheden kunnen de systeemprestaties sterk nadelig beïnvloeden. Daarom is een robuust voorspellend controleschema wenselijk. Voorheen zijn in de internationale wetenschappelijke literatuur enkele MPC-regelingen met parameterwaarnemers voorgesteld. Dergelijke schema's gebruiken een waarnemer om tijdens werking van de machine de motorparameters te identificeren die gebruikt worden in het MPC-algoritme. De robuustheid van de parameter wordt met dergelijke schema's echter verbeterd ten koste van een hogere systeemcomplexiteit en meer berekeningen. Bovendien houden de waarnemers aanvullende parameters in die moeten afgestemd worden en kunnen zich daarbij ook convergentieproblemen voordoen.

Door het toepassen van de schakeltoestanden gedurende een controleperiode wordt een stroomverandering bekomen die kan worden gemeten. Dergelijke stroominformatie kan later gebruikt worden om het machinemodel te vervangen in het maken van voorspellingen voor een gegeven toestand van de vermogensomvormer. Daarom wordt in dit proefschrift een Current-Difference Sample Based Predictive Current Control (CDSPCC) geïntroduceerd. Dit schema omvat geen parameterwaarnemers en verzamelt data omtrent stroomveranderingen als gevolg van iedere schakeltoestand. Aangezien geen motorparameters gebruikt worden bij de voorgestelde CDSPCC, kan de invloed van eventuele parameteronzekerheden of systeemvariaties sterk worden gereduceerd. Om de betrouwbaarheid van de huidige voorspellingen te garanderen, wordt bovendien een geavanceerd mechanisme voor het bijwerken van de data geïntroduceerd zodat de huidige informatie in elke controleperiode vernieuwd wordt. Als gevolg hiervan kan de voorgestelde CDSPCC een vergelijkbare prestatie

bereiken als de modelgebaseerde aanpak steunend op de juiste parameters. In vergelijking met de op waarnemers gebaseerde MPC-schema's bereikt de voorgestelde CDSPCC een verbetering in de robuustheid tegen parametervariaties en dit op een eenvoudige en intuïtieve manier zonder complexe formuleringen. De prestaties van het voorgestelde CDSPCC worden aangetoond door verschillende experimentele tests die op de bovengenoemde opstelling zijn uitgevoerd.

List of Abbreviations

PMSM	Permanent Magnet Synchronous Machine
AC	Alternating Current
MPC	Model Predictive Control
CNC	Computer Numerical Control
EV	Electric Vehicle
BEV	Battery Electric Vehicle
HEV	Hybrid Electric Vehicle
FCEV	Fuel Cell Electric Vehicle
DTC	Direct Torque Control
DPC	Direct Power Control
PI	Proportional Integration
FOC	Field Oriented Control
PWM	Pulse Width Modulation
DC	Direct Current
MIMO	Multiple-Input Multiple-Output
SISO	Single-Input Single-Output
VSI	Voltage Source Inverter
MPTC	Model Predictive Torque Control
LUT	Lookup Table

FCS-MPC	Finite Control Set MPC
RVV-MPC	Voltage Vector Based MPC
PM	Permanent Magnet
SVM	Space Vector Modulation
CB-PWM	Carrier-Based PWM
OSV-MPC	Optimal Switching Vector MPC
OSS-MPC	Optimal Switching Sequence MPC
CCS-MPC	Continuous Control Set MPC
GPC	Generalized Predictive Control
EMPC	Explicit MPC
MPCC	Model Predictive Current Control
RMS	Root Mean Square
IPMSM	Interior PMSM
THD	Total Harmonic Distortion
MTPA	Maximum Torque Per Ampere
CDSPCC	Current-Difference Sample Based Predictive Current Control

Chapter 1
Introduction

Permanent Magnet Synchronous Machine (PMSM) is a kind of Alternating Current (AC) machine for electromechanical energy conversion. PMSM with high power density, torque density and efficiency has been widely used in various applications, e.g. automotive, robotics and high-precision servo systems. Thus, the control of PMSM drive system is always an important research topic.

In this chapter, the applications and the conventional control schemes of PMSM drive are introduced. Then, the challenges facing by conventional control schemes are discussed and Model Predictive Control (MPC) as a promising alternative are introduced. Furthermore, the challenges of MPC and the research questions as well as the outline of this thesis are presented.

1.1 Application of PMSM

PMSM is a type of high-performance synchronous machine. In the 1980s, the successful development of permanent magnet materials, such as NdFeB, and the development of permanent magnet related manufacturing technology promoted the wide application of PMSM in industry and life. PMSM has high efficiency and high power density. At the same power level, PMSM is smaller and lighter than induction motors, and the torque-to-inertia ratio is higher. Thus, PMSM, with fast dynamic response, high operating reliability and good low speed performance, has considerable application prospects in modern industry.

PMSM plays an important role in the field of high-end Computer Numerical Control (CNC) machine tools, robots, advanced rail transit equipment, new energy vehicles, etc. PMSM and its high-performance servo motion control system are the core foundation of high-end CNC machine tools and robots. In the field of advanced rail transportation equipment, high-performance PMSM instead of asynchronous traction motor as an electric locomotive transmission device is the trend of future development. In addition, PMSM has played a vital role in the field of public transportation and Electric Vehicle (EV).

1.1.1 Electric Vehicle

Energy shortage and environmental pollution are the great obstacles to the sustainable development of human society. As one of the important symbols of industrial civilization, automobile brings convenience to people, but also makes environmental problems more prominent. With the increasing production and quantity of traditional automobiles fueled by gasoline or diesel fuel in the world, the shortage of petroleum resources is increasing and environmental pollution is gradually aggravating. Under the dual pressure of energy crisis and environmental protection, the development of new clean energy vehicles has been pushed into the focus of automotive research, and EVs are becoming the focus of governments, enterprises and research institutions all over the world. The term EV includes Battery Electric Vehicles (BEVs), Hybrid Electric Vehicles (HEVs) and Fuel Cell Electric Vehicles (FCEVs). BEVs use battery as an energy source, which in turn drives the vehicle by the electromagnetic torque output of the motor. HEVs generally contain two power units, electric motor and engine. Through energy management and control, the vehicle is driven completely or partially by the motor output torque. FCEVs are a type of electric vehicle in which hydrogen combines with oxygen in a fuel cell to generate the electricity needed to power an electric motor.

In the face of the global energy crisis and environmental problems, governments, automobile manufacturers and research institutes around the world are vigorously promoting the development, manufacture and promotion of electric vehicles. According to the ‘Global EV Outlook’ of International Energy Agency, the global sales of electric cars exceeded 2.1 million in 2019. Figure 1.1 shows the global electric car stock during the past decade [1]. It is seen that electric car sales have

soared during the past years. In 2010, there were only about 17000 electric cars in the world, but this number had swelled to 7.2 million by 2019.

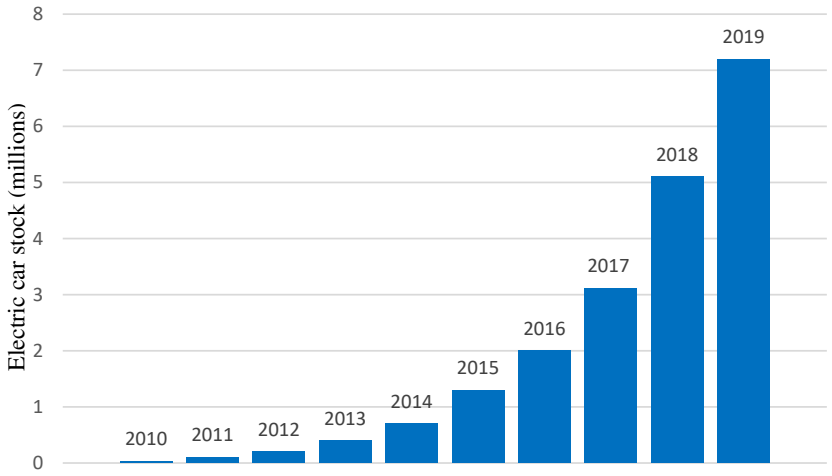

Figure 1.1: Global electric car stock, 2010-2019.

1.1.2 PMSM for EVs

The electric drive system is the core of the energy conversion unit of EVs. Whether for BEV, HEV or FCEV, electric drive system is the key and generic technology. The task of an electric drive system is to convert electrical energy from the battery of an electric vehicle into momentum on the wheels. Unlike ordinary industrial motor control systems, EVs have high vibration and temperature changes, which put forward higher demands for the reliability, durability and safety of the drive system. Due to the complex operating conditions of EVs, the electric drive system is required to have fast dynamic response, strong robustness, and wide constant power output capacity. The space of EVs is limited, the power density and volume of the drive system are then more demanding. In addition, low cost and low noise are also the key to the development of electric drive system.

Motor is the main energy conversion component of electric drive system. Motors commonly used in EVs include switched reluctance motor, induction motor and PMSM. In particular, considering the

requirements of electric drive system, PMSM has been a main choice due to following advantages:

- High power density, its size is much smaller than that of asynchronous motors with the same speed and same power.
- High efficiency, the output of the same power results in a low loss.
- Reasonable cost.
- Easy maintenance.

1.2 Control Strategies for Motor Drives

In electric drives, the main aspect is control. With the development of semiconductor devices and the introduction of new control platforms, motor control strategies are constantly evolving. Figure 1.2 shows the most commonly used control strategies for motor drive systems [2].

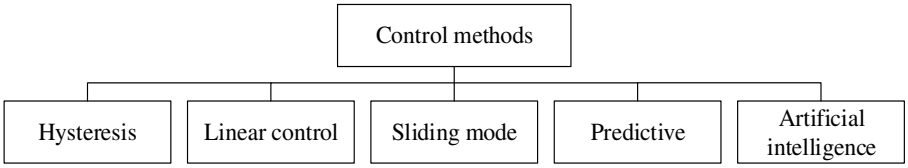

Figure 1.2: Control methods for power electronics and drives.

Hysteresis control takes into account the nonlinear nature of power converters and selects suitable voltage vector based on hysteresis controllers. This control scheme can be used in current control, Direct Torque Control (DTC) [3] and Direct Power Control (DPC) [4]. This control scheme originates from the power relay, and its implementation on digital platform requires a high sampling frequency. The nonlinear nature of the system and the width of the hysteresis cause the switching frequency of this control method to be not fixed. This may cause resonance problems in some applications. Therefore, the control of switching frequency needs to be studied [2].

On the other hand, linear controllers are also widely used in power converter applications, with the most widely choice being the use of Proportional Integration (PI) regulators. A conventional linear control strategy for motor drives is Field Oriented Control (FOC) [5]. In

contrast to hysteresis control, linear control can achieve fixed switching frequency. However, a disadvantage of linear controller is that it is difficult to handle constraints. Some system constraints and technical requirements, e.g. current boundary settings, maximum switching frequency, that need to be taken into account in motor drive systems cannot be directly included within the design of linear control strategy.

With the development of more advanced control platforms, more and more attention has been paid to the new control strategies, including sliding mode control, artificial intelligence control, predictive control, etc. In particular, predictive control with intuitive concept is considered to replace the traditional control schemes for motor drives. Predictive control includes many kinds of controllers with different approaches. However, the main idea of all predictive control schemes is similar, which is to use system model to predict the future behaviors of controlled variables and to use optimization principle to determine the most suitable actuation.

Deadbeat control is a typical predictive control scheme. It uses a system model to compute the desired voltage so that the tracking error can be zero in a sampling cycle and then outputs the desired voltage through a modulation stage [2]. MPC, on the other hand, is a powerful predictive control scheme that has been widely used in power electronics and motor drives in recent years.

1.3 Conventional Control Schemes of PMSM

Over recent decades, control of motor drive systems has been widely studied. The most widely used linear control scheme for PMSM drives is FOC. On the other hand, nonlinear control strategies, such as DTC, also play an important role in high-performance applications.

A. Field Oriented Control

FOC is a classical linear control scheme for PMSM drive [6-9]. FOC performs with cascading structure and it uses PI controllers to regulate the stator currents. The current controllers manipulate the desired voltage, which is synthesized by the inverter with Pulse Width Modulation (PWM) to drive the motor. The main advantage of FOC is that it can achieve high system steady-state accuracy such that FOC-based PMSM control system has comparable to Direct Current (DC)

machine control performance. Thus, FOC has been widely used. However, it still suffers from some shortcomings, one of which is that it is difficult to optimize the overall control performance. This is because each PI controllers operates individually. In addition, the complexity of the control system increases remarkably when multiple control objectives need to be considered. Moreover, as PI controllers involve proportional coefficient and integral coefficient to be designed, additional tuning work is required.

B. Direct Torque Control

On the other hand, the most widely used nonlinear control strategy for PMSM drive system is DTC [10-22]. Its main difference from FOC is that DTC uses torque and flux linkage hysteresis controllers to replace the PI regulators of current loop. In DTC, the decoupling of FOC is abandoned. Instead, the instantaneous space vector theory is considered to estimate the electromagnetic torque and stator flux. As a result, the direct control of torque and flux can be achieved with the help of hysteresis. DTC uses hysteresis to control torque and flux, thus avoiding the introduction of current control loop. Simple system structure and fast dynamic response are then achieved. Nevertheless, DTC suffers from significant steady-state torque and flux ripple. With hysteresis controller only the sign of the error is manipulated, but its magnitude is not considered. Often, a same vector is chosen to be applied during the whole control period for both larger and smaller error, thus resulting in unsatisfactory steady-state control performance. Additionally, the low-speed performance is not good enough with DTC. Moreover, the switching frequency of DTC is variable depending on the operating conditions.

1.4 Challenges for Control Schemes

Traditional control requirements are primarily related to the dynamic performance and the system stability, while more technical specifications and constraints are required in the current industrial applications. Many control requirements should not be handled by hardware only, but also need to be considered by control system. Thus, the development of more improved control schemes is motivated. The design of motor drive systems can be considered as an optimization problem that requires multiple control objectives to be accomplished at

the same time. There are two main challenges when applying control schemes to power electronics and motor drives.

Challenge 1: system nonlinearities

Generally, motor drive systems are nonlinear systems. For instance, nonlinearity problems appear when machine variables such as the torque or stator flux amplitude are directly controlled, as both variables are nonlinear functions of currents or flux linkages [23]. In addition, the inductance saturation effect and any required limitations on currents can cause additional nonlinearities, which should be the problems to be considered in the design of control system.

Challenge 2: multiple-input multiple-output (MIMO) systems

To simplify the design of a MIMO system, the control problem can be decomposed into multiple Single-Input Single-Output (SISO) loops and cascading control loops can be used. This method is effective when the system operates at (quasi) steady-state conditions. However, during transient state and faults, different control loops often start to interact, thus complicating the regulation of control loops. In addition, the bandwidth and the robustness of controller are limited.

Hence, for applications with high control requirements, the MIMO problem of motor drive systems needs to be considered by MIMO-supported controllers. A main benefit of this is that a faster dynamic response during transient state and a simpler controller tuning process can be achieved [23].

1.5 MPC in Power Electronics and Drives

1.5.1 Development of MPC

In the late 1970s, MPC was used in the petrochemical industry [24]. MPC includes a variety of control strategies, the main idea of which is to use the system mathematical model and an objective function to obtain the optimal control solution. At first, MPC did not receive too much attention from the community of power electronics and drives, and its application in this field was inadequate. By contrast, MPC had been seen an effective control scheme in the area of process control since 1980s. In the late 1990s, linear MPC was used in more than 4,500 applications in various industries, mainly in petrochemicals, refining and chemicals. Some applications can also be found in the fields of food

processing, mining and metallurgy, aerospace and defense, and the automotive industry [25].

The first ideas to apply MPC to power electronics and electric drives appeared in the 1980s [26, 27]. There are several reasons for the late adoption of MPC in this field. A main reason is the limited processor capacity available in the last century to solve real-time control problems. Moreover, the time constants of power electronic and drive systems are often short, thus requiring short sampling periods. In addition, the nonlinear characteristics of power electronic and drive system make the design, analysis and verification of the controller complex [23]. Nowadays, the use of digital signal processors and the development of powerful and advanced control platform have made it possible for MPC to be used in the field of power electronics and drives. Over the past decade, MPC has grown rapidly in the field of power electronics and machine drives. This can be revealed by the number of publications in the IEEE *Xplore*. A search with the search term "predictive control and machine" or "predictive control and motor" in the abstract has been done. The result shows that the number of annual publications per year has been rapidly increased since 2010 (see Figure 1.3). This progress is due not only to the huge increase in computing power available in the control platform, but also to the significant increase in the computing speed of solvers that calculate the underlying optimization problems.

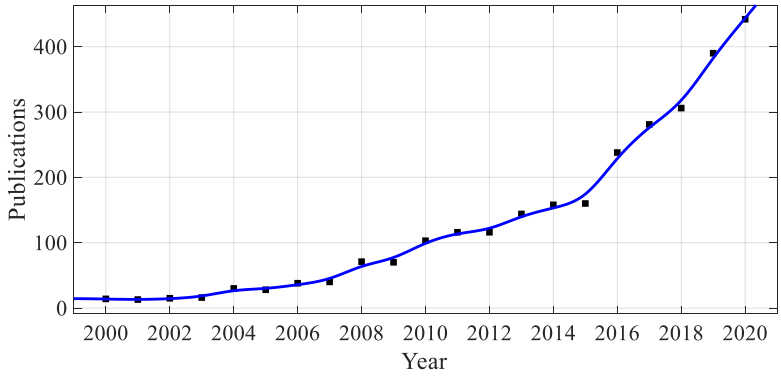

Figure 1.3: Annual number of MPC related publications in IEEE *Xplore* since 2000.

1.5.2 Advantages of MPC for Power Electronics and Drives

The two challenges faced by traditional control schemes of motor drives have been discussed before. The advantages of MPC in addressing these issues will be discussed here.

First, MPC is performed in the time domain rather than in the frequency domain, which allows MPC to handle nonlinear systems in a systematic manner, especially those consisting of switching devices. This is achieved by incorporating the nonlinear system behavior into the control structure of MPC in the form of an internal system model [23]. In addition, the ability of MPC to deal with system constraints on manipulated variables, states, and controlled variables is excellent.

In MPC, the use of an objective function enables collaborative control of system variables with coupling relationships. These controlled variables can be prioritized, giving MPC the ability to integrate multiple control objectives in one controller. Moreover, additional constraints can also be included into the MPC system.

On the other hand, different from PI-based controllers, MPC is a multivariate control scheme, which is very suitable for MIMO systems, especially for those complex control systems. It is noted that decomposing a MIMO system into multiple SISO control loops could be a solution for such problems. However, this behavior means that a separate design for each control loop is required. In addition, in practice, these control loops may interact with each other in a negative way. The situation could be even worse during dynamic states and faults, thus making the commissioning and adjustment of the control loops complex. The control performance of closed-loop systems is then impacted. In contrast to classical control schemes formulated in frequency domain, MPC does not require multiple control loops when dealing with multivariable problems. Instead, only one loop is sufficient, which greatly simplifies the design, analysis and adjustment process of the controller [23].

In general, power converters and motor drive systems can be seen as hybrid nonlinear systems, as both linear and nonlinear parts with a finite number of switches are involved. The input signals of the drive system are discrete signals that are used to control the turn-on and turn-off of the switching devices. Control systems often need to consider constraints. Some constraints are inherent in the system, such as the

maximum output voltage of the inverter, and some additional constraints can be considered for safety reasons. For example, current limits can be added to protect the drive system hardware and load. Additionally, as mentioned before, the control platforms today provide increased computing power and feasibility for more computation-demanding control algorithms. Therefore, all the characteristics of motor drive systems and control platforms and the advantages of MPC make it very suitable for use in the field of motor drive, and this is the reason why MPC has received more and more attention in this field [2].

1.5.3 Challenges for MPC

In recent years, the application of the MPC in power electronics and drives has been widely investigated. However, the implementation of MPC also faces some challenges, such as the steady-state error and the computational efficiency. The main challenges are discussed here.

A. Steady-State Error

For power electronics and motor drive systems, such as PMSM systems, MPC scheme is performed in discrete time. It selects a voltage vector that minimizes an objective function to drive the motor during each sampling period. However, for conventional Voltage Source Inverter (VSI), the amount of the possible voltage vectors is limited. Similar to DTC, conventional MPC applies a fixed voltage vector over a full sampling period without taking into account the system performance between samples, hence resulting in relatively high torque or current ripples [28]. These ripples can arouse additional noise and vibrations and lead to disturbances in the rotating shaft. Reducing the torque and flux ripples is therefore desired to gain a smoother torque output and to improve the motor efficiency. Such improvements are very important if we consider for example that PMSMs are widely used in automotive applications.

B. Computational Efficiency

MPC uses a system prediction model and a defined objective function to obtain the optimal control input of the system by solving an optimization problem. This MPC algorithm needs to be executed online in each sampling period. In addition, for a motor drive system, all the

possible voltage vectors need to be evaluated, leading to a low computational efficiency. This problem could be more serious in cases where multiple candidate solutions and optimization methods are introduced to improve the steady-state performance of MPC. In practice, however, a characteristic of power electronic applications is that the sampling period tends to be short [29]. Therefore, improving the computational efficiency of MPC should be studied.

C. Influence of Parameter Uncertainty

MPC predicts the future behaviors based on a discrete-time system model. It means the system parameters must be known. However, because MPC directly uses the system model to select the optimal control action, its control performance can be largely affected by modeling errors or parameter uncertainties [30]. In addition, nonlinear factors from inverter in the drive system can also impact the control performance of MPC [31]. Therefore, the influence of errors in the prediction model remains as a main challenge for MPC.

1.6 Research Questions

The main objective of this study is to develop adaptive solutions with predictive control for PMSM drives addressing the aforementioned challenges of conventional MPC. The objectives, technological barriers and methodologies are discussed in three aspects as follow.

A. Improvement of Steady-State Performance

Objective The first objective is to develop an adaptive solution with Model Predictive Torque Control (MPTC) that can achieve improved steady-state performance on a global time scale. The torque ripple should be minimized in a straightforward way. Moreover, the MPTC scheme should remain a simple structure without involving complex formulations. The weighting factor within the conventional MPTC should be omitted and the computational cost should be looked after.

Technological Barrier In a conventional MPTC scheme, a single voltage vector is activated during a fixed sampling period. Meanwhile, the number of the candidate voltage vectors is limited. For example, in a two-level VSI fed PMSM drive system, there are only six active voltage vectors with fixed amplitude and phase angle and two zero

vectors. Thus, such limitations result in high current or torque ripple and unsatisfactory steady-state performance. Usually, MPC algorithm needs to configure a higher sampling frequency to improve the steady-state performance. However, the improvement is limited and higher switching cost is aroused. This stimulates some researchers to work on two-vectors MPC schemes [32-34]. In such schemes, two voltage vectors are applied in a sampling period and a duty ratio control is introduced. The state of art two-vectors MPC schemes focus on restricting the torque ripple at a certain point, i.e. at the end of a sampling period. As the instantaneous torque ripple is not looked after, a scheme that can reduce the overall torque ripple is desirable to further improve the steady-state performance.

In addition, in a MPTC, there are two controlled variables, torque and stator flux, which have different dimensions. A weighting factor is then used to keep the balance between the two variables in an objective function. An appropriate weighting factor can help to improve the MPTC performance, otherwise the system control performance will deteriorate. However, it is difficult to set the weighting factor, which needs to be verified by empirical methods and experiments. Moreover, the setting of the weighting factor is related to the operating conditions of the machine. Thus, some methods that perform based on online calculation or Lookup Table (LUT) are introduced to realize the selection of weighting factor according to different machine working conditions [35, 36]. However, this is performed with involving additional computational efforts, which increase the complexity of the control scheme. Therefore, the elimination of the weighting factor is desired for a MPTC.

Methodology To achieve the first objective and considering the technical barriers aforementioned, an improved two-vectors MPTC that can restrict the torque ripple within desired boundaries during the whole operating period can be of great interest. The defined boundaries should be able to be adjusted automatically so that the torque performance can be optimized at different working conditions. Moreover, the weighting factor should be eliminated in the MPTC to facilitate the design of the control scheme. In addition, as a two-vectors scheme introduces more candidate solutions that can increase the computational efforts, a selective mechanism can be considered to reduce the computational efforts.

B. Simplification and Control Flexibility

Objective The second objective is to develop an adaptive MPC with simplified solution and flexible control structure. With such a scheme, the computational efficiency should be improved through the simplification of MPC. In addition, such a scheme should have a high control flexibility. It means the characteristic of inclusion of constraints within an objective function should not be affected, as this is an important advantage of MPC.

Technological Barrier The computation effort required to solve the optimization problem underlying MPC is often considerable. With a Finite Control Set MPC (FCS-MPC), the control variables need to be evaluated under all admissible voltage vectors. The computational cost is then relatively high. For a two-level VSI, eight switching states need to be considered. When a two-vectors scheme is used, the computational burden will be heavier, as more possible vector combinations ($8\times8=64$) are involved. Actually, in each control period, there is always a number of candidate vectors that obviously do not meet the current control objectives. Thus, evaluating all the candidate vectors in each control period could reduce the computational efficiency. A Reference Voltage Vector Based MPC (RVV-MPC) that focuses on the simplification of FCS-MPC was then proposed to reduce the computational burden [37, 38]. Such a strategy obtains a reference voltage vector based on the machine model and selects an optimal voltage vector directly according to the location of the reference voltage vector. As a result, the optimal solution is obtained without evaluating each candidate, thus improving the computational efficiency. However, as the number of the candidate solutions is strongly reduced, additional constraints are less likely to be included within the objective function, affecting the control flexibility of FCS-MPC. An important advantage of FCS-MPC is then lost. It also means the extensibility of such scheme is limited and achieving further control performance improvement becomes difficult.

Methodology The RVV-MPC reduces the computational effort through the simplification of FCS-MPC, however affecting the control flexibility due to the use of a single reference point. Thus, to develop an improved MPC scheme with flexible control structure to handle system constraints, setting up of adaptive reference variants can be introduced rather than considering a fixed reference point. A referent variant region can be constructed to include more candidate solutions

so that additional constraints can be fulfilled. The region should have flexible structure to comply truly with constraints. In addition, a trade-off should be made between the computational efficiency and the system performance.

C. Robustness Against System Parameter Uncertainty

Objective The third objective is the adaption to counter the parameter dependence problem with predictive current control. This controller should be independent of motor parameters, thus being robust against parameter uncertainties and system nonlinearities. This controller should achieve improved robustness without affecting the control performance. Moreover, any observer with additional parameters should not be involved to achieve a low system complexity.

Technological Barrier For an MPC-based PMSM system, the discrete-time model is used to predict motor behaviors. It means the controller is dependent on the motor parameters. However, the parameters may not match with their actual values due to measurement error or they may change during the operation of motor. All these uncertainties and model inexactitude lead to inaccurate prediction of the motor behavior and thus deteriorating the performance and stability of the controller. It is desirable that the controller should be insensitive to these kinds of model uncertainties, i.e. the controller should be robust [39]. To improve the robustness of MPC, observers were introduced to online identify the motor parameters so that more accurate predictions can be achieved [40-42]. However, such observers perform with additional parameters that need to be well tuned. Also, the complexity of controller will be increased and the convergence problem requires to be considered with observers. Therefore, a model-free controller without involving observer is desirable.

Methodology In order to achieve this objective, an improved current-difference sample based predictive controller is of interest. Such a controller does not depend on the motor parameters, and instead uses online sampled current differences to achieve current predictions. In addition, in order not to affect the control performance with this method, the reliability of the current difference information should be guaranteed so that this controller can achieve the similar performance as a model-based controller with correct parameters does.

To summarize, a diagram is given as Figure 1.4 to explain the three research questions. Three shortcomings of conventional MPC are pointed out at the first level. Then, the conventional methods that solve the problems are given. However, even though improvements are achieved, further problems are raised with these conventional methods, as described at the third level. Thus, adaptive solutions are proposed to reach the final goals given at the fifth level. The three research questions will be discussed in Chapter 4, Chapter 5 and Chapter 6, respectively. The contents linked to each block in Figure 1.4 will also be pointed out in those chapters.

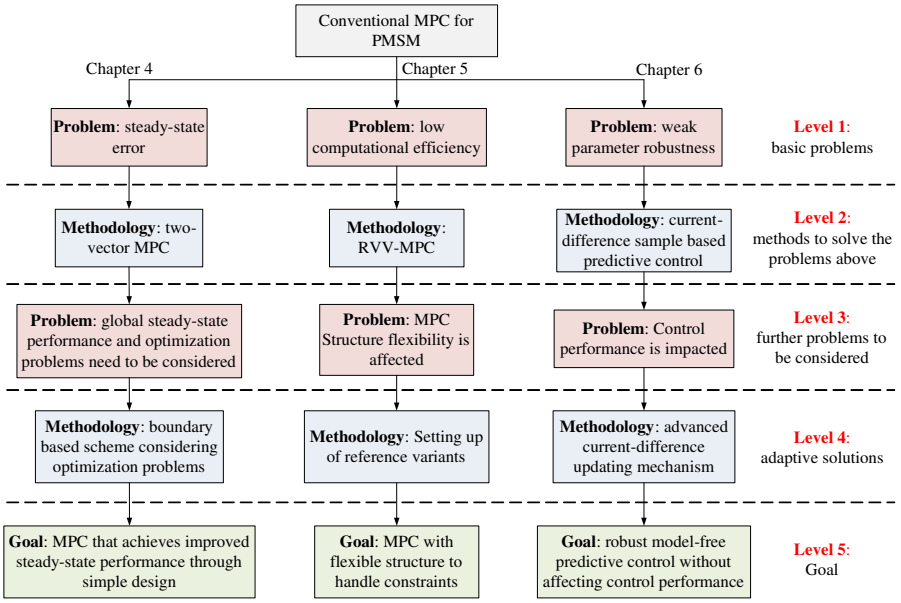

Figure 1.4: Diagram of the research questions.

1.7 Outline

This thesis is organized in seven chapters.

Chapter 1 introduces the main control schemes for power electronics and motor drives, and their main challenges are discussed. Furthermore, MPC and its advantages for motor drives are introduced. In addition, three main research questions on MPC are discussed.

In Chapter 2, the PMSM models are given. The conventional control schemes for PMSM, FOC and DTC, are introduced, and their characteristics are discussed. The classifications and the basic principles of predictive control are elaborated in Chapter 3. Then, the MPTC of PMSM is presented to discuss the application of MPC to PMSM drive. In addition, the three research issues on MPC, which are the steady-state performance, computational efficiency and parameter robustness, are pointed out. These three issues are further studied in the following chapters.

In Chapter 4, the improvement of the steady-state performance of MPC is discussed. First, two-vectors MPC strategy is introduced and the effects of different duty ratio optimization methods on improving the steady-state performance are studied. Then, aiming at minimizing the steady-state error, a torque boundary based MPTC is developed for PMSM taking into account some optimization issues, e.g. computational burden reduction, weighting factor elimination and boundary optimization. To show the effectiveness and improvements of the proposed boundary based MPTC, it is compared with conventional one-vector MPTC and conventional two-vectors MPC by experiments.

In Chapter 5, to reduce the computational burden, the simplification of FCS-MPC is firstly discussed by introducing a reference voltage vector based MPC. Then, the limitations of such strategy are pointed out. The control flexibility of FCS-MPC is influenced, as the advantage of easy inclusion of system constraints is lost with such a reference based MPC. A reference-variant-MPC strategy is then introduced aiming at retrieving this important advantage and thus achieving a trade-off between the computational efficiency and the control performance. The effectiveness of the proposed reference-variant-MPC is demonstrated by simulations and experiments. Moreover, this strategy is compared with the reference based MPC in terms of steady-state performance and dynamic performance to show its improvements.

Chapter 6 focuses on solving the parameter dependence problem of MPC. First, the parameter sensitivity of model predictive PMSM current control is analyzed. Then, to eliminate the influence of parameter uncertainties, a current-difference sample based predictive current control is developed for PMSM. Such a strategy abandons machine model, and instead uses sample current difference to achieve current prediction. As a result, a strong robustness against parameter mismatches is achieved. Experimental studies are provided to reveal the

validity of the proposed strategy. In addition, this strategy is compared with the conventional model based predictive current control and the conventional current-difference sample based predictive current control to show its improvements.

Finally, Chapter 7 draws a number of conclusions and looks ahead to further research.

1.8 Scientific Publications

Articles in International SCI Journals

An overview of publication in peer-reviewed international journals:

1. C. Ma, H. Li, X. Yao, Z. Zhang and F. De Belie, "An Improved Model-Free Predictive Current Control with Advanced Current difference Updating Mechanism," in *IEEE Transactions on Industrial Electronics*, doi: 10.1109/TIE.2020.3044809.
2. C. Ma, X. Yao, H. Li, H. Vansompel, C. Garcia, J. Rodriguez and F. De Belie, "A Novel Torque Boundary-Based Model Predictive Torque Control for PMSM Without Weighting Factor," in *IEEE Journal of Emerging and Selected Topics in Power Electronics*, doi: 10.1109/JESTPE.2020.3039687.
3. C. Ma, X. Yao, H. Li and F. De Belie, "Setting up Reference Variants to Comply with Current Boundary Settings in Finite Set Model Predictive PMSM Control," in *IEEE Journal of Emerging and Selected Topics in Power Electronics*, doi: 10.1109/JESTPE.2021.3062868.
4. X. Yao, C. Ma, J. Zhao and F. De Belie, "Rapid estimation and compensation method of commutation error caused by Hall sensor installation error for BLDC motors" in *IET Electric Power Applications*, 2020, 14(3):337-347.
5. H. Li, J. Van Damme, C. Ma, J. Melkebeek and F. De Belie, "A Geometrical Interpretation of Current Transient Responses to Predict Current differences for IPMSM Model Predictive Control," in *IEEE Transactions on Industrial Electronics*, doi: 10.1109/TIE.2020.3028816.

Articles in Conference Proceedings

An overview of conference papers:

6. C. Ma, X. Yao, H. Li and F. De Belie, "An Improved Two-Vector Model Predictive Torque Control Based on RMS Duty Ratio Optimization for PMSM," *2019 IEEE International Electric Machines & Drives Conference (IEMDC)*, 2019, pp. 1674-1679, doi: 10.1109/IEMDC.2019.8785176.
7. C. Ma, X. Yao, H. Li and F. De Belie, "Reference Voltage Vector Based Model Predictive Torque Control with RMS Solution for PMSM," *2019 IEEE 28th International Symposium on Industrial Electronics (ISIE)*, 2019, pp. 384-389, doi: 10.1109/ISIE.2019.8781392.
8. C. Ma, X. Yao, H. Li and F. D. Belie, "Current Boundary Based Model Predictive torque control of PMSM," *2019 22nd International Conference on Electrical Machines and Systems (ICEMS)*, 2019, pp. 1-6, doi: 10.1109/ICEMS.2019.8922178.
9. H. Li, C. Ma and F. D. Belie, "High Loading Distortion Effect on EIectric Pulse Sensing in Rotor Position Estimators for EIectric Machines," *2020 IEEE Transportation Electrification Conference & Expo (ITEC)*, 2020, pp. 906-911, doi: 10.1109/ITEC48692.2020.9161513.

Some of the work presented in the journal and conference papers above has been implemented in this thesis. The link between the chapters of this thesis and the papers listed above is given in Table 1.1.

Table 1.1: Link between the chapters and the published papers

Chapter	1	2	3	4	5	6	7
Paper				2,6,8	3,7	1	

Chapter 2
PMSM Drive and Conventional Control Strategies

The characteristics of PMSM, such as high torque, high power density, high efficiency and rapid dynamic response, make it highly attractive in industrial applications. Due to these characteristics, PMSMs are suitable for a wide range of applications, including general purpose industrial drives, high-performance servo drives, and several specific applications where size and weight are limited, such as automotive and aerospace applications. Generally, PMSMs consists of three-phase stator windings and an iron rotor with permanent magnets. The permanent magnets can be mounted on the rotor surface or inside the rotor core. As a result, the magnetic field is fixed to the rotor position. Typically, a voltage source inverter is required to drive the PMSM.

Several control schemes have been proposed for PMSM. Well-known methods are FOC and DTC. In this chapter the dynamic model of PMSM and the conventional control strategies (FOC and DTC) will be introduced.

2.1 Dynamic Model of Salient-Pole PMSM

A salient-pole PMSM with three-phase stator windings and a sinusoidal flux distribution is studied in this thesis. The machine fed by a two-level VSI and the admissible voltage vectors are shown in Figure 2.1.

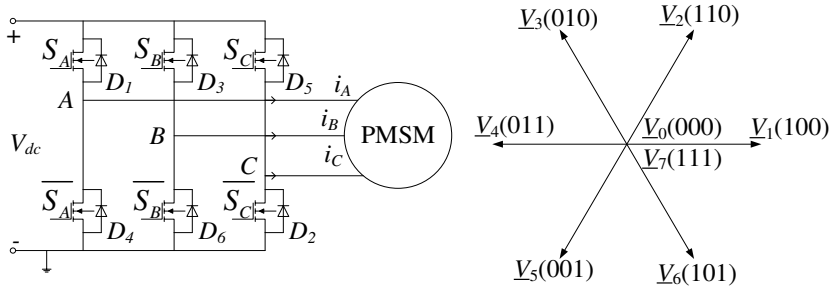

Figure 2.1: Three-phase PMSM fed by a two-level VSI and the admissible voltage vectors.

It can be seen that a two-level VSI generates eight admissible voltage vectors that can be expressed as:

$$\underline{V}_j = \frac{2}{3} V_{dc} (S_A + e^{i2\pi/3} S_B + e^{i4\pi/3} S_C) \tag{2.1}$$

where $\underline{V}_j (j = 0,...,7)$ represent the admissible voltage vectors, S_A, S_B, S_C denote the switching states of the three inverter arms and V_{dc} is the DC voltage.

Here, some assumptions are made:

- the magnetomotive force is considered sinusoidal along the air gap.
- the windings of PMSM are assumed symmetrical.
- the core losses and eddy current are ignored.
- the inverter switches and diodes have ideal switching characteristics.

Under the above assumptions, the space vector of the stator voltage, stator current and stator flux can be defined as:

$$\underline{v}_s = \frac{2}{3} (v_A + a v_B + a^2 v_C) \tag{2.2}$$

$$\underline{i}_s = \frac{2}{3} (i_A + a i_B + a^2 i_C) \tag{2.3}$$

$$\underline{\psi}_s = \frac{2}{3}(\psi_A + a\psi_B + a^2\psi_C) \tag{2.4}$$

respectively. v_A, v_B, v_C are stator voltage, i_A, i_B, i_C are stator current and ψ_A, ψ_B, ψ_C are stator flux. Then, the stator dynamics can be expressed as:

$$\underline{v}_s = R_s \underline{i}_s + \frac{d\underline{\psi}_s}{dt} \tag{2.5}$$

where R_s is the stator resistance.

As sinusoidal quantities under stationary reference frame would become constant under rotary reference frame in steady state, the dynamic model of PMSM is usually established in the rotary reference frame aligned with the rotor axis. Therefore, considering $v_s = \underline{v}_s e^{-j\theta_r}$, $i_s = \underline{i}_s e^{-j\theta_r}$ and $\psi_s = \underline{\psi}_s e^{-j\theta_r}$, the stator equation (2.5) can be transformed from the static three-phase reference frame to the rotary two-phase reference frame as:

$$v_s = R_s i_s + \frac{d\psi_s}{dt} + j\omega_r \psi_s \tag{2.6}$$

where v_s, i and ψ_s denote stator voltage vector, stator current vector and stator flux vector in rotary reference frame, respectively, θ_r is the rotor position, $\omega_r = d\theta_r / dt$ is rotor speed.

Then, the stator voltage equation (2.6) model can be written as:

$$v_d = R_s i_d + \frac{d\psi_d}{dt} - \omega_r \psi_q \tag{2.7}$$

$$v_q = R_s i_q + \frac{d\psi_q}{dt} + \omega_r \psi_d \tag{2.8}$$

where v_d and v_q are the d-axis and q-axis stator voltage, respectively; i_d and i_q are the d-axis and q-axis stator current, respectively; ψ_d and ψ_q are d-axis and q-axis stator flux respectively. It is noted that the stator voltage, current and flux vectors can be expressed as $v_s = v_d + jv_q$, $i_s = i_d + ji_q$ and $\psi_s = \psi_d + j\psi_q$, respectively.

The stator flux linkage is produced by the stator currents and the rotor magnets. Thus, the stator flux in rotary reference (d-q) frame can be given as:

$$\psi_d = L_d i_d + \psi_f \tag{2.9}$$

$$\psi_q = L_q i_q \tag{2.10}$$

where L_d and L_q are the d-axis and q-axis inductance, respectively; ψ_f is the Permanent Magnet (PM) flux linkage. Figure 2.2 shows the stator flux vector in the rotary reference (d-q) frame.

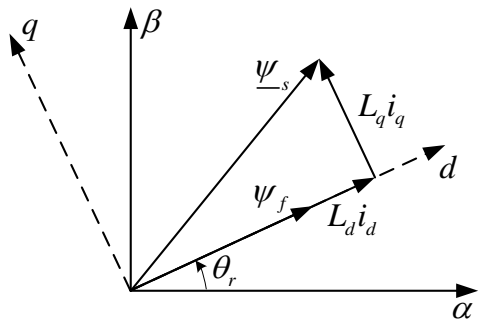

Figure 2.2: Stator flux vector in rotary reference (d-q) frame.

The electromagnetic torque of salient-pole PMSM is produced by the stator current and the PM flux. It can be expressed as:

$$T_e = \frac{3}{2} p(\psi_d i_q - \psi_q i_d) \tag{2.11}$$

where p is the number of pole pairs. The mechanical rotor dynamics can be represented as:

$$\frac{d\omega_m}{dt} = \frac{1}{J}(T_e - T_l) - \frac{B}{J}\omega_m \tag{2.12}$$

where ω_m is the mechanical rotor speed, J is the rotor inertia, B is the friction coefficient and T_l is the load torque. Here, the relationship between the electrical rotor speed and the mechanical rotor speed is given as:

$$\omega_r = p\omega_m \tag{2.13}$$

2.2 Conventional Control Strategies for PMSM

Over the past few decades, two main control strategies of PMSM drive have played an important role in the high-performance applications: FOC and DTC. These two control schemes will be presented hereafter.

2.2.1 Field Oriented Control

In the late 1960s, FOC entered the field of AC drive research. FOC, a type of vector control, was vigorously developed in the 1980s mainly to deal with the flux and torque oscillation problem in inverter fed induction and synchronous motor drives.

FOC establishes a rotary reference frame that rotates synchronously either with the stator, the air-gap or the rotor flux vector. In the rotary reference frame, the stator current vector can be decomposed into a d-axis component and a q-axis component, and these two current components are orthogonal. In addition, in the rotating reference frame, the machine variables are DC quantities during steady-state operation. It is noted that the two components of stator current, d-axis component and q-axis component, are effectively decoupled, simplifying the design of the control scheme [23].

It can be concluded that the main idea of FOC is to decouple the electromagnetic torque and the magnitude of the rotor flux using a proper coordinate transformation. This can be achieved by aligning the coordinate system with the rotor flux.

The reference frame in rotor FOC is shown in Figure 2.3. It can be seen that the d-axis of the rotating reference frame is aligned with the rotor flux vector ψ_r. The coordinate frame rotates synchronously with the rotor flux and is displaced by θ_r with respect to the stationary $\alpha\beta$ reference frame. As the variables are given in a rotating coordinate frame, the electromagnetic torque can be controlled via the q-axis component of the stator current i_q, and the rotor flux magnitude can be controlled by the d-axis component of the stator current i_d. Here, an estimator can be employed to obtain the angular position of the reference frame. Thus, the rotor flux vector can be estimated based on

the measured stator currents. The magnitude and the angular position of the rotor flux vector, $|\psi_r|$ and θ_r, can be then obtained [2].

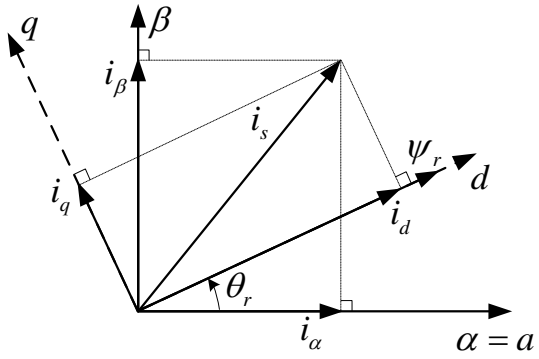

Figure 2.3: Reference frame in rotor FOC.

The block diagram of rotor FOC is shown in Figure 2.4. It can be seen that the reference for the d-component of the stator current reference i_d^* is translated from the reference for the rotor flux magnitude $|\psi_r^*|$. Here, in order to achieve a fast control of the rotor flux magnitude, a PI controller is typically used. The error between the rotor speed ω_r and its reference is given as the input of the speed PI controller, which manipulates the reference value for the q-component of the stator current i_q^*.

The d-component and q-component of the measured stator current i_d and i_q with the corresponding stator current references i_d^* and i_q^* are fed to the current controllers. Here, i_d and i_q are obtained by transforming the phase currents from the static abc frame to the rotary dq frame with the angular position θ_r. The outputs of the two current controllers are the stator voltage reference v_d^* and v_q^*, respectively. Then, v_d^* and v_q^* are translated into the three-phase abc frame, resulting in the three-phase reference voltages v_a^*, v_b^* and v_c^*. Next, with a PWM stage, typically Space Vector Modulation (SVM) or Carrier-Based PWM (CB-PWM), the three-phase switching commands are generated.

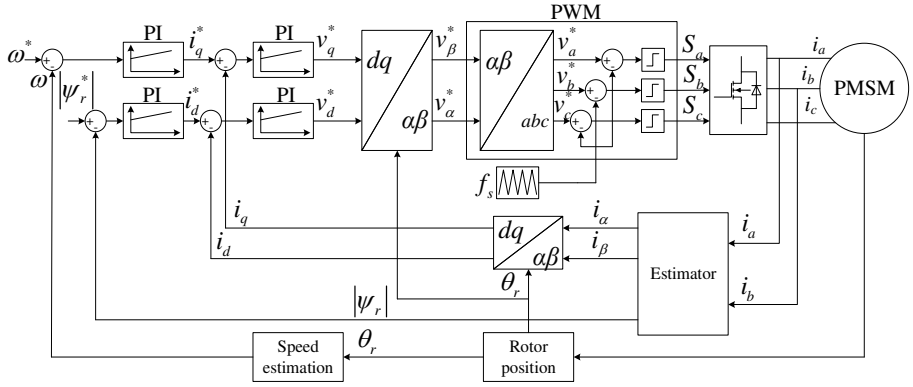

Figure 2.4: Block diagram of rotor FOC.

Here, two main advantages inherent in the combination of FOC and CB-PWM or SVM can be identified. First, the stator current ripple at the peaks of the triangular carrier waveform can be guaranteed as zero by using CB-PWM. Similarly, this benefit can also be given by SVM. Only the fundamental component of the AC current waveform can be captured when the stator currents are sampled at the carrier peaks. Directly related to this is the fact that fixed-length modulation cycles are used with CB-PWM and SVM. This facilitates sampling at equally spaced time instants. For this purpose, in the case of CB-PWM, where sampling is asymmetrical and regular, the sampling interval is set to half of the carrier interval, $0.5T_s$ [23].

Second, the stator current can be converted from AC quantity to a DC quantity by transforming the stator current from abc reference frame into a dq reference frame. This transformation rotates synchronously with the rotor (or stator) flux vector. The same conversion applies to the orthogonal components of the flux vectors. It is noted that the stator current references are also effectively DC quantities because the bandwidth of the current controller is much higher than that of the outer flux and speed controllers. As (quasi) DC quantities are involved with the current control loop, the use of PI controllers is facilitated. It can be seen from Figure 2.4 that two PI control loops are commonly used: one for the d-axis component of the stator current, and another one for the q-axis component.

On the other hand, the performance of the two PI loops can be limited by two fundamental issues. First, a digital implementation of the current controller arouses a computational delay of one sampling period. In case of an asymmetric, regularly sampled CB-PWM, an additional delay of half a sampling period can be incurred by the modulator. Then, the overall delay in the current control loop will be $1.5T_s$. This delay can largely limit the bandwidth that a current control loop can achieve when the switching frequency is low, the carrier period is long and the corresponding sampling period is long [23].

Second, the maximum voltage that the modulator can generate is limited. As a result, a physical constraint is imposed on the manipulated variables. If no proper countermeasures are applied, the integrator of an aggressively tuned PI current controller may wind up when the PI controller operating close to its voltage limit. Thus, an anti-wind-up mechanism is often added to prevent this situation from happening. These schemes are typically used to monitor the difference between the commanded and the generated modulator voltage. The integrators of the PI controllers will be turned off in case the difference is nonzero [23].

2.2.2 Direct Torque Control

As previously mentioned, with FOC the electromagnetic torque and the machine magnetization of PMSM are controlled indirectly through controlling the stator currents. On the other hand, in the mid-1980s Takahashi and Noguchi proposed a method, in which the torque and magnetization can be directly controlled. Due to this characteristic, this method is called “direct torque control” (DTC) or “direct torque and flux control.” After decades of development, DTC has been a mature and well-established control scheme for motor drives and is considered as an alternative to FOC [43, 44].

In a DTC, upper and lower boundaries are imposed on the electromagnetic torque and the stator flux amplitude, and hysteresis controllers are used to limit the controlled variables within the boundaries. The hysteresis controllers manipulate the input of LUT, which is used to set the switching states of the inverter. Like FOC, DTC achieves the control of torque and flux independently of each other. The direct manipulation of the voltage vector applied to the stator windings exploits the fast stator flux dynamics of the machine. This makes the

concept of DTC simple. In addition, DTC is almost independent of the machine parameters, and it can achieve a very fast closed-loop torque and flux response. The main difference between DTC and other control methods is that it uses closed-loop torque and flux amplitude controllers instead of current control loops [45].

DTC relies on fast stator flux control. (2.14) can be obtained from the stator equation (2.5):

$$\frac{d\psi_s}{dt} = v_s - R_s i_s \tag{2.14}$$

Here, as the stator resistance R_s is negligible, the variation of stator flux over a control period T_s can be derived as:

$$\Delta\psi_s = v_s T_s \tag{2.15}$$

It can be seen from (2.15) that a direct manipulation of the stator flux vector can be achieved by choosing a suitable voltage vector and applying it to the stator windings. Here, the voltage vector v_s is assumed as a constant over T_s. It is noted that the stator flux vector is controlled in the direction of the voltage vector and the change rate corresponds to the length of the voltage vector. The available DC-link voltage defines an upper limit on $\|\Delta\psi_s\|$ [23].

Here, the electromagnetic torque (2.11) can be rewritten as:

$$T_e = \frac{3p|\psi_s|}{4L_d L_q}[2\psi_f L_q \sin\theta_{sr} + |\psi_s|(L_d - L_q)\sin 2\theta_{sr}] \tag{2.16}$$

where θ_{sr} is the angle between the stator flux vector and the rotor flux vector. It is noted that (2.16) is independent of the adopted reference frame. It can be seen torque is composed of the permanent-magnet torque and the reluctance torque caused by the rotor saliency [46]. The control of torque can be then achieved by manipulating the angle θ_{sr}, which is the basic principle of conventional DTC.

The change of the angle θ_{sr} can only be achieved by applying appropriate voltage vectors. This is because the fact that the voltage vector is the sole controllable input variable for a VSI-fed DTC. It is seen from (2.15) that the stator flux ψ_s can be rapidly controlled by

applying different voltage vectors. As the rotor time constant is long, the amplitude of the rotor flux vector can be assumed as a constant within several control periods (several milliseconds). Therefore, the angle θ_{sr} changes with the stator flux, resulting in a fast torque response. Figure 2.5 shows that the angle θ_{sr} can be controlled by applying a proper stator voltage vector [2].

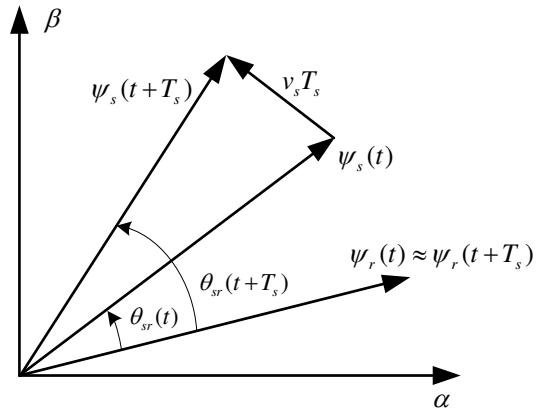

Figure 2.5: Principle of direct torque control.

Figure 2.6 shows the schematic diagram of a standard DTC [2]. It can be seen that the torque reference T_e^* is obtained by the external speed controller and the reference for the stator flux amplitude is constant. The torque and the amplitude and angle of the stator flux vector are estimated based on the PMSM model. Then, the torque error can be obtained by computing the difference between the estimated torque and the reference torque, and the error of stator flux amplitude is calculated accordingly. Two individual hysteresis comparators are used to control the torque and flux errors. The outputs of the two hysteresis controllers, h_T and h_ψ, with the stator flux angle θ_s are fed to a LUT, which is used to select a suitable voltage vector. Finally, the most suitable voltage vector is selected and directly applied to the VSI, allowing the PMSM to respond to the control action according to the DTC principle [2].

The key parts of a DTC strategy are the hysteresis comparators and the LUT that includes a switching table. The inputs of the switching table are the outputs of the hysteresis controllers, h_T and h_ψ. The LUT

provides a suitable voltage vector for each of the input combinations. The applied voltage vector is selected according to the sign and amplitude of the torque and flux errors with the location of the stator flux vector. Here, this location means the number of the sector that contains the stator flux vector. In case the torque or the flux error exceeds a boundary of hysteresis, a new voltage vector will be applied aiming at driving the stator flux vector to a position such that the torque and flux errors can be limited within the corresponding hysteresis bounds.

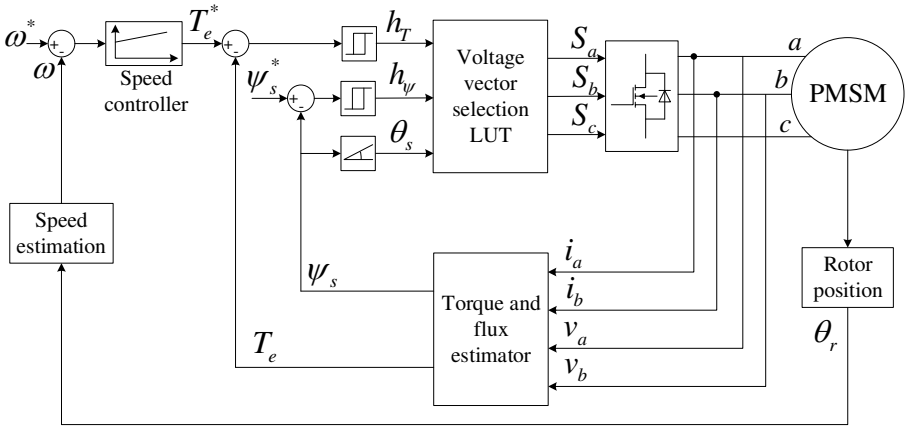

Figure 2.6: Block diagram of direct torque control.

With a two-level VSI six active voltage vectors are generated. Thus, as shown in Figure 2.7, the complex plane can be divided into six sectors, each of which covers 60°. The six sectors are enumerated from 1 to 6. Then, the design of the LUT can be restricted to the first sector with angles between -30° and 30°, while the LUT for the remaining five sectors can be easily obtained by rotating the voltage vectors in the first sector by multiples of 60°.

The electromagnetic torque can be increased or decreased by applying a voltage vector that acts in a direction that is orthogonal to the stator flux vector. Thus, the orthogonal component of the voltage vector can be controlled to achieve torque control. Based on this principle, a switching logic can be obtained: $h_T = 1$ means an increase of the electromagnetic torque is required, while $h_T = -1$ necessitates a

decrease of the electromagnetic torque. Accordingly, voltage vectors that are parallel to the stator flux vector can increase or decrease the stator flux amplitude.

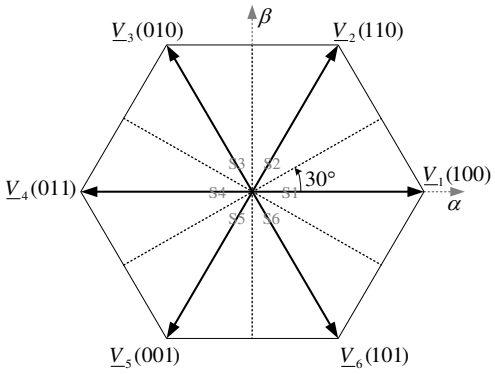

Figure 2.7: Sector definition for DTC.

On this basis, the influence of each voltage vector on the behavior of the torque and flux can be evaluated for each sector. For instance, as shown in Figure 2.8, in case the stator flux vector ψ_s is located in sector 2, applying vector V_3 will increase the torque T_e and the stator flux amplitude $|\psi_s|$, while applying V_1 will decrease T_e and increase $|\psi_s|$. Accordingly, taking into account the increase or decrease of T_e and $|\psi_s|$ for each sector, a LUT can be derived [2].

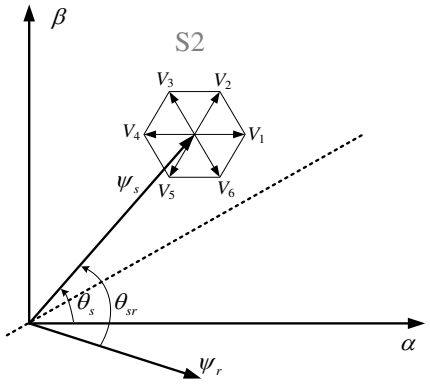

Figure 2.8: Control principle of torque and stator flux amplitude.

The switching table can be derived by combining the reasoning for the torque and flux hysteresis controllers [23]. The $\alpha\beta$ -plane of the voltage vectors is divided into orthogonal bands that correspond to the integer outputs of the two hysteresis controllers. Each combination of the controller outputs corresponds to one voltage vector. The selected voltage vector is applicable to any stator flux vector that lies within this subsector. Thus, DTC only requires knowledge of the subsector that contains the stator flux, rather than of its precise angular position. Table 2.1 shows the resulting LUT for DTC. Based on the inputs of the table, which are the sector of the stator flux, as defined in Figure 2.8, and the outputs of the hysteresis controllers h_T and h_ψ , a proper voltage vector is selected and applied to the drive system.

Table 2.1: Voltage vector selection LUT for DTC

Sector	(h_ψ, h_T)			
	(1,1)	(1,-1)	(-1,1)	(-1,-1)
1	V_2	V_6	V_3	V_5
2	V_3	V_1	V_4	V_6
3	V_4	V_2	V_5	V_1
4	V_5	V_3	V_6	V_2
5	V_6	V_4	V_1	V_3
6	V_1	V_5	V_2	V_4

2.3 Characteristics and Discussions

After introducing the two conventional control schemes of PMSM drive, their characteristics will be discussed hereafter.

With DTC, the control of torque and flux are realized by hysteresis controllers. Different from FOC, which includes inner current control loop, DTC uses the hysteresis controllers to replace the PI controllers. A switching table is introduced with DTC, thus avoiding the use of a modulator. In addition, DTC aims to restrict the torque and flux within certain bounds around their references, rather than to regulate the controlled variables to their corresponding reference values.

In DTC, the switching frequency is determined by the widths of the hysteresis bounds. In case the width of hysteresis band is fixed, the switching frequency is related to the operating conditions and varies with the fundamental frequency and the reference torque [47]. With the

hysteresis controllers, high ripples of stator currents and electromagnetic torque are aroused. In order to minimize the current and torque ripples, multi-level hysteresis controllers should be used. This is particularly important for the torque hysteresis controller, which controls the angular position of the stator flux vector [23].

In contrast to FOC, DTC shows the following advantages in terms of implementation and performance:

- **Simplicity** In DTC, hysteresis controllers are employed instead of PI control loops, thus avoiding the modulation stage. Compared to a PI controller, a hysteresis controller is simpler in concept with lower computational cost. In addition, the tuning and commissioning effort of DTC is less than those of FOC.
- **Fast response** In FOC, the dynamic torque response is limited by the bandwidth of the inner control loop. In contrast, DTC can achieve a fast dynamic response due to the absence of inner control loop. The dynamic response is limited only by the available DC-link voltage [48].

On the other hand, the following disadvantages are typically associated with DTC:

- **Steady-state performance** Due to the use of hysteresis controllers, DTC produces significant steady-state errors, particularly in the torque control loop. A conventional DTC tends to suffer from higher torque and current ripples compared to FOC, especially in case a two-level VSI is employed, as limited admissible voltage vectors are provided [49]. In addition, the harmonic distortion of stator current produced by DTC is also pronounced.
- **Switching frequency** The use of hysteresis control loops results in a variable switching frequency, which is dependent on the operating condition. A variable switching frequency can affect the noise in a negative way, and the estimation of the heat produced by variable switching frequency could also be affected by the uncertainty. The widths of the hysteresis bounds need to be adjusted to achieve a fixed switching frequency, however requiring additional control efforts. For instance, this can be achieved by monitoring the switching frequency and adjusting the bound widths through a closed-loop switching frequency control loop.

- **Sampling frequency** In order to restrict the controlled variable, torque and stator flux amplitude, within the hysteresis bounds, a high sampling frequency is needed with DTC. Basically, achieving a similar steady-state performance as FOC does requires a much higher switching frequency.

2.4 Conclusions

The basic PMSM equations and the conventional control strategies, FOC and DTC, are introduced in this chapter. In addition, the characteristics of FOC and DTC have been discussed. Compared to FOC, DTC realizes the control of torque and stator flux through hysteresis controllers rather than modulators, thus achieving a simpler control structure and lower tuning effort. In addition, due to the absence of inner control loop, DTC can achieve a fast dynamic response. On the other hand, the noticeable steady-state error, especially torque ripple, is a main disadvantage of DTC. To achieve a similar steady-state performance as FOC does, a higher sampling frequency is often required. Moreover, the hysteresis controllers lead to variable switching frequency, which is another disadvantage of DTC.

Chapter 3
Model Predictive Control for Power Electronic and Drives

The research and development of MPC has been more than four decades. Initially, MPC was applied to the process industry. Then, some scholars put forward the application of MPC to the field of power electronics and motor drives in 1980s. For example, [26] presents a predictive current controller for AC machines. In recent years, due to advances in microprocessor technology, MPC is considered a promising alternative to traditional motor control strategies, e.g. FOC and DTC [50, 51]. Thus, the concept and implementation of MPC to power electronics and drives will be studied in-depth in this chapter.

3.1 Classification of Predictive Control Strategies

Predictive control includes a variety of control strategies, which have recently been used in the field of power electronics and motor drives. Different predictive control schemes can be classified as shown in Figure 3.1 [52].

The main feature of predictive control is the use of a system model to predict the future behaviors of the controlled variables. The controller then utilizes the predicted results to determine the best input (often denoted as the optimal control action) based on the desired way how the system should behave, which is translated mathematically into a predefined optimization criterion.

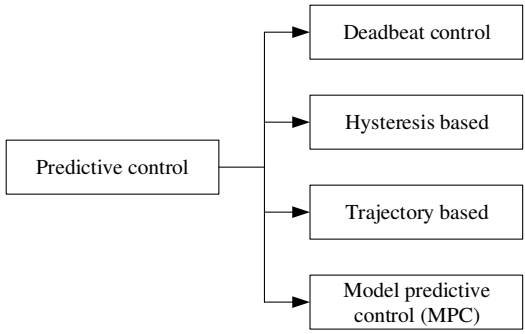

Figure 3.1: Classification for different predictive control methods.

In a deadbeat predictive control, the selection principle for the most suitable actuation is to nullify the error at the next sampling instant [53, 54]. For a hysteresis-based predictive control scheme, the optimization principle is to limit the controlled variables within the boundaries of a hysteresis band [55]. The controlled variables in a trajectory-based control scheme are forced to follow a predefined trajectory [56]. MPC, on the other hand, uses a more flexible optimization criterion, which is represented as an objective function to be minimized to determine the optimal actuation [57].

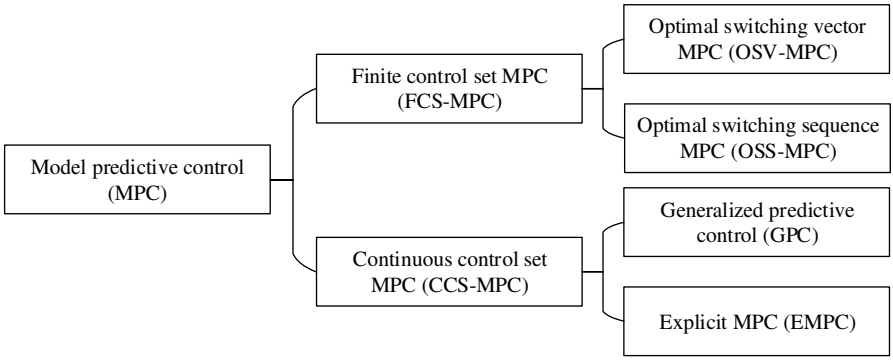

Figure 3.2: Classifications of MPC methods.

According to the type of the optimization problem, the MPC schemes applied to power electronics and drives can be classified into two main categories. The classification of MPC schemes is shown in

Figure 3.2, as proposed in [29]. On one hand, FCS-MPC, which is the most widely investigated predictive control scheme for power electronics and drives, takes the advantage of the discrete nature of power converters to formulate the MPC algorithm. It should be noted that FCS-MPC does not contain a modulation stage. The diagram of a FCS-MPC is shown in Figure 3.3(a). FCS-MPC schemes can be further classified into two types. The first one is Optimal Switching Vector MPC (OSV-MPC), which is the first FCS-MPC technique and is currently the most popular MPC scheme applied to power electronics and drives. Thus, OSV-MPC is often referred to as FCS-MPC in literature. In such a scheme, all the possible voltage vectors produced by the power converter are composed as a control set. Then, the predictions of system behavior are performed for this control set, reducing the optimization problem to an enumerated search problem. As a result, a very intuitive formulation is achieved with the OSV-MPC. In a conventional OSV-MPC, only one voltage vector is applied over a whole switching period. Moreover, the same voltage vector may be applied during several continuous switching periods without additional constraints. As a result, a variable switching frequency can be generated with OSV-MPC, which is a main disadvantage of this scheme [29].

A second type of FCS-MPC is Optimal Switching Sequence MPC (OSS-MPC). With OSS-MPC, a limited number of possible switching sequences are composed as a control set in each switching period. In this way, OSS-MPC considers the time as an additional decision variable, i.e. the instant that the switching state is changed.

On the other hand, a Continuous Control Set MPC (CCS-MPC) can be identified. With such a scheme, a continuous control signal is calculated and then a modulation stage is used to generate a desired output voltage of the power converter. Here, the modulator can be any strategy that is applicable to the power converter under consideration [58]. A typical diagram of CCS-MPC is illustrated in Figure 3.3(b). CCS-MPC can produce a constant switching frequency, which is a main benefit of this scheme. It is noted that the most widely used CCS-MPC schemes for power electronics and drives are Generalized Predictive Control (GPC) and Explicit MPC (EMPC). GPC is primarily used in systems with linear and unconstrained problems, while EMPC has the ability to deal with nonlinear and constrained systems. When applied to power electronics and motor drive systems, the main disadvantage of

GPC and EMPC is that both schemes contain complex formulations [29].

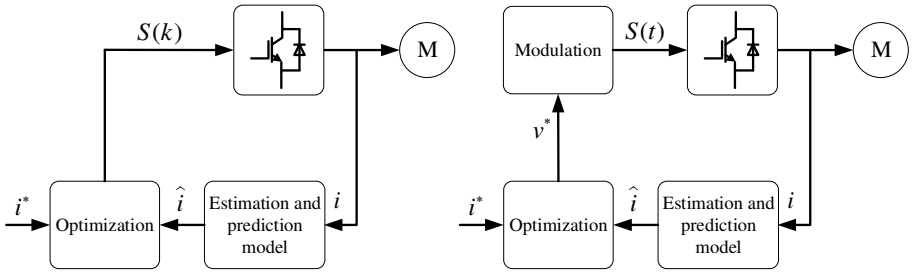

(a) FCS-MPC (b) CCS-MPC

Figure 3.3: Diagram of FCS-MPC and CCS-MPC.

It should be noted that CCS-MPC can solve part or all of the optimization problem by offline calculations. Thus, the computational cost of CCS-MPC is lower than that of FCS-MPC. For this reason, CCS-MPC can be used to address long prediction horizon problems. For example, GPC uses an expression to determine the control action that can be precalculated, therefore reducing the online computational cost [59]. On the other hand, with EMPC the optimization problem can be solved offline and the solution can be stored. As a result, the online computation contains only a search algorithm that can be fulfilled through a binary search tree technique.

Table 3.1: Main features of different MPC strategies

Item description	GPC	EMPC	OSV-MPC	OSS-MPC
Switching frequency	Fixed	Fixed	Not fixed	Fixed
Optimization	Online	Offline	Online	Online
Modulator	SVM or PWM	SVM or PWM	Not required (optional)	Not required (optional)
Inclusion of constraints	Supported with high computational burden	Supported	Supported	Supported
Long prediction horizon	Achievable	Achievable	Achievable with special search algorithm	Achievable with special search algorithm
Formulation	Complex	Complex	Intuitive	Intuitive

In contrast, FCS-MPC needs to solve optimization problems involving a large amount of calculations online. Thus, for power electronics and motor drive systems, FCS-MPC is often used to achieve short prediction horizons. The main characteristics of different MPC strategies are summarized in Table 3.1, as concluded in [29]. It should be noted that the most widely used MPC strategy for power electronics and drives is FCS-MPC, which is thus the focus of this thesis.

3.2 Basic Principles of Model Predictive Control

MPC covers a variety of controllers, rather than a specific control scheme [7]. What this kind of controllers has in common is that they use a system model to predict the future behaviors of the controlled variables over a predefined horizon and select the optimal control action by minimizing an objective function.

3.2.1 Control Problem

Typically, a general control problem can be summed up as designing a controller in which the system output y is regulated to follow its reference value y^*. To achieve this goal, the measured output y should be fed back and compared with the reference value y^*, and the input u should be manipulated accordingly to minimize the error. A closed-loop control is then achieved by feeding the output back to the input. It should be mentioned that the stability of controller should be guaranteed and the system constraints should be always complied with. In addition, to achieve these three objectives, the controller needs to be robust in some degree, as disturbances and model uncertainties may exist.

As shown in Figure 3.4, a general power electronic system that includes input vector $u \in \mathbb{R}^{n_u}$ and output vector $y \in \mathbb{R}^{n_y}$ is considered. Both vectors may contain real-valued and integer components. Typically, physical constraints in the form of actuator limits exist on the input. Here, the system input u is considered as the manipulated variable, while the system output y is referred to as the controlled variable. The controller manipulates the system input u such that the system output y can be regulated to track its reference y^*. An optional modulator can be used to translate u into the switching state of power

converter. In addition, an estimator is used to reconstruct the system state x.

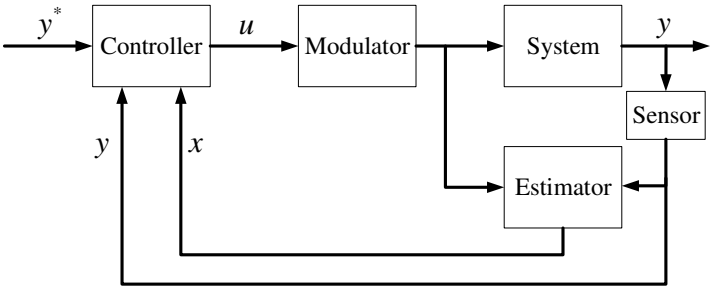

Figure 3.4: General power electronic system.

Two kinds of control problem are considered here. If a modulator is included within the system, the manipulated variable is real-valued. It is usually a reference voltage. In this case, the control problem can be referred to as an indirect control problem. The switching phenomenon can be masked by the use of averaging. Additionally, using integer variables in the system model is avoided. On the other hand, in case the modulation stage is removed from the system, it becomes a direct control problem, in which the manipulated variable is corresponded to the switching state of power converter. In this way, integer variables are included within the system model.

The state vector of the system $x \in \mathbb{R}^{n_x}$ is required for MPC. Here, some variables that cannot be obtained by measurements, e.g. the stator flux of PMSM, need to be estimated by an observer. The state and the output of the system can be computed based on the system model including the system input. The design of estimator can be achieved through feeding back the difference between the measured and the estimated system outputs. When the estimator is asymptotically stable and the system is observable, the estimated states converge to the real states [23].

3.2.2 Control Principle

Although MPC comes in several types, the key attributes of MPC can be summed up in five aspects, which are the system model, constraints,

objection function, optimization and receding horizon policy, respectively. These five aspects will be discussed in the following.

3.2.2.1 System Model

The dynamic model of the system to be controlled is required with MPC. The vector $x \in \mathbb{R}^{n_x}$ represents the state vector of the system, which typically contains both real-valued component and integer component. Starting from the current state, the sequence of future system states and outputs due to a given sequence of manipulated variables is predicted based on the internal dynamic model.

Here, state-space representation can be used to describe the dynamic evolution of the system in the continuous-time domain:

$$\frac{dx(t)}{dt} = f(x(t), u(t)) \tag{3.1}$$

$$y(t) = h(x(t), u(t)) \tag{3.2}$$

where (3.1) is a nonlinear first-order differential equation that captures the change of the state vector over the time $t \in \mathbb{R}$. The outputs y are a nonlinear function $h(\cdot,\cdot)$ of the state and input vectors.

For power electronics and drive systems, the state-space equations (3.1) and (3.2) can be considered linear when voltages, currents, or flux linkages are considered as state and output variables. Then, they can be described in the following well-known matrix form:

$$\frac{dx(t)}{dt} = Fx(t) + Gu(t) \tag{3.3}$$

$$y(t) = Cx(t) \tag{3.4}$$

where F is the system matrix, G is the input matrix and C is the output matrix.

For switching power converters, due to the switching nature, linear MPC schemes are performed in the discrete-time domain with a constant control period T_s. The manipulated variables are forced to change their values only at the start of each control period, i.e. the time instants $t = kT_s$, where $k \in \mathbb{N} = \{0,1,2,...\}$ is the number of each control period. The discrete-time equations of the continuous-time state-space

model (3.3) and (3.4) can be derived. For this, (3.3) can be integrated from $t = kT_s$ to $t = (k+1)T_s$. Meanwhile, by holding $u(t)$ to be equal to $u(k)$ during this period, the discrete-time state-space representation can be derived as:

$$x(k+1) = Ax(k) + Bu(k) \tag{3.5}$$

$$y(k) = Cx(k) \tag{3.6}$$

The matrices A and B can be obtained from their continuous-time counterparts according to:

$$A = e^{FT_s} \quad \text{and} \quad FB = -(I - A)G \tag{3.7}$$

where e represents the matrix exponential, and I denotes the identity matrix of appropriate dimensions.

It is noted that the matrix exponentials can cause computational difficulties, while the forward Euler approximation is accurate enough for the cases where the sampling intervals are up to several tens of microseconds and short prediction horizons are considered. Therefore, the discrete-time system matrices can be given by:

$$A = I + FT_s \quad \text{and} \quad B = GT_s \tag{3.8}$$

The output matrix C remains the same when deriving the discrete-time system equation.

3.2.2.2 Constraints

As mentioned before, the state-space representations (3.5) and (3.6) are linear. However, additional constraints imposed can make the system nonlinear. The constraints on the system inputs, states, and outputs can be given as:

$$u(k) \in \mathbf{u} \subseteq \mathbb{R}^{n_u} \tag{3.9}$$

$$x(k) \in \mathbf{x} \subseteq \mathbb{R}^{n_x} \tag{3.10}$$

$$y(k) \in \mathbf{y} \subseteq \mathbb{R}^{n_y} \tag{3.11}$$

In case a modulation stage is included within the system, an indirect control problem arises, and the manipulated variable is typically the

voltage reference for the PWM, which is real-valued. Thus, the manipulated variable is limited to a bounded continuous set, such as:

$$\mathbf{u} = [-1,1]^{n_u} \tag{3.12}$$

On the other hand, when a direct control problem is considered, the manipulated variable is constituted by the switching state of the power converter. In this case, the manipulated variable is limited to a finite set of integers. For instance, A two-level VSI can synthesize two voltage levels in each phase, and this feature can be captured by constraint on the input:

$$\mathbf{u} = [0,1]^{n_u} \tag{3.13}$$

Typically, the dimension of the input vector in a three-phase system is $n_u = 3$, and the constraints imposed on u are physical.

To prevent the system from running beyond the safe operating range, limitations are sometimes imposed on states. For instance, to avoid trips and damages caused by over currents in a converter, upper constraints on the absolute value of the currents can be imposed slightly below the trip level. It is noted that such constraints are usually added in the form of soft constraints, implying that they can be slightly violated.

Through imposing soft constraints on the controlled variables, they can be limited within upper and lower boundaries instead of tracking their reference values. For example, in a PMSM control, an upper and a lower boundary can be applied to the electromagnetic torque and the stator flux amplitude, which is similar to the hysteresis band in DTC.

3.2.2.3 Objective Function

The MPC converts the control objectives into an objective function. In this function, the future states, outputs, and manipulated variables are translated into a scalar cost value to be evaluated. With the objective function the impacts of different sequences of manipulated variables on the system can be assessed and compared. This enables MPC to select the control action that minimizes the value of the objective function as the optimal solution.

A general objective function can be expressed as:

$$J(x(k),U(k)) = \sum_{\ell=k}^{k+N_p-1} \Lambda(x(\ell),u(\ell)) \tag{3.14}$$

(3.14) represents the sum of all the stage costs $\Lambda(\cdot,\cdot)$ over a finite time step horizon, Np. The stage cost values are used to evaluate the predicted system behavior, e.g. the difference between the controlled variables and their reference values and the control cost, e.g. the switching frequency. Here, the stage cost value should be nonnegative. The objective function uses the current state vector $x(k)$ and the sequence of manipulated variables

$$U(k) = [u^T(k)u^T(k+1)...u^T(k+N_p-1)]^T \tag{3.15}$$

as arguments. Then, the future system states and the controlled variables over the prediction horizon can be predicted and evaluated based on the two arguments and the system model.

3.2.2.4 Optimization

For switching power converters, MPC can be considered as a constrained finite-time optimal control problem, i.e. minimizing an objective function subject to the evolution of the discrete-time internal system model over the prediction horizon and the system constraints. The solution to the optimization problem results in an optimal sequence of manipulated variables, $U_{opt}(k)$. The control problem based on a linear state-update equation, a nonlinear output equation, and constraints on the manipulated variable can be given as

$$U_{opt}(k) = \arg\text{minimize}\, J(x(k),U(k)) \tag{3.16}$$

$$\begin{aligned} \text{subject to } & x(\ell+1) = Ax(\ell) + Bu(\ell) \\ & y(\ell+1) = h(x(\ell+1)) \\ & u(\ell) \in \mathbf{u} \;\; \forall \ell = k,...,k+N_p-1 \end{aligned} \tag{3.17}$$

In a general MPC, the system model is nonlinear, and the system variables contain integers. Therefore, the optimization problem of MPC can be considered as a mixed-integer nonlinear problem. Typically, the optimal solution is required to be available in real time, and thus the optimization problem is solved online.

3.2.2.5 Receding Horizon Policy

At the time step k, the solution to the optimization problem (3.16) and (3.17) is obtained, which is an open-loop optimal sequence of manipulated variables $U_{opt}(k)$ from time step k to $k+N$-1. Then, often only the first element of this sequence, e.g. $u_{opt}(k)$, is applied to the system to provide feedback. At the next time step k+1, a new state estimate is performed and the optimization problem is solved again over the shifted horizon from k+1 to k+N. This policy is referred to as receding horizon control, which is illustrated in Figure 3.5.

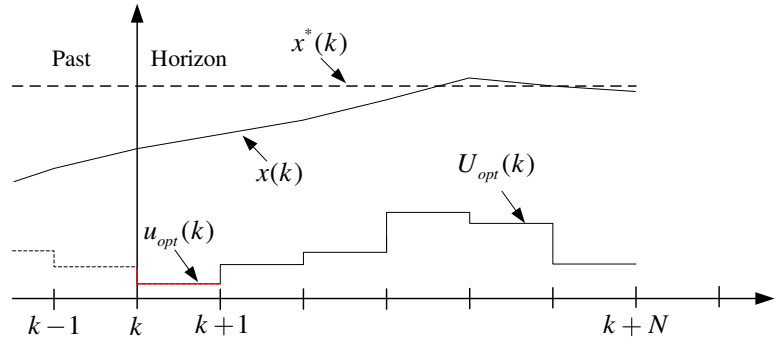

(a) prediction horizon at time step k

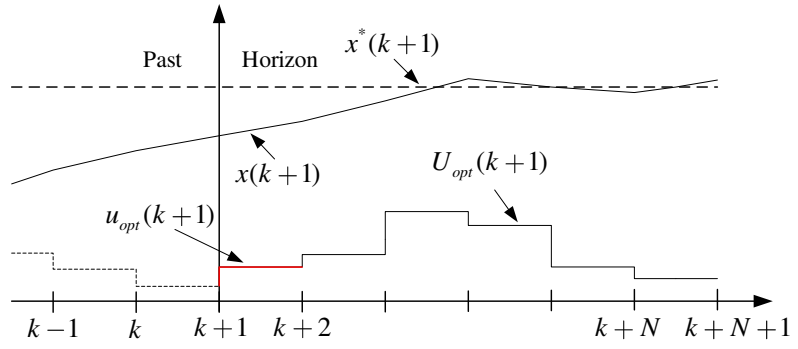

(b) prediction horizon at time step k+1

Figure 3.5: Receding horizon policy.

In summary, the main principle of MPC is to obtain the optimal manipulated variable at each time step by solving a constrained optimal control problem over a defined prediction horizon. MPC considers the

current state of the system, which needs to be estimated, as the initial state and utilizes the system dynamic model to predict the future system states and the controlled variables. The control objectives are included in an objective function, and the minimization of the objective function is subject to the evolution of the system model as well as the system constraints. An optimal sequence of manipulated variables can be obtained by solving the underlying optimization problem. Typically, MPC adopts a receding horizon policy in which only the first element of the optimal manipulated variable sequence is applied to the system and the manipulated variable sequence is recalculated at the next time step over a shifted horizon. Therefore, a constrained optimal control and the receding horizon policy with system feedback are combined in MPC, achieving a closed-loop control [23].

3.3 Model Predictive Torque Control of PMSM

The main idea of MPC is to obtain the optimal values for the manipulated variables based on the predictions of the future system behavior. The execution of MPC includes three main steps. Due to the existence of a one-step delay in a digital implementation, the first step is to estimate the variables in the next sampling period. A second step is the prediction of future system behaviors according to the estimated variables, and the final step is the output optimization based on a predefined control law.

For a motor drive system, MPC uses measured variables, e.g. stator currents, rotor speed, and the discrete-time machine model to estimate the variables that cannot be measured, e.g. stator flux. The machine model is then used to predict the future behaviors of the controlled variables due to each of the possible voltage vectors. Finally, the voltage vector that minimizes an objective function will be selected as the optimal control action. Thus, three stages can be identified with a standard MPC: estimation, prediction and objective function optimization. As both estimations and predictions depend on the machine model, it can be seen as the most important part of an MPC.

MPC strategies applied to PMSM drive can be classified as MPTC and Model Predictive Current Control (MPCC). The main difference between these two strategies is the control objective. For MPTC, the control objectives are the electromagnetic torque and stator flux amplitude, whereas the control objectives for MPCC are the stator

currents. Here, the conventional MPTC applied to PMSM drive is introduced.

3.3.1 Structure of Conventional MPTC

For a PMSM, the stator flux ψ_s and the electromagnetic torque T_e can be controlled by applying a proper voltage vector sequence such that the stator flux amplitude can be modified and the angle between the stator flux and rotor flux can be changed. This idea corresponds to the principle of DTC. The same principle is adopted by MPTC. The difference is that MPTC predicts the future stator flux and torque, and evaluates the predicted results through an objective function. The predictions of controlled variables are performed for each of the possible voltage vectors and the voltage vector that optimizes the reference tracking is selected. The block diagram of a conventional MPTC is shown in Figure 3.6.

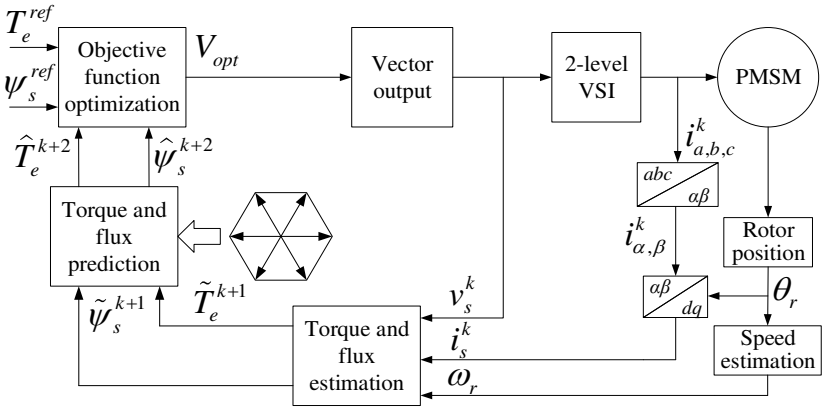

Figure 3.6: Diagram of conventional MPTC.

As mentioned above, three main steps can be identified with a conventional MPTC scheme. The first step is the estimation of the variables that cannot be measured based on the machine model, i.e. the torque and stator flux at the time step k+1, $\tilde{T}_e^{k+1}$ and $\tilde{\psi}_s^{k+1}$. It is noted that in this thesis " ~ " on the top of a variable represents an estimated value. Then, the future values of torque and stator flux at the time step k+2 are

predicted, i.e. $\hat{T}_e^{k+2}$ and $\hat{\psi}_s^{k+2}$. Here, " ˆ " on the top of a variable represents a predicted value. This step needs to be performed for each of the possible voltage vectors produced by the inverter. As a two level VSI is used in this study, eight switching states with seven different voltage vectors are generated. The final step is the optimization, in which the optimal switching state is determined according to the principle of an objective function minimization. In a standard MPTC, the control objective within the objective function is to reach the torque and stator flux references, T_e^{ref} and ψ_s^{ref}.

3.3.2 State Estimation

Since the controlled variables in a MPTC are the stator flux and the electromagnetic torque, their behaviors need to be estimated. In a discrete-time implementation, the optimal voltage vector computed is to be applied during the next control period. This means that the stator flux vector and torque at the end of the current control period, occurring at the start of next control period as well, have to be estimated based on the voltage vector as computed in the previous control period [60]. The stator flux estimation $\tilde{\psi}_s^{k+1}$ can be obtained by means of the stator voltage equation (2.5). Using the Euler formula to discretize (2.5) and shifting the result to a single time step [53], the stator flux vector at the start of the next control period (k+1) can be estimated as:

$$\tilde{\psi}_s^{k+1}=\psi_s^k+[v_s{}^k-R_s i_s{}^k+\omega_r A_e]T_s \tag{3.18}$$

where $\psi_s=[\psi_d,\psi_q]^T$, $i_s=[i_d,i_q]^T$, $v_s=[v_d,v_q]^T$ are the stator voltage, current and voltage vector values at the start of a control period, T_s is the duration of the control period, $A_e=[\psi_q,-\psi_d]^T$. According to the PMSM model, the electromagnetic torque can be estimated as:

$$\tilde{T}_e^{k+1}=\frac{3}{2}p[\psi_f\tilde{i}_q^{k+1}+(L_d-L_q)\tilde{i}_d^{k+1}\tilde{i}_q^{k+1}] \tag{3.19}$$

Here, the stator current at the start of the next control period (k+1) can be obtained according to the stator dynamics as:

$$\tilde{i}_s^{k+1}=B_e i_s^k+C_e v_s^k+D_e \tag{3.20}$$

where $B_e = \begin{bmatrix} 1-\frac{R_s T_s}{L_d} & \frac{L_q T_s \omega_r}{L_d} \\ -\frac{L_d T_s \omega_r}{L_q} & 1-\frac{R_s T_s}{L_q} \end{bmatrix}$, $C_e = \begin{bmatrix} \frac{T_s}{L_d} & 0 \\ 0 & \frac{T_s}{L_q} \end{bmatrix}$,

$D_e = [0, -\psi_f T_s \omega_r / L_q]^T$.

3.3.3 Behavior Prediction

As the motor states at the start of the control period (k+1) have been estimated, the stator flux, torque and stator current due to the admissible voltage vectors can be then predicted at the start of the control period (k+2):

$$\hat{\psi}_s^{k+2} = \tilde{\psi}_s^{k+1} + [v_s^{k+1} - R_s \tilde{i}_s^{k+1} + \omega_r A_e] T_s \tag{3.21}$$

$$\hat{T}_e^{k+2} = \frac{3}{2} p [\psi_f \hat{i}_q^{k+2} + (L_d - L_q) \hat{i}_d^{k+2} \hat{i}_q^{k+2}] \tag{3.22}$$

$$\hat{i}_s^{k+2} = B_e \tilde{i}_s^{k+1} + C_e v_s^{k+1} + D_e \tag{3.23}$$

3.3.4 Objective Function Optimization

The next step in MPC is the optimization of an appropriate control law that is defined as an objective function. For a MPTC, a typical structure can be given as:

$$g = \left| T_e^{ref} - \hat{T}_e^{k+2} \right| + k_\psi \left| |\psi_s^{ref}| - |\hat{\psi}_s^{k+2}| \right| \tag{3.24}$$

where T_e^{ref} is the reference torque, $|\psi_s^{ref}|$ is the reference flux amplitude, and k_ψ is a weighting factor that is used to adjust the importance of the torque versus flux control. As the tuning of the weighting factor often requires additional trial tests, its elimination is always desirable, and thus will be discussed later on in Chapter 4.

As the objective function (3.24) can be used to evaluate the predictions due to all the voltage vectors, an optimal voltage vector that minimizes the objective function will be selected and applied in the next control period.

To summarize, the flow chart of a conventional MPTC is shown in Figure 3.7. First, the torque and stator flux at the start of next control period k+1 are estimated based on the motor states at the current control period k and the voltage vector decided in the last control period. Next, the torque and stator flux at the start of the control period k+2 are predicted under all the possible voltage vectors. Finally, an objective function is used to evaluate all the predicted results and select an optimal voltage vector that minimize the objective function. This optimal vector is then applied in the next control period. It is noted that eight switching states are produced by a two level VSI, but only seven voltage vectors are considered with the MPC routing, as the effects of the two zero vectors are the same. However, a zero vector can be selected in a reasonable way to lower the switching frequency, which will be discussed in Chapter 4.

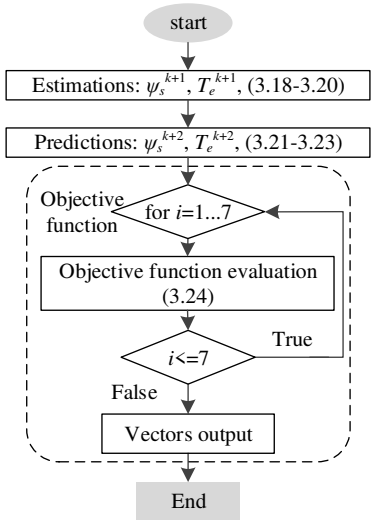

Figure 3.7: Flow chart of conventional MPTC.

In an MPC, a real-time optimization is achieved because the control strategy considers the real applied voltage value instead of the average voltage as with FOC. This is possible because the inverter model is considered in the control algorithm, avoiding the use of modulators [61].

As previously mentioned, the control variables for an MPCC are the stator currents, rather than torque and stator flux for an MPTC. Thus, the objective function of a conventional MPCC can be given as:

$$g = \left| i_d^{ref} - \hat{i}_d^{k+2} \right| + \left| i_q^{ref} - \hat{i}_q^{k+2} \right| \tag{3.25}$$

where i_d^{ref} and i_q^{ref} are the reference d-axis and q-axis current, respectively. The schematic diagram of MPCC is shown as Figure 3.8.

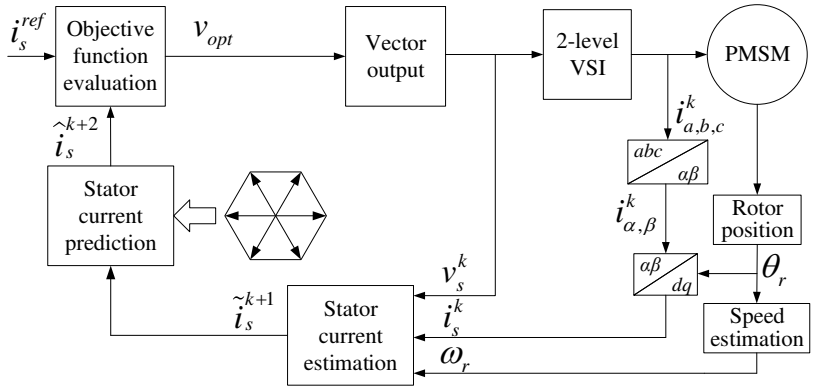

Figure 3.8: Diagram of conventional MPCC.

3.4 Research Questions Related to Model Predictive PMSM Control

A. Steady-state performance

FCS-MPC has intuitive concept, flexible control structure and can achieve fast dynamic performance. However, a main disadvantage of FCS-MPC is the unsatisfactory steady-state performance. This is because only one voltage vector is applied in an entire control period, resulting in high torque or current ripples. Thus, the improvement of steady-state performance is an important research question for model predictive PMSM control.

In addition, as mentioned before, there is a weighting factor in the objective function of the MPTC, as shown in (3.24). However, it is difficult to find a theoretical guideline to determine this weighting factor, which means tedious tuning works are required. Thus, an

effective way to eliminate the weighting factor is needed to be found to facilitate the design process of an MPC strategy.

B. Computational efficiency

FCS-MPC needs to evaluate the motor behaviors due to all the possible inputs, and thus resulting in relatively high computational burden. In particular, many optimization methods have been introduced to improve the steady-state performance of an FCS-MPC. In such cases, the computational burden could even remarkably increase. An increased computational effort and corresponding time delay could hamper the development of a higher dynamic drive performance in practical application. The problem is more severe, as recent development efforts on the power supply try to increase the switching frequency and hence lower the time available to perform calculations [62]. Hence, reducing the computational burden and reaching a balance between the computational efficiency and the control performance without affecting the control flexibility of an MPC need to be well considered.

C. Robustness against parameter uncertainties

As previously discussed, MPC directly uses the system model to predict the behavior of the system. It is desirable that the model used for the prediction is accurate enough. However, parameter mismatches and model uncertainties commonly exist in practice. In particular, motor parameters may vary during the operation of the motor. For PMSM system, resistance can be affected by temperature effects, PM flux is related to back-EMF, and inductance can also change due to a variable magnetic state of the machine (magnetic saturation) and frequency effects. The control performances can be deteriorated with such parameter uncertainties. The challenges of parameter mismatches and model uncertainties to MPC have gained increasing attention from the academic society. Therefore, the robustness against parameter uncertainties is also required to be investigated for MPC.

The questions above can be considered as the research focus for MPC, and thus will be studied in detail in the following chapters of this thesis.

3.5 Conclusions

In this chapter, the classifications of predictive control schemes are firstly given. MPC schemes applied to power electronics and drives mainly includes a CCS-MPC and a FCS-MPC. In particular, FCS-MPC as the most commonly used MPC scheme is the research focus of this thesis. Then, the basic principles of MPC, including the system model, constraints, objection function, optimization and receding horizon policy are elaborated. To show an exemplary MPC scheme applied to PMSM drive system, a standard MPTC is given, which mainly includes three steps: estimation, prediction and objective function optimization. Finally, three main research questions for MPC, also being the focus of this book are pointed out. These questions are the improvement of the steady-state performance, achieving a computationally efficient scheme with flexible control structure and the improvement of robustness against parameter uncertainties.

Chapter 4
Optimization of FCS-MPC for PMSM to Improve Steady-State Performance

4.1 Introduction

PMSM drives are widely employed thanks to their high efficiency and power density. Often, FOC and DTC are considered as they are proven control strategies nowadays for many synchronous as well as asynchronous drives. FOC can achieve good steady-state performance with high reliability. Nevertheless, the dynamic response is restricted by the bandwidth of the internal current control loop [63-65]. On the other hand, DTC has a direct and less complex control loop structure that can achieve faster dynamic response than FOC but with less certainty on the transient evolution. Furthermore, DTC suffers from an important torque ripple, being a hysteresis controller due to the finite amount of possible input voltage vectors [66]. By contrast, FOC relies on PWM or SVM strategies to reduce the average value during a control action of the voltage drop over the phase inductances compared to DTC.

More recently, MPC, which is able to model and counter future distortions, has received increased attention. The main advantage of MPC is that it is suitable for multivariable systems with fast dynamic response. Additionally, MPC allows the inclusion of physical constraints and nonlinearities in a straightforward way. The MPC schemes applied to electric drives can be classified as a CCS-MPC and a FCS-MPC.

For power converter and drive applications, FCS-MPC is the most widely investigated MPC scheme due to its intuitive structure without a modulation stage and the ability to handle constraints [67]. However, a main disadvantage of FCS-MPC is the steady-state performance [68, 69]. This has been pointed out in Figure 1.4 with the first block of Level 1. Just like DTC, the voltage supply is often done through power electronic switching converters, hence strongly limiting by hardware the amount of input variants. Moreover, only one voltage vector is applied over a single sampling period in conventional FCS-MPC. Therefore, the torque or current ripples are relatively high compared to the strategies involving a modulator.

In [70], the ratio between the sampling frequency and the switching frequency is seen as a metric, and the relationship between the ratio and the steady-state performance is investigated. It has been revealed that a high sampling-to-switching-frequency ratio is required to achieve a good steady-state performance. However, to obtain such a high ratio, control effort penalization is needed to lower the switching frequency, and an advanced microprocessor (e.g. field-programmable gate array) is required to enable a high sampling frequency.

The high torque or current ripple is largely caused by the lack of candidate inputs and the application of a single voltage vector over a fixed control period. Thus, to overcome the input limitation, some two-vectors-based MPC strategies have been proposed aiming at producing more possible inputs to reduce the steady-state ripple (see Figure 1.4, the first block of Level 3). Such strategies use two voltage vectors in a control period and define a duty ratio (or switching moment) to be determined to reduce ripple. This behavior brings the MPC strategy closer to SVM strategies but at a lower switching cost. A key of such two-vectors-based MPCs is the rule of the duty ratio optimization. Thus, the effects of different duty ratio optimization rules on improving the steady-state performance will be discussed for a MPTC in Section 4.2.

On the other hand, as the conventional two-vectors-MPTCs often aim to reduce the torque ripple at a certain point, e.g. the end of the control period, the reduction of the global torque ripple in a straightforward way can be further considered. Basically, two-vectors based schemes reduce the steady-state ripple by introducing more input possibilities, which also implies the increase in computational burden. Thus, the computational burden reduction is desired. In addition, a

weighting factor exists in the objective function of a conventional MPTC to keep a balance between the two controlled variables (torque and stator flux) with different dimensions. Due to the lack of theoretical tuning guidelines for the weighting factor, its elimination is always desirable. It is noted that these problems have been summarized in Figure 1.4 with the first block of Level 3. In this chapter, these problems will be countered by introducing adaptive solutions with a boundary-based MPTC strategy (see Figure 1.4, the first block of Level 4). Such a strategy will be discussed in Section 4.3, and the experimental verifications are given in Section 4.4.

4.2 Effects of Different Optimization Solutions on the Steady-State Performance

In a first step of the conventional two-vectors MPC strategy [71], an active vector is selected based on an objective function evaluation. Here, a fixed control period is considered, and the time duration of this first active voltage vector (illustrated in Figure 4.1 as T_1) is calculated according to some rules, e.g. nullifying the torque error at the end of a control period. Then, a zero vector is applied during the remaining control period. However, as the duty ratio calculation is done after the objective function evaluation, it means the rules of the duty ratio optimization are not considered in the objective function evaluation. Moreover, after inserting a zero vector, it could be non-optimal to apply a new active voltage vector.

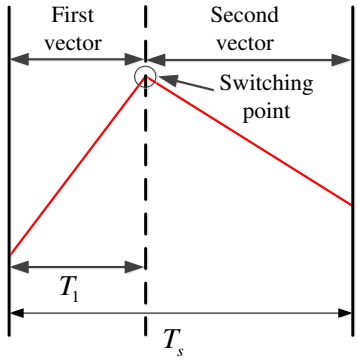

Figure 4.1: Illustration of the time duration.

To address this problem, it is suggested in [32] to consider both vector duration and vector selection in the objective function. Compared to the conventional MPC, much better steady-state performance, especially at low speed, can be obtained with the method from [32] even if the sampling frequency is reduced by half. However, the second voltage vector is fixed to a zero vector in prior methods [32, 36, 72]. This behavior poses some limitations on the performance improvement because the best second voltage vector is not necessarily a zero vector. In fact, the combination of an active vector and a zero vector is only a subspace of possible voltage vector combinations, which cannot achieve global minimization of objective function in true sense [73].

Therefore, a generalized two-vectors-based MPTC method is proposed in [33]. In this method, the restriction of the second vector is released from a zero vector to an arbitrary vector. It means that $7 \times 7=49$ voltage vector combinations can be selected, which provides more possibilities to reduce the torque ripple. However, a torque deadbeat solution is used in [33] when determining the duty ratio, which considers only the instantaneous minimum torque error at the end of the control period. It means the minimization of the mean error is not guaranteed during the whole control period. In addition, the flux error is not taken into account during the duty ratio optimization, which can affect the flux tracking performance.

To reduce the steady-state error in a more average sense, the Root Mean Square (RMS) duty ratio optimization is considered here and its effects on the steady-state performance are compared with the torque deadbeat solution used in [33].

4.2.1 Control Structure of a Two-Vectors MPTC

Here, a MPTC strategy that utilizes two voltage vectors in one control period is studied to improve the steady-state performance and to reduce the torque ripple and current harmonic. For a two-vectors MPC, some strategies use zero vector as the second vector, which achieve limited improvement in torque performance, since zero vector may not be the optimal one for the second vector. Alternatively, selecting a nonzero vector as the second vector could lead to high switching frequency and increased computational burden. To reach a balance among switching frequency, computational burden and steady-state performance, this

scheme uses an active vector as the first vector, and for the second vector, the two adjacent vectors of the first one and zero vector are considered as the candidates. Thus, $6\times3=18$ vectors combinations are provided. In this strategy, the duty ratio is calculated for every vector combination before the selection of the optimal one. This behavior guarantees the optimal vector combination with the corresponding duty ratio can be selected during the objective function evaluation.

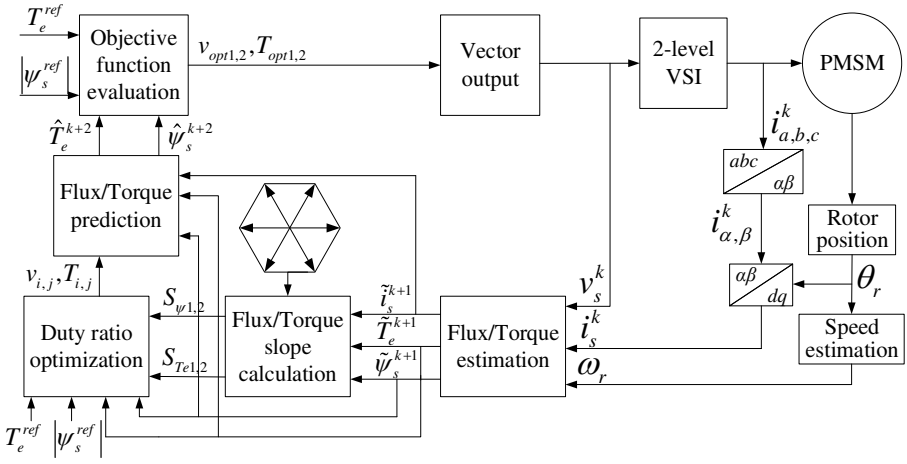

Figure 4.2: Diagram of a two-vectors MPTC.

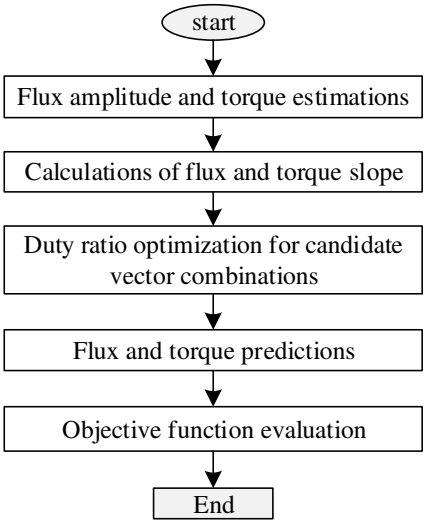

Figure 4.3: Flowchart of a two-vectors MPTC.

A diagram and a flow chart are given as Figure 4.2 and Figure 4.3 respectively to show the control structure of the two-vectors MPTC. First, the torque and flux at the next time step k+1 are estimated based on the measurements. Then, the slope of torque and flux is calculated under the application of each VSI vector that are used for the duty ratio optimization. It is noted that different duty ratio optimization solutions have different effects on the steady-state performance improvement. In this study, both deadbeat solution and RMS solution are discussed for comparison. With the well-constructed candidate inputs, the torque and flux at the time step k+2 can be predicted under all the candidates. Finally, the vector combination that minimizes the objective function will be selected as the optimal control action to be applied. All the steps will be discussed hereafter.

4.2.2 Torque and Flux Estimation

The PMSM equations have been given as (2.7)-(2.11). Then, based on the discrete PMSM model and the motor variables, the stator flux and the torque at the next sampling instant k+1 can be estimated. For this purpose, vector combination and corresponding durations determined in the previous control period are used. The estimations of flux and torque can be derived as:

$$\begin{cases} \tilde{\psi}_d^{k+1}=\psi_d^k+v_{d1}^k T_1+v_{d2}^k T_2-(R_s i_d^k-\omega_r \psi_q^k)T_s \\ \tilde{\psi}_q^{k+1}=\psi_q^k+v_{q1}^k T_1+v_{q2}^k T_2-(R_s i_q^k+\omega_r \psi_d^k)T_s \end{cases} \tag{4.1}$$

$$\tilde{T}_e^{k+1}=\frac{3}{2}p[\psi_f \tilde{i}_q^{k+1}+(L_d-L_q)\tilde{i}_d^{k+1}\tilde{i}_q^{k+1}] \tag{4.2}$$

$$\begin{cases} \tilde{i}_d^{k+1}=i_d^k+\frac{T_s}{L_d}(L_q\omega_r i_q^k-R_s i_d^k)+\frac{1}{L_d}(T_1 v_{d1}^k+T_2 v_{d2}^k) \\ \tilde{i}_q^{k+1}=i_q^k+\frac{T_s}{L_q}(-L_d\omega_r i_d^k-R_s i_q^k-\omega_r \psi_f)+\frac{1}{L_q}(T_1 v_{q1}^k+T_2 v_{q2}^k) \end{cases} \tag{4.3}$$

where T_s is the duration of the control period, v_{s1} and v_{s2} are the first and the second optimal stator voltage vector, which are determined in the last control period, T_1 and T_2 are their time durations respectively. $T_1 \le T_s$ and $T_2 = T_s - T_1$.

4.2.3 Calculation of Flux and Torque Slope

For a PMSM drive system, the voltage vector is the sole input and the flux and torque are considered the most important states for an MPTC. Therefore, it is of interest to deduce the flux and torque variations under the input voltage vector for the further duty ratio optimization. First, the derivative of the stator flux amplitude can be given as:

$$\begin{aligned}\frac{d|\psi_s|}{dt} &= \frac{d(\sqrt{\psi_d^2+\psi_q^2})}{dt} \\ &= \frac{1}{2}(\psi_d^2+\psi_q^2)^{-\frac{1}{2}}(2\psi_d\frac{d\psi_d}{dt}+2\psi_q\frac{d\psi_q}{dt})\end{aligned} \tag{4.4}$$

Then, substituting the PMSM equations (2.7-2.10) into (4.4), the derivative of stator flux amplitude under the voltage vector applied can be derived as:

$$\frac{d|\psi_s|}{dt} = \frac{\psi_s \bullet (v_s - Ri_s)}{|\psi_s|} \tag{4.5}$$

where $\psi_s = [\psi_{sd}, \psi_{sq}]^T$, $i_s = [i_d, i_q]^T$, $v_s = [v_d, v_q]^T$. Then, flux variation under the two voltage vectors can be then represented as:

$$\Delta|\psi_{s1}| = \frac{\psi_s \bullet (v_{s1} - Ri_s)}{|\psi_s|}T_1 \triangleq S_{\psi 1}T_1 \tag{4.6}$$

$$\Delta|\psi_{s2}| = \frac{\psi_s \bullet (v_{s2} - Ri_s)}{|\psi_s|}T_2 \triangleq S_{\psi 2}T_2 \tag{4.7}$$

respectively, where $S_{\psi 1} = \frac{\psi_s \bullet (v_{s1} - Ri_s)}{|\psi_s|}$, $S_{\psi 2} = \frac{\psi_s \bullet (v_{s2} - Ri_s)}{|\psi_s|}$, denote the flux slopes under the first and the second voltage vector, respectively.

According to the torque equation (2.11), the torque derivative can be given as:

$$\frac{dT_e}{dt} = \frac{3p}{2}(i_q\frac{d\psi_d}{dt} + \psi_d\frac{di_q}{dt} - i_d\frac{d\psi_q}{dt} - \psi_q\frac{di_d}{dt}) \tag{4.8}$$

Similarly, substituting the PMSM equations (2.7-2.10) into (4.8), the torque derivative and the torque variation under the two voltage vectors can be derived as:

$$\frac{dT_e}{dt} = \frac{3p}{2}[(v_q - R_s i_q - \omega_r \psi_d)(\frac{\psi_d}{L_q} - i_d) + (v_d - R_s i_d + \omega_r \psi_q)(i_q - \frac{\psi_q}{L_d})] \tag{4.9}$$

$$\Delta T_{e1} = \frac{3p}{2}[(v_{q1} - R_s i_q - \omega_r \psi_d)(\frac{\psi_d}{L_q} - i_d) + (v_{d1} - R_s i_d + \omega_r \psi_q)(i_q - \frac{\psi_q}{L_d})]T_1 \triangleq S_{Te1}T_1 \tag{4.10}$$

$$\Delta T_{e2} = \frac{3p}{2}[(v_{q2} - R_s i_q - \omega_r \psi_d)(\frac{\psi_d}{L_q} - i_d) + (v_{d2} - R_s i_d + \omega_r \psi_q)(i_q - \frac{\psi_q}{L_d})]T_2 \triangleq S_{Te2}T_2 \tag{4.11}$$

respectively, where

$$S_{Te1} = \frac{3p}{2}[(v_{q1} - R_s i_q - \omega_r \psi_d)(\frac{\psi_d}{L_q} - i_d) + (v_{d1} - R_s i_d + \omega_r \psi_q)(i_q - \frac{\psi_q}{L_d})]$$

$$S_{Te2} = \frac{3p}{2}[(v_{q2} - R_s i_q - \omega_r \psi_d)(\frac{\psi_d}{L_q} - i_d) + (v_{d2} - R_s i_d + \omega_r \psi_q)(i_q - \frac{\psi_q}{L_d})]$$

are the torque slopes under the first and the second voltage vector, respectively. As the control period T_s is much smaller than the electrical time constant, all the variables can be assumed constant within a control period. Therefore, both flux slope and torque slope can be regarded as fixed value within one control period.

4.2.4 Duty Ratio Optimization

For a two-vectors MPC, the duty ratio has to be optimized, resulting in the time duration T_1 to apply the first vector from the start of the next control period. Duty ratio optimization is an important issue for a two-vectors MPC, since different solutions can lead to different control performances. In [72] and [33], deadbeat torque control principle is used to nullify the torque tracking error at the end of the next control period. It means a reduction of the mean error is not aimed at in such strategy. On the other hand, a solution that aims to minimize the RMS error over the whole control period can be considered to achieve an improved tracking trajectory [11]. The principles of these two solutions used in a two-vectors scheme are illustrated in Figure 4.4. Moreover, the tracking of flux is not taken into account in [72] and [33], which can influence the flux control performance.

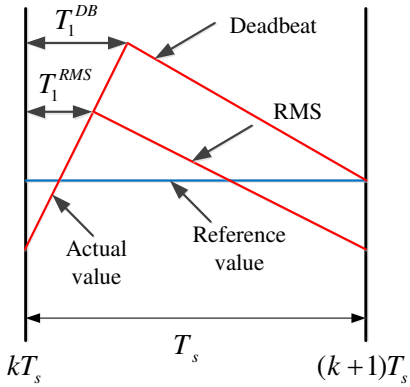

Figure 4.4: Principle of deadbeat and RMS solution.

A. Deadbeat Solution

For a torque deadbeat solution in [72] and [33], the control principle is to achieve the instantaneous minimum error of torque at the end of a control period. According to Figure 4.4, the torque error at the end of each control period can be given as:

$$E_{Te}^{DB} = \left| T_e^e + S_{Te1} T_1 + S_{Te2} (T_s - T_1) \right| \tag{4.12}$$

where $T_e^e = T_e - T_e^*$ is the initial torque error at the beginning of the control period. Then, to nullify the torque error at the end of the control

period ($E=0$), the time duration of the first vector T_1 can be obtained as:

$$T_1^{DB}=\frac{T_e^e+S_{Te2}T_s}{S_{Te2}-S_{Te1}} \tag{4.13}$$

B. RMS Solution

For a RMS solution, the reduction of error during the entire control period is aimed at. The RMS error of torque can be given as:

$$E_{Te}^{RMS}=\frac{1}{T_s}\int_0^{T_1}(T_e^e+S_{Te1}t)^2dt+\frac{1}{T_s}\int_{T_1}^{T_s}[T_e^e+S_{Te1}t+S_{Te2}(t-T_1)]^2dt \tag{4.14}$$

Here, to improve the flux tracking performance, the flux error is also considered. The RMS error of stator flux amplitude can be expressed as:

$$E_{\psi}^{RMS}=\frac{1}{T_s}\int_0^{T_1}(\psi_s^e+S_{\psi 1}t)^2dt+\frac{1}{T_s}\int_{T_1}^{T_s}[\psi_s^e+S_{\psi 1}t+S_{\psi 2}(t-T_1)]^2dt \tag{4.15}$$

where $\psi_s^e=|\psi_s|-|\psi_s^*|$ is the initial flux error at the beginning of the control period. Then, the RMS error of torque and stator flux amplitude can be obtained as:

$$E^{RMS}=E_{Te}^{RMS}+\lambda_{\psi}E_{\psi}^{RMS} \tag{4.16}$$

Here, due to the different dimensions of torque and flux amplitude, a weighting coefficient λ_{ψ} is used to combine these two variables. Therefore, letting $dE/dT_1=0$, the time duration of the first voltage vector is deduced as [11]:

$$T_1^{RMS}=\frac{-B+\sqrt{B^2-4AC}}{2A} \tag{4.17}$$

where

$$A=-\lambda_{\psi}S_{\psi}'(S_{\psi 1}+S_{\psi}')-S_{Te}'(S_{Te1}+S_{Te}')$$

$$B=2\lambda_{\psi}S_{\psi}'(T_sS_{\psi}'-\psi_s^e)+2S_{Te}'(T_sS_{Te}'-T_e^e)$$

$$C = T_s\lambda_\psi S_\psi{}'(T_s S_{\psi 2} + 2\psi_s^e) + T_s S_{Te}{}'(T_s S_{Te2} + 2T_e^e)$$

$S_\psi{}' = S_{\psi 1} - S_{\psi 2}$, $S_{Te}{}' = S_{Te1} - S_{Te2}$. In this study, as two vectors are applied in one control period, the corresponding time duration should be calculated for every vector combination before prediction. Different from the method [71], which determines the time duration after objective function evaluation, the method used in this study guarantees that both the vector and the time duration can be evaluated in the objective function.

4.2.5 Prediction and Objective Function Evaluation

Based on the torque and flux estimations and the constructed candidate vector combinations for the (k+1)th control period, flux and torque at the (k+2)th sampling instant due all the candidates can be predicted as:

$$\begin{cases} \hat{\psi}_d^{k+2} = \tilde{\psi}_d^{k+1} + v_{d1}^{k+1} T_1 + v_{d2}^{k+1} T_2 - (R_s \tilde{i}_d^{k+1} - \omega_r \tilde{\psi}_q^{k+1}) T_s \\ \hat{\psi}_q^{k+2} = \tilde{\psi}_q^{k+1} + v_{q1}^{k+1} T_1 + v_{q2}^{k+1} T_2 - (R_s \tilde{i}_q^{k+1} + \omega_r \tilde{\psi}_d^{k+1}) T_s \end{cases} \tag{4.18}$$

$$\hat{T}_e^{k+2} = \frac{3}{2} p[\psi_f \hat{i}_q^{k+2} + (L_d - L_q)\hat{i}_d^{k+2} \hat{i}_q^{k+2}] \tag{4.19}$$

$$\begin{cases} \hat{i}_d^{k+2} = \tilde{i}_d^{k+1} + \frac{T_s}{L_d}(L_q \omega_r \tilde{i}_q^{k+1} - R_s \tilde{i}_d^{k+1}) + \frac{1}{L_d}(T_1 v_{d1}^{k+1} + T_2 v_{d2}^{k+1}) \\ \hat{i}_q^{k+2} = \tilde{i}_q^{k+1} + \frac{T_s}{L_q}(-L_d \omega_r \tilde{i}_d^{k+1} - R_s \tilde{i}_q^{k+1} - \omega_r \psi_f) + \frac{1}{L_q}(T_1 v_{q1}^{k+1} + T_2 v_{q2}^{k+1}) \end{cases} \tag{4.20}$$

The vector combination, which can minimize an objective function will be selected as the optimal vector combination and applied in next control period. Here, the objective function is given as:

$$g = (T_e^{ref} - \hat{T}_e^{k+2})^2 + k_\psi(|\psi_s^{ref}| - |\hat{\psi}_s^{k+2}|)^2 \tag{4.21}$$

where k_ψ is the weighting factor of stator flux.

4.2.6 Comparative Results and Discussions

The conventional MPTC [74], the MPTC with torque deadbeat solution (referred to as DB-MPTC) [71] and the MPTC with RMS solution

(referred to as RMS-MPTC) are compared by simulation in the environment of Matlab/Simulink to show the effects of different duty ratio optimization solutions on the steady-state performance, i.e. the reduction of torque and flux ripple. The machine parameters used in this test are listed in Table 4.1.

Table 4.1: Machine parameters used in the simulation study of Section 4.2.6

Motor parameter	Symbol	Value
DC voltage	V_{dc}	200 V
Permanent magnet flux linkage	ψ_f	1 Wb
Stator resistance	R_s	1.91 Ω
d-axis inductance	L_d	16 mH
q-axis inductance	L_q	32 mH
Flux amplitude reference	$\lvert\psi_s^*\rvert$	1.0227 Wb

For the conventional MPTC, one active voltage vector is applied in a fixed control period and the sampling frequency is set at 10 kHz. The sampling frequency of the DB-MPTC and the RMS-MPTC is set to 5 kHz. It should be noticed that the sampling frequency of the conventional MPTC strategy is twice as high as other two MPTC strategies. It is reasonable to set this inequality, since one vector is applied in one control period for the conventional MPTC, whereas two vectors are applied in one control period for the other two MPTC strategies. The waveforms of torque, flux, and phase current for the three strategies are shown in Figure 4.5.

It can be seen in Figure 4.5(a) and Figure 4.5(b) that lower torque ripple and flux ripple are achieved with the DB-MPTC compared to the conventional MPTC. However, due to the torque deadbeat duty ratio solution, the torque under the DB-MPTC can only reach the reference value at the end of every control period. Furthermore, it can be seen in Figure 4.5(b) that the flux tracking performance with the DB-MPTC is not satisfactory enough, because it does not consider the flux ripple when determining the duty ratio. For the RMS-MPTC, an RMS solution considering both torque and flux is employed. The torque error can be minimized over the whole control period, which can be observed in Figure 4.5(c). In addition, the RMS-MPTC takes the flux error into account in the duty ratio optimization. Therefore, the RMS-MPTC achieves better flux performance compared to the DB-MPTC, as shown in Figure 4.5(c).

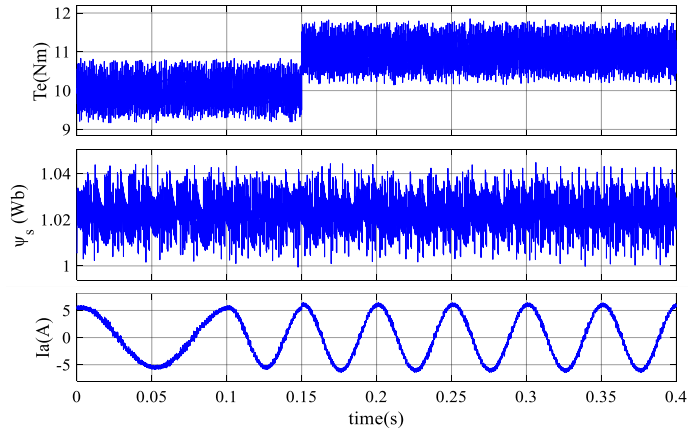

(a) conventional MPTC

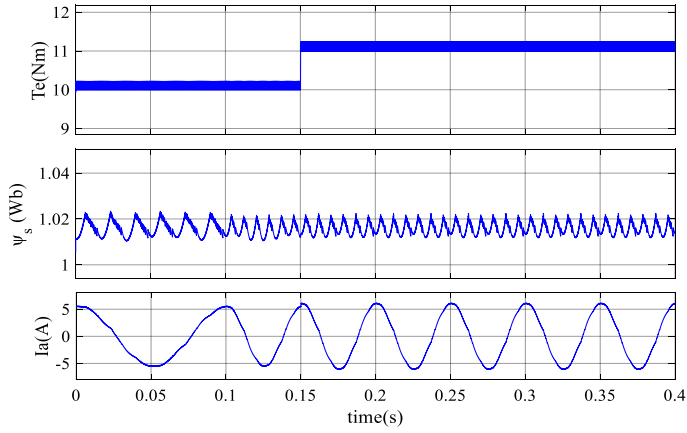

(b) DB-MPTC

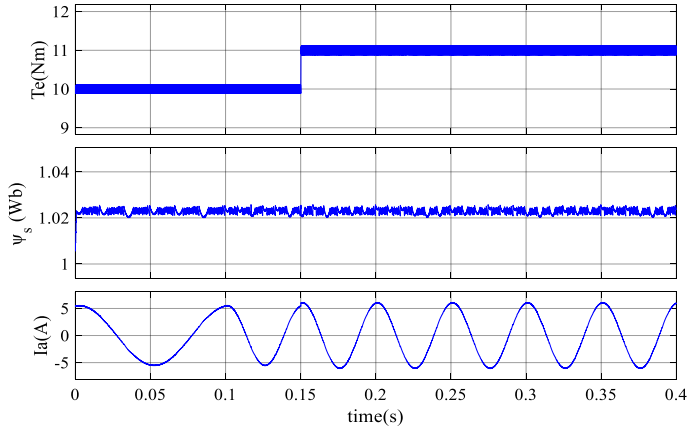

(c) RMS-MPTC

Figure 4.5: Waveforms of torque, stator flux and phase current.

Figure 4.6 shows the tracking trajectories of the DB-MPTC and the RMS-MPTC. It can be seen that the RMS-MPTC strategy performs better than the DB-MPTC in terms of torque and flux steady-state performance. The mean torque error is reduced and the tracking performance of stator flux is improved with the RMS-MPTC.

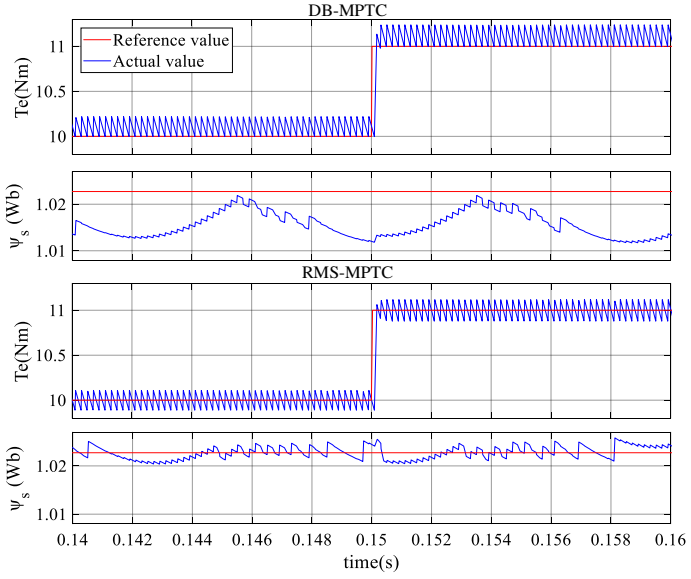

Figure 4.6: Tracking trajectory with the DB-MPTC and the RMS-MPTC.

The average torque and flux ripples under the three MPTC strategies are listed in Table 4.2, which are calculated based on (4.22). It can be seen that the lowest torque and flux ripple is achieved with the RMS-MPTC, which reveals the improved performance of the RMS solution on reducing the steady-state ripple.

$$\begin{cases} T_{rip} = \sqrt{\dfrac{1}{n}\sum_{i=1}^{n}(T_e(i) - T_e^{ref})^2} \\ \psi_{rip} = \sqrt{\dfrac{1}{n}\sum_{i=1}^{n}(\psi_s(i) - \psi_s^{ref})^2} \end{cases} \tag{4.22}$$

where n represents the sampling number. Figure 4.7 shows the switching states of the three strategies. It can be seen that different switching states are generated with the RMS-MPTC strategy to offer better steady-state performance. It should be noted that even though

there are similarities in the switching state selection under the DB-MPTC and the RMS-MPTC, they employ different duty ration optimization principles, and thus resulting in different control performance.

Table 4.2: Comparation of steady-state performance

Parameter	Conventional MPTC	DB-MPTC	RMS-MPTC
T_{rip}	0.3024Nm	0.1386Nm	0.0701Nm
ψ_{rip}	0.0067Wb	0.0074Wb	0.0011Wb

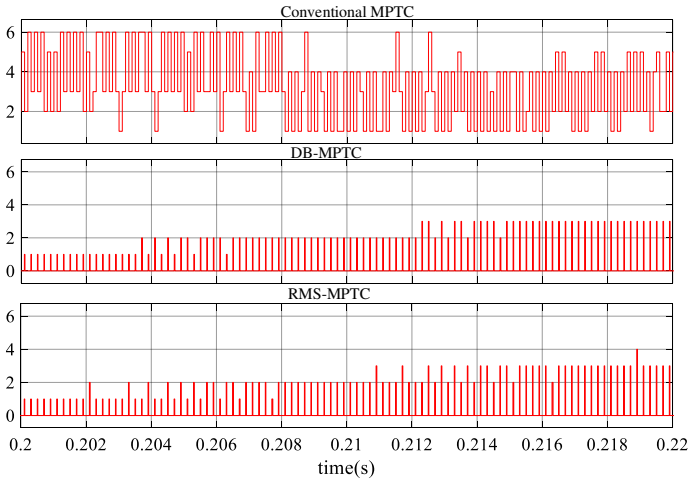

Figure 4.7: Switching states under the three MPTC strategies.

Generally, a two-vectors MPTC considering a duty ratio optimization can achieve improved steady-state performance compared to a conventional one-vector MPTC. Different duty ratio optimization principles give different tracking performances. In contrast to a torque deadbeat solution, an RMS solution considering both torque and flux error can achieve globally better torque performance by minimizing the mean torque error during the whole control period. In addition, as the flux error is also taken into account with the RMS solution, improved flux tracking performance can be obtained.

4.3 A Boundary-Based MPTC with Consideration of Optimization Problems

As presented above, a two-vectors MPTC can achieve better steady-state performance than a conventional MPTC. However, there are still some problems that need to be well considered. In a DB-MPTC, the switching instant of the two vectors is determined based on the deadbeat solution, which aims at forcing the torque to reach the reference value at the end of the control period. This behavior means the torque ripple at the switching point of the two applied vectors (as illustrated in Figure 4.1) has not been looked after. On the other hand, the RMS-MPTC considers the ripples during the whole control period. However, such a strategy involves a more complex formulation. Therefore, an improved strategy that can reduce the global torque ripple in a more straightforward way is desired.

In addition, a two-vectors MPTC reduces the torque ripple by introducing a larger set of candidate input vectors. As a result, the computational burden caused by the objective function evaluation and duty ratio optimization is increased. Thus, the reduction of the computational burden caused by the increased amount of candidate inputs should be aimed at. Furthermore, the weighting factor existing in the objective function requires additional design works, and thus its elimination is also desirable.

Actually, the problems mentioned above (algorithm complexity, computational burden and weighting factor elimination) also occur in some existing works. In [75], a symmetrical three-vector-based MPC is proposed for PMSM. In this strategy, the steady-state performance can be improved by applying a symmetrical three-vector switching sequence in a control period. However, two switching instants need to be determined for the three vectors, which introduces complexity to the control algorithm. In addition, applying a symmetrical three-vector switching sequence can lead to an increase in switching losses. To provide more possible inputs, an extended control set is introduced in [76] by creating a group of virtual vectors that are synthesized by basic VSI vectors. The steady-state performance can be then improved with the additional set of candidate vectors. However, more candidate solutions lead to an increased computational effort, which can hamper the high dynamic drive performance.

To lower the average torque ripple and flux ripple, an RMS based MPTC strategy is proposed in [77]. In this strategy, an RMS based solution is introduced to determine the time duration of the two voltage vectors to be applied. Even though the average ripples of torque and stator flux amplitude can be reduced, the algorithm leads to an increase in the computation burden due to a more complex formulation. Additionally, two weighting factors, one for the objective function and one for the time duration calculation, are required in such a strategy, which introduce complex and tedious tunings [78, 79].

A stator flux vector-based MPTC has been proposed to eliminate the weighting factor of the objective function [34, 37]. In such a strategy, the reference torque and reference stator flux amplitude are equally converted into a stator flux vector reference based on the relationship among torque, stator flux and the phase angle of flux vector. As a result, the control variables in the objective function are changed from torque and stator flux to an equivalent stator flux vector, thereby eliminating the weighting factor. In [80], a parallel MPTC approach is proposed, in which the torque and stator flux are optimized simultaneously with mutual influence. Then, the weighting factor in the conventional objective function can be omitted. In addition, this strategy tries to restrain the torque and flux within corresponding boundaries. However, just like conventional MPTC, a one-vector based approach has limited possible inputs to improve steady-state performance.

On the other hand, to lower the torque and flux ripple, an MPTC strategy with torque hysteresis is proposed in [81]. In such a strategy, after the torque reaches a preset boundary due to the supply of an active vector, a zero vector is employed as a second vector over the rest of the control period. However, the zero vector may not be the optimal choice for the second vector. For example, if the torque hits the lower boundary, the zero vector could make the torque even lower, exceeding the torque ripple band, and then worsening the torque performance.

A similar approach is introduced in model predictive current control in [82]. First, an error limit is set for the stator current amplitude. Then, a proper vector is first selected and applied until the stator current error hits the limit. After that, a zero vector is used for the remaining time of the control period. However, since the current error has already reached the limit border, it may exceed the limit under the zero vector during the rest of the control period, as in [81]. Generally, the torque ripple or current ripple cannot be guaranteed within the limit borders during the

whole control period under such a strategy. Moreover, as the limit border may vary according to the working conditions and the specifications of machine, the definition of the border could be a challenging task, which is not discussed in [81] and [82].

A current boundary-based MPTC, in which the torque ripple of a surface PMSM can be reduced by restricting the q-axis current ripple with the help of the defined boundaries, is proposed in [83]. However, as two voltage vectors are applied in a control period and a relatively large set of vector combinations are considered as candidates, reducing the computational cost is desirable. In addition, the weighting factor remains in the objective function and the design of the boundaries is not considered, as in [81, 82].

In this study, such a boundary based two-vectors MPTC is further developed and applied to an Interior PMSM (IPMSM) drive. This strategy aims to improve the torque and flux performance by restricting the torque ripple within certain boundaries and then minimizing the flux ripple during the whole control period. For this purpose, an optimal sequential list of two voltage vectors is considered as candidate input and the time durations of the two vectors to be applied are determined based on a predefined torque ripple tolerance band. Considering the torque outcomes both at the switching instant and at the end of the control period, the torque can be limited within the upper and lower boundaries of the preset tolerance band during the whole control period. Moreover, by monitoring the number of the defined valid vector sequences that can restrict the global torque ripple within the boundaries, the torque boundaries can be optimized online such that the manual boundary design work is avoided.

The proposed MPTC scheme considers 18 solutions (two-vectors combinations) from the start by using the six nonzero (active) vectors as the candidates for a first vector and selecting the second vector from the two neighbours of the first vector and the zero vector. However, according to the predicted torque outcomes of the candidate inputs, a group of vector sequences can be excluded from the control set before optimization, reducing the computation cost. Moreover, due to the preset torque ripple tolerance, the weighting factor in the objective function is eliminated, thereby avoiding the corresponding tuning work. Figure 4.8 shows the main steps of the proposed boundary based MPTC. All the steps will be discussed in the following. It is noted that a full flow chart will be given later on with more details.

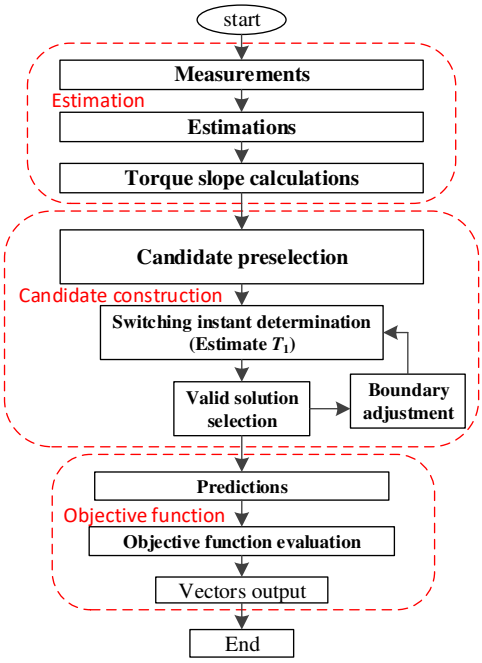

Figure 4.8: The main steps of the proposed boundary-based MPTC.

Compared to the previous boundary-based MPTC [81], an important improvement of the proposed strategy is that the torque ripple can be restricted within preset boundaries during the whole control period. This is achieved by forcing the torque to reach a boundary at the end of the control period and taking care of the torque at the switching instant. Additionally, the torque boundaries can be automatically adjusted to guarantee that the torque ripple can be restrained within a small enough range. Lower torque ripple is then achieved compared to the conventional MPTC and the existing boundary-based MPTC strategy [81].

Compared to [83], a reduced computational burden is achieved by preselecting the candidate vector combinations based on the torque slope. Furthermore, a self-adjustment mechanism is utilized to seek the optimal torque boundary settings. Here, the vector combination that can guarantee the torque to be within the boundaries over the whole control period is defined as a valid solution. Then, by monitoring the amount of the valid solutions, the torque boundaries can be adjusted accordingly, trying to restrict the torque ripple to as low as possible. An important benefit of this mechanism, compared to [81-83], is that only

an initial value of the ripple tolerance is required, avoiding the work of designing the torque boundaries. In addition, as the torque error under every candidate solution is forced to be equal to a preset ripple tolerance at the end of a control period, the weighting factor in the objective function can be omitted, hence avoiding the corresponding tuning work.

4.3.1 Structure of the Proposed Boundary Based MPTC

The diagram of the proposed boundary based MPTC strategy is shown in Figure 4.9. The first step is to estimate the states of torque and stator flux, followed by the calculation of torque slope. Secondly, with proper preselection, the switching instants of candidate vector sequences are determined based on the preset torque boundaries. Then, by counting the valid candidate solutions that make the torque within the boundaries during the whole control period, the number of candidates can be further reduced and the torque boundaries used in the next control period can be properly adjusted. Finally, based on the predictions, the optimal vector combination can be determined according to the objective function evaluations. All the steps will be described hereafter.

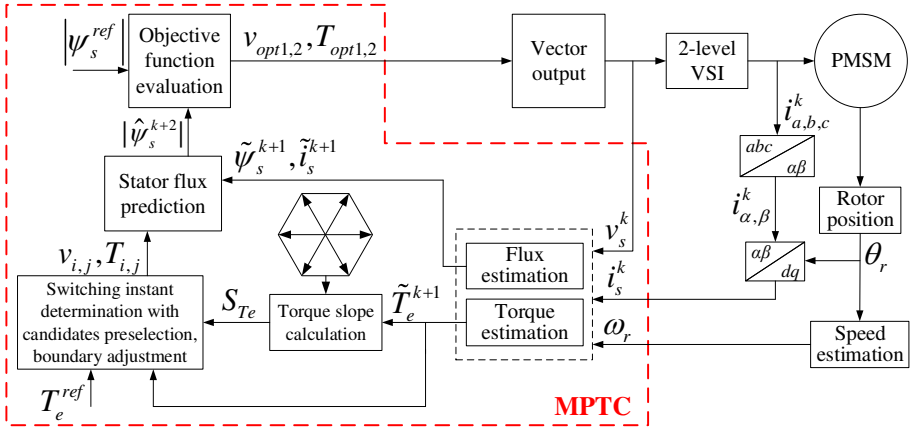

Figure 4.9: Diagram of the proposed MPTC strategy.

4.3.2 Construction of Candidate Inputs

It should be mentioned that the flux and torque estimations have been presented in Section 4.2.2. In addition, as discussed in Section 4.2.3,

the torque variation due to the applied voltage vector can be approximated as:

$$\begin{aligned}\Delta T_e = \frac{3p}{2}[(v_q - R_s i_q - \omega_r \psi_d)(\frac{\psi_d}{L_q} - i_d) \\ + (v_d - R_s i_d + \omega_r \psi_q)(i_q - \frac{\psi_q}{L_d})]T_s \triangleq S_{Te} T_s\end{aligned} \tag{4.23}$$

S_{Te} is the torque slope under the voltage vector v_s.

The construction of the candidate inputs includes the switching instant determination of two voltage vectors applied, candidate preselection and the valid solution selection with torque boundary adjustment, which will be discussed in the following.

It is noted that the candidate preselection should be performed before the switching instant determination in practice, as seen in Figure 4.8. Here, the preselection mechanism can be seen as a benefit of the proposed boundary-based switching-instant determination strategy, which will be explained later on. Thus, the switching instant determination will be discussed first, and both the strategy in the prior methods and the proposed strategy are presented.

4.3.2.1 Analysis of the Switching Instant Determination in Prior Methods

For two-vectors MPTC strategies, determining the switching instant is a key issue. To restrict the torque ripple, a ripple band is employed in [81] to calculate the switching instant. In such a strategy, an active voltage vector is applied first. When the torque hits the boundary of the ripple band, a zero vector will be activated. The goal of this approach is to limit the torque within the ripple band. However, it can be deduced from (4.23) that if a zero vector is applied, the slope of torque will become:

$$\begin{aligned}S_{Te|V_0} = \frac{3p}{2}[(-R_s i_q - \omega_r \psi_d)(\frac{\psi_d}{L_q} - i_d) \\ + (-R_s i_d + \omega_r \psi_q)(i_q - \frac{\psi_q}{L_d})]\end{aligned} \tag{4.24}$$

The sign of (4.24) is negative in motoring mode [11], which means the zero vector will decrease the torque. It is noted if the machine is in regenerative mode, the current will be negative, the slope of the torque under a zero vector (4.24) is therefore positive. This is because a zero vector makes the torque tend to zero. Here, the motoring mode is discussed.

Even though a zero vector has a weak effect on torque variation, it may still lead the torque to exceed the ripple band if the time duration is relatively long. This could happen in case the first active vector results in the torque hitting the upper boundary in a short time, as shown in Figure 4.10(a). Even worse, if the active voltage vector leads the torque to reach the lower boundary of the ripple band, the zero vector will further decrease the torque. Obviously, it can result in the torque exceeding the ripple boundary during the rest of the control period, hence causing torque ripple, as shown in Figure 4.10(b). This behaviour means the torque ripple cannot be limited within the boundaries during the whole control period under such a strategy. In addition, as the active vector is first decided and the zero vector combined with the active vector is not evaluated by the objective function, this solution may not be the globally optimal one.

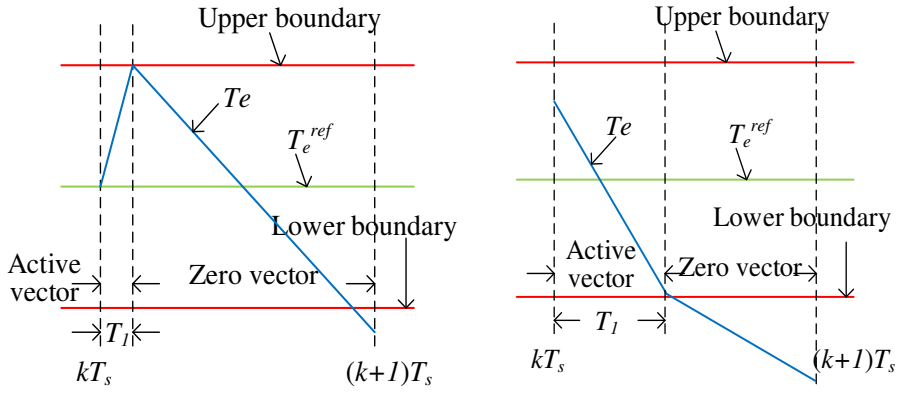

(a) Upper boundary hitting after T_1 (b) Lower boundary hitting after T_1

Figure 4.10: Illustrations of switching instant determination in [81]

Figure 4.11 reports the simulated results of torque under the MPTC of [81]. It can be seen that the torque exceeds the lower ripple boundary in some cases. As analyzed above, it is caused by the switching scheme,

since the zero vector can further decrease the torque after it reaches the lower boundary, which results in torque ripple.

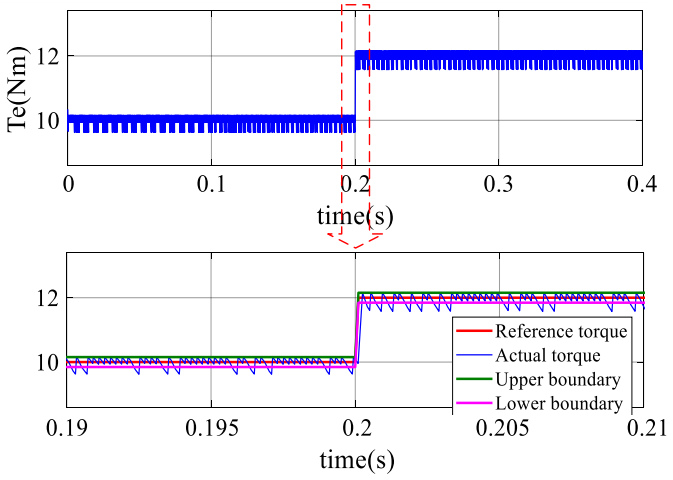

Figure 4.11: Simulated torque waveform under the MPTC from [81].

These problems also occur in the similar approach presented in [82], which is more focused on a similar concept for current error in model predictive current control rather than torque. Therefore, to guarantee that the torque can be restricted within the boundaries on a global time scale, an improved approach to determine the switching instant based on the torque boundary is introduced in the following.

4.3.2.2 Proposed Torque Boundary based Switching Instant Determination

In this study, to globally restrain the torque ripple within the set boundaries, a novel and simple approach to determine the switching instant of the two vectors is proposed. In the proposed approach, a torque ripple tolerance band is predefined before calculating the switching instant, as shown in Figure 4.12.

Unlike the strategy in [81, 82], which first select an active vector then apply a zero vector after torque reaching the corresponding preset border, the proposed strategy computes the switching instant for the well-selected candidate vector combinations first and then selects an

optimal one according to an objective function. This behavior can guarantee that the selection of the vector combination can achieve the best global control performance.

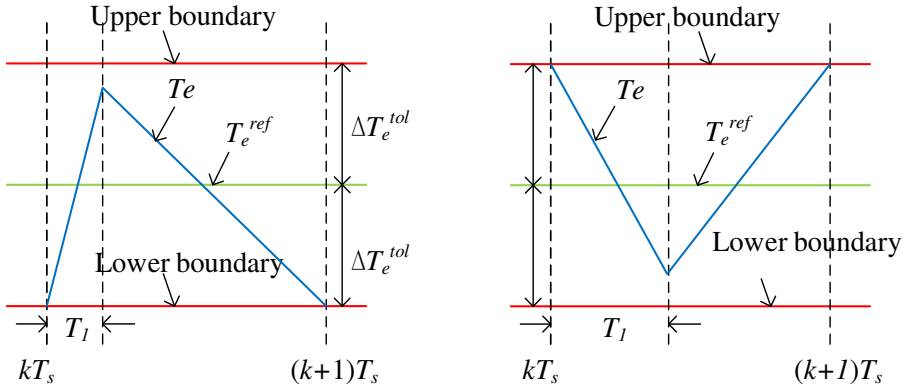

(a) Lower boundary hitting (b) Upper boundary hitting

Figure 4.12: Proposed boundary based switching instant determination.

It is noted that an assumption is made that the torque changes linearly during a control period. In the proposed method, the principle of calculating the switching instant is to force the torque to reach a boundary of the tolerance ripple band at the end of the control period. Based on this principle, the torque ripple can be limited within the tolerance band during the whole control period by also taking care of the torque at the switching instant. In addition, another significant advantage of this principle is that it makes it possible to conduct candidate preselection, which will be presented in the following.

For a given vector combination, the torque slopes under the two vectors can be obtained by (4.23). Thus, the solution to compute the switching instant can be expressed as:

$$\tilde{T}_e^{k+1}+S_{Te1}T_1+S_{Te2}(T_s-T_1)=T_e^{ref}\pm\Delta T_e^{tol} \tag{4.25}$$

where T_e^{ref} is the torque reference, $\tilde{T}_e^{k+1}$ is the estimated torque at the start of $(k+1)T_s$, S_{Te1} and S_{Te2} are the torque gradient under the first and the second candidate voltage vectors, respectively, T_1 and (T_s-T_1) are their respective time duration and ΔT_e^{tol} is a predefined ripple tolerance of

torque, which is shown in Figure 4.12. Thus, $T_e^{ref}+\Delta T_e^{tol}$ and $T_e^{ref}-\Delta T_e^{tol}$ are the upper and lower torque boundary, respectively.

Since the torque slopes are known before the switching instant determination, a target boundary can be decided according to the sign of the torque slope under the second vector S_{Te2}. If the second vector makes the torque descend, which means S_{Te2} is negative, the torque should reach the lower boundary $T_e^{ref}-\Delta T_e^{tol}$ at the end of the control period, as shown in Figure 4.12(a). Conversely, if S_{Te2} is positive, the torque will be forced to hit the upper boundary ($T_e^{ref}+\Delta T_e^{tol}$), as shown in Figure 4.12(b). Therefore, from (4.21), the time duration for the first vector T_1—and hence also for the switching moment—can be deduced as:

$$T_1=\begin{cases}\dfrac{\left(T_e^{ref}+\Delta T_e^{tol}-\tilde{T}_e^{k+1}-S_{Te2}T_s\right)}{(S_{Te1}-S_{Te2})}, & S_{Te2}>0\\ \dfrac{\left(T_e^{ref}-\Delta T_e^{tol}-\tilde{T}_e^{k+1}-S_{Te2}T_s\right)}{(S_{Te1}-S_{Te2})}, & S_{Te2}<0\end{cases} \tag{4.26}$$

The value of the time duration T_1 depends on the boundary settings, and for a feasible vector combination it should satisfy $0<T_1<T_s$, otherwise this vector combination should not be considered as a candidate.

4.3.2.3 Candidates Preselection

In the proposed MPTC strategy, two voltage vectors are applied in one control period to achieve better steady-state performance. The six nonzero (active) vectors are the candidates for a first vector. To reduce the computational burden and the amount of switching instants, the second vector is selected from the two neighbours of the first vector and the zero vector. Hence, 6×3=18 possible inputs are generated.

In the conventional strategy [34], all the vector combinations are required to be considered as candidates for the duty ratio optimization. However, thanks to the proposed boundary-based switching instant determination principle, here, nearly half of the possible inputs can be removed according to the torque slope of the previous control period.

For example, at steady state, if the second voltage vector applied in the kT_s decreases the torque, as shown in Figure 4.12(a), the first voltage vector in the $(k+1)T_s$ should increase the torque to guarantee that it remains within the ripple band. Accordingly, as shown in Figure 4.12(b),

when the second vector in the kT_s increases the torque, the first vector applied in the next control period should decrease the torque.

This behaviour means that the torque slope under the first voltage vector applied in the next control period should be opposite in sign to that under the second vector of the previous control period. It should be noted that such candidate preselection is a benefit of the proposed boundary-based switching instant determination. Since the torque reaches a boundary at the end of the last period, improper candidates (nearly half of the 18 possible inputs) can be removed by simply judging the sign of the torque slopes for which the torque can be limited within the boundaries during the next period. The amount of the remaining candidates is defined as M. Then, the switching instants needed to be calculated only for the M reduced solutions.

4.3.2.4 Torque Boundary On-Line Adjustment

The aim of the proposed torque-boundary based MPTC is to minimize the torque ripple within a tolerance band on a global time scale. Thus, the setting of the torque boundaries needs to be well considered. Different from the conventional boundary-based approaches that require offline boundary design [81-83], here, a boundary self-optimizing mechanism is employed to properly adjust the torque boundaries and to avoid the tuning of boundary. As a result, only an initial value is required for the torque tolerance and the optimal boundary setting can be online obtained. Such a mechanism includes two steps:

- First, the torque at the switching instant $(k+1)T_s+T_1$ should be estimated for all the M candidate solutions. It can be computed based on the switching instant T_1 and the torque slope under the first vector. Then, the vector combinations that can restrain the torque within the boundaries at the switching instant will be considered as valid solutions, which can be expressed by:

$$\begin{cases} \tilde{T}_e^{k+1}+S_{Te1}T_1-T_e^{ref} \le \left|\Delta T_e^{tol}\right| \\ 0<T_1<T_s \end{cases} \tag{4.27}$$

- The second step is to adjust the torque boundaries according to the number of the valid solutions, which is defined as N. Obviously, if N is close to M, it means the torque tolerance ΔT_e^{tol} is too large, which has limited effect on reducing the torque

ripple. Conversely, in case ΔT_e^{tol} is too small, there will be insufficient or even no valid solutions provided. Therefore, ΔT_e^{tol} can be optimized by intuitively controlling N within a proper range. In this study, based on an initial torque tolerance, when N >5, the ΔT_e^{tol} will be decreased by 2%. If N<3, ΔT_e^{tol} will be increased by 2% in the next control period [80].

By online implementing this principle, the torque boundaries can be optimally adjusted to restrict the torque ripple within a proper band. Then, 3-5 candidate solutions are left for the further stator flux evaluation, which will be introduced in the following section. It means torque has the priority to be firstly looked after, which is reasonable since torque is a more important variable than stator flux for an MPTC strategy. Figure 4.13 illustrates the torque waveform under the proposed boundary-based MPTC. It can be observed that the torque is limited within a fairly small tolerance band over the entire operation period.

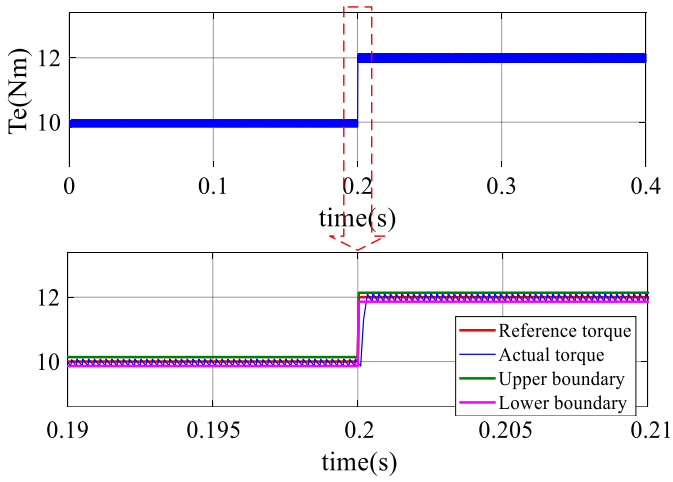

Figure 4.13: Simulated torque waveform under the proposed boundary-based MPTC.

4.3.3 Prediction and Objective Function Minimization

Based on the state estimations and the input constructions at the (k+1)th control period, flux and torque at the (k+2)th sampling instant under the candidate vector sequences can be predicted. The control action that minimizes the objective function, will be selected as the optimal one and

applied during the next control period. In conventional MPTC, the objective function contains two control objectives, which are the torque and the stator flux amplitude. Thus, a weighting factor is required to keep a balance between the two control objectives. The objective function can be expressed as:

$$g=\left|T_e^{ref}-\hat{T}_e^{k+2}\right|+k_\psi\left|\left|\psi_s^{ref}\right|-\left|\hat{\psi}_s^{k+2}\right|\right| \tag{4.28}$$

where $\left|\psi_s^{ref}\right|$ is the reference flux amplitude and k_ψ is the weighting factor of the stator flux amplitude.

Unfortunately, there is no effective and generic theoretical guideline to determine the weighting factor for the strategies published up to now. In practical applications, it is tedious and time-consuming to tune the weighting factor [84]. To eliminate the weighting factor, a stator flux vector-based MPTC [34, 37] has been developed based on the deadbeat MPTC [33]. In such a strategy, an equivalent reference stator flux vector is constructed from the reference torque and reference stator flux amplitude based on the deadbeat solution. Even though such a strategy can eliminate the weighting factor, it gives similar torque performance compared to the deadbeat MPTC with proper weighting factor [33], as the control variables are equally converted based on the intrinsic relationship between torque and stator flux. The torque is aimed to be equal to the reference only at the end of the control period. In contrast, as previously mentioned, the proposed MPTC seeks the optimal torque tolerance that can restrain the torque ripple within an adaptive range on a global time scale. Gaining lower torque ripple is then aimed at.

In the proposed MPTC strategy, the weighting factor in the objective function is omitted. This advantage is a result of the preset torque boundaries since all the valid candidate solutions can force the torque to reach a boundary at the start of $(k+2)T_s$. This behaviour means that the difference between the reference torque and the predicted torque under all candidate inputs can be given as $|T_e^{ref}-\hat{T}_e^{k+2}|=\Delta T_e^{tol}$, which is a fixed value in each period. Meanwhile, the valid solutions can guarantee the torque within the boundaries at the switching point of the two vectors. Therefore, evaluating the predicted torque is no longer required. Then, only the stator flux amplitude exists in the objective function, avoiding the use of the weighting factor.

In this study, two voltage vectors are applied in one control period. As opposed to [33, 34, 37], which evaluate the variables only at the end of the control period, here, an objective function that evaluates the stator flux at two instants is used to select a globally optimal solution:

$$\overline{g}=\left|\left|\psi_s^{ref}\right|-\left|\widehat{\psi}_s^{t1}\right|\right|+\left|\left|\psi_s^{ref}\right|-\left|\widehat{\psi}_s^{k+2}\right|\right| \tag{4.29}$$

where $\left|\widehat{\psi}_s^{t1}\right|$ and $\left|\widehat{\psi}_s^{k+2}\right|$ are the predicted stator flux amplitudes at the switching instant and the start of (k+2)th control period, respectively. They can be derived from (4.1) considering $\left|\psi_s\right|=\sqrt{\psi_d^2+\psi_q^2}$ and a one-step delay compensation:

$$\begin{cases}\widehat{\psi}_d^{t1}=\widetilde{\psi}_d^{k+1}+v_{d1}^{k+1}T_1-(R_s\widetilde{i}_d^{k+1}-\omega_r\widetilde{\psi}_q^{k+1})T_s\\ \widehat{\psi}_q^{t1}=\widetilde{\psi}_q^{k+1}+v_{q1}^{k+1}T_1-(R_s\widetilde{i}_q^{k+1}+\omega_r\widetilde{\psi}_d^{k+1})T_s\end{cases} \tag{4.30}$$

$$\begin{cases}\widehat{\psi}_d^{k+2}=\widetilde{\psi}_d^{k+1}+v_{d1}^{k+1}T_1+v_{d2}^{k+1}(T_s-T_1)-(R_s\widetilde{i}_d^{k+1}-\omega_r\widetilde{\psi}_q^{k+1})T_s\\ \widehat{\psi}_q^{k+2}=\widetilde{\psi}_q^{k+1}+v_{q1}^{k+1}T_1+v_{q2}^{k+1}(T_s-T_1)-(R_s\widetilde{i}_q^{k+1}+\omega_r\widetilde{\psi}_d^{k+1})T_s\end{cases} \tag{4.31}$$

$\widetilde{\psi}_s^{k+1}=[\widetilde{\psi}_d^{k+1},\ \widetilde{\psi}_q^{k+1}]^T$ and $\widetilde{i}_s^{k+1}=[\widetilde{i}_d^{k+1},\ \widetilde{i}_q^{k+1}]^T$ are the estimated stator flux and stator current at the start of $(k+1)T_s$ based on the voltage vectors applied in kT_s respectively. $v_{s1}^{k+1}=[v_{d1}^{k+1},\ v_{q1}^{k+1}]^T$ and $v_{s2}^{k+1}=[v_{d2}^{k+1},\ v_{q2}^{k+1}]^T$ are the first and second vector to be applied in $(k+1)T_s$ respectively.

Figure 4.14 shows the flow chart of the proposed MPTC to illustrate the three stages of the strategy. First, the states of torque and flux amplitude in the next control period are estimated based on the vector combinations decided in the previous control period, following the corresponding slope calculations. Second, after preselecting the candidates based on torque slopes, switching instants are optimized for the reduced M candidates according to the torque boundaries. Then, the defined valid solutions are selected for the objective function evaluation. At the same time, the torque boundaries to be used in the next control period can be adjusted according to the number of valid solutions. Finally, the stator flux amplitude will be predicted under the N candidates and an objective function evaluation will be conducted to finally select the optimal vector combination.

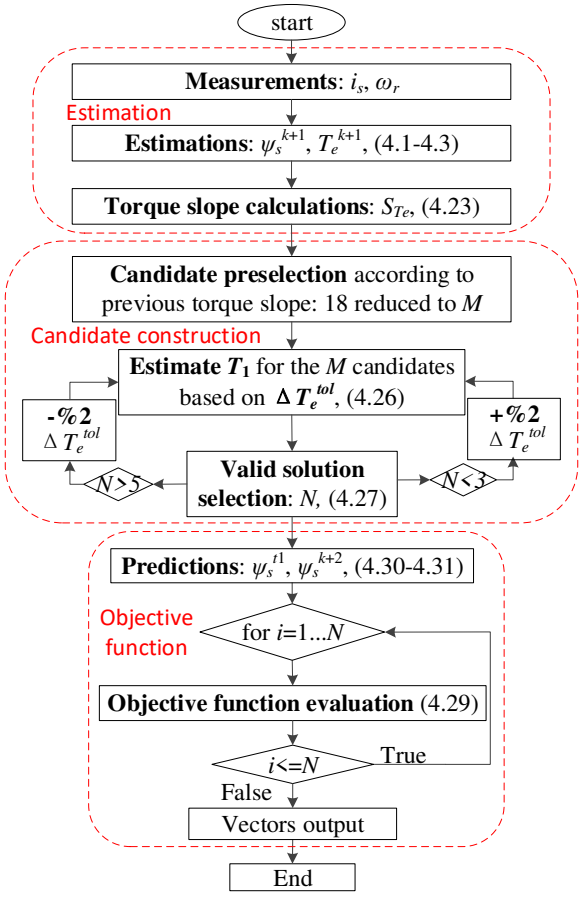

Figure 4.14: Flow chart of the proposed boundary based MPTC strategy.

4.4 Experimental Verifications

To demonstrate the effectiveness of the proposed MPTC strategy, comparative experiments are carried out on a real PMSM drive setup, which is shown in Figure 4.15. The schematic of the setup is illustrated as Figure 4.16. In this setup, a dSPACE MicroLabBox DS1202 is employed to implement the control algorithms. All the data of the tests are monitored and saved from Controldesk, a software of dSPACE, then transferred to Matlab/Simulink to be displayed and analysed. The parameters of the salient-pole PMSM are shown in Table 4.3. In addition, to show the improvements of the proposed MPTC, it is experimentally compared with the conventional MPTC [74] and two double-vector MPTCs, which are the boundary based MPTC from [81]

(referred to as MPTC-I), and the deadbeat MPTC from [33] (referred to as MPTC-II).

There are two vectors applying in a control period in the proposed MPTC. Therefore, to lower the switching frequency, the second vector to be applied is selected in a reasonable manner in case it is zero vector. For instance, if the two vectors are $\underline{V_2}$ (110) and zero vector, $\underline{V_7}$ (111) rather than $\underline{V_0}$ (000) will be selected as the second vector. As a result, only one switching action is aroused, reducing the switching losses.

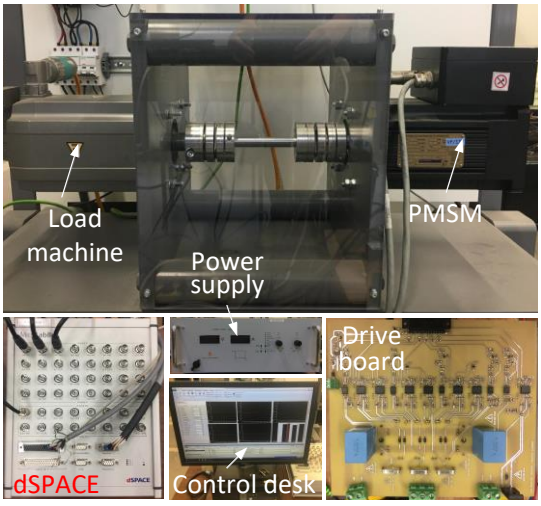

Figure 4.15: Experimental setup.

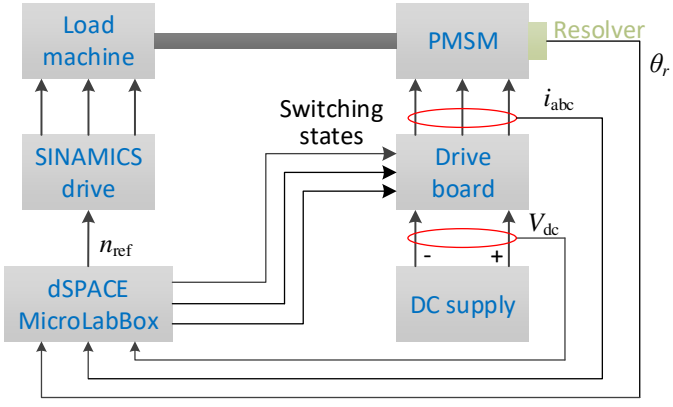

Figure 4.16: Schematic of the experimental setup.

Table 4.3: Parameters of salient-pole PMSM

Parameter	Symbol	Value
Rated power	P_N	3.7 kW
Rated speed	n_N	3000 r/min
Rated torque	T_N	12 Nm
Rated current	I_N	6.7 A
Number of pole pairs	p	3
Permanent magnet flux linkage	ψ_f	0.343 Wb
Stator resistance	R_s	0.95 Ω
d-axis inductance	L_d	7.5 mH
q-axis inductance	L_q	18 mH
Rotor moment of inertia	J	10.3 kg cm^2

In the following, experimental results will be given in several aspects. First, the effects of fixed torque boundary settings are discussed in Section 4.4.1 to show the influence of different boundary settings on the steady-state performance. Then, the proposed boundary self-adjustment mechanism is validated in Section 4.4.2 to reveal its effectiveness. The experimental results of steady-state performance are presented in Section 4.4.3 with comparisons to the conventional MPTCs abovementioned, while the results regarding dynamic performance are given in Section 4.4.4. In Section 4.4.5, a simulated torque reversal test is presented to show the performance of the proposed MPTC in regenerative mode. Next, the computational burden of different schemes is analysed in Section 4.4.6. Finally, the parameter sensitivity of the proposed MPTC is discussed in Section 4.4.7 to show the influence of parameter uncertainties on the control performance.

4.4.1 Effects of Fixed Torque Boundary Settings

In the proposed MPTC strategy, adaptive boundaries are set to restrict torque ripple. The goal of this approach is to limit the torque within a tolerance band globally. It means that different torque boundaries can lead to different control performances. Therefore, the effects of different torque boundary settings on the control performance are firstly investigated.

The proposed MPTC strategy with different torque boundaries is tested at 300 r/min and the experimental results are shown in Figure 4.17. The reference torque is set at 8 Nm. In Stage 1, the torque ripple tolerance is set to 0.5 Nm. It can be seen that the torque and flux ripple

are significant in this stage. Meanwhile, due to the large tolerance band, torque deviations can be observed. When the ripple tolerance is set to 0.3 Nm, the torque ripple and flux ripple are reduced, which is shown in Stage 2. In Stage 3, the torque and flux performance is further improved when the torque ripple tolerance is reduced to 0.1 Nm. It is therefore demonstrated that proper torque boundary setting can give good system performance.

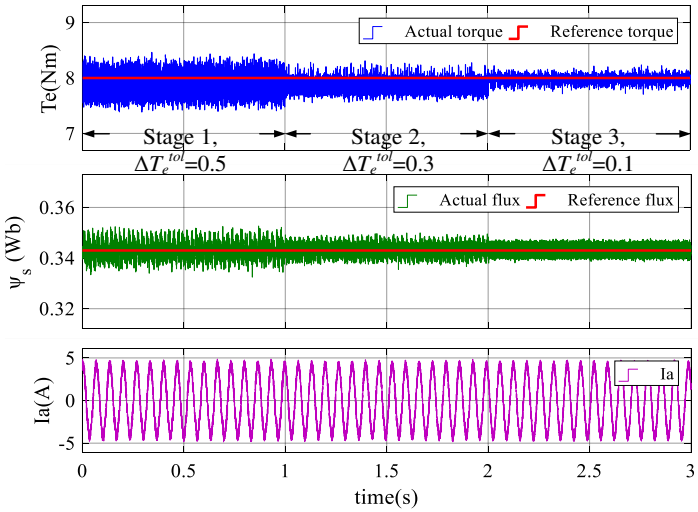

Figure 4.17: Experimental results of the proposed MPTC with different torque boundary settings.

Table 4.4: Torque ripple and flux ripple of proposed MPTC with different torque boundaries

	Stage 1	Stage 2	Stage 3
T_{rip}	0.2310Nm	0.1855Nm	0.0601Nm
ψ_{rip}	0.00274Wb	0.00234Wb	0.00191Wb

The torque and flux ripples of the three stages are shown in Table 4.4. It can be seen that much lower torque and flux ripples are achieved in Stage 3. The stator current harmonic spectrums are shown in Figure 4.18. It is observed in Stage 1 that some important spikes occur between 50 Hz and 120 Hz, and the Total Harmonic Distortion (THD) rate is 11.36%. Such spikes are lower in Stage 2 and are disappeared in Stage 3. It is also seen that all harmonics are less than 0.6% of the fundamental

component in Stage 3, where a lower THD rate (9.72%) is also achieved compared to the other two stages.

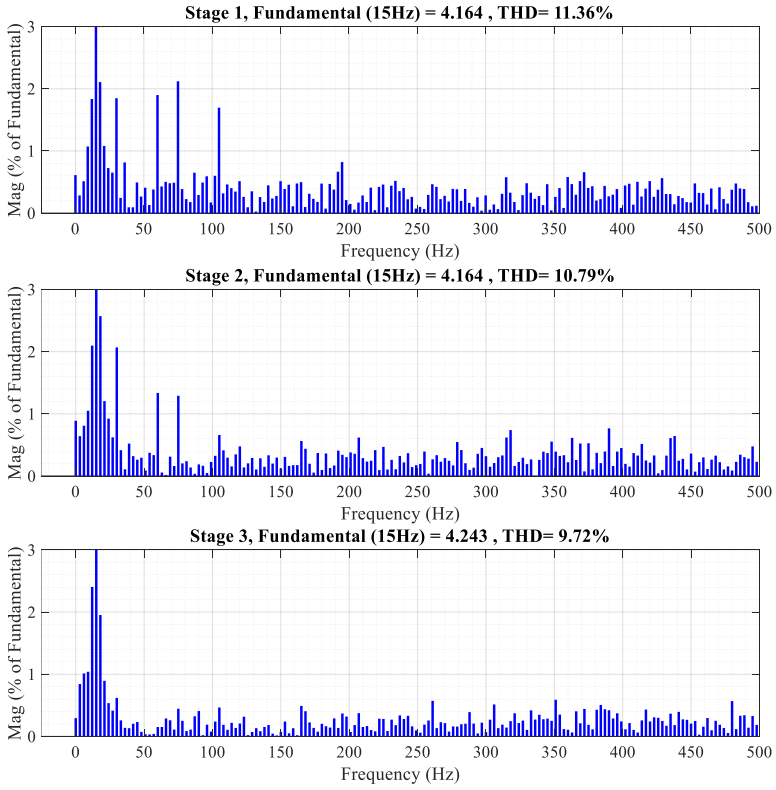

Figure 4.18: Harmonic spectrum of phase current under different torque boundary settings.

4.4.2 Validation of the Torque Boundary Self-Adjustment

It has been previously confirmed that proper torque boundary setting can improve the steady-state performance. However, the design of the torque boundaries requires additional efforts. In the proposed MPTC strategy, the boundaries of the torque ripple tolerance can be optimized online, as discussed in Section 4.3.2.4, which means only an initial value of the ripple tolerance is required.

A test to show the dynamic process of the self-adjustment is carried out with a motor operating at 300 r/min, the results are shown in Figure 4.19. The stator flux and torque are estimated based on the measured

currents and the PMSM equations. During 0–0.1 s, the initial torque ripple tolerance is set at 0.5 Nm. Then, the torque boundary setting is switched to the self-optimization mode at 0.1 s. It can be observed that the ripple tolerance is regulated to a proper range in a short time. As a result, the torque ripples and the flux ripples are effectively reduced, which reveals the validity of this mechanism.

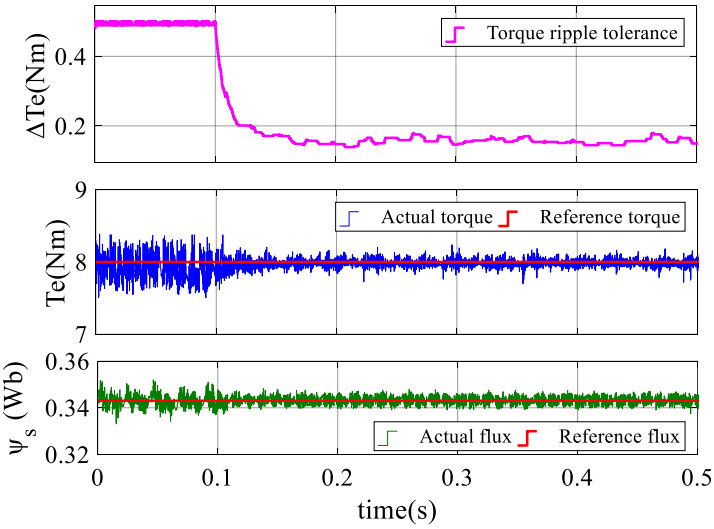

Figure 4.19: Validation of the Torque boundary self-adjustment.

4.4.3 Steady-State Performance

The steady-state performance of the conventional MPTC, MPTC-I and the proposed MPTC are compared at 500 r/min with the rated load (12 Nm). The sampling frequency of the conventional MPTC is set to 10 kHz. To fairly compare the three strategies, the sampling frequency of MPTC-I and the proposed strategy is adjusted to 6.67 kHz so that their average switching frequencies are similar to that of the conventional MPTC. Figure 4.20 shows the waveforms of torque, stator flux amplitude and stator current under the three strategies. It can be seen that the MPTC-I achieves lower torque and flux ripple compared to the conventional MPTC. The drawbacks of MPTC-I are discussed in Section 4.3.2.1. Even though the switching instant of the two voltage vectors is determined based on a torque boundary, the torque may still exceed the ripple band during the rest of the control period.

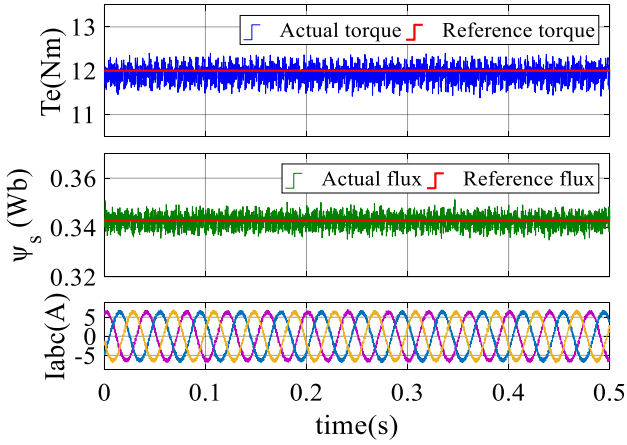

(a) Conventional MPTC

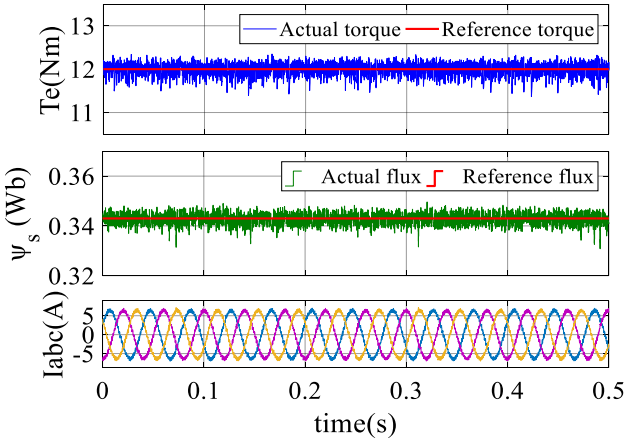

(b) MPTC-I

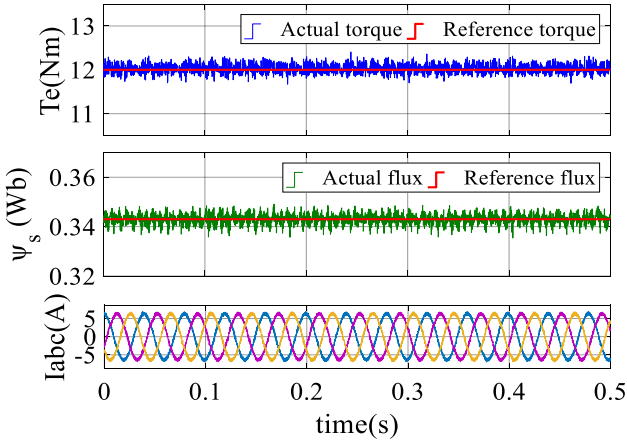

(c) Proposed boundary based MPTC

Figure 4.20: Experimental results of torque, stator flux amplitude and phase current at 500 r/min.

Unlike MPTC-I, the proposed MPTC can restrict the torque ripple within a tolerance band over the whole control period. Therefore, as seen in Figure 4.20, the torque ripple and the flux ripple are further reduced in the proposed MPTC strategy. In addition, compared to MPTC-I, another advantage of the proposed MPTC is that the torque boundaries can be self-adjusted without manual design.

The phase current harmonic spectrums under the three strategies are reported in Figure 4.21. It can be seen that the conventional MPTC and the MPTC-I achieve similar THD rate that are 7.97% and 7.85%, respectively. In contrast, the proposed MPTC strategy reduces the THD rate to 6.78%, which further confirms its improved steady-state performance.

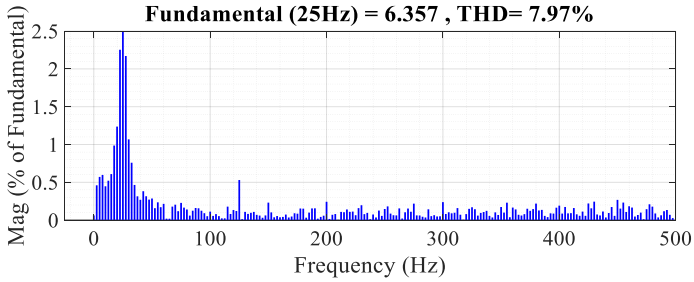

(a) Conventional MPTC

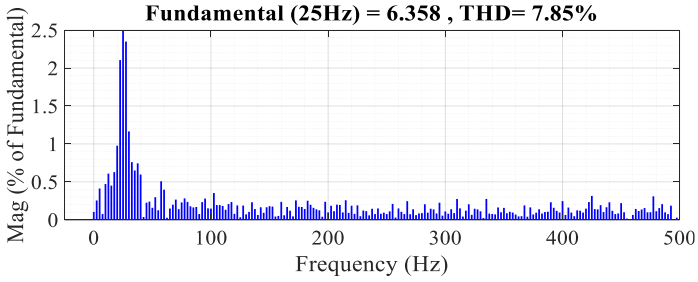

(b) MPTC-I

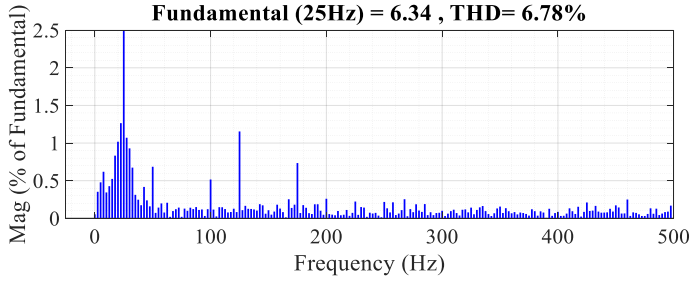

(c) Proposed boundary based MPTC

Figure 4.21: Harmonic spectrum of phase current.

The torque and flux ripple and the average switching frequencies under the three strategies are summarized in Table 4.5. The ripples include both the average errors that are calculated based on (4.18) and the percentages of their reference values. The average switching frequency f_{av} is obtained by counting the total switching actions N of the six VSI switches over a test period t_N and then calculating $f_{av}=N/6/t_N$. This analysis reveals the proposed MPTC strategy achieves much lower torque ripple and flux ripple than the conventional MPTC and MPTC-I at a similar switching frequency.

Table 4.5: Comparison of steady-state performance at 500 r/min

Method	T_{rip}		ψ_{rip}		f_{av}
	Nm	%	Wb	%	kHz
Conventional MPTC	0.1819	1.52	0.00241	0.71	5.52
MPTC-I	0.1561	1.30	0.00235	0.69	5.65
Proposed MPTC	0.1015	0.85	0.00194	0.56	5.68

In the following, the experiments will be shown at different rotational speeds and at different load conditions. Figure 4.22 shows the comparative results of the MPTC-II and the proposed MPTC when the machine runs at 1000 r/min with a 6 Nm load, and Figure 4.23 shows the results of these two strategies at 3000 r/min with a 12 Nm load. The sampling frequency of the two strategies is set at 6.67 kHz. To focus more on the control performance comparison for the MPTC-II and the proposed MPTC, the candidate vector combinations in the MPTC-II are defined the same as those in the proposed MPTC, which means 18 different candidates are provided.

The switching instant of the two vectors applied in the MPTC-II is calculated based on the deadbeat solution. However, the torque ripple at the switching instant is not considered. On the other hand, the torque ripple in the proposed MPTC is aimed to be limited within a minimal range on a global time scale with the help of the torque boundary online optimizing mechanism. As a result, the proposed MPTC strategy performs better in torque ripple, as can be seen in Figure 4.22 and Figure 4.23. Moreover, a lower flux ripple is also achieved in the proposed MPTC since the flux amplitudes both at the switching point and at the end of the period are considered in the objective function. Additionally, compared to the steady-state performance at 500 r/min, more current

harmonics are aroused as the rotational speed increases, as can be seen in the phase current waveform of Figure 4.23.

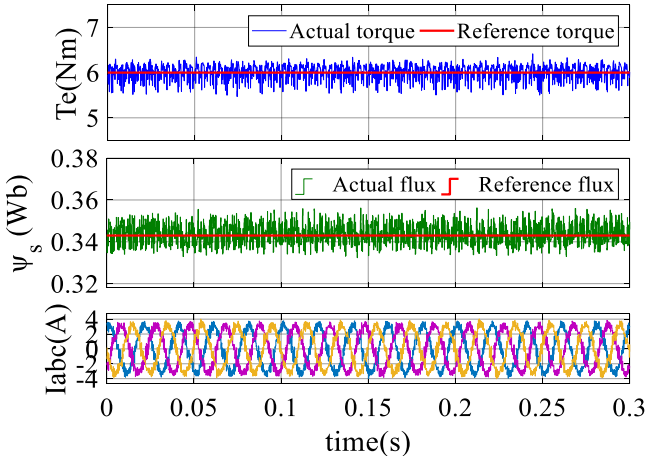

(a) MPTC-II

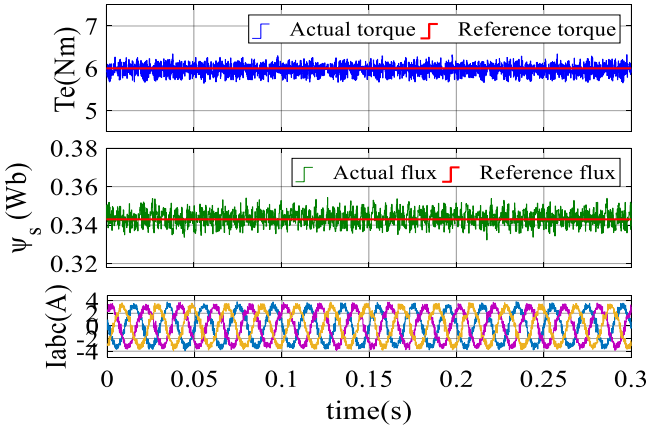

(b) Proposed boundary based MPTC

Figure 4.22: Experimental results of torque, stator flux amplitude and stator current at 1000 r/min.

To be concluded, the quantitative results are summarized in Table 4.6 and Table 4.7. The proposed MPTC strategy achieves lower torque ripple, flux ripple and THD rate compared to MPTC-II at a similar average switching frequency. In addition, due to the candidate preselection mechanism, the proposed MPTC can achieve lower computational burden in contrast to MPTC-II. The detailed comparative

results will be shown later. Moreover, as previously presented, the proposed MPTC successfully omits the weighting factor, which exists in the objective function of the MPTC-II, reducing the tuning efforts to be done.

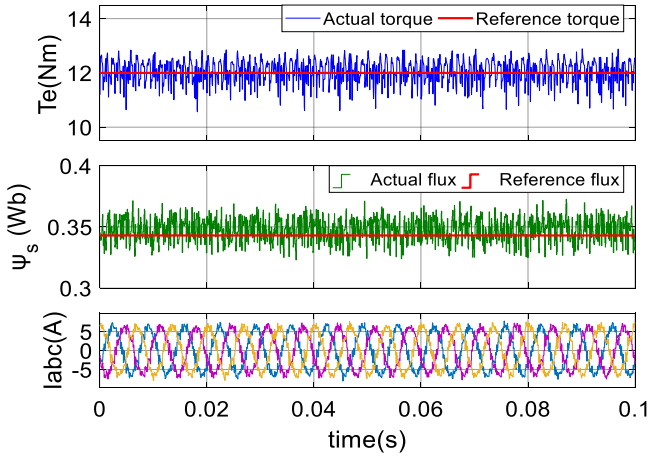

(a) MPTC-II

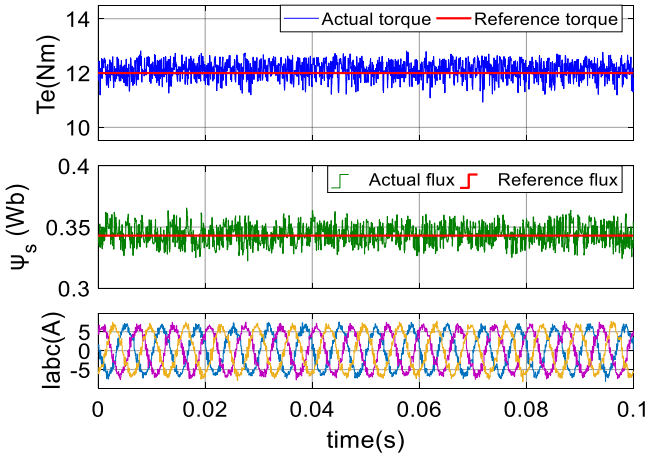

(b) Proposed MPTC

Figure 4.23: Experimental results of torque, stator flux amplitude and stator current at 3000 r/min.

Table 4.6: Comparison of steady-state performance at 1000 r/min

Method	T_{rip}		ψ_{rip}		f_{av}
	Nm	%	Wb	%	kHz
MPTC-II	0.1621	2.70	0.004696	1.37	5.56
Proposed MPTC	0.1376	2.29	0.003752	1.09	5.44

Table 4.7: Comparison of steady-state performance at 3000 r/min

Method	T_{rip}		ψ_{rip}		THD	f_{av}
	Nm	%	Wb	%	%	kHz
MPTC-II	0.4320	3.60	0.01049	3.06	18.35	5.62
Proposed MPTC	0.3492	2.91	0.00803	2.34	16.21	5.57

Generally, with comparison to the conventional MPTC, MPTC-I and MPTC-II, the improvements in the steady-state performance of the proposed MPTC have been revealed. For example, compared to MPTC-II, the proposed MPTC reduces the torque ripple from 0.4320 Nm to 0.3492 Nm at the rated speed. Such improvements are important for the applications of PMSMs, such as electromobility, where torque and efficiency in the limited use of battery power are crucial [85].

4.4.4 Dynamic Performance

In this section, the dynamic performance of the proposed MPTC is compared with that of the conventional MPTC. First, start-up tests are carried out for the conventional MPTC and the proposed MPTC.

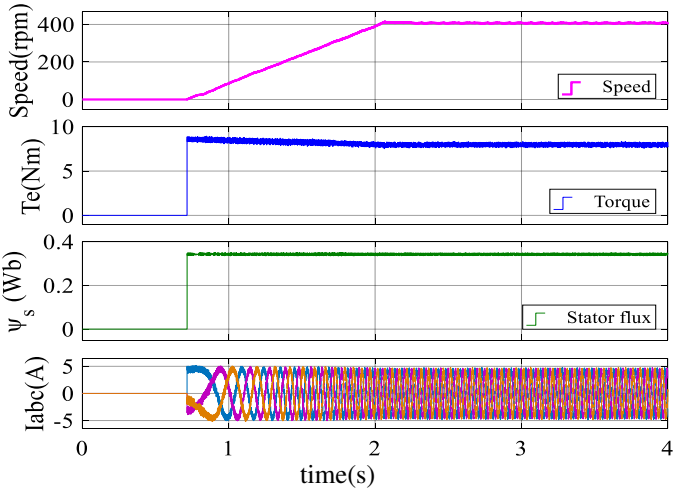

(a) Conventional MPTC

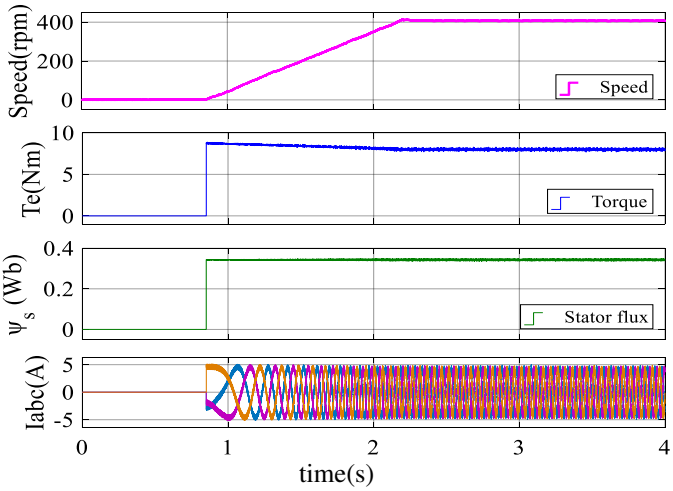

(b) Proposed MPTC

Figure 4.24: Experimental results of start-up test.

Figure 4.24 shows the responses during start-up under the two strategies, all the measured data are set as zero before starting the motor. It can be observed that the motor accelerates from 0 to 400 r/min without large overshoot or torque and flux fluctuation. Even though both strategies achieve fast torque and flux responses, the proposed strategy has much lower torque and flux ripple compared to the conventional MPTC strategy.

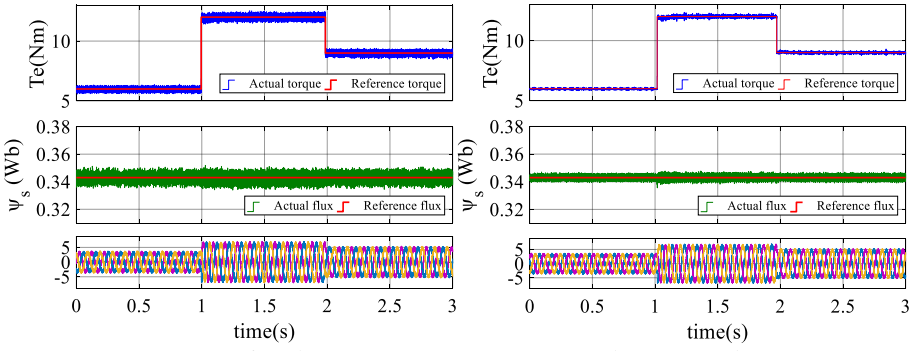

(a) Conventional MPTC (b) Proposed MPTC

Figure 4.25: Experimental results of dynamic performance comparison in the condition of load changing.

In addition, dynamic tests are carried out at 200 r/min for the two MPTC strategies when the load suddenly changes from 6 Nm to 12 Nm, then to 9 Nm, while the reference flux remains constant. The results are demonstrated in Figure 4.25. The actual torque of the two strategies changes in a short time without arousing large flux fluctuations, which means that the two strategies can achieve extremely fast dynamic response as well as good disturbance rejection performance. Meanwhile, the proposed MPTC strategy achieves much lower torque and flux ripples.

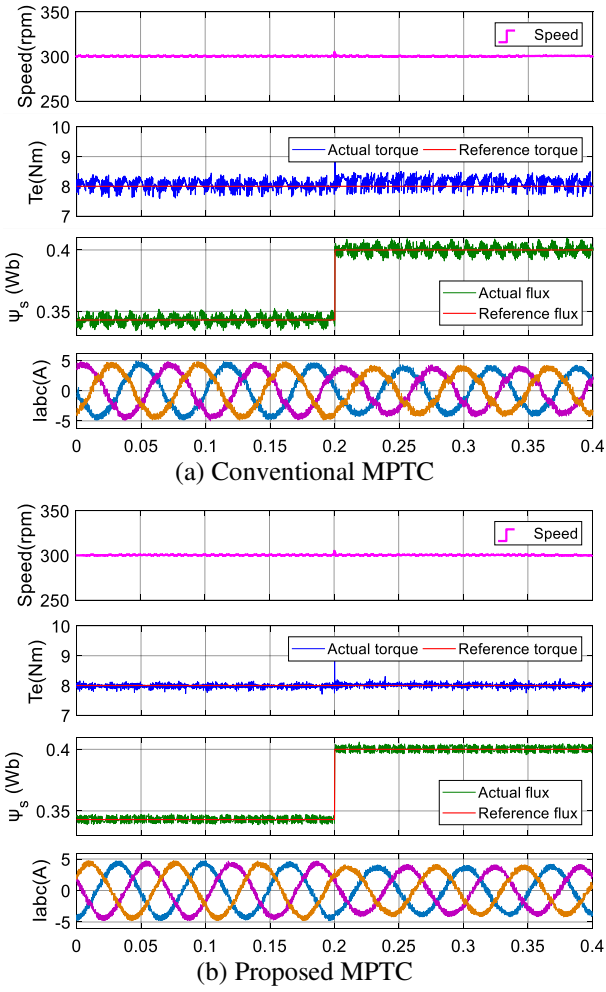

Figure 4.26: Experimental results of dynamic performance comparison in the condition of flux changing.

Furthermore, the flux step performance of the two strategies is investigated when the flux amplitude changes from 0.343 Wb to 0.4 Wb at 300 r/min with an 8 Nm load, the results are shown in Figure 4.26. It can be seen that a torque spike appears at the stepping instant in both strategies. The steady torque ripple of the conventional MPTC increases slightly as the flux amplitude increases. In contrast, with the help of the proposed boundary-based approach, in which the torque ripple can be restricted within the torque boundaries, the proposed MPTC achieves improved torque performance.

4.4.5 Simulation Results of Torque Reversal Operation from Regenerative Mode to Motoring Mode

To confirm the capability of the proposed MPTC strategy both in regenerative mode and motoring mode, a simulated torque reversal test is conducted. Here, the torque is demanded to reverse from the negative rated value in generation to the positive rated value in motoring (-12 Nm to 12 Nm) at the rated speed (3000 r/min). The results are shown in Figure 4.27. It can be seen the proposed MPTC performs well also in the regenerative mode. In addition, the torque is correctly reversed in a very short time without any overshoot or arousing ripples in the stator flux amplitude. The full capability of the proposed MPTC is therefore demonstrated.

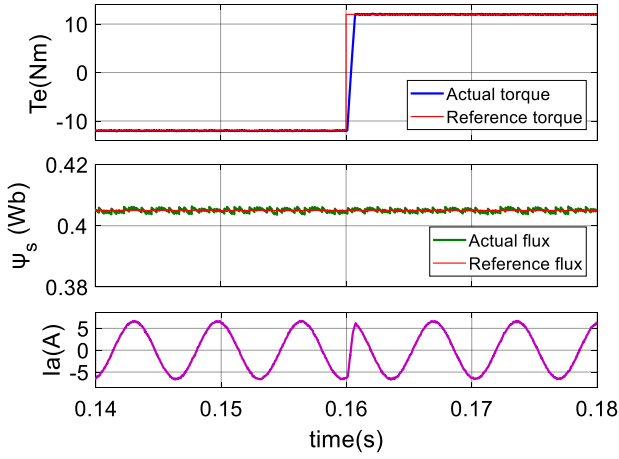

Figure 4.27: Simulated torque reversal test (3000 r/min) under the proposed MPTC from the negative rated value in generation to the positive rated value in motoring.

4.4.6 Computation Burden Analysis

The computational burdens of the four MPTC strategies are compared and the results are given in Table 4.8. A dSpace MicroLabBox with a dual-core 2-GHz real-time processor is used to implement the algorithms. Here, the execution time of an MPTC algorithm is obtained by setting a signal to 1 at the start of the algorithm and setting it to 0 at the end of the algorithm. In the conventional MPTC strategy, 6 active vectors are considered. The computational burden is relatively low, 20.4 μs is required to carry out the MPTC algorithm. In the MPTC-I, there are 6 possible inputs to be evaluated as well, even though a zero vector is inserted. As it is necessary to calculate the switching instant, the execution time is slightly increased to 21.8 μs. In the MPTC-II, 18 candidate vector combinations and their switching instants need to be considered, which costs 43.5 μs to conduct the algorithm. In the proposed MPTC strategy, there are also 18 possible vector combinations from the start. However, a number of them can be excluded before the stage of switching instant calculation due to the preselection mechanism. Hence, the algorithm execution time decreases to 29.7 μs, which means the computational burden is effectively reduced compared to the MPTC-II.

Table 4.8: Computation burden comparison

	Conventional MPTC	MPTC-I	MPTC-II	Proposed MPTC
Execution Time	20.4μs	21.8μs	43.5μs	29.7μs
Amount of candidates	6	6	18	≤9

4.4.7 Analysis of Parameter Sensitivity

Due to the parameter dependence of the model-based predictive control, the proposed MPTC is tested when motor parameter mismatches exist in the machine model [86]. The resistance, d-axis inductance and q-axis inductance are varied within ± 40% of their nominal values. With such a variation, the torque ripple and stator flux ripple are reported when the motor is operating at 100 r/min with 12 Nm load. The results of the resistance variation are shown in Figure 4.28(a). As the resistance variation increases, the flux ripple varies almost linearly. On the other

hand, underestimated resistance can lead to an up to 0.79% increase in torque ripple when the resistance is 60% of the nominal value, while resistance overestimation has a weaker effect on the torque ripple.

Figure 4.28(b–c) shows the results when d-axis and q-axis inductance vary within 40% of their nominal values, respectively. The variation tendencies of torque ripple are similar in the two cases but the influence of q-axis variation on the torque ripple is much larger. The flux ripple presents opposite variation trends for d-axis inductance deviation and q-axis inductance deviation. Meanwhile, it can be seen from Figure 4.28(c) that the flux ripple shows a relatively large variation from 0.74% to 0.59% as the q-axis inductance increases. Generally, the variations of d-axis and q-axis inductance have a greater effect on the torque ripple and stator flux ripple than the resistance variation.

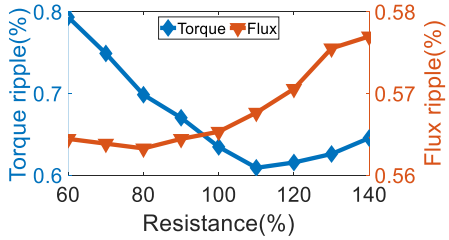

(a) Resistance variation

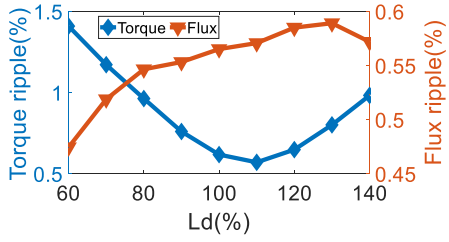

(b) d-axis inductance variation

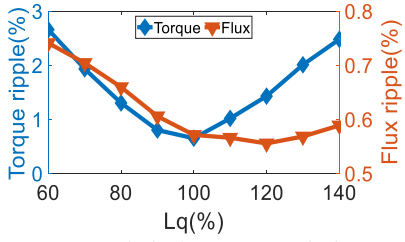

(c) q-axis inductance variation

Figure 4.28: Analysis of parameter sensitivity for the proposed strategy.

4.5 Conclusions

In this chapter, the optimization of MPTC is discussed aiming at improving the steady-state performance of a PMSM drive system. Two-vectors MPCs are studied and the effects of classical duty ratio optimization rules are analysed. The results show that the MPTC with considering the RMS error of torque and flux in the duty ratio optimization achieves improved torque and flux performance compared to the MPTC with a torque deadbeat solution.

Then, adaptive solutions with a novel boundary-based MPTC are introduced taking into account the optimization problems of the conventional methods, i.e. global steady-state ripple, computational burden and weighting factor elimination. This goal is pointed out in Figure 1.4 with the first block of Level 5. Here, Figure 4.29 is used to conclude the main ideas and the benefits of the proposed boundary based MPTC.

In this two-vectors MPTC strategy, a torque ripple tolerance is used to determine the switching instant of the two voltage vectors. Compared to conventional boundary based MPTC, the proposed MPTC can restrict the torque within the adaptive boundaries in a global manner. In addition, a torque boundary self-optimized mechanism is employed to online adjust the boundaries aiming at limiting the torque ripple within a proper range. Experimental results reveal that the proposed torque boundary based MPTC achieves better steady-state performance than the standard MPTC, the conventional boundary-based MPTC, and the deadbeat MPTC. Compared to the standard MPTC and the conventional boundary based MPTC, the proposed MPTC reduces the torque ripple from 1.52% and 1.30% to 0.85% at 500 r/min. The experimental results conducted at 3000 r/min indicate that the proposed MPTC reduces the torque ripple from 3.6% to 2.91% compared to the deadbeat MPTC.

Due to the presented torque boundary self-adjustment mechanism, the tuning of the boundaries is avoided, which is required for the conventional boundary based MPTC. Here, valid solutions that can restrict the torque ripple within the boundaries during the whole control period are counted, and the boundaries will be adjusted automatically if the number of the valid solutions exceeds a certain range. The dynamic performance of the proposed MPTC is demonstrated by experiments, and its performance in regenerative mode is confirmed by simulations.

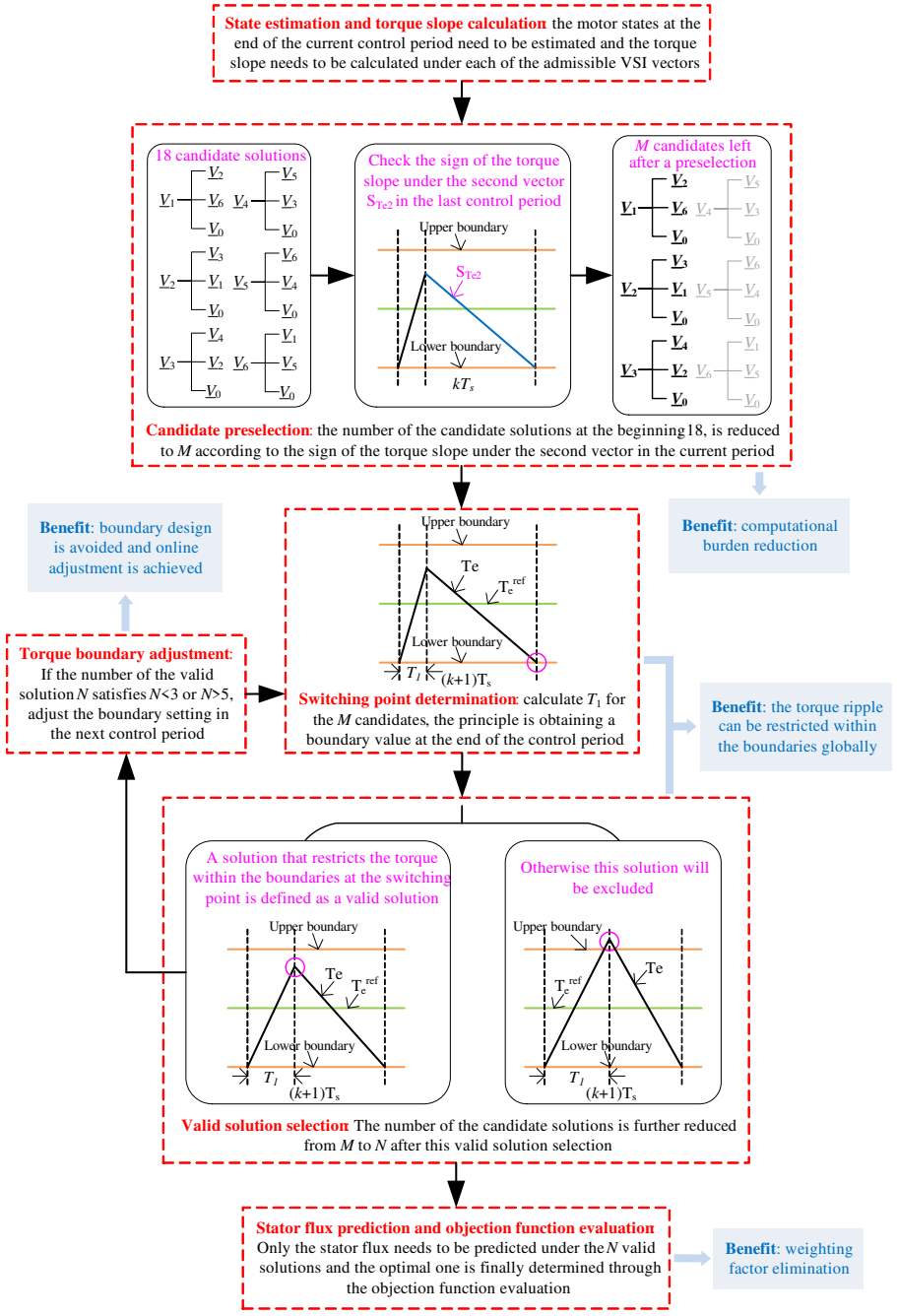

Figure 4.29: Illustration of the main ideas and the benefits of the proposed boundary based MPTC.

In addition, with a proper preselection, a group of the initial candidate solutions are excluded, which effectively decreases the computational efforts compared to the deadbeat MPTC. This is revealed by the results of the computational time. The weighting factor of objective function is omitted in the proposed MPTC, hence avoiding the tedious tuning work. This is achieved by considering the torque and flux in a sequential manner. Finally, the parameter sensitivity of the proposed MPTC is studied. The results show that inductance mismatches have relatively large influence on the steady-state performance of the proposed MPTC, which reveals the parameter dependence problem of a model based predictive control scheme.

Chapter 5
Simplification and Control Flexibility of FCS-MPC

5.1 Introduction

MPC presents several advantages. For instance, it can be used in a variety of processes, simple to apply in multivariable systems, and presents a fast dynamic response. Furthermore, it supports the incorporation of system constraints and nonlinearities into the control law in a straightforward way. In addition, nested control loops can be integrated in only one loop with MPC [87, 88]. On the other hand, a well-known disadvantage of MPC is that it performs with a larger computational burden compared to the conventional control schemes. The computational cost of MPC depends on the algorithm used to solve the optimization problem. The algorithm is related to the MPC method applied to control the system [29].

For power electronics and drive systems, CCS-MPC, and FCS-MPC are the main MPC strategies. The classifications have been illustrated in Figure 3.2. As a type of CCS-MPC, EMPC solves an optimization problem for all possible states by offline calculations and stores the solution in a LUT. As a result, the online computations are reduced to a search algorithm that can be done simply based on a binary search tree technique [89, 90]. A main disadvantage of EMPC is that it requires a lot of memory to store the required information, therefore limiting its application range. As the size of the stored LUTs is dependent on the amount of the optimization variables and the prediction horizon, EMPC

is appropriate only for small-scale problems [29]. GPC is another type of CCS-MPC scheme that often applied to power electronics and drive systems. In contrast to EMPC, an analytical solution to the optimization problem is considered with GPC. As the analytical solution can be precalculated, the online calculation amount is reduced [91, 92].

FCS-MPC is a more widely used MPC scheme for power electronics and drives. In an FCS-MPC, the optimization problem needs to be solved for each of the possible solutions in the control set. For large numbers of control possibilities, this behavior means a high computational burden is required, lowering the computational efficiency. This is the second disadvantage shown in Figure 1.4 with the second block of Level 1. This disadvantage can affect the implementation of FCS-MPC in a low-budget control platform. In addition, the steady-state performance of a conventional FCS-MPC is not good, as a single voltage vector is applied over a control period. Thus, to achieve a satisfactory enough steady-state performance, the control period of a conventional FCS-MPC needs to be much shorter than that of a conventional linear control, e.g. FOC [93, 94]. Therefore, it is desirable to complete the FCS-MPC algorithm in a short time interval [95]. Furthermore, the computational effort increases with more complex converter topology or additional system constraints, e.g. current boundary settings and common-mode voltage reduction. Therefore, the reduction of the computational burden of FCS-MPC requires investigations.

As mentioned above, the computational burden of a FCS-MPC is increased when a multilevel power converter topology is used [96]. As a result, hierarchical FCS-MPCs has been proposed in [97-100]. Such methods reduce the computational burden by taking into account the redundant vectors in multilevel converters and splitting the objective function into two functions. To evaluate the first objective function, its value is calculated for each of the possible voltage levels and the one that minimizes the objective function is selected as the optimal voltage level. This optimal voltage level is then combined with a group of redundant voltage vectors, and this new set is used to minimize the second objective function. Finally, the voltage vector that minimizes the second objective function is selected as the optimal input [29].

In recent years, the simplification of FCS-MPC scheme has been discussed [101-105]. For instance, [101] aims at reducing the number of candidate vectors during prediction by a sector distribution on a

source voltage vector. This method can significantly reduce the computational burden of MPC, however at the cost of a control performance degradation as the simplification algorithm involves an inequivalent transformation.

More recently, the simplification of FCS-MPC by the mean of equivalent transformation has been investigated. In a MPCC of [106], the reference currents are transformed to an equivalent reference voltage. As a result, the objective function evaluation becomes an optimization problem involving the equivalent reference voltage and the candidate voltage vectors [107]. Then, by identifying which voltage vector is closest to the reference voltage vector, the optimal switching state can be determined. Traditional FCS-MPC needs to predict the behaviors of controlled variables due to all the candidate voltage vectors, whereas this simplified FCS-MPC utilizes a calculation of reference voltage vector instead of the system behavior predictions. As this calculation performs only once in each control period, the computational burden is reduced. It should be mentioned that such a simplified FCS-MPC ensures its performance is the same as that of the conventional FCS-MPC, as the controlled variables are equivalently transformed according to the system model.

This concept has also been applied to MPTC [34, 37, 38, 108]. The reference torque and reference stator flux amplitude are equally converted to a reference voltage vector. As a result, the computational burden is reduced by selecting an optimal voltage vector in a straightforward way. Such a RVV-MPC strategy (linked to Figure 1.4, the second block of Level 2) will be presented in this chapter. As discussed in Chapter 4, multi-vector MPCs are introduced to improve the steady-state performance. The main idea behind such strategies is to involve more possible control actions. For example, in [33], an MPTC strategy that applies two arbitrary voltage vectors during each control period is proposed. As more possible vector combinations are provided, the torque and flux ripple can be further reduced. However, despite the improvement of steady-state performance, the computational burden is remarkably increased, requiring a controller with high computational power or with parallelization of computations and reusable resources. Indeed, for a two-level VSI, eight times eight (i.e. 64) possibilities have to be evaluated, according to a predefined objective function. For each possibility, the corresponding duty ratio optimizations have to be conducted. Considering this, the RVV-MPC

can be particularly useful for the multi-vector MPCs to reduce the computational burden. The RVV-MPC will be explained in this chapter.

On the other hand, even though the computation burden is reduced, the control flexibility is affected with the RVV-MPC (has been pointed out in Figure 1.4 with the second block of Level 3). An optimal voltage vector is determined in a straightforward way through a generation of reference voltage vector without evaluating all the candidate voltage vectors. However, considering that an advantage of FCS-MPC is that it can handle system constraints, and the main reason is that a finite set of candidates are considered, the strongly reduced amount of candidates with the RVV-MPC means that an inclusion of additional constraints is not feasible to be implemented. As a result, an important advantage of FCS-MPC is lost. It also means further development on control performance becomes difficult with this RVV-MPC. Therefore, an extension of the RVV-MPC is desired to retrieve the advantage of easy constraint inclusion and to find a trade-off between the computational efficiency and the control performance, which will be discussed later on in this chapter.

In Section 5.2, the RVV-MPC is presented and the simulation results are provided. Even though such a scheme can reduce the computational burden without affecting the control performance, it hides an important benefit of FCS-MPC, i.e. the inclusion of constraints. It also means that the control flexibility of FCS-MPC is influenced. This problem will be discussed in Section 5.3 and an improved scheme with setting up of adaptive reference variants will be introduced to solve this problem (linked to Figure 1.4, the second block of Level 4). To demonstrate the effectiveness of the proposed scheme, simulation results and experimental results are given in Section 5.4 and Section 5.5, respectively. In Section 5.6, the characteristics of different control schemes are discussed for a comparison. The conclusions for this chapter are given in Section 5.7.

5.2 Reference Voltage Vector based MPTC

5.2.1 Control Principle

Compared to conventional two-vectors control solutions as presented in the Chapter 4, a reduction of the computational burden is aimed at with

the RVV-MPTC. Rather than evaluating all two-vectors control possibilities, a reduced finite control set is looked at. For this, the RVV-MPTC converts the given reference flux amplitude and reference torque to a reference voltage vector, which is then computed that can be generated through the VSI. According to the location of this reference voltage vector, the first optimal vector in the two-vectors solution can be determined directly through a closed analytical formulation. As a consequence, the multi-solution evaluation of the conventional MPTC strategy is avoided, resulting in a lower computational burden. In addition, the reference torque and reference flux are replaced by a single variable, being the reference voltage vector, which means the two variables are reduced to one. As a result, the use of a weighting factor in the objective (cost) function becomes obsolete, hence its tuning is avoided.

To explain the MPC strategy based on a reference voltage vector, consider in Figure 5.1 the diagram of the RVV-MPTC strategy. Additionally, a flow chart is given in Figure 5.2 to illustrate the process of the RVV-MPTC. The whole scheme can be divided into 6 steps, which include the state estimation, calculation of torque and flux slope, prediction of reference voltage vector, selection of the first vector and the candidates of the second vector, duty ratio optimization and the objective function evaluation.

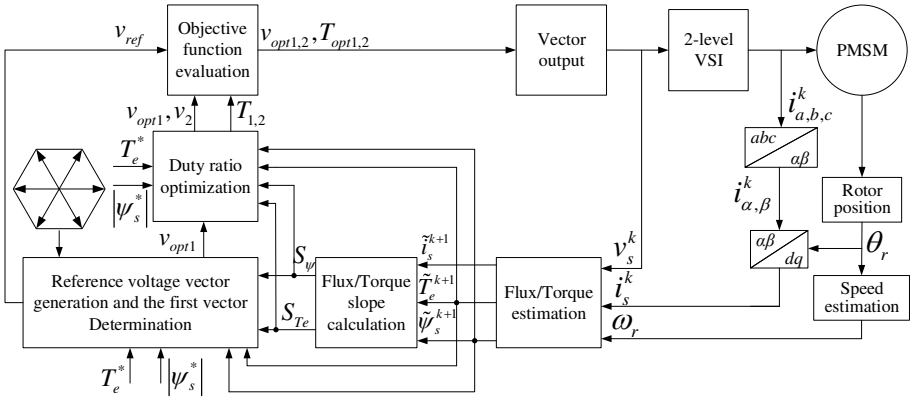

Figure 5.1: Diagram of the RVV-MPTC.

It is noted that the steps that are different compared to the two-vectors MPTC illustrated in Figure 4.3 have been highlighted in Figure

5.2. The two-vectors MPTC computes the duty ratio for all the candidate vector combinations and then performs predictions accordingly. In the RVV-MPTC, however, a reference voltage vector is created from the reference torque and flux based on the PMSM prediction model. As a result, the first optimal vector and the candidates of the second vector are determined. Then, the duty ratio is computed for a reduced amount of candidate vector combinations.

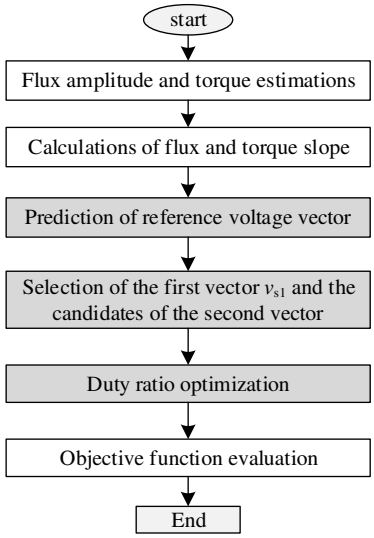

Figure 5.2: Flow chart of the RVV-MPTC.

A short overview of all the steps is given in this paragraph. First, the motor states are estimated based on the current measurements, the vector combinations decided in the previous control period and the machine model. In a second step, the torque and flux slopes are calculated, which are used for the reference voltage prediction and the duty ratio calculation. Next, a reference voltage vector is generated based on the reference torque and flux amplitude using the machine model. Consequently, the first optimal vector can be selected from the control set according to the location of the reference voltage vector. Next, candidates can be considered for the second vector and the corresponding duty ratios should be computed. Finally, the best solution is decided based on the objective function evaluation. The main steps will be elaborated hereafter.

5.2.2 Reference Voltage Vector Generation

The flux vector and torque at the control period (k+1) can be estimated, and the flux and torque slopes S_ψ and S_{Te} can be computed, as presented in Section 4.2.2 and Section 4.2.3, respectively. Then, a reference voltage vector can be generated from the reference torque and the reference flux amplitude. Here, different solutions can be used to determine the reference voltage vector. In the following, the deadbeat solution that aims to force the torque and flux to reach their reference values at the end of the control period and the RMS solution that aims to reduce the error of flux and torque over the whole control period will be discussed.

A. Deadbeat Solution

First, the deadbeat solution can be used to generate the reference voltage vector. It aims at forcing the torque and flux to be equal to the reference values at the end of each control period. The error of stator flux and torque at the end of the control period (k+2) is given as:

$$E_\psi^{DB} = \psi_s^e + S_\psi T_s \tag{5.1}$$

$$E_{Te}^{DB} = T_e^e + S_{Te} T_s \tag{5.2}$$

respectively, where $\psi_s^e=\tilde{\psi}_s^{k+1}-\psi_s^{ref}$, $T_e^e=\tilde{T}_e^{k+1}-T_e^{ref}$ are the estimated flux and torque error at the beginning of the next control period (k+1) respectively. By letting $E_\psi^{DB}=0$ and $E_{Te}^{DB}=0$, the reference voltage vector under deadbeat solution can be derived as:

$$v_{ref}^{DB} = \begin{bmatrix} v_d^{DB} \\ v_q^{DB} \end{bmatrix} \tag{5.3}$$

where

$$\begin{cases} v_d^{DB}=-\dfrac{\psi_s^e\left|\tilde{\psi}_s^{k+1}\right|}{T_s\tilde{\psi}_d^{k+1}}+\dfrac{\tilde{\psi}_q^{k+1}(R_s\tilde{i}_q^{k+1}-v_q^{k+1})}{\tilde{\psi}_d^{k+1}}+R_s\tilde{i}_d^{k+1} \\ v_q^{DB}=\dfrac{1.5p\left|\tilde{\psi}_s^{k+1}\right|\psi_s^e\tilde{\psi}_q^{k+1}(L_d-L_q)-\tilde{\psi}_d^{k+1}L_dL_qT_e^e+E_e}{1.5T_sp[\tilde{\psi}_d^{k+1}L_d(\tilde{\psi}_d^{k+1}-\tilde{i}_d^{k+1}L_q)-(\tilde{\psi}_q^{k+1})^2(L_d-L_q)]}+R_s\tilde{i}_q^{k+1} \end{cases} \tag{5.4}$$

in which $E_e=2pT_s\omega_r\tilde{\psi}_d^{k+1}L_q(\left|\tilde{\psi}_s^{k+1}\right|^2-L_d\tilde{\psi}_s^{k+1}\cdot\tilde{i}_s^{k+1})$.

B. RMS Solution

Except for the deadbeat solution, the RMS solution can also be considered to generate the reference voltage vector aiming at minimizing the global mean errors of torque and flux. The RMS errors of the flux and torque can be expressed as:

$$E_{\psi}^{RMS} = \frac{1}{T_s}\int_0^{T_s}(\psi_s^e + S_{\psi}t)^2 dt = (\psi_s^e)^2 + \psi_s^e S_{\psi} T_s + \frac{1}{3}(S_{\psi}T_s)^2 \tag{5.5}$$

$$E_{Te}^{RMS} = \frac{1}{T_s}\int_0^{T_s}(T_e^e + S_{Te}t)^2 dt = (T_e^e)^2 + T_e^e S_{Te} T_s + \frac{1}{3}(S_{Te}T_s)^2 \tag{5.6}$$

Then by letting $dE_{\psi}^{RMS} / dv_s = 0$ and $dE_{Te}^{RMS} / dv_s = 0$, a reference voltage vector under the RMS solution can be deduced as:

$$v_{ref}^{RMS} = \begin{bmatrix} v_d^{RMS} \\ v_q^{RMS} \end{bmatrix} \tag{5.7}$$

where

$$\begin{cases} v_d^{RMS} = -\dfrac{3\psi_s^e \left|\tilde{\psi}_s^{k+1}\right|}{2T_s\tilde{\psi}_d^{k+1}} + \dfrac{\tilde{\psi}_q^{k+1}(R_s\tilde{i}_q^{k+1} - v_q^{k+1})}{\tilde{\psi}_d^{k+1}} + R_s\tilde{i}_d^{k+1} \\ v_q^{RMS} = \dfrac{3p\left|\tilde{\psi}_s^{k+1}\right|\psi_s^e\tilde{\psi}_q^{k+1}(L_d - L_q) - 2\tilde{\psi}_d^{k+1}L_dL_qT_e^e + E_e}{2T_sp[\tilde{\psi}_d^{k+1}L_d(\tilde{\psi}_d^{k+1} - \tilde{i}_d^{k+1}L_q) - (\tilde{\psi}_q^{k+1})^2(L_d - L_q)]} + R_s\tilde{i}_q^{k+1} \end{cases} \tag{5.8}$$

5.2.3 Optimal Voltage Vector Determination

For now, the reference voltage vector has been obtained, but it should be implemented by a switching power converter. As a limited amount of voltage vectors are produced by the VSI, the reference voltage vector can be realized in average by combining these voltage vectors.

In the conventional FCS-MPC, the optimal voltage vector is determined based on the predictions due to all the candidate voltage vectors. In particular, in a two-vectors MPC, such as [33], variable predictions, as well as the duty ratio optimizations require to be conducted for all possible vector combinations ($7 \times 7 = 49$ possibilities in [33]), which means many calculations are required. In the RVV-MPTC, since the reference torque and flux amplitude are converted to

a single variable, being reference voltage vector, the whole selecting process of the optimal voltage vector is simplified and the computational burden is reduced. Instead of evaluating the objective function for all possible finite control sets, a reference voltage vector allows to select an optimal voltage vector in the two-vectors approach in a straightforward way according to the position of the reference voltage vector only.

In a two-vectors approach, the first VSI vector is selected from the six nonzero VSI vectors being the active vectors. To determine the first voltage vector, the stationary $\alpha - \beta$ reference frame can be divided into six sectors of sixty degrees as shown in Figure 5.3. Each of these sectors contains a single active or nonzero vector. The first optimal vector to be applied is determined by the sector that holds the reference voltage vector. For instance, in Figure 5.3, according to the phase angle of the reference voltage vector, the reference voltage vector is located in sector 1, and hence the vector $\underline{V}_1$ will be the first optimal voltage vector.

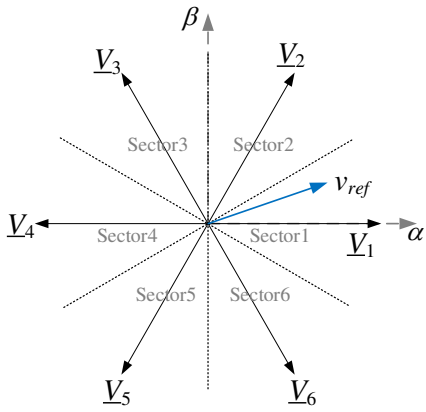

Figure 5.3: Principle Diagram of Vector Selection.

After choosing the first optimal voltage vector, the candidates for the second optimal vector can be identified and combined with the first vector to approximate the reference voltage vector. The second vector can be a zero vector, resulting in only one candidate vector combination. In this case, the objective function evaluation can be omitted. On the other hand, the second vector could not be fixed as a zero vector, but could be selected from the nonzero voltage vectors. As

done in Chapter 4, the second vector is selected from the two neighbors of the first vector and the zero vector. For instance, if the first optimal vector is determined as $\underline{V}_1$, the candidates of the second optimal vector will be $\underline{V}_2$, $\underline{V}_6$ and $\underline{V}_0$, resulting in three candidate vector combinations. In this case, an objective function evaluation is required to determine an optimal solution from the three candidates. The duty ratio optimization of a vector combination will be discussed in the following.

5.2.4 Duty Ratio Optimization

After obtaining the first optimal voltage vector and the candidates for the second optimal vector, the duty ratio of every candidate vector combination needs to be calculated, resulting in the time duration to apply the first vector. As the control variables, torque and stator flux, have been transformed resulting in a reference voltage vector, one way to determine the duty ratio can be minimizing the tracking error of reference voltage vector. Here, an error function can be defined as:

$$J^2 = \left| T_s v_{ref} - T_1 v_{s1} - (T_s - T_1) v_{s2} \right|^2 \tag{5.9}$$

where v_{s1}, v_{s2} are the first and second vector respectively, T_1 is the time duration of the first vector. Thus, by forcing $dJ^2 / dT_1 = 0$, the time duration of the first vector T_1 can be derived as:

$$T_1 = \frac{T_s (v_{ref} - v_{s2}) \bullet (v_{s1} - v_{s2})}{(v_{s1} - v_{s2})^2} \tag{5.10}$$

where $\bullet$ is dot product of two vectors.

5.2.5 Objective Function Evaluation

As previously discussed, if the second vector is fixed as a zero vector, the objective function evaluation can be omitted, as only one candidate solution is involved. In case more candidates are considered for the second vector, an objective function evaluation is necessary to determine the optimal solution. To track the reference voltage vector, the objective function can be given as:

$$g = \left| v_{ref} - d_1 v_{s1} - (1 - d_1) v_{s2} \right| \tag{5.11}$$

where $d_1 = T_1 / T_s$ is the duty ratio of the first vector. Then, the optimal vector combination that minimizes the objective function will be selected.

5.2.6 Simulation Results

Figure 5.4 shows the waveforms of the torque, stator flux and a phase current under the RVV-MPTC with deadbeat solution, and the results under the RVV-MPTC with RMS solution are reported in Figure 5.5. Both the results under the deadbeat reference voltage vector generation, as (5.3), and the results under the RMS reference voltage vector generation, as (5.7), are presented.

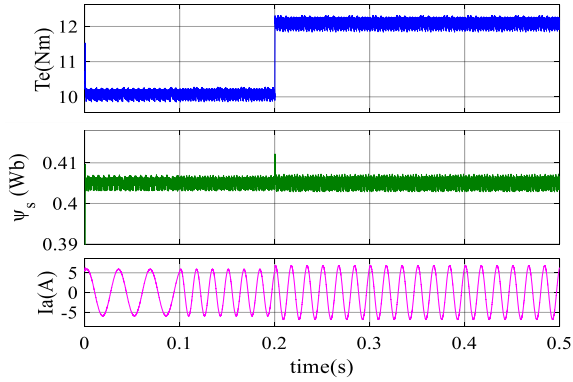

(a) Waveforms of torque, flux and phase current

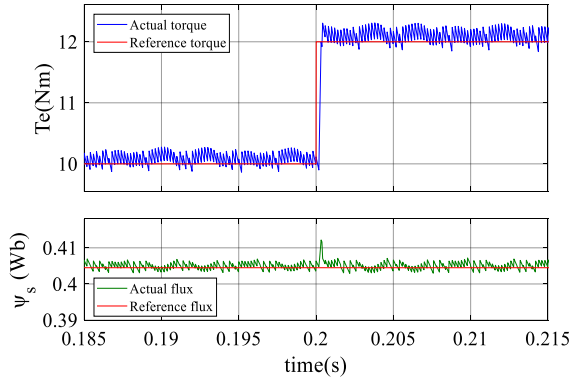

(b) Waveforms of torque and flux during 0.185-0.215s

Figure 5.4: Simulated results under the RVV-MPTC with deadbeat solution

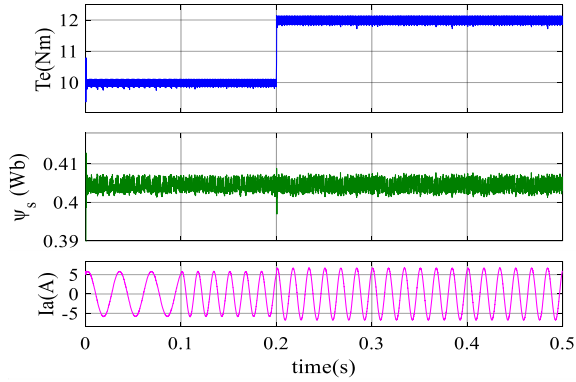

(a) Waveforms of torque, flux and phase current

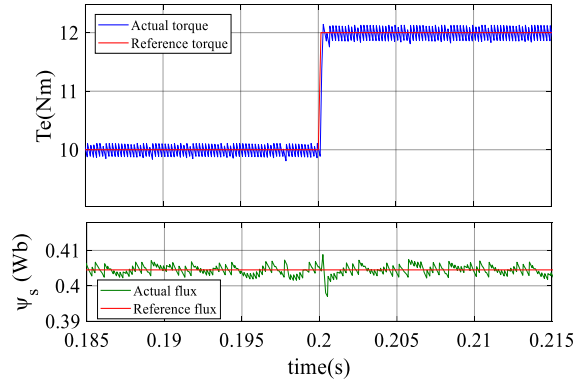

(b) Waveforms of torque and flux during 0.185-0.215s

Figure 5.5: Simulated results under the RVV-MPTC with RMS solution

It can be seen from Figure 5.4 that the torque reaches the reference value at the end of the control period only under the RVV-MPTC with deadbeat solution. In contrast, rather than forcing the torque to reach its reference value at the end of control period, the RMS error of the flux and torque is minimized with the RVV-MPTC with RMS solution, as can be observed in Figure 5.5. In addition, both solutions achieve a similar flux performance, although spikes are aroused during the torque transient state.

It should be noted that the RVV-MPTC achieves a similar performance as the conventional two-vectors MPTC that presented in Section 4.2 does, as the control variables are equally transformed based on the intrinsic relationship within the machine model. However, as the RVV-MPTC determines the optimal vector using a reference voltage vector without evaluating all the candidate solutions, it can achieve a

lower computation cost compared to the conventional two-vectors MPTC.

5.3 Improvement of RVV-MPC with Setting Adaptive Reference Variants

As presented above, the RVV-MPC is introduced to reduce the computational burden of a conventional FCS-MPC. The main idea is to convert the variable reference, e.g. reference torque and reference flux, to a single-reference voltage vector based on a machine model. Then, according to the location of this reference voltage vector, a strongly reduced amount of vector combinations will be considered to approximate the reference vector. In this manner, evaluating every possible solution is avoided, hence reducing the computation burden. However, due to the limited amount of candidate inputs, additional constraints, such as maximum allowed peak currents or maximum switching frequency, cannot truly be achieved, which hides a main advantage of the conventional FCS-MPC.

Motivation and Contribution

Generally, in a conventional RVV-MPC, during each control period, a single-fixed reference voltage is calculated based on the principle of tracking the reference torque and flux. This reference voltage vector relates to only one or two candidate control actions. This is because the amount of the possible vector combinations increases with long receding horizon, and it comes down by selecting one or two candidates. Hence, such a focus on a single reference point, and with short impact, means that including additional restraints (e.g. current peak value or motor efficiency) into the objective function is less likely to be upheld. An important advantage of FCS-MPC, the inclusion of constraints and nonlinearities, is then lost with this RVV-MPC, although it can lower the computational burden. It also means that further development on the control performance is violated, as only limited candidate inputs are offered. To solve this, an improved reference-based MPC that allows the inclusion of additional constraints is desired to achieve a better control performance.

On this basis, a further innovation is proposed here for the reference-based MPC under the assumption of a correct linear model. Here, as a salient pole PMSM is studied, the reference current can be obtained

based on the Maximum Torque Per Ampere (MTPA) principle. However, rather than considering a fixed reference point, as done in the conventional RVV-MPC [37, 38, 108], a well-considered neighborhood of the MTPA reference is introduced. These reference variants are processed, resulting in a larger set of optimal candidate solutions. With the multiple, but still finite amount of, optimal candidates; additional constraints can then be incorporated within the objective function. In this study, current boundaries are included in the objective function to achieve improved system performance. Furthermore, the size of the current reference space can be adjusted online to generate proper candidate solutions that truly comply with the current boundary settings.

5.3.1 Control Structure of Reference-Variant-Based MPC

The structure of the proposed reference-variant-based MPTC is introduced here. The diagram of the proposed MPC strategy is shown in Figure 5.6.

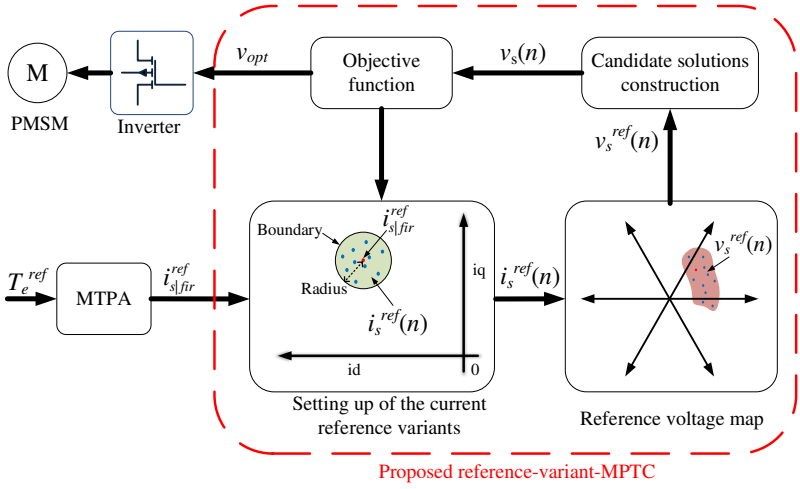

Figure 5.6: Diagram of the proposed reference-variant-MPC strategy.

The first step is a conventional one that calculates the reference current according to the reference torque based on the MTPA principle. Here, however, reference variants are considered as contributions, generating a set of reference currents in the neighborhood of the aforementioned MTPA reference. Then, as a VSI is used, for each of

these reference variants, a reference voltage vector is computed, using the machine model. Next, optimal solutions are constructed to approximate the corresponding reference voltage vectors. Finally, taking the benefit of the multiple solutions, an objective function with extra constraints evaluates the candidates, and the optimal one will be selected to be applied during the next control period. These different steps will be described in more detail later on.

5.3.2 Calculation of Reference Current under MTPA Control

Using salient pole PMSM drives to obtain the maximum efficiency considering Joule losses only, MTPA control can be achieved by selecting the suitable current vector as a function of torque. It aims to maximize the ratio between the torque and current amplitude [109], hence minimizing Joule losses. In this work, to achieve MTPA control, the direct calculation approach of the reference current vector from [12] is utilized. As the electromagnetic torque is expressed as (2.11), by neglecting the magnet saturation the relationship between the d-axis and q-axis current under the MTPA principle can be represented as [12, 110]:

$$i_d = \frac{\psi_f}{2(L_q - L_d)} - \sqrt{\frac{\psi_f^2}{4(L_q - L_d)^2} + i_q^2} \tag{5.12}$$

Here, to simplify the analysis and to obtain the reference current for MTPA control, the active flux $\psi_D = \psi_f - (L_q - L_d) i_d$ [111] is used. Then, (5.12) can be rewritten as:

$$(L_q - L_d)^2 i_q^2 = \psi_D (\psi_D - \psi_f) \tag{5.13}$$

Therefore, by substituting (5.13) into (2.11), T_e can be expressed as:

$$\left(\frac{L_q - L_d}{p} T_e\right)^2 = (\gamma_D - 1)\gamma_D^3 \tag{5.14}$$

where $\gamma_D = \psi_D / \psi_f$. Then, the solution of (5.14) can be deduced as:

$$\gamma_D = \frac{(1 + x_R)}{4}\left(1 + \sqrt{\frac{2}{x_R} - 1}\right) \tag{5.15}$$

where

$$x_R = \sqrt{\frac{1}{2}\{(\sqrt{3x_T^2+1}+1)^{\frac{1}{3}} - (\sqrt{3x_T^2+1}-1)^{\frac{1}{3}}\}^3}$$

$$x_T = (\frac{4}{3})^2 \frac{(L_q - L_d)}{p\psi_f^2} T_e$$

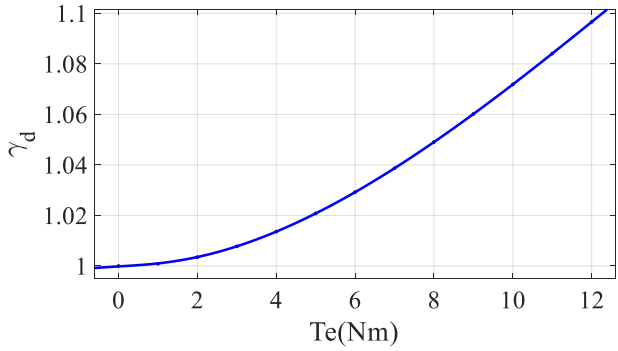

Figure 5.7: Relationship between γ_D and torque

Here, the relationship between γ_D and torque is shown in Figure 5.7 in which the motor parameters listed in Table 4.3 are used. Then, the first reference point of stator current for MTPA control can be expressed as:

$$i_{s|fir}^{ref} = \left[i_d^{ref}, i_q^{ref} \right]^T \tag{5.16}$$

$$\begin{aligned} i_d^{ref} &= \frac{\psi_f}{L_d - L_q}(\gamma_D - 1) \\ i_q^{ref} &= \frac{2T_e^{ref}}{3p\psi_f}\frac{1}{\gamma_D} \end{aligned} \tag{5.17}$$

The locus of currents under different torque values is shown in Figure 5.8. It is noted that linear IPMSM models are used in this study, where magnet saturation is neglected. The effect of saturation and mutual coupling of both orthogonal magnetic axes on an MTPA-controlled IPMSM has been analyzed in [112], in which a flux model taking into account the saturation of the dq-axis and the magnetic coupling between these axes is considered with the help of an equivalent magnetizing

current [113]. In particular, the locus of current vectors that correspond to MTPA with and without considering cross-saturation are compared in [112]. It is concluded that the cross-saturation little modifies the optimal operating points, and in contrast to an MTPA method that neglects the cross-saturation, the MTPA strategy includes cross-saturation predicts a stronger field-weakening for a given q-axis current. Although such a study has been given, this paper considers linear models that neglect the magnetic interaction to simplify the analysis, as the focus of this study is the development of MPC strategies rather than MTPA control.

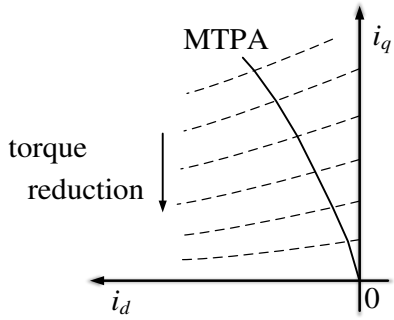

Figure 5.8: Current locus under different torque values.

5.3.3 Setting Up of Current Reference Variants

In the RVV-MPC approaches discussed so far in international literature, a single reference value is used to generate the VSI control actions during each control period [37, 38, 108]. In such strategies, the reference voltage vector is computed based on the principle of achieving the reference torque and reference flux at the end of the next control period. Then, the required effect of the reference voltage on the torque and flux, only stated at the end of the control action, will be replaced by a set of two succeeding VSI vectors. Such strategies can reduce the computational burden by considering a strongly reduced number of candidates.

However, even though such a strategy obtains the same control performance as the conventional two-vectors strategy [33], multi-objective strategies, such as restricting the switching losses or limiting the current peak value, are less likely to be achieved due to the limited number of candidates. This means that the ability to consider extra

constraints or nonlinearities, which is a significant advantage of FCS-MPC, is lost in such a strategy. A better trade-off between computational burden and sufficient control solutions has to be found. For this, reference variants will be considered and discussed hereafter.

In the proposed strategy, to better comply to additional constraints (in this work current boundaries are considered), multiple current reference variants are introduced to be able to involve more candidate solutions. As current boundaries are included in this study, it is better to start the setting up of reference variants with the current reference. These will be transformed later on into voltage references. Here, a first reference point is determined based on the principle of achieving the main control objective (MTPA control in this work). This reference is considered as the first reference point, as it is obtained from the main control objective. However, if additional constraints are considered, the optimal point may not be this first reference, but could locate near this point. Thus, a neighborhood of this reference point is introduced and a finite set of reference variants is considered to generate more optimal candidate solutions. It means proper freedom is given to the reference current, and a region of the reference current is considered.

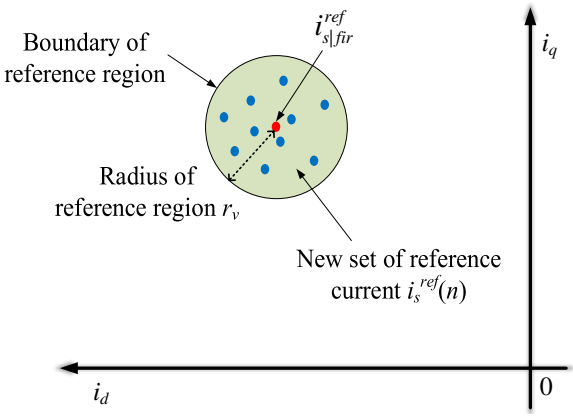

Figure 5.9: Setting up of reference variants.

This defined region could be a circle, triangle, or a different shape around the original point given in (5.16). For now, the optimal shape of this region with respect to fasten the search action toward a proper reference current is not discussed, and in this study, a circular shape is proposed. The center of this circle falls together with the first reference

current vector, as shown in Figure 5.9. The radius of the circle is predefined as r_v and can be adjusted later on to comply truly with boundaries.

Instead of considering the infinite amount of possible current reference variants in the recently defined circle, a finite set of points within the circle will be selected. For now, the reference variant points are randomly selected in the hope of fully exploiting the surface covered by the circle, though existing techniques can be used to select samples in an optimal way [114]. Thus, a new set of reference currents can be defined as:

$$i_s^{ref}(n) = \begin{cases} i_{s|fir}^{ref}, & n = 1 \\ rand(i_{s|fir}^{ref}, r_v), & n = 2,...,N \end{cases} \tag{5.18}$$

where $rand(x, y)$ denotes a random point within a circle with x as the center and y as the radius. Obviously, more reference points offer more possibilities to achieve better system performance, however, elevating the computational burden. In this work, to make a trade-off between the system performance and the computational burden, the number of referent variants is set to 10. Thus, including the original reference value, a new reference set with 11 points (N=11) is constructed.

5.3.4 Mapping of Reference Voltage

As described above, with the introduction of the reference variants, a new set of reference current vectors is created as $i_s^{ref}(n)$ within the neighborhood of the MTPA reference current $i_{s|fir}^{ref}$. Thus, a closed region of reference voltage vectors can be deduced based on modeling the relationship between the current and the required voltage vector to obtain such current, which will be described in the following text.

In an MPC strategy, the stator current prediction is based on a machine model and the voltage vector selected. However, in the practical discrete-time implementation, there is a one-step delay between the finally selected vector and the applied vector. This means that the voltage vector selected in the present control period kT_s will be applied in the next period $(k+1)T_s$. Thus, as described in Chapter 3, the stator current at the end of the present control period, being the start of the next period, needs to be first estimated based on the voltage vector

selected in the previous control period. According to the discrete-time model of the IPMSM derived from (2.7-2.10), the stator current for the given voltage vector v_s^k at the start of the next control period $(k+1)T_s$ can be estimated as:

$$\begin{aligned} \tilde{i}_d^{k+1} &= i_d^k - \frac{R_s T_s}{L_d} i_d^k + \frac{L_q T_s \omega_r}{L_d} i_q^k + \frac{T_s}{L_d} v_d^k \\ \tilde{i}_q^{k+1} &= i_q^k - \frac{R_s T_s}{L_q} i_q^k - \frac{L_d T_s \omega_r}{L_q} i_d^k + \frac{T_s}{L_q} v_q^k - \frac{\psi_f T_s \omega_r}{L_q} \end{aligned} \tag{5.19}$$

Based on this estimated stator current (5.19), the currents at the end of the next control period can be predicted for different voltage vectors in $(k+2)T_s$ as:

$$\begin{aligned} \hat{i}_d^{k+2} &= \tilde{i}_d^{k+1} - \frac{R_s T_s}{L_d} \tilde{i}_d^{k+1} + \frac{L_q T_s \omega_r}{L_d} \tilde{i}_q^{k+1} + \frac{T_s}{L_d} v_d^{k+1} \\ \hat{i}_q^{k+2} &= \tilde{i}_q^{k+1} - \frac{R_s T_s}{L_q} \tilde{i}_q^{k+1} - \frac{L_d T_s \omega_r}{L_q} \tilde{i}_d^{k+1} + \frac{T_s}{L_q} v_q^{k+1} - \frac{\psi_f T_s \omega_r}{L_q} \end{aligned} \tag{5.20}$$

Here, to compute the corresponding reference voltages, the deadbeat solution is employed, which aims at tracking the reference value at the end of the control period, namely setting $\hat{i}_s^{k+2} = i_s^{ref}$. Hence, due to the relationship between the stator current and voltage vector (5.20), the set of reference voltage vectors with respect to the set of reference currents $i_s^{ref}(n)$, defined in the neighborhood of the MTPA reference current, can be derived as:

$$v_s^{ref}(n) = \left[v_d^{ref}(n), v_q^{ref}(n) \right]^T \tag{5.21}$$

$$\begin{aligned} v_d^{ref}(n) &= (i_d^{ref}(n) - \tilde{i}_d^{k+1} + \frac{R_s T_s}{L_d} \tilde{i}_d^{k+1} - \frac{L_q T_s \omega_r}{L_d} \tilde{i}_q^{k+1}) \frac{L_d}{T_s} \\ v_q^{ref}(n) &= (i_q^{ref}(n) - \tilde{i}_q^{k+1} + \frac{R_s T_s}{L_q} \tilde{i}_q^{k+1} + \frac{L_d T_s \omega_r}{L_q} \tilde{i}_d^{k+1} + \frac{\psi_f T_s \omega_r}{L_q}) \frac{L_q}{T_s} \end{aligned} \tag{5.22}$$

It should be noted that the set of reference voltage vectors, $v_s^{ref}(n)$, can be located within a closed region for each control period, as shown in Figure 5.10. Such a region may span more than one 60 degrees sector, which means that various vector combinations will be considered during the next step. This variety of candidate solutions provides more

possibilities to comply better to any additional boundary. A circle with a defined radius will allow an expansion of the region in the case boundaries are not met later by any of the candidate solutions.

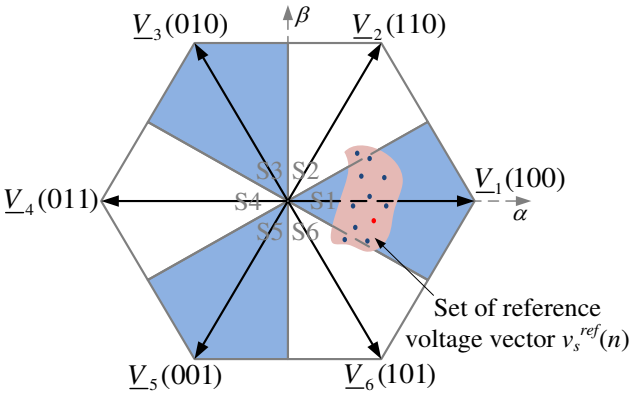

Figure 5.10: Set of reference voltage vectors.

5.3.5 Candidate Solutions Construction

With the group of reference voltage vectors, $v_s^{ref}(n)$, given by (5.21) and (5.22), proper vectors need to be combined within a control period to approximate each of them, resulting in candidate solutions for the MPC routing. With the six active VSI vectors, the stationary α-β reference frame is divided into six sectors, each of which contains a VSI vector. In this work, and for each of the reference voltage vectors, the sector that holds the reference will be determined first. Then, the VSI vector of this sector will be selected so that combined with a zero vector will approximate the reference vector. Combining here means setting the time durations of the two vectors for which the calculation will be given hereafter. The principle of optimization is to track the reference value. For this, an error function to be minimized is defined as:

$$J^2 = \left| T_s v_s^{ref} - T_{1|opt} v_{c|1} - (T_s - T_{1|opt}) v_{c|2} \right|^2 \tag{5.23}$$

where $v_{c|1}$ and $v_{c|2}$ are the two successive vectors, respectively. Here, $v_{c|1}$ has been decided according to the location of the reference voltage vector, $v_{c|2}$ is a zero vector ($\underline{V}_0$ or $\underline{V}_7$), depending on which gives only

one switching jump compared to the previous VSI vector. $T_{1|opt}$ is the optimal time duration of the first vector. Therefore, to minimize the error by enforcing $\partial(J^2)/\partial T_{1|opt}=0$, the optimal time duration for the first vector $T_{1|opt}$ can be deduced as:

$$T_{1|opt}=\frac{T_s(v_s^{ref}-v_{c|2})\bullet(v_{c|1}-v_{c|2})}{(v_{c|1}-v_{c|2})^2} \tag{5.24}$$

where • represents dot product of two vectors. Then, a vector combination can be expressed as:

$$v_c^i=v_{c|1}^i T_{1|opt}^i+v_{c|2}^i(T_s-T_{1|opt}^i) \tag{5.25}$$

where $i=1,2,...,N$. Hence, a group of candidate control actions with respect to the reference voltage set $v_s^{ref}(n)$ is constructed as:

$$v_c(n)=\{v_c^i\}\ (n=i) \tag{5.26}$$

5.3.6 Objective Function Evaluation

In conventional RVV-MPC strategies [37, 38, 108], the error function (5.23) is also employed as the objective function to minimize the error between the reference and the candidate vector combinations. In this method, a single reference voltage vector is obtained based on the deadbeat solution, which aims at reaching the reference value at the end of the control period. This means the timing is computed to approximate the reference voltage vector as well as possible, leaving no freedom to optimize for the current peak value during the control period.

As described above, the original reference current vector for MTPA control is given by (5.16-5.17). Remember, due to the switching nature of the VSI, this cannot be achieved at each moment, hence setting this reference at (for instance) the end of a control period. If current boundaries are considered, having the reference current does not imply the current remains within those boundaries all moments. Hence, even though the reference is achieved, the voltage solution may not be optimal, as it could result in too high instantaneous currents. Due to the limited number of solutions in a finite set RVV-MPC, the problem could remain.

In the proposed strategy here, as a proper solution could be provided to approximate a given reference voltage, as is done in (5.25), and as n reference voltage vectors (5.21-5.22) are considered, efforts can be made to take on additional boundaries through a minimization of an objective function. This objective function will be discussed hereafter and will try to reduce torque ripples (using a g_1 equality function) as much as possible and to truly comply to current boundaries (using a g_2 inequality function).

To restrict the instantaneous torque deviations from the reference torque, both the torque at the switching moment $\hat{T}_e^{t1}$, and the torque at the end of the next control period $\hat{T}_e^{k+2}$ are evaluated in the objective function, expressed as:

$$g_1 = \left| T_e^{ref} - \hat{T}_e^{t1} \right| + \left| T_e^{ref} - \hat{T}_e^{k+2} \right| \tag{5.27}$$

Note that $\hat{T}_e^{k+2}$ corresponds to the predicted torque at the start of the $(k+2)T_s$ due to its continuity, as shown in Figure 5.11. Assumption is made that the torque gradient during the control period will not change sign; hence, for this period, extreme torque values remain in the interval between $\hat{T}_e^{t1}$ and $\hat{T}_e^{k+2}$.

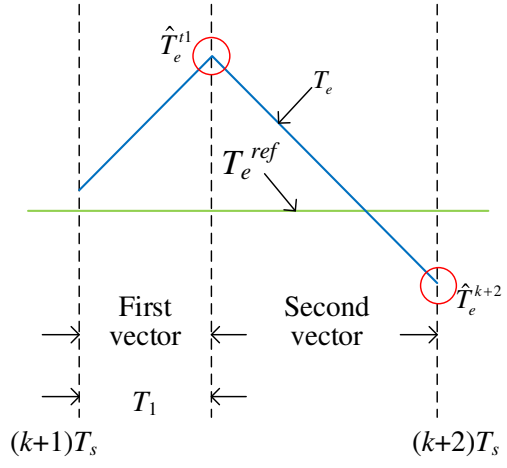

Figure 5.11: Predicted torque at different instants.

As the peak value of the phase currents has to be limited, a tolerance band Δi_s^{tol} is defined on the current amplitude (assuming the common mode current in the IPMSM is zero). This tolerance band is used in the objective function to penalize in case the deviation of the stator current vector amplitude goes outside the tolerance band $\left|i_{s|fir}^{ref}\right| \pm \Delta i_s^{tol}$ [115], where $\left|i_{s|fir}^{ref}\right|$ is the reference of the stator current amplitude, which can be derived from (5.17):

$$\left|i_{s|fir}^{ref}\right| = \sqrt{(i_d^{ref})^2 + (i_q^{ref})^2} \tag{5.28}$$

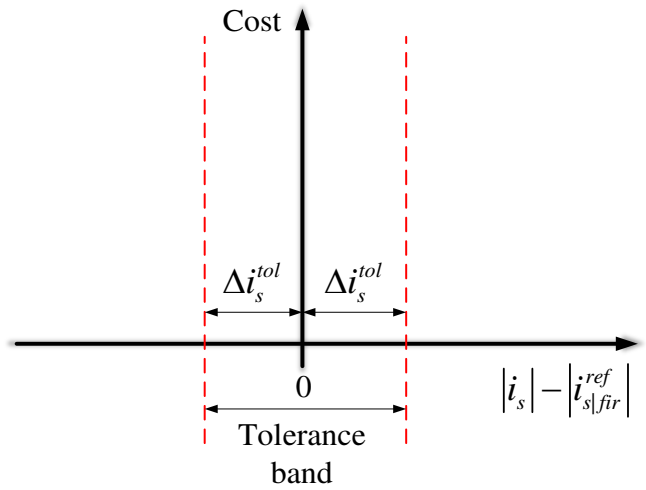

Figure 5.12: Objective function for stator current amplitude.

As stator currents should truly comply to the boundary, an objective function, as illustrated in Figure 5.12 will be used, assuming current predictions and hence machine models are accurate. If the error between the predicted current amplitude and the reference exceeds the tolerance band, it will increase the objective function to infinite; otherwise, it will have no effect on the objective function. Like the objective term function, g_1 for the torque, the current amplitude will be evaluated at the two switching instants for each control period. This is illustrated in Figure 5.13, for either the case of a current exceeding the boundaries, Figure 5.13(a), as for a current that remains within the boundaries, Figure 5.13(b).

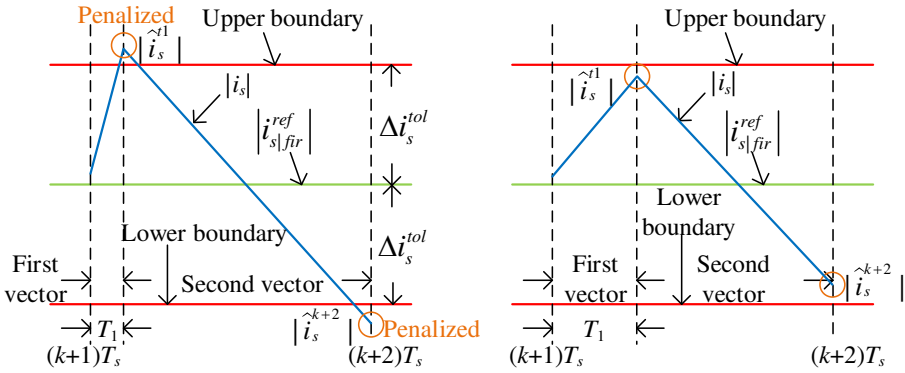

(a) Exceeds the tolerance band (b) Within the tolerance band

Figure 5.13: Predicted stator current amplitude.

In a mathematical way, the objective function term to evaluate the stator current amplitude is given here as:

$$g_2 = \begin{cases} 0, & \left|\left|i_{s|fir}^{ref}\right| - \left|\hat{i}_s^{t1}\right|\right| \le \Delta i_s^{tol} \ \ and \ \ \left|\left|i_{s|fir}^{ref}\right| - \left|\hat{i}_s^{k+2}\right|\right| \le \Delta i_s^{tol} \\ K, & \left|\left|i_{s|fir}^{ref}\right| - \left|\hat{i}_s^{t1}\right|\right| > \Delta i_s^{tol} \ \ or \ \ \left|\left|i_{s|fir}^{ref}\right| - \left|\hat{i}_s^{k+2}\right|\right| > \Delta i_s^{tol} \end{cases} \tag{5.29}$$

where K denotes the value goes to infinity, $|\hat{i}_s^{t1}|$ and $|\hat{i}_s^{k+2}|$ are the predicted stator current amplitude at the switching instant and the one at the start of $(k+2)T_s$, respectively.

Based on the evaluations of the torque and the stator current amplitude, an objective function to be minimized is defined as:

$$g = g_1 + g_2 \tag{5.30}$$

To summarize, the flowchart of the proposed reference-variant-MPC in Figure 5.14 is used. Four phases are distinguished to implement the proposed MPC strategy. The unique steps to the proposed MPC are highlighted in a different color. The first phase is a conventional one to obtain the optimal reference current based on the MTPA principle and the reference torque. In the second phase, a new step is added, where a set of current reference variants is constructed. From these and a machine model, voltage vector variants are computed aiming at a deadbeat solution. In the third phase, corresponding candidate switching actions are constructed for each reference voltage vector. Then, a conventional optimization is performed based on an objective function

evaluation. Finally, the optimal two-vectors combination is determined. Meanwhile, an assessment is made: If the objective function turns infinite for the optimal solution, then the radius of the reference current region is made larger.

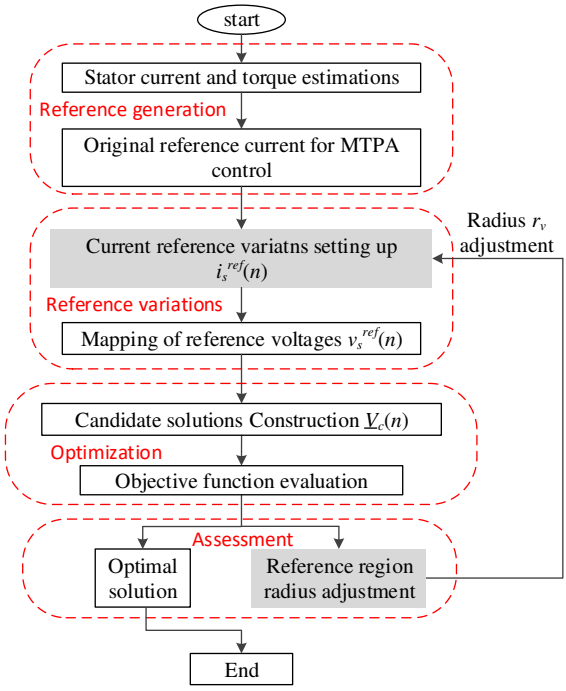

Figure 5.14: Flow chart of the proposed reference-variant-MPC strategy.

5.4 Simulation Results

Simulation studies are given in this section. The proposed MPC scheme introduces multiple reference variants rather than considering a single reference point. As a result, current boundary setting can be included in the objective function. This benefit is revealed in Section 5.4.1. Both the results under the fixed reference and the results under the setting up reference variants are presented to show how the proposed reference-variant-MPC brings the current back within the imposed boundaries. In 5.4.2, the proposed MPC is compared with the RVV-MPC to show it improvements in imposing the boundaries. As the proposed MPC is parameter-dependent, its parameter sensitivity is studied in Section 5.4.3.

5.4.1 Current Boundary

The proposed reference-variant-MPC is compared here with the fixed reference-based approach. Figure 5.15(a) shows the stator current amplitude when the first MTPA reference current is considered. It can be seen that such a fixed reference cannot guarantee the current within the boundaries during the whole period. On the other hand, with the help of the reference variants, the current is restricted within the boundaries imposed in the proposed strategy, which is shown in Figure 5.15(b). The current and voltage reference regions during the period 0.0238-0.024s in Figure 5.15(b) are shown in Figure 5.16. It reveals that one of the setting up reference variants, rather than the original reference, is finally selected and successfully brings the current back within the boundaries.

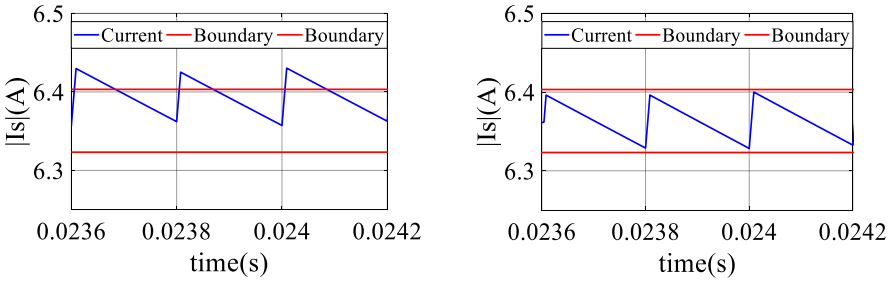

(a) Under the original MTPA reference (b) Under the proposed approach

Figure 5.15: Waveforms of the stator current amplitude.

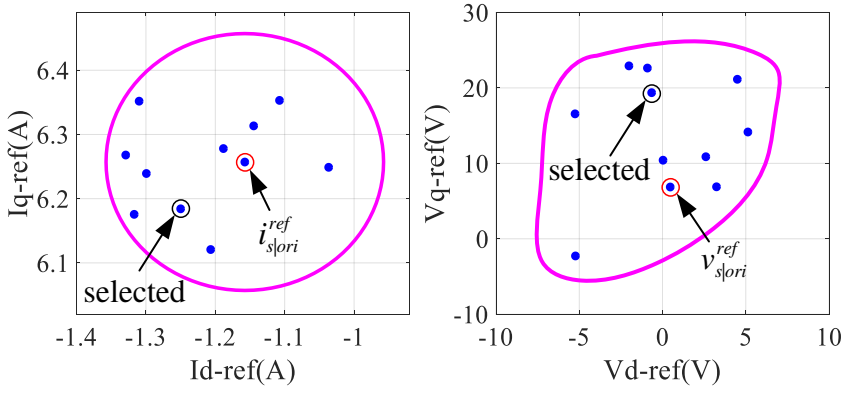

(a) Current reference region (b) Voltage reference region

Figure 5.16: Reference regions under the proposed strategy.

5.4.2 Comparison with RVV-MPC

Here, the proposed reference-variant-MPC is compared with the RVV-MPC which considers only a single reference point. Figure 5.17 and Figure 5.18 show the simulated waveforms of torque, dq-axis current and current amplitude under the RVV-MPC and the proposed reference-variant-MPC at 500 r/min, respectively. In order to show the dynamic performance, the load suddenly changes from 10 Nm to 10.5 Nm at t=0.15s. It can be found that in RVV-MPC, uneven fluctuations can be observed in the waveforms of the torque, q-axis current and the stator current amplitude.

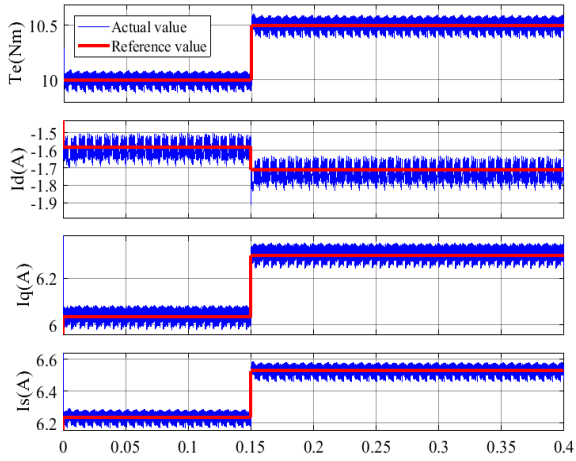

(a) Waveforms of torque, d-axis current, q-axis current and stator current amplitude

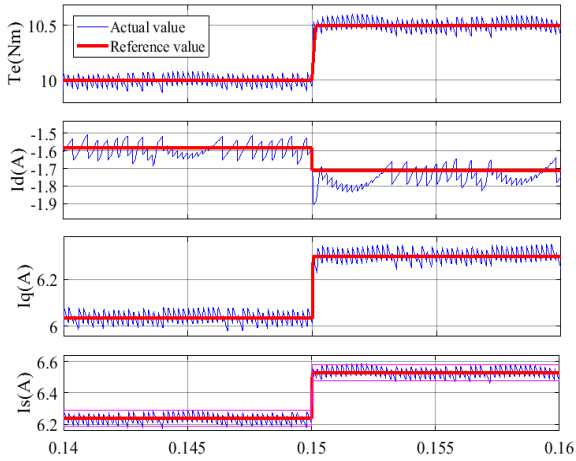

(b) Transient state between 0.14s and 0.16s

Figure 5.17: Simulated results under the RVV-MPC at 500 r/min.

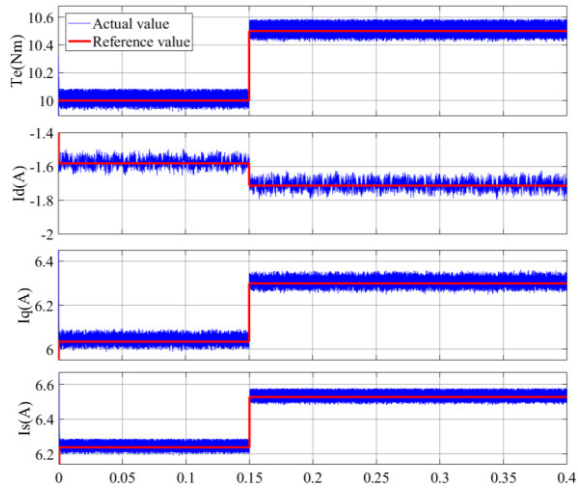

(a) Waveforms of torque, d-axis current, q-axis current and stator current amplitude

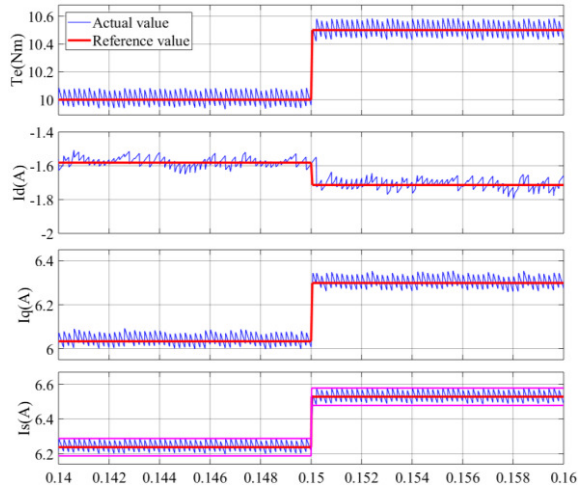

(b) Transient state between 0.14s and 0.16s

Figure 5.18: Simulated results under the proposed MPC at 500 r/min.

In Figure 5.18, with the help of the setting up reference variants and the current boundary limitation, the mean ripples of torque and current are reduced with the proposed MPC. The corresponding ripples are shown in Table 5.1. Moreover, due to the current boundary limitation, the stator current amplitude can be restricted within the certain tolerance boundaries, as shown in Figure 5.18(b). Besides, the overshoot of d-axis current, which can be seen in RVV-MPC at t=0.15s, is eliminated with the proposed MPC.

Table 5.1: Statistic results of steady-state performance

Method	T_e^{rip}	i_d^{rip}	i_q^{rip}	$\lvert i_s^{rip} \rvert$
RVV-MPC	0.0437Nm	0.0465A	0.0231A	0.0253A
Proposed MPC	0.0409Nm	0.0267A	0.0229A	0.0237A

In addition, the phase currents and the corresponding harmonic spectrums under the two MPC strategies are illustrated in Figure 5.19. It can be observed that even though both strategies have low THD, the proposed reference-variant-MPC can achieve lower THD rate compared to the RVV-MPC, which can further confirm the improvement of the proposed strategy. It is noted that in this simulation study, the improvement of the proposed reference-variant-MPC is not so much on reducing ripple or harmonic, but mainly being able to impose the boundaries.

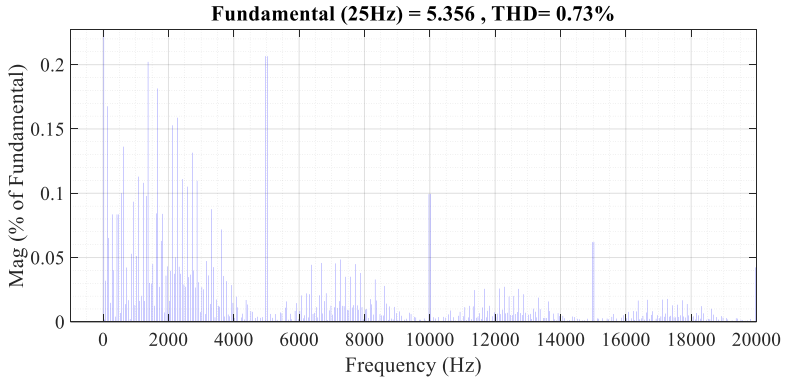

(a) RVV-MPTC

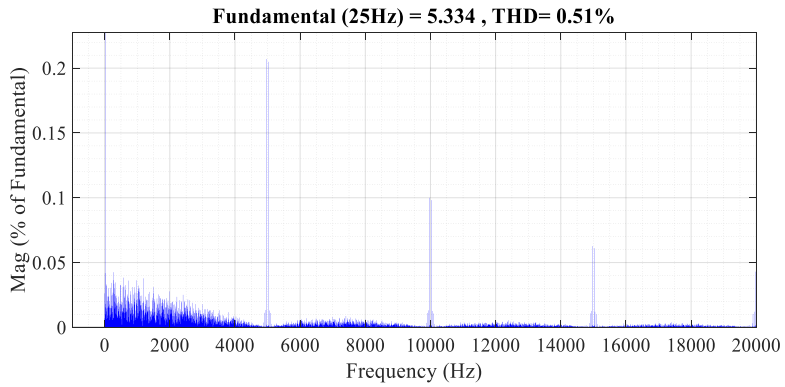

(b) Proposed reference-variant-MPTC

Figure 5.19: Phase currents and the harmonic spectrums under the two MPTC strategies.

5.4.3 Parameter Sensitivity

For an MPC strategy, the machine behaviors at the next control period are predicted based on the discrete machine model; therefore, the accuracy of motor parameters in the model is crucial for an MPC. However, there are some factors, such as flux saturation, system non-linearities, measurement error, or other disturbances that can affect the accuracy of the parameters. Such parameter uncertainties can result in prediction errors and affect the control performance.

Here, the parameter sensitivity is studied for the proposed reference-variant-MPC here to analyze the influence of parameter uncertainties on the control performance. In particular, resistance uncertainties are studied referring to temperature effects, PM flux uncertainties are investigated related to the back-EMF, as well as inductance uncertainties, due to a variable magnetic state of the machine (flux saturation) and frequency effects. Torque to reference torque and current to reference current amplitude are studied for stator resistance, permanent magnet flux, and dq-axis inductance uncertainty of ± 20% with respect to the rated values.

To study the influence on torque and current control of the uncertainty in a single parameter, this uncertainty is included within the simulation model and into the different MPC steps of the phases that require a model. Steps involving a model are the MTPA reference current vector generation, the deadbeat solution to obtain reference voltage vectors, and the model-based prediction. To better understand the impact, an additional in-depth study is conducted by varying the parameter only for one step in the MPC, while having the model for the remaining steps unvaried, referred to as the rated model.

Figure 5.20(a) shows the results when resistance uncertainties are involved in the models of all steps. The percentage torque and current errors occurring are negligible in the case of resistance uncertainty, which can be the result of the small voltage resistance drops with respect to the main voltages applied and the short control period with respect to the electrical time constant. Larger errors in Figure 5.20(a) can be explained at higher values of resistances as the voltage drop assumed and current prediction made deviate from those of the rated model. For resistance values below rated one, the current prediction is still affected while the effect of resistance voltage drops becomes even

smaller. It can be noticed from (5.17) that the MTPA reference generation does not require knowledge of stator resistance.

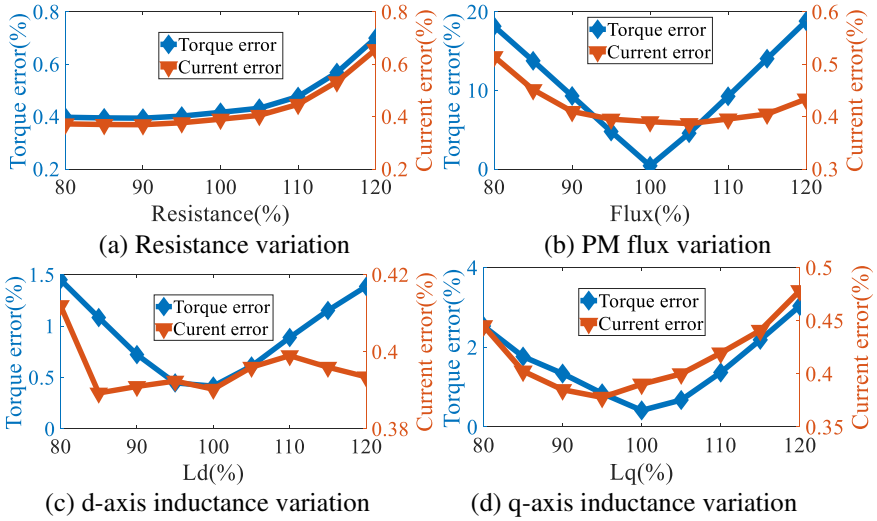

(a) Resistance variation (b) PM flux variation

(c) d-axis inductance variation (d) q-axis inductance variation

Figure 5.20: Analysis of parameter sensitivity for the proposed reference-variant-MPC.

The results for PM flux uncertainty are shown in Figure 5.20(b). Torque errors vary mainly linear with the flux identification error, which can be expected from PM flux being mainly a proportional factor in the torque function. For the torque setting given, an error in the PM flux value identified has a bigger and, for torque noticeable, impact compared to an identification mistake in the resistance. The PM flux is used in all three steps, and the uncertainty largely affects the outcome of the MTPA reference generation, and results in large deviations between the reference torque and actual torque.

The effects of d-axis and q-axis inductance uncertainties are shown in Figure 5.20(c) and Figure 5.20(d), respectively. It shows a similar trend for both inductances and with a rather symmetrical effect around the correct values. The impact of q-axis inductance uncertainty, however, is larger: a torque error rate of 3% can be seen for a q-axis inductance at 120% of the rated value, while this is half of it, 1.5%, for a d-axis inductance at 120%. This is the result of the salient pole PMSM used, being an IPMSM with a q-axis inductance more than twice the values of the d-axis inductance. Hence, a q-axis inductance

identification error has a higher proportional impact on the torque and MTPA reference generation than the d-axis identification error.

For prediction, the effect of inductance errors is inversely proportional to the predicted current (5.19-5.20) for which the highest current ripples can occur in the d-axis for the same voltage supplied. This could explain the asymmetrical trend in Figs. 5.20(c-d) for the current error. In addition, despite prediction errors occurring due to inductance uncertainties, the current measurements and feedback loop reduce the effect of such uncertainties. As a result, the main effect is to be found within the MTPA reference generation.

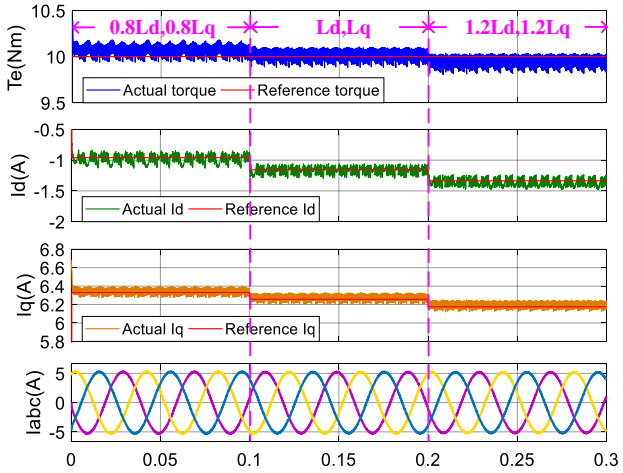

(a) RVV-MPC

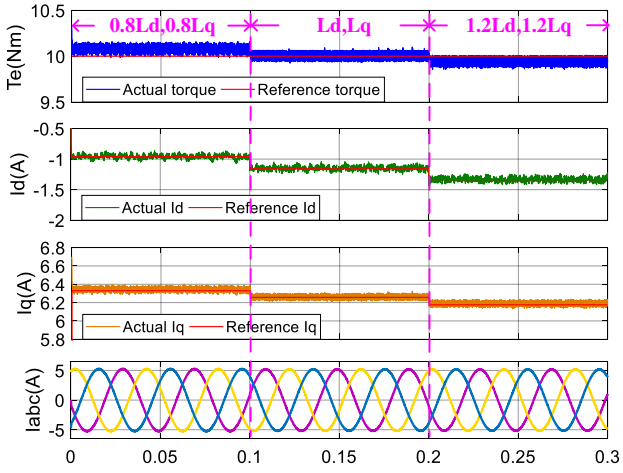

(b) Proposed reference-variant-MPC

Figure 5.21: Steady-state performance under different inductance values.

The parameter sensitivity of the proposed MPC is further compared to that of the conventional RVV-MPC. As discussed above, inductance uncertainty has a relatively great influence on steady-state performance. Different inductance values are introduced to the two strategies, and the results are shown in Figure 5.21. In the three phases, the d-axis inductance and q-axis inductance are set as 80%, 100%, and 120% of their nominal values. It can be seen that inductance uncertainties affect the generation of the MTPA reference. Additionally, the two strategies show similar performance under inductance uncertainties, revealing that the proposed MPC does not deteriorate the parameter sensitivity of the system compared to the conventional RVV-MPC.

Generally, the parameter dependence problem is a well-known challenge for MPCs. However, there are some alternative strategies introduced to deal with this problem. An effective alternative could be model-free predictive control, in which the system model is abandoned and instead online measured input/output data are used to predict the system behaviors. In this way, the parameter uncertainties caused by any disturbances can be avoided, and the influence of system non-linearities can also be eliminated.

5.5 Experimental Verification

The proposed reference-variant-MPC strategy is tested on a real PMSM drive setup, as shown in Figure 4.15, to verify its effectiveness. In the setup, a dSPACE MicroLabBox is used to execute the control algorithms. For the sake of analysis, all the measured data are monitored and saved from Controldesk, a dSPACE software, then transferred to Matlab/Simulink to be displayed. The motor parameters have been listed previously in Table 4.3. Additionally, to show the validity and the improvements of the proposed MPC, it is experimentally compared with the conventional RVV-MPC. The comparative results regarding steady-state performance are given in Section 5.5.1, and the results regarding dynamic performance are presented in Section 5.5.2.

5.5.1 Steady-State Performance

The steady-state performance of the proposed reference-variant-MPC strategy is investigated and compared with the conventional RVV-MPC.

Figure 5.22 shows the experimental results when the motor is operating at 300 r/min with rated load torque of 12 Nm. From top to bottom, the waveforms are torque, d-axis current, q-axis current, and stator current. It is noticed that the electromagnetic torque is estimated based on the measured currents and the torque equation (2.11). In Figure 5.22(a), it can be seen that there are oscillations in the waveforms of torque and q-axis current under the conventional RVV-MPC. Meanwhile, the ripple of the d-axis current is remarkable.

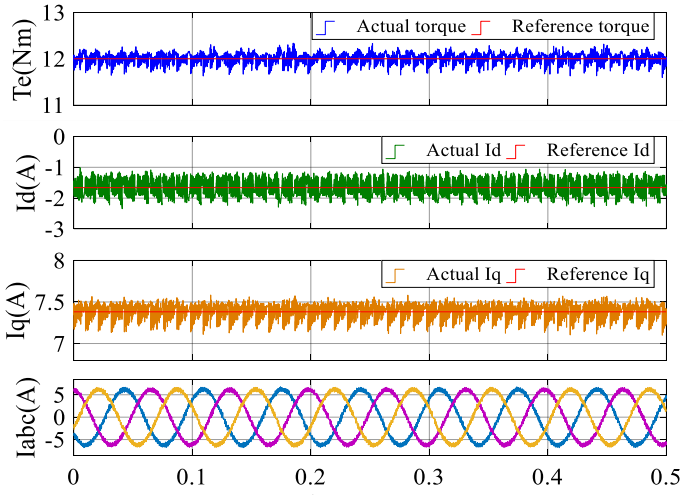

(a) RVV-MPC

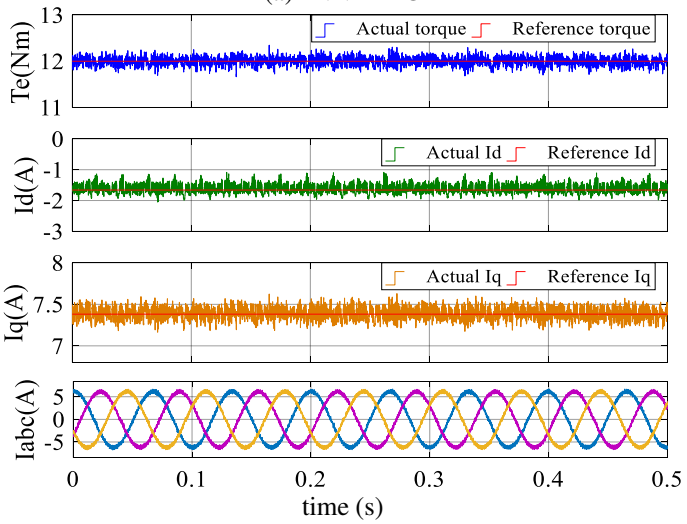

(b) Proposed reference-variant-MPC

Figure 5.22: Experimental results of torque, dq-axis current and stator current at 300 r/min.

On the other hand, more possible control actions are involved in the proposed reference-variant-MPC, the result of which is extra restraints on current can be added in the objective function. In Figure 5.22(b), the tolerance of stator current amplitude Δi_s^{tol} is set as 0.15 A. According to the objective function described in 5.3.6, a vector combination that can limit the stator current within the tolerance band over the whole control period will be optimally selected. Therefore, significant fluctuations and spikes are reduced in the waveforms of torque and dq-axis currents, which can be observed in Figure 5.22(b).

Table 5.2: Experimental results related to steady-state performance at 300 r/min

Method	T_e^{rip} (Nm)	i_d^{rip} (A)	i_q^{rip} (A)	$\lvert i_s^{rip}\rvert$ (A)	$\lvert \psi_s^{rip}\rvert$ (Wb)	f_{av} (kHz)
RVV-MPC	0.1043	0.2485	0.0835	0.0633	0.0020	5.17
Proposed MPC	0.0933	0.1522	0.0739	0.0560	0.0014	5.24

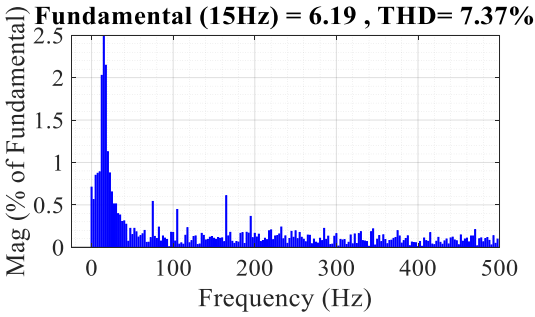

(a) RVV-MPC

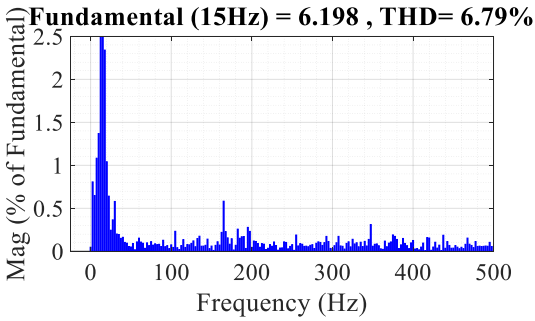

(b) Proposed reference-variant-MPC

Figure 5.23: Harmonic spectrums of stator current at 300 r/min.

The statistic results from Figure 5.22 are given. The average ripples of torque, dq-axis current, stator current amplitude that are calculated according to (4.22) and the average switching frequencies under the two MPC strategies are summarized in Table 5.2. The average switching frequency f_{av} is obtained by counting the total switching jumps N of the six VSI switches over a test period t_N and then calculating f_{av}=N/6/t_N. Due to the introduction of the reference variants and the current limitations, it can be seen from Table 5.2 that the steady-state performance of the proposed MPC strategy is improved compared to the RVV-MPC at a similar switching frequency. Also, Figure 5.23 shows the harmonic spectrums of the stator current under the two strategies. It can be observed that the THD of the proposed MPC is lower than that of RVV-MPC, which further confirms the improved steady-state performance of the proposed MPC strategy.

Figure 5.24 shows the comparative results of the two MPC strategies at 800 r/min at an 8 Nm load. The current spectrums are shown in Figure 5.25. The tolerance of the stator current amplitude Δi_s^{tol} in the proposed MPC is set as 0.4 A. The quantitative results are listed in Table 5.3. It can be seen that the proposed MPC still performs better in terms of torque and stator current compared to the RVV-MPC at a similar switching frequency. It can be confirmed that better steady-state performance is achieved with the proposed MPC strategy under different working conditions.

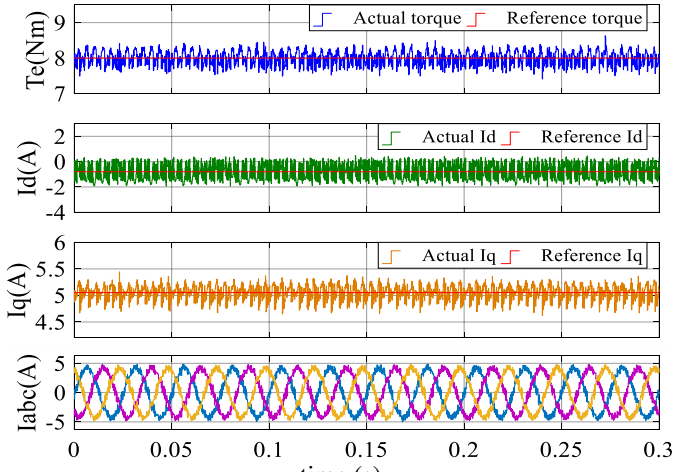

(a) RVV-MPC

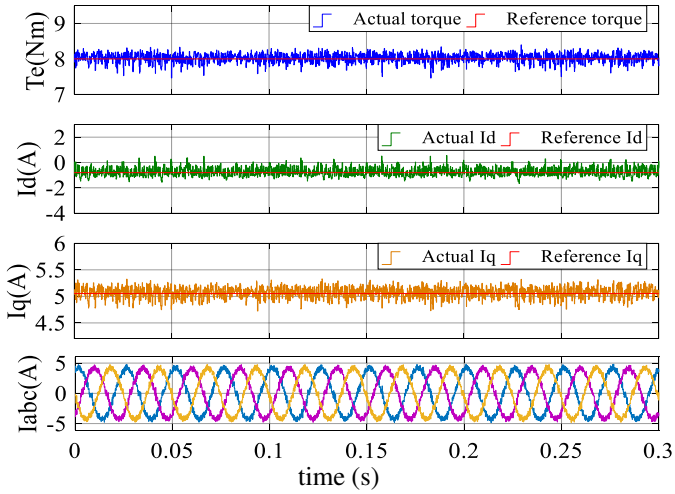

(b) Proposed reference-variant-MPC

Figure 5.24: Experimental results of torque, dq-axis current and stator current at 800 r/min.

Table 5.3: Experimental results related to steady-state performance at 800 r/min

Method	T_e^{rip} (Nm)	i_d^{rip} (A)	i_q^{rip} (A)	$\lvert i_s^{rip}\rvert$ (A)	$\lvert \psi_s^{rip}\rvert$ (Wb)	f_{av} (kHz)
RVV-MPC	0.1893	0.5894	0.1323	0.1259	0.00430	5.21
Proposed MPC	0.1290	0.3297	0.0988	0.0779	0.00278	5.33

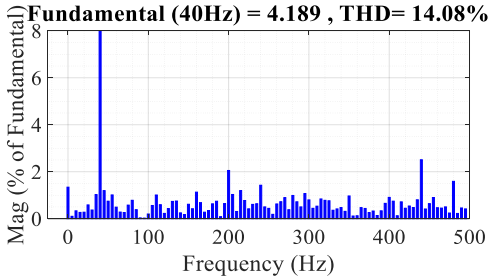

(a) RVV-MPC

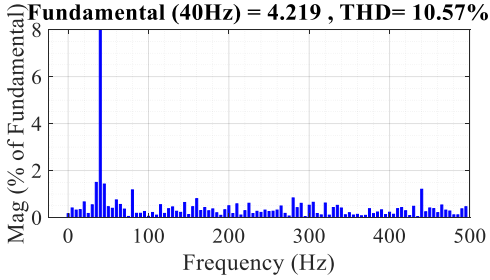

(b) Proposed reference-variant-MPC

Figure 5.25: Harmonic spectrums of stator current at 800 r/min.

5.5.2 Dynamic Performance

To demonstrate the dynamic performance, start-up tests are carried out for the two MPC strategies. The waveforms of speed, torque, stator flux amplitude, and stator current are shown in Figure 5.26. All the values are set at zero before motor start-up. It can be seen that the torque ripple and flux ripple increase during the process of start-up as the rotor speed increases. In addition, both strategies achieve fast torque and flux responses during the accelerating process from 0 to 400 r/min without considerable fluctuations or overshoots.

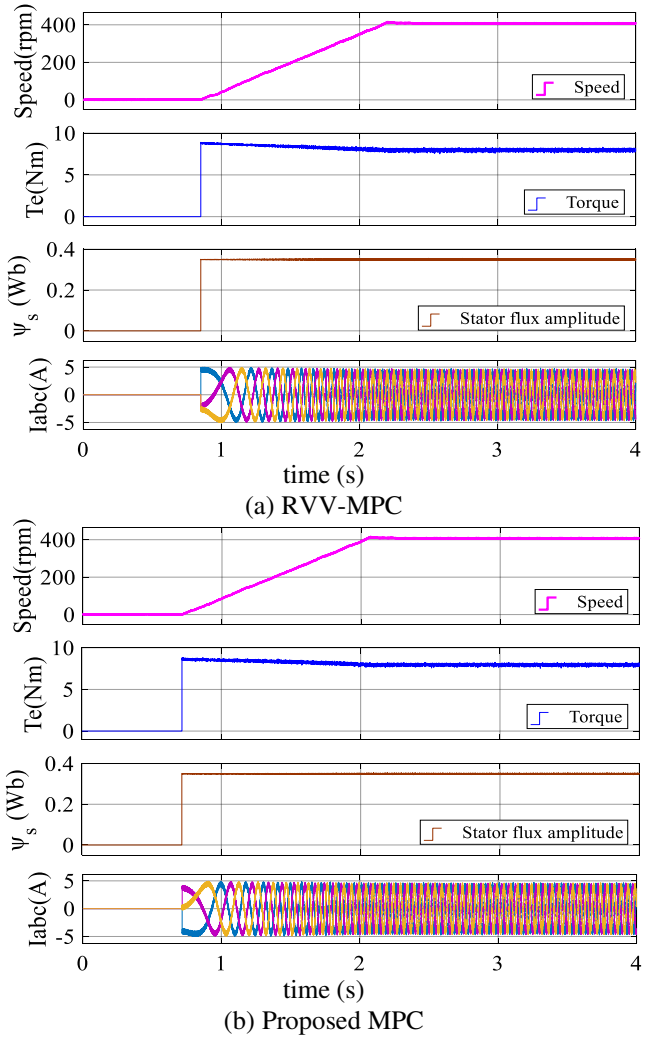

Figure 5.26: Dynamic performance comparison when speed changing.

Comparative tests are carried out when the load abruptly changes from 4 Nm to 10 Nm at 300 r/min, as shown in Figure 5.27. It can be seen in Figure 5.27(a) that there is an overshoot in the waveform of the d-axis current in the transient state during load changing under the conventional RVV-MPC. It takes 2 ms to reach the new steady state.

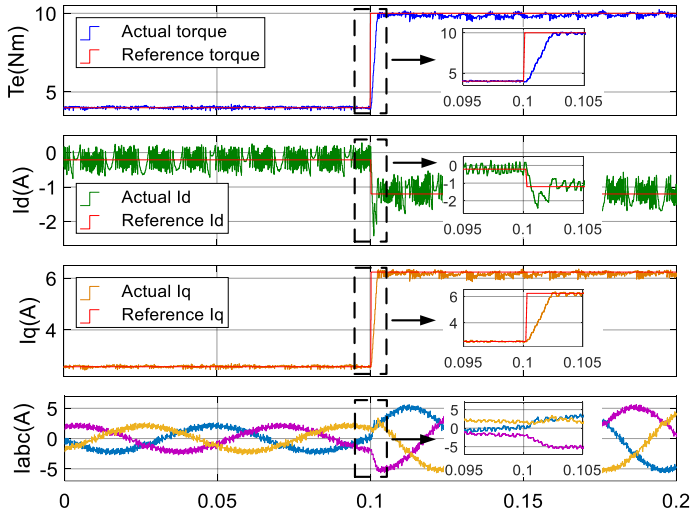

(a) RVV-MPC

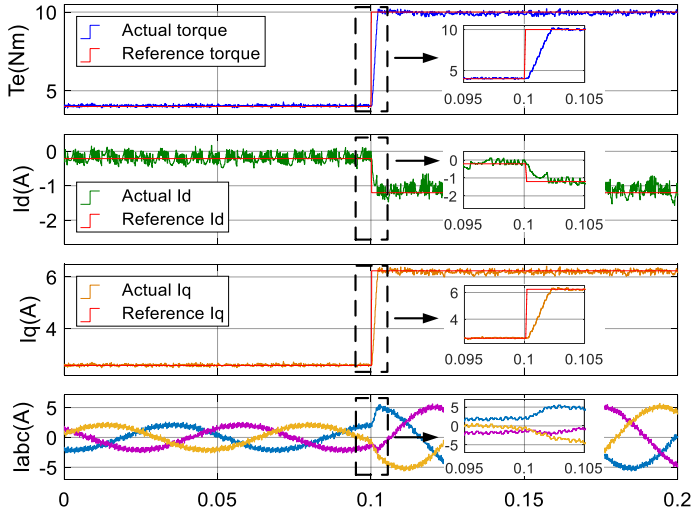

(b) Proposed MPC

Figure 5.27: Dynamic performance comparison when load changing.

In contrast, as more candidate solutions are provided with the proposed MPC, combined with the current boundary imposed in the objective function, a more suitable solution can be selected, which is helpful to improve the dynamic performance as well. The results under the proposed MPC strategy are illustrated in Figure 5.27(b). It can be seen that the overshoot of the d-axis current is eliminated, which verifies the better dynamical performance of the proposed MPC strategy.

5.6 Discussions on Characteristics of Different Control Schemes

The characteristics of different control strategies are discussed here. As previously mentioned, the MPC schemes applied to electric drives can be classified as a CCS-MPC and a FCS-MPC. In a CCS-MPC, a modulator is used to generate the desired voltage output from a continuous control signal [116-118]. On the other hand, FCS-MPC takes advantage of the discrete nature of power converters to solve an optimization problem. It has been revealed in [61] that, compared to conventional FOC, MPC can achieve a faster dynamic response due to the absence of internal current loops. In addition, the relationship between the voltage and the current is dependent on the magnetic state, and the tuning of the PI controllers in FOC is often done for the fixed magnetic state. However, when the magnetic state varies, the PI controllers are not optimally tuned any more. It means that FOC is sensitive to variable operating conditions. In contrast, MPC can cope with the variation of operating point through the use of model.

Generally, FCS-MPC has a finite number of control actions, whereas CCS-MPC has an infinite number of solutions and considers the duty cycle as the control action. Some comparative studies between FCS-MPC and CCS-MPC have been conducted [119-121]. The results indicate that both strategies can achieve good dynamic performance. The switching frequency of FCS-MPC is variable according to the operating conditions, whereas CCS-MPC has a fixed switching frequency [119]. On the other hand, the problem with CCS-MPC is that the constraint inclusion is not straightforward, whereas FCS-MPC can include additional constraints directly in the objective function [51, 120]. This problem also exists in the RVV-MPC, as only limited solutions can be provided with such strategy.

In contrast to a standard CCS-MPC and RVV-MPC, the proposed reference-variant-MPC strategy can provide a more flexible control structure to include additional constraints and nonlinearities in a straightforward way, thus being suitable and giving more potential to a multi-objective system. In addition, considering the utilization of two voltage vectors and the corresponding duty ratio optimization, a good control performance is also guaranteed with the proposed MPC strategy. This means that the proposed MPC inherits not only the good steady-state performance from CCS-MPC but also the inclusion of constraints from FCS-MPC, being a more flexible and effective MPC strategy.

For comparison, the main characteristics of FOC, standard FCS-MPC, standard CCS-MPC, conventional RVV-MPC, and the proposed MPC are summarized in Table 5.4. It can be seen that the proposed reference-variant-MPC can achieve fast dynamic response, low stead-state ripple, and high control flexibility simultaneously, giving an improved MPC strategy.

Table 5.4: Main Characteristics of Different Control Strategies

Item description	Dynamic response	Steady-state ripple	Sensitivity to variable operating point	Control flexibility
FOC	Slow	Low	Bad	Low, difficult to include constraints
Standard FCS-MPC	Fast	High	Good, due to the use of model	High, constraints can be included straightforwardly
Standard CCS-MPC	Fast	Low	Good, due to the use of model	Low, difficult to include constraints
Conventional RVV-MPC	Fast	Low	Good, due to the use of model	Low, difficult to include constraints
Proposed MPC	Fast	Low	Good, due to the use of model	High, constraints can be included straightforwardly

5.7 Conclusions

In this chapter, the simplification of conventional FCS-MPC is firstly discussed by introducing a RVV-MPC. Even though such strategy can reduce the computational burden, the flexible control structure of a FCS-MPC is impacted, as additional constraints are less likely to be included with this RVV-MPC. Thus, the development of the RVV-MPC is studied and a reference-variant-MPC is then introduced.

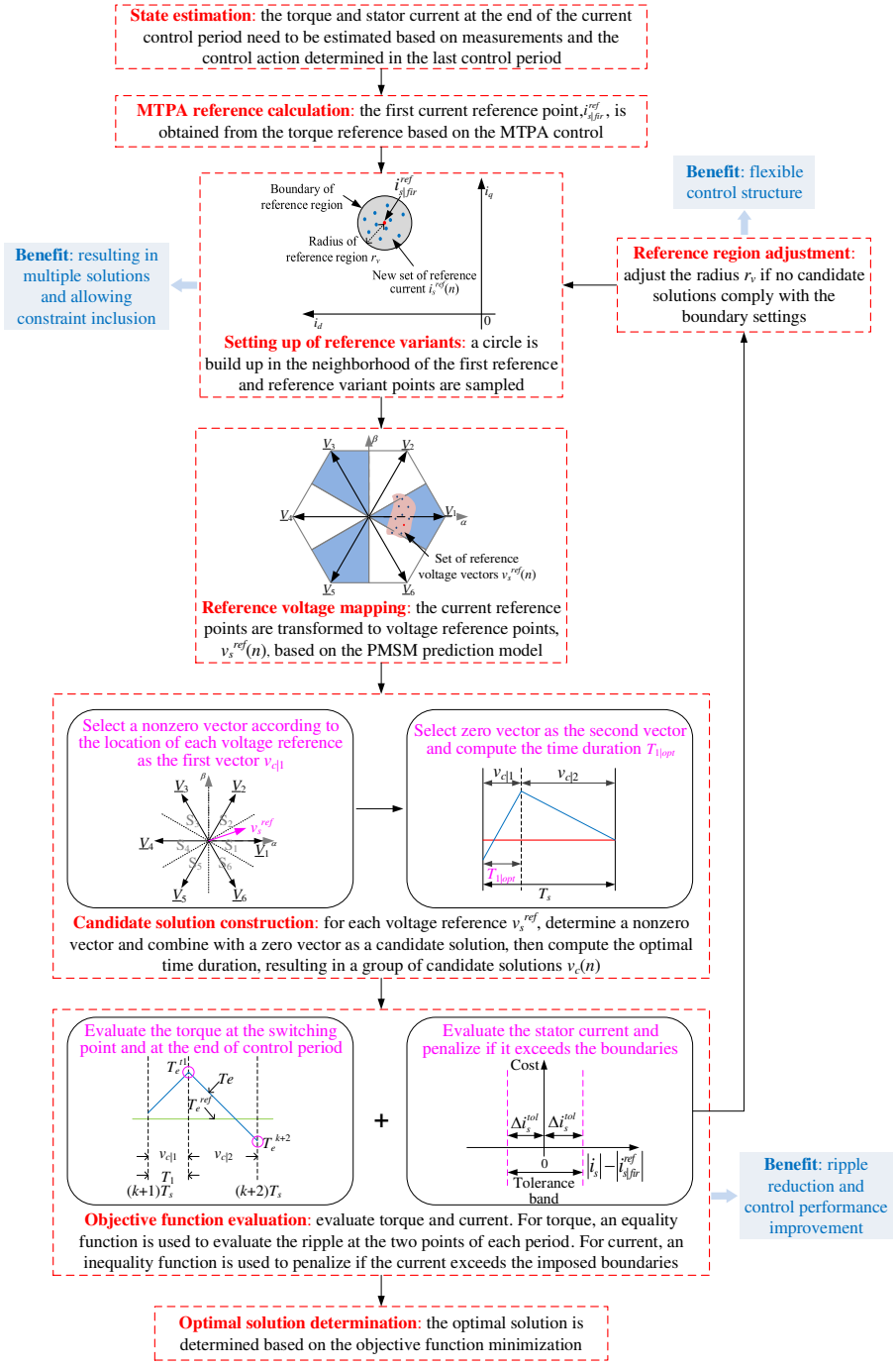

Figure 5.28: Illustration of the proposed reference-variant-MPC and its benefits.

In the conventional FCS-MPC strategies, especially RVV-MPC, additional boundaries are difficult to include due to a missing freedom in input references. In this study, a current-reference-variant based MPC strategy is proposed to deal with such problem. Based on the introduction of adaptive MTPA current reference variants, current boundaries can be included in the objective function, in an effort to truly comply to such boundaries, even if this would mean a deviation from the current reference. An optimization strategy is given in which the region of current references can be adjusted by proper assessment of the control outcome, resulting in a flexible control structure. These benefits are linked to Figure 1.4, the second block of Level 5. The whole scheme and its main benefits are illustrated in Figure 5.28.

As the MPC method proposed relies on an accurate model, a parameter sensitivity of the proposed strategy is analyzed in this work. The results show that uncertainties concerning the PM flux value and value of the largest qd-inductance have a non-neglectable impact on the torque and current performance. In addition, experimental results reveal that the proposed MPC strategy can track the reference torque and reference current well and outperforms conventional RVV-MPC by resulting in bounded and lower ripples. Compared to the RVV-MPC, the proposed reference-variant-MPC reduces the average torque ripple, d-axis current ripple and q-axis current ripple from 0.1893 Nm, 0.5894 A and 0.1323 A to 0.129 Nm, 0.3297 A and 0.0988 A, respectively, at 800 r/min with an 8 Nm load. With the help of the current boundaries, the dynamic control performance is improved as well, as is shown by the elimination of current overshoot during a torque step transient.

Chapter 6
Current-Difference Sample Based Predictive Current Control

6.1 Introduction

In Chapter 4 and Chapter 5, a boundary-based MPTC and a reference-variant-MPC are introduced, respectively. Such MPCs are model-based approaches that highly depend on system mathematical model. However, the model quality cannot always be guaranteed. For PMSM system, motor parameters maybe inaccurate due to measurement error or they may change due to the variable operating state, e.g. variable temperature and magnetic state. The parameter dependence problem is third disadvantage of conventional MPC to be countered in this thesis (see Figure 1.4, the third block of Level 1).

In Section 4.4.7 and Section 5.4.3, the proposed MPC strategies are tested with motor parameter uncertainties. It can be seen that the parameter uncertainties affect the accuracy of predictions and further impact the control performance. For example, the torque ripple under the proposed torque boundary based MPTC with different parameter values is analyzed in Section 4.4.7. The results show that the torque ripple is about 0.5% when the rated q-axis inductance value is used, while the ripple increases to 2.7% in case the q-axis inductance is set as 60% of its nominal value. Considering the control performance degradation caused by parameter uncertainties, improved predictive control with enhanced parameter robustness is then desired. Therefore, the goal of this chapter is the adaption to counter the influence of

parameter uncertainties with predictive control. This will be fulfilled by introducing a current-difference sample based predictive control that depends on online sampled current differences rather than system parameters.

In [40], the parameter sensitivity of MPCC is analyzed for PMSM. It concludes that the current predictions can be significantly affected by incorrect motor inductances. In contrast, the influence of resistance inaccuracy on the control performance is relatively weak. The results of the parameter sensitivity analysis presented in Section 4.4.7 and Section 5.4.3 also confirm this conclusion. Some robust MPCC strategies with inductance disturbance observers have therefore been proposed for the purpose of online parameter identification [40-42]. However, although the inductance parameter mismatch can be reduced by employing observers, this introduction increases the complexities of the control strategies due to the involvement of additional parameters.

Instead of using an observer, an alternative solution that utilizes a newly designed objective function in PI form is proposed in [122] to improve the robustness of MPCC. In such a strategy, the past current tracking errors and future tracking errors are included in the objective function to be evaluated. A reduction of the steady-state error caused by parameter mismatches can be then achieved. However, the PI-based controller involves additional coefficients to be tuned, although a selective optimization method is introduced in such a strategy to facilitate the design of integral coefficients. In addition, the convergence problem is also needed to be considered for a PI-based controller.

On the other hand, a Current-Difference Sample Based Predictive Current Control (CDSPCC) is proposed in [123] to eliminate the influence of parameter uncertainties (linked to Figure 1.4, the third block of Level 2). This scheme predicts the optimal control input based on the present and previous input/output data without the need of a system model, which is required in a conventional MPCC [124]. In [123], the traditional model-based prediction is abandoned. Instead, the current differences caused by each voltage vector over a control period are stored in two LUTs for the d-axis and q-axis, respectively. Then, assuming that a subsequent current difference is equal to the previous one due to the same voltage vector, the predictions of the stator current can be approximately obtained based on the measured currents and the stored current differences. In this way, only measured data are required, thereby skipping the motor parameters and system nonlinearities.

Because the accuracy of the current prediction depends on the information in the LUTs, which must be updated online, the reliability of the LUTs is quite important for this approach. In [123], however, because only the current difference caused by the applied voltage vector can be updated in one control period, the other elements in the LUT will be stagnant. Even worse, if a voltage vector is not applied over many periods, a long stagnation can therefore result in unreliable predictions and even impact the system stability. Generally, the control performance is impacted with such a conventional CDSPCC (pointed out in Figure 1.4 with the third block of Level 3).

The same problem can also occur in the robust predictive current control presented in [125], which includes a prediction error correction. To lessen the impact of this stagnation effect in the CDSPCC, a minimum updating frequency is defined in [126], such that a voltage vector must be applied in the next control period if it has not been selected in a predefined number of past periods. However, the updating frequency for the LUTs is still not sufficient with this method, as it is related to the defined number of periods. Furthermore, applying a non-optimal voltage vector frequently will cause a negative impact on the control performance. Therefore, such a conventional CDSPCC requires further developments and improvements.

To enhance the reliability of the LUTs, an indirect LUT reconstruction approach is proposed in [127, 128]. In such strategies, the current differences caused by the last three applied voltage vectors are used to estimate the current differences for the remaining vectors. However, this update can be fulfilled only when the three successive voltage vectors are different from each other, such that the LUT update can be corrupted if only two voltage vectors are activated for many periods, which often occurs in conventional MPCC and CDSPCC. In addition, to reconstruct the LUTs, all the possible vector sequences (up to 210) need to be considered. This means additional efforts are required to reduce the computational burden to improve the feasibility of this strategy.

In this work, an improved CDSPCC is proposed for PMSM drives by introducing an advanced current difference updating mechanism (linked to Figure 1.4, the third block of Level 4). Such a CDSPCC does not require a mathematical model, and instead employs information about the current differences to predict future currents. In this way, the impact of motor parameter mismatches can be strongly reduced. The accuracy of the current differences can be considered as key to this strategy.

In this chapter, the relationship between the current difference and the applied voltage vector is first analyzed. The current differences can be then derived for all the voltage vectors in one control period by further analyzing the relationships between the applied voltage vector and the other vectors. As a result, the stagnation problem that exists in the conventional CDSPCC can be effectively solved by keeping all the current difference information up to date.

Compared to [127, 128], which require three successive current differences, the proposed mechanism utilizes samples from only two control periods to update all the LUT elements, significantly reducing the stagnation caused by having only two voltage vectors applied for long intervals. In addition, in contrast to [127, 128], which involve considering all the possible vector sequences and taking action according to a predefined LUT, here, the current difference update is performed based on equations with basic mathematical operators. With reliable information about current differences, the future currents can be accurately predicted and improved control performance therefore can be achieved. This strategy can prove valuable under conditions where the motor parameters cannot be properly given.

In the following, the current-difference based predictive control will be discussed in detail. First, the parameter sensitivity of model-based predictive current control is analyzed in 6.2. Then, the current-difference based predictive current control will be presented in 6.3. It includes the basic principle, the current difference construction in conventional methods and the proposed current difference estimation approach. The proposed strategy is validated by experiment studies and the results are presented in 6.4. Finally, some conclusions are given in 6.5.

6.2 Parameter Sensitivity Analysis for Model Predictive Current Control

The principle of a model predictive torque control has been introduced in Section 3.3, and it has been explained the main difference between a torque control and a current control is the control variable. The current estimation and current prediction are given as (3.20) and (3.23), respectively, and the objective function of a conventional MPCC is given as (3.25).

Conventional MPCC is dependent on a PMSM model that includes motor parameters (resistance, inductance, and PM flux linkage). It means that MPCC is parameter sensitive. The system performance can be directly affected by the accuracy of the prediction model. In order to evaluate how the MPCC is sensitive to a parameter mismatch, the parameter sensitivity of a MPCC is studied here.

Based on the current estimation model (3.20), if parameter mismatch exists, the current estimation model can be represented as:

$$\begin{aligned}
\tilde{i}_d^{k+1'} &= i_d^k - \frac{(R_s+\Delta R_s)T_s}{(L_d+\Delta L_d)} i_d^k + \frac{(L_q+\Delta L_q)T_s\omega_r}{(L_d+\Delta L_d)} i_q^k + \frac{T_s}{(L_d+\Delta L_d)} v_d^k \\
\tilde{i}_q^{k+1'} &= i_q^k - \frac{(R_s+\Delta R_s)T_s}{(L_q+\Delta L_q)} i_q^k - \frac{(L_d+\Delta L_d)T_s\omega_r}{(L_q+\Delta L_q)} i_d^k + \frac{T_s}{(L_q+\Delta L_q)} v_q^k \\
&\quad - \frac{(\psi_f+\Delta\psi_f)T_s\omega_r}{(L_q+\Delta L_q)}
\end{aligned} \tag{6.1}$$

where ΔR_s, ΔL_d, ΔL_q and $\Delta\psi_f$ are the parameter uncertainties added in the current estimation model. Then, the estimation errors between the accurate model (3.20) and the model including parameter uncertainties can be derived as:

$$\begin{aligned}
E_d^{k+1} &= \tilde{i}_d^{k+1'} - \tilde{i}_d^{k+1} = \frac{(R_s\Delta L_d - L_d\Delta R_s)T_s}{L_d(L_d+\Delta L_d)} i_d^k + \frac{(L_d\Delta L_q - L_q\Delta L_d)T_s\omega_r}{L_d(L_d+\Delta L_d)} i_q^k \\
&\quad - \frac{T_s\Delta L_d}{L_d(L_d+\Delta L_d)} v_d^k \\
E_q^{k+1} &= \tilde{i}_q^{k+1'} - \tilde{i}_q^{k+1} = \frac{(R_s\Delta L_q - L_q\Delta R_s)T_s}{L_q(L_q+\Delta L_q)} i_q^k + \frac{(L_d\Delta L_q - L_q\Delta L_d)T_s\omega_r}{L_q(L_q+\Delta L_q)} i_d^k \\
&\quad - \frac{T_s\Delta L_q}{L_q(L_q+\Delta L_q)} v_q^k + \frac{(\psi_f\Delta L_q - L_q\Delta\psi_f)T_s\omega_r}{L_q(L_q+\Delta L_q)}
\end{aligned} \tag{6.2}$$

It can be seen from (6.2) that parameter uncertainty can lead to current estimation error. In addition, such estimation error will be further involved in the current prediction. Considering the current estimation error, the current prediction model including parameter uncertainties can be expressed as:

$$\begin{aligned}
\hat{i}_d^{k+2'} &= [1-\frac{(R_s+\Delta R_s)T_s}{(L_d+\Delta L_d)}](\tilde{i}_d^{k+1}+E_d^{k+1})+\frac{(L_q+\Delta L_q)T_s\omega_r}{(L_d+\Delta L_d)}(\tilde{i}_q^{k+1}+E_q^{k+1}) \\
&\quad +\frac{T_s}{(L_d+\Delta L_d)}v_d^{k+1} \\
\hat{i}_q^{k+2'} &= [1-\frac{(R_s+\Delta R_s)T_s}{(L_q+\Delta L_q)}](\tilde{i}_q^{k+1}+E_q^{k+1})-\frac{(L_d+\Delta L_d)T_s\omega_r}{(L_q+\Delta L_q)}(\tilde{i}_d^{k+1}+E_d^{k+1}) \\
&\quad +\frac{T_s}{(L_q+\Delta L_q)}v_q^{k+1}-\frac{(\psi_f+\Delta\psi_f)T_s\omega_r}{(L_q+\Delta L_q)}
\end{aligned} \tag{6.3}$$

Accordingly, the current prediction error can be then obtained by subtracting (3.23) from (6.3) as:

$$\begin{aligned}
E_d^{k+2} &= [1-\frac{(R_s+\Delta R_s)T_s}{(L_d+\Delta L_d)}]E_d^{k+1}+\frac{(R_s\Delta L_d-L_d\Delta R_s)T_s}{L_d(L_d+\Delta L_d)}\tilde{i}_d^{k+1} \\
&\quad +\frac{(L_d\Delta L_q-L_q\Delta L_d)T_s\omega_r}{L_d(L_d+\Delta L_d)}\tilde{i}_q^{k+1}+\frac{(L_q+\Delta L_q)T_s\omega_r}{L_d+\Delta L_d}E_q^{k+1} \\
&\quad -\frac{T_s\Delta L_d}{L_d(L_d+\Delta L_d)}v_d^{k+1} \\
E_q^{k+2} &= [1-\frac{(R_s+\Delta R_s)T_s}{(L_q+\Delta L_q)}]E_q^{k+1}+\frac{(R_s\Delta L_q-L_q\Delta R_s)T_s}{L_q(L_q+\Delta L_q)}\tilde{i}_q^{k+1} \\
&\quad +\frac{(L_d\Delta L_q-L_q\Delta L_d)T_s\omega_r}{L_q(L_q+\Delta L_q)}\tilde{i}_d^{k+1}-\frac{(L_d+\Delta L_d)T_s\omega_r}{L_q+\Delta L_q}E_d^{k+1} \\
&\quad -\frac{T_s\Delta L_q}{L_q(L_q+\Delta L_q)}v_q^{k+1}+\frac{(\psi_f\Delta L_q-L_q\Delta\psi_f)T_s\omega_r}{L_q(L_q+\Delta L_q)}
\end{aligned} \tag{6.4}$$

It can be seen from (6.4) that the current prediction error is further expanded with the error involved current estimation, which can impact the control performance. Thus, to eliminate the impact of parameter uncertainties on the system performance, it is necessary to develop an improved prediction control strategy that is insensitive to parameter uncertainties.

6.3 Current Difference Sample Based Predictive Current Control

6.3.1 Basic Principle

In MPCC, the current estimations and predictions are both parameter dependent. However, the motor parameters may be inaccurate due to measurement error or they may vary due to the changes in operating conditions. Such parameter uncertainties can result in estimated and predicted error, which can further influence the control performance. Therefore, CDSPCC, able to avoid the influence of parameter uncertainties by using measured data without system parameters, is introduced. In this strategy, the current estimation can be expressed as:

$$\tilde{i}_{s|j}^{k+1} = i_s^k + \Delta i_j^k \tag{6.5}$$

where $i_s^k = [i_d^k, i_q^k]^T$ is the measured stator current vector at kT_s and $\tilde{i}_{s|j}^{k+1} = [\tilde{i}_{d|j}^{k+1}, \tilde{i}_{q|j}^{k+1}]^T$ is the estimated current vector at $(k+1)T_s$ under the voltage vector applied in kT_s, $\underline{V}_j^k$, $j \in \{0,1,...,7\}$, which is determined in the last control period. Because each of the eight voltage vectors results in current difference on the d-axis and q-axis, which can be measured, all the current differences can be stored in two LUTs for current estimations and predictions. Thus, $\Delta i_j^k = [\Delta i_{d|j}^k, \Delta i_{q|j}^k]^T$ in (6.5) denotes the current difference caused by the $\underline{V}_j^k$. Then, the current at the start of $(k+2)T_s$ can be predicted as:

$$\hat{i}_{s|j}^{k+2} = \tilde{i}_{s|j}^{k+1} + \Delta i_j^{k+1} \tag{6.6}$$

where $\hat{i}_{s|j}^{k+2} = [\hat{i}_{d|j}^{k+2}, \hat{i}_{q|j}^{k+2}]^T$ is the predicted current at $(k+2)T_s$ under the voltage vector applied in $(k+1)T_s$, $\underline{V}_j^{k+1}$, $j \in \{0,1,...,7\}$, and $\Delta i_j^{k+1} = [\Delta i_{d|j}^{k+1}, \Delta i_{q|j}^{k+1}]^T$ is the current difference caused by the $\underline{V}_j^{k+1}$.

6.3.2 Current Difference Construction in Conventional Methods

On the basis of the introduction above, it can be concluded that the current differences under all the candidate voltage vectors are the most important factors for the CDSPCC, as their accuracy can directly affect the current estimations and current predictions. However, as only one voltage vector is applied in a control period, measured current difference can be obtained for this applied voltage vector only. Thus, the current difference constructions for the remaining voltage vectors need to be considered.

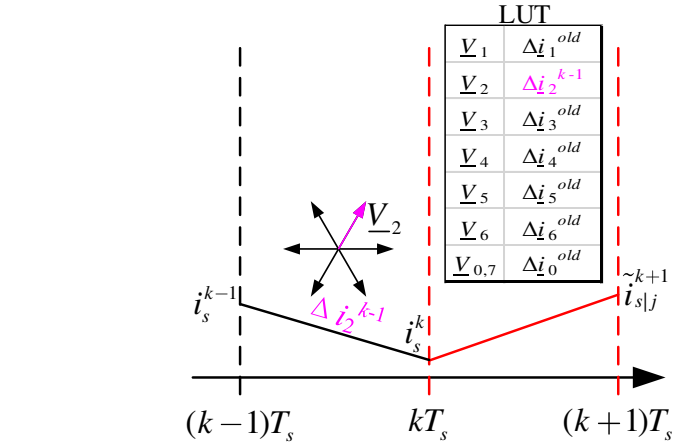

(a) Method in [123]

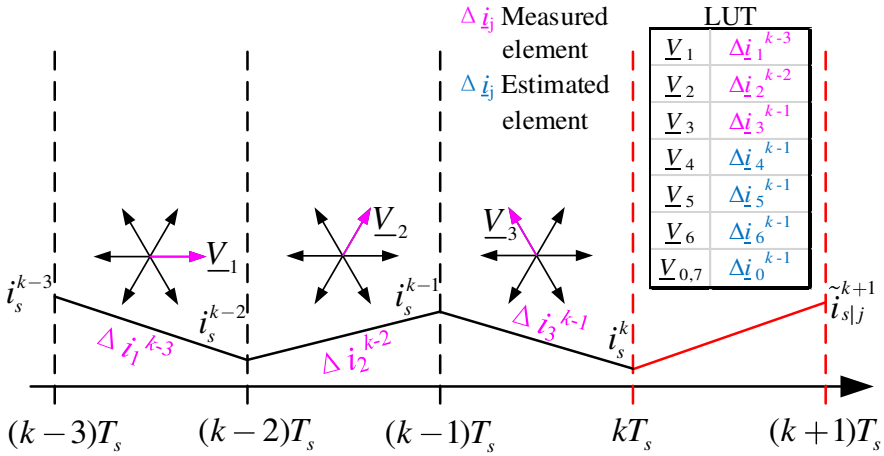

(b) Method in [127, 128]

Figure 6.1: Mechanism of current-difference construction in prior methods.

Figure 6.1(a) illustrates the current difference updating mechanism in [123]. In this strategy, once one of the voltage vectors is applied over a control period, the resulting current difference is updated in an LUT, whereas the remaining elements are approximated as the old values. Stagnation then occurs with updates to the current differences under the unapplied voltage vectors. Even worse, if a voltage vector is not applied for many control periods, the long stagnation could even impact the stability of the control system. Thus, a minimum updating frequency is guaranteed in [126] by applying a voltage vector in the next period if it has not been activated during a defined time frame. Nevertheless, because the minimum updating frequency is linked to a predefined time frame, the improvement on the stagnation problem is limited. Moreover, applying a non-optimal voltage vector frequently can result in current ripples and worsen the control performance of the system.

In [127, 128], to increase the LUT updating frequency, the last three measured current differences are used to reconstruct the four under the remaining four voltage vectors, this principle is illustrated in Figure 6.1(b). A stringent requirement in this approach, however, is that the last three voltage vectors applied must be different from one another. This means that two different voltage vectors alternately applied for a long interval could corrupt this mechanism, resulting in stagnation. A typical case that often occurs in an MPC is shown in Figure 6.2.

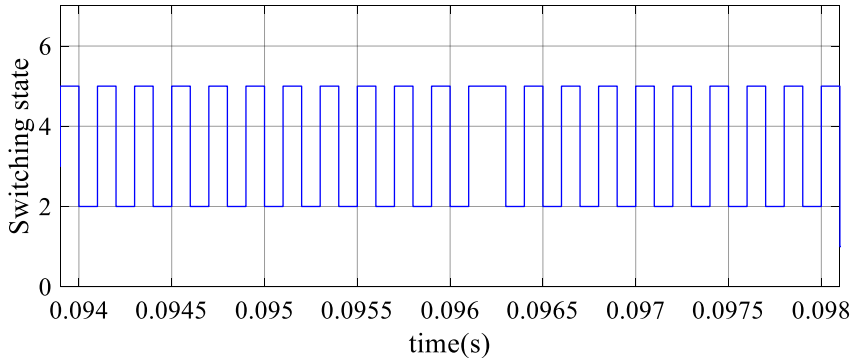

Figure 6.2: Two voltage vectors applied for long intervals that can result in stagnation in [127, 128].

This requirement can limit the LUT updating frequency of this approach. Furthermore, this approach necessitates identifying all the possible combinations of three-state voltage vectors, which means 210

different vector sequences that need to be considered. Thus, to avoid such considerable computations in each control period, a more selective algorithm is required. Even though an identification mechanism that can classify all the vector combinations into six groups is reported in [128], a more intuitive current-difference updating approach that depends on simple computations is desirable.

Due to the aforementioned disadvantages, an improved current difference updating mechanism that uses two succeeding current differences to estimate the remaining ones is proposed in this work. This more effective method will be introduced hereafter.

6.3.3 Proposed Current Difference Updating Mechanism

6.3.3.1 Relationship Between Applied Voltage Vector and Current Difference

In order to provide reliable and accurate current differences under different voltage vectors, an advanced estimating approach is proposed in this paper, which aims to maximize the LUT updating frequency. To this end, the current difference due to the applied voltage vector is first investigated.

Because the mechanical time constant τ_m is much larger than the electrical time constants $\tau_d = L_d / R_s$ and $\tau_q = L_q / R_s$, the mechanical speed can be assumed constant over a few time steps and $\omega_r = \omega_{r0} = \Omega$, with ω_{r0} being the electrical rotor speed in the steady state. The steady-state model of PMSM can be described as:

$$\begin{aligned} V_{sd} &= R_s I_{sd} - \Omega L_q I_{sq} \\ V_{sq} &= R_s I_{sq} + \Omega L_d I_{sd} + \Omega \psi_f \end{aligned} \tag{6.7}$$

where V_{sd} and V_{sq} are the steady-state voltage components, I_{sd} and I_{sq} are the steady-state current components. By subtracting the steady-state PMSM model from the voltage model, a small-signal model of PMSM can be deduced as [129]

$$\begin{aligned}\frac{d}{dt}\delta i_d &= \frac{1}{L_d}Dv_d - \frac{R_s}{L_d}\delta i_d + \Omega\frac{L_q}{L_d}\delta i_q \\ \frac{d}{dt}\delta i_q &= \frac{1}{L_q}Dv_q - \frac{R_s}{L_q}\delta i_q - \Omega\frac{L_d}{L_q}\delta i_d\end{aligned} \tag{6.8}$$

where $\delta i_d = i_d - I_{sd}$, $\delta i_q = i_q - I_{sq}$ are small current deviations from the steady state, $Dv_d = v_d - V_{sd}$, $Dv_q = v_q - V_{sq}$ are voltage deviations from the steady state. Here, the voltage deviations Dv_d and Dv_q is to be regarded as step functions with amplitude DV_d and DV_q, respectively. Based on (6.8), if one of the basic voltage vectors $\underline{V}_j = [V_{d|j}, V_{q|j}]^T, j \in \{0,1,...,7\}$, is applied for one control period $T_s \ll \min(\tau_d, \tau_q)$, it is shown in [129] that the time gradients of the resulting current deviations $\delta i_{d|j}$ and $\delta i_{q|j}$ can be approximated as:

$$\begin{aligned}\frac{d\delta i_{d|j}}{dt} &= \frac{DV_{d|j}}{L_d} \\ \frac{d\delta i_{q|j}}{dt} &= \frac{DV_{q|j}}{L_q}\end{aligned} \tag{6.9}$$

For a control period T_s, (6.9) can be written as:

$$\begin{aligned}\Delta\delta i_{d|j} &= \frac{T_s}{L_d}DV_{d|j} \\ \Delta\delta i_{q|j} &= \frac{T_s}{L_q}DV_{q|j}\end{aligned} \tag{6.10}$$

Considering $\Delta\delta i_{d|j} = \delta i_{d|j}^{t=T_s} - \delta i_{d|j}^{t=0}$, $\delta i_{d|j}^{t=T_s} = i_{d|j}^{t=T_s} - I_{sd}$, $\delta i_{d|j}^{t=0} = i_{d|j}^{t=0} - I_{sd}$ and $\Delta\delta i_{q|j} = \delta i_{q|j}^{t=T_s} - \delta i_{q|j}^{t=0}$, $\delta i_{q|j}^{t=T_s} = i_{q|j}^{t=T_s} - I_{sq}$, $\delta i_{q|j}^{t=0} = i_{q|j}^{t=0} - I_{sq}$, (6.10) can be rewritten as:

$$\begin{aligned}\Delta i_{d|j} &= \frac{T_s}{L_d}DV_{d|j} \\ \Delta i_{q|j} &= \frac{T_s}{L_q}DV_{q|j}\end{aligned} \tag{6.11}$$

where $\Delta i_{d|j} = i_{d|j}^{t=T_s} - i_{d|j}^{t=0}$, $\Delta i_{q|j} = i_{q|j}^{t=T_s} - i_{q|j}^{t=0}$ are the dq-axis current differences over T_s due to the applied voltage vector $\underline{V}_j$.

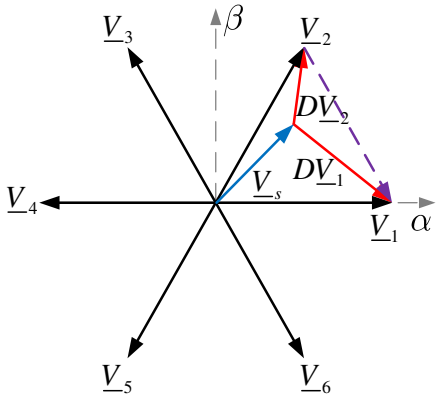

Figure 6.3: Principle of voltage deviation.

It can be seen from (6.11) that the current difference is related to the voltage deviation, which is the difference between the voltage vector and the steady-state voltage, as shown in Figure 6.3. If the applied voltage vector $\underline{V}_j$ is $\underline{V}_1$, the voltage deviation $D\underline{V}_1$ should be the difference between $\underline{V}_1$ and the steady-state voltage $\underline{V}_s = [V_{sd}, V_{sq}]^T$. However, estimating $\underline{V}_s$ would introduce error that can affect the current difference estimation in a negative way. Thus, avoiding the use of the steady-state voltage $\underline{V}_s$ is desired here. As shown in (6.7), the steady-state voltage contains the voltage drop on the stator resistor and the back EMF. It is noted that, even though current is fast variable that may change during adjacent control periods, the resulting variation of voltage drop across the resistor is still negligible, compared to the steady-state voltages, V_{sd} and V_{sq}. In addition, it has been previously discussed the mechanical speed that related to the back EMF can be assumed as constant over a few time steps. Thus, considering that the control period T_s is very short, the steady-state voltage can be considered unchanged during adjacent control periods. Then, a subtraction of two contiguous current differences caused by two applied voltage vectors can be made as:

$$\begin{aligned}\Delta i_{d|j}^1 - \Delta i_{d|j}^2 &= \frac{T_s}{L_d}(DV_{d|j}^1 - DV_{d|j}^2)\\ \Delta i_{q|j}^1 - \Delta i_{q|j}^2 &= \frac{T_s}{L_q}(DV_{q|j}^1 - DV_{q|j}^2)\end{aligned} \tag{6.12}$$

where $\Delta \underline{i}_j^1 = [\Delta i_{d|j}^1, \Delta i_{q|j}^1]^T$ and $\Delta \underline{i}_j^2 = [\Delta i_{d|j}^2, \Delta i_{q|j}^2]^T$ are the current differences related to the voltage deviations $D\underline{V}_j^1 = [DV_{d|j}^1, DV_{q|j}^1]^T$ and $D\underline{V}_j^2 = [DV_{d|j}^2, DV_{q|j}^2]^T$, respectively, the indexes "1" and "2" represent the variables of the first and second control period. Then, considering $D\underline{V}_j^1 = \underline{V}_j^1 - \underline{V}_s$, $D\underline{V}_j^2 = \underline{V}_j^2 - \underline{V}_s$, (6.12) can be rewritten as:

$$\begin{aligned}\Delta i_{d|j}^1 - \Delta i_{d|j}^2 &= \frac{T_s}{L_d}(V_{d|j}^1 - V_{d|j}^2)\\ \Delta i_{q|j}^1 - \Delta i_{q|j}^2 &= \frac{T_s}{L_q}(V_{q|j}^1 - V_{q|j}^2)\end{aligned} \tag{6.13}$$

Thus, the relationship between the two succeeding current differences and the two corresponding voltage vectors is derived without the use of the steady-state voltage $\underline{V}_s$. It can be seen from Figure 6.3 that, if the two applied voltage vectors are $\underline{V}_1$ and $\underline{V}_2$, the difference between the two voltage vectors can be used instead of the difference between the two voltage deviations, $D\underline{V}_1$ and $D\underline{V}_2$. For simplicity, (6.13) can be described in a one-dimensional format as:

$$\Delta i_j^1 - \Delta i_j^2 = \frac{T_s}{L_s}(\underline{V}_j^1 - \underline{V}_j^2) \tag{6.14}$$

where $\Delta i_j^1 = [\Delta i_{d|j}^1, \Delta i_{q|j}^1]^T$, $\Delta i_j^2 = [\Delta i_{d|j}^2, \Delta i_{q|j}^2]^T$ are the current differences caused by the two applied voltage vectors $\underline{V}_j^1 = [V_{d|j}^1, V_{q|j}^1]^T$ and $\underline{V}_j^2 = [V_{d|j}^2, V_{q|j}^2]^T$, $L_s = [L_d, L_q]^T$.

6.3.3.2 Estimation of Current Difference for All Voltage Vectors

Based on the analysis above, (6.14) can be used to estimate the current differences for all the voltage vectors to be stored in the LUTs. Figure

6.4 illustrates the time sequence of the LUT update. At the start of kT_s, the current difference over $(k-1)T_s$ due to the applied voltage vector $\underline{V}_j^{k-1}$, $j \in \{0,1,...,7\}$ can be derived based on the current measurements as $\Delta i_j^{k-1} = i_s^k - i_s^{k-1}$. Here, it is noted that the currents are sampled immediately before a new switching state is activated to avoid the current spikes that may occur at the switching instants. Then, with the information from the $(k-2)T_s$, (6.15) can be obtained according to (6.14).

$$\Delta i_j^{k-1} - \Delta i_j^{k-2} = \frac{T_s}{L_s}(\underline{V}_j^{k-1} - \underline{V}_j^{k-2}) \tag{6.15}$$

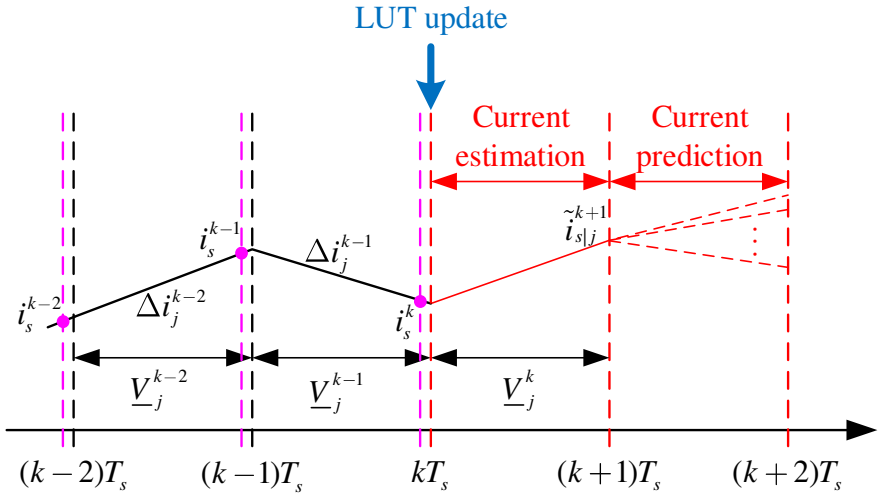

Figure 6.4: Time sequence of the LUT update.

Apart from $\underline{V}_j^{k-1}$, if one of the remaining seven voltage vectors $\underline{V}_{j'}^{k-1}$ ($j' \in \{0,1,...,7\}, j' \neq j$), is applied during $(k-1)T_s$, a similar relationship can be established as:

$$\Delta i_{j'}^{k-1} - \Delta i_j^{k-2} = \frac{T_s}{L_s}(\underline{V}_{j'}^{k-1} - \underline{V}_j^{k-2}) \tag{6.16}$$

Since the control period T_s is short enough to assume the phase inductance L_s as constant during adjacent control periods, the term T_s/L_s can be eliminated by combining (6.15) and (6.16) as:

$$\frac{\Delta i_{j'}^{k-1} - \Delta i_j^{k-2}}{\Delta i_j^{k-1} - \Delta i_j^{k-2}} = \frac{\underline{V}_{j'}^{k-1} - \underline{V}_j^{k-2}}{\underline{V}_j^{k-1} - \underline{V}_j^{k-2}} \tag{6.17}$$

Then, the current difference under the remaining voltage vector can be estimated as:

$$\Delta i_{j'}^{k-1} = \frac{(\underline{V}_{j'}^{k-1} - \underline{V}_j^{k-2})(\Delta i_j^{k-1} - \Delta i_j^{k-2})}{\underline{V}_j^{k-1} - \underline{V}_j^{k-2}} + \Delta i_j^{k-2} \tag{6.18}$$

It can be seen that the current difference estimations are based on measured data only without any dependence on the motor parameters. As the control period T_s is very short, the rotor electrical position can be considered unchanged during a few adjacent control periods, the current differences over kT_s and over $(k+1)T_s$ can be therefore approximated as those over $(k-1)T_s$. The current differences obtained by (6.18) can be then used in (6.5) and (6.6) as Δi_j^k and Δi_j^{k+1} for current estimation and current prediction, respectively.

It should be mentioned that two succeeding similar voltage vectors could lead to inaccurate estimations in (6.18). Thus, such a situation needs to be well considered. In this paper, a threshold σ is introduced. If the denominator of (6.18) $\underline{V}_j^{k-1} - \underline{V}_j^{k-2} \geq \sigma$, the current differences would be estimated by (6.18). Otherwise, if two succeeding similar vectors occur ($\underline{V}_j^{k-1} - \underline{V}_j^{k-2} < \sigma$), the current differences would be kept at the previous values. In particular, based on the new outcome of the controller, if more than two succeeding similar vectors would be applied, a suboptimal voltage vector selection could instead be decided upon to avoid the occurrence of several succeeding similar vectors. Otherwise, such a sequence of similar vectors could impede obtaining new accurate current difference estimations. Such a decision allows for frequent updates to the current differences, but comes at a cost of operating in a suboptimal manner. Fortunately, a sequence of more than two similar voltage vectors does not occur frequently in normal operating conditions in an MPCC or CDSPCC. The corresponding influence on the control performance is therefore limited.

Generally, based on the relationship between two succeeding applied voltage vectors and the resulting current differences, the current differences under all the vectors can be estimated using the relationships between different voltage vectors. Such an advanced current difference updating mechanism can effectively solve the stagnation problem in a conventional CDSPCC [123] and can also reduce the stagnation caused by applying only two voltage vectors for many periods, which can corrupt the method in [128]. Another improvement of the proposed approach is the simple and intuitive calculation. The current differences can be estimated based on an equation with basic mathematical operators (6.18), rather than an identification mechanism with an LUT, as in [128].

Figure 6.5 and Figure 6.6 show the diagram and the flow chart of the proposed CDSPCC strategy, respectively. In general, there are three phases to implement the proposed CDSPCC. First, the current differences based on all the possible voltage vectors are estimated using the measured currents, thereby refreshing the information in the LUTs. In the second phase, the stator currents under the corresponding voltage vectors in the following control periods are estimated and predicted based on the updated LUTs. Finally, the optimal voltage vector is decided upon according to the results of the objective function evaluation.

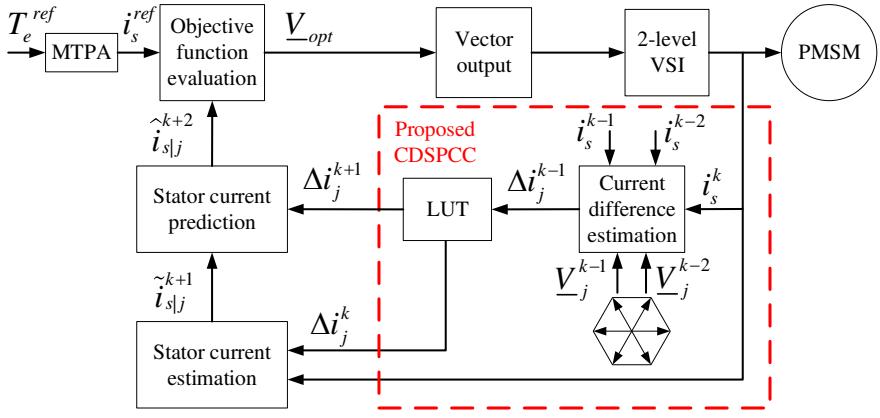

Figure 6.5: Diagram of the proposed CDSPCC strategy.

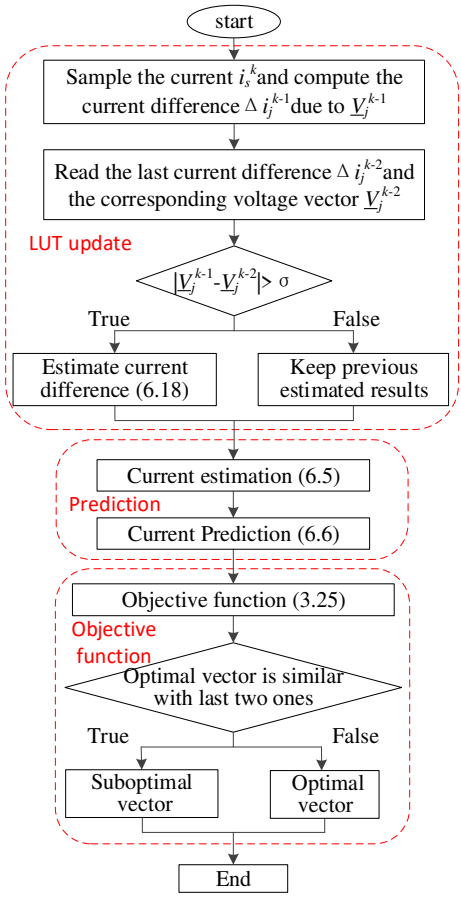

Figure 6.6: Flow chart of the proposed CDSPCC strategy.

6.4 Experimental Verifications

To reveal the validity and improvements of the proposed CDSPCC strategy, experiments are carried out on a real PMSM drive setup, as shown in Figure 4.15. The parameters of the tested motor are listed in Table 4.3. In addition, to show the improvements of the proposed CDSPCC strategy, the conventional MPCC and the CDSPCC from [126] (referred to as CDSPCC-I) are involved for comparison. The control period T_s is set at 100 μs in all the experimental tests.

In the following, the experimental results are discussed in several aspects. In Section 6.4.1, the current difference update under the proposed CDSPCC is analyzed and compared with the CDSPCC-I to

show the effectiveness of the proposed CDSPCC in obtaining reliable current difference information. The results regarding the steady-state performance are given in Section 6.4.2. In particular, the conventional MPCC is tested with different motor parameter settings to show its sensitivity to parameter uncertainties. The proposed CDSPCC needs to be validated to reveal if it can achieve the similar performance as a MPCC with nominal parameters does. In Section 6.4.3, a low load test is given to see if the proposed CDSPCC can obtain enough current difference information when the reference currents are almost zero. A torque step test is presented in Section 6.4.4 to verify the dynamic performance of the proposed CDSPCC. In Section 6.4.5, a speed reversal test is performed to confirm the performance of the proposed CDSPCC over the entire speed range. Next, the executed time of different strategies is discussed in Section 6.4.6 to show their computational burden. Finally, as the proposed CDSPCC relies on measured current difference, an additional simulated stability test is given in Section 6.4.7. This study is used to confirm the stability of the proposed CDSPCC under different current noise levels.

6.4.1 Current Difference Update

In this section, the current differences stored in the LUTs under the proposed CDSPCC are reported and compared to those under the CDSPCC-I when the motor operates at 300 r/min with an 8 Nm load. The current differences due to all the possible voltage vectors under the CDSPCC-I are shown in Figure 6.7(a). In this strategy, only the current difference under the applied voltage vector is updated in each control period, whereas the remaining ones are approximated as the old values. At the same time, a minimum updating frequency mechanism is applied in this strategy. If a voltage vector is not selected in the last contiguous 50 control periods, it will be imposed in the next period to refresh the corresponding current difference information. Nevertheless, a significant stagnation effect can still be observed in both the d-axis and q-axis currents. Figure 6.7(b) shows the predicted current error, which is the difference between the predicted current and the measured current. The unreliable current difference information leads to large current prediction errors with error spikes, which can further affect the control performance.

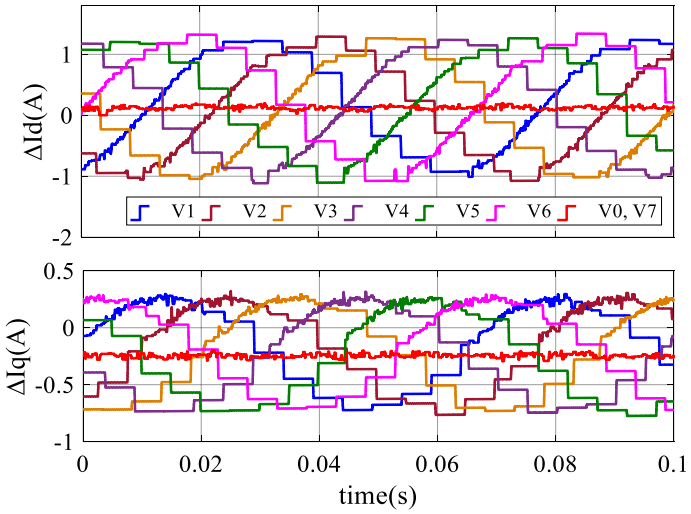

(a) Current differences under different voltage vectors

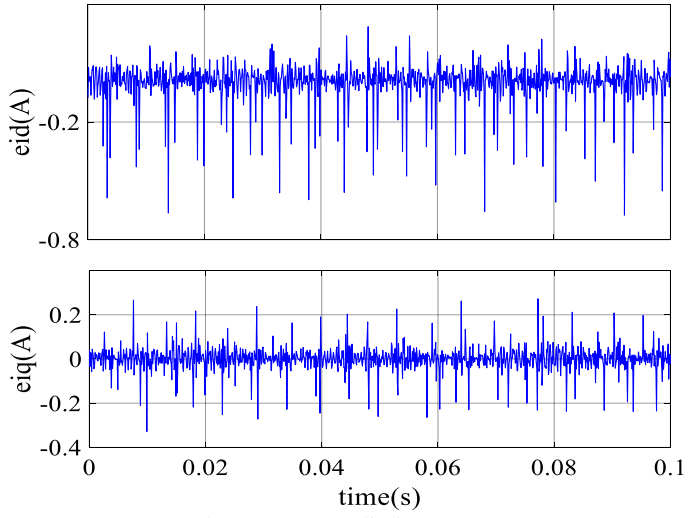

(b) Current prediction errors

Figure 6.7: Current differences and prediction errors under the CDSPCC-I at 300 r/min at 8 Nm load.

On the other hand, the results under the proposed CDSPCC are shown in Figure 6.8. The proposed strategy aims at updating the current differences for all the possible voltage vectors in one control period. As a result, a high updating frequency is guaranteed and stagnations are significantly reduced, although some current measurement noises are involved, as can be seen in Figure 6.8(a). Here, resistors are used to measure the phase currents. The current noise could be further reduced

by using more advanced current sensors. Figure 6.8(b) shows the current prediction errors under the proposed CDSPCC. As can be seen, reliable current difference information has been obtained in the proposed CDSPCC, such that the proposed CDSPCC effectively eliminates the error spikes in the CDSPCC-I and reduces the current prediction errors.

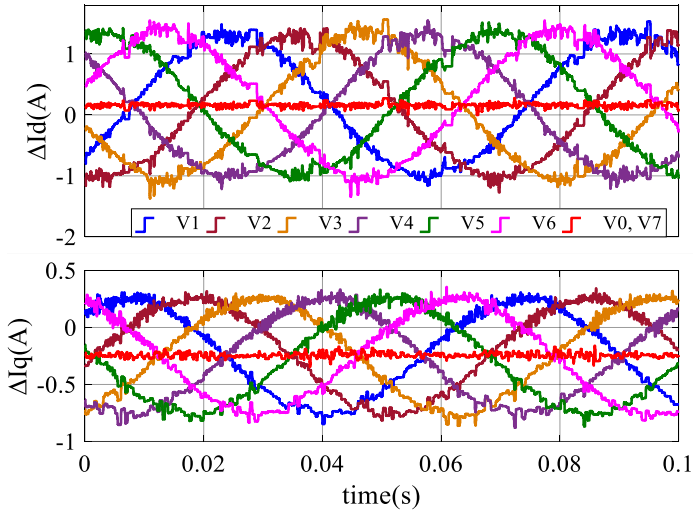

(a) Current differences under different voltage vectors

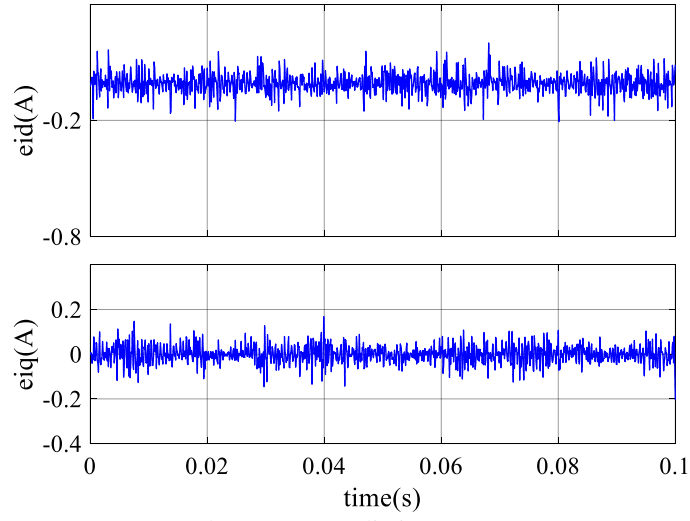

(b) Current prediction errors

Figure 6.8: Current differences and prediction errors under the proposed CDSPCC at 300 r/min at 8 Nm load.

To statistically compare the results shown in Figure 6.7(b) and Figure 6.8(b), the standard deviations of the dq-axis current prediction error under the two strategies are calculated using (6.19), and the results are summarised in Table 6.1. It can be seen that the proposed CDSPCC can reduce the current prediction error significantly compared to the CDSPCC-I.

$$S = \sqrt{\frac{1}{n}\sum_{i=1}^{n}[e(i)-\mu]^2} \tag{6.19}$$

S is the standard deviation of the d-axis (S_d) or q-axis (S_q) current prediction error, n is the sampling number, e is the d-axis (e_{id}) or q-axis (e_{iq}) current prediction error, and $\mu=\frac{1}{n}\sum_{i=1}^{n} e(i)$ is the mean of e.

Table 6.1: Standard deviation of current prediction error

Method	S_d (A)	S_q (A)
CDSPCC-I	0.1102	0.0544
Proposed CDSPCC	0.0599	0.0423

6.4.2 Steady-State Performance

The steady-state performance of the proposed CDSPCC strategy is investigated and compared with the conventional MPCC and the CDSPCC-I. As previously mentioned, inductance and PM flux linkage uncertainty has a greater impact on the control performance than resistance uncertainty [40]. Thus, the conventional MPCC is tested with rated motor parameters, as listed in Table 4.3, and with inductance and PM flux linkage uncertainties. The reference stator currents are given by a reference torque based on MTPA principle, using the parameters in Table 4.3 in all the tests.

Figure 6.9(a) shows the torque, d-axis current, q-axis current and phase currents of the conventional MPCC with nominal parameters at 500 r/min with a 12 Nm load. It is noted that the electromagnetic torque is estimated based on measured currents and the torque equation, considering the motor parameters in Table 4.3.

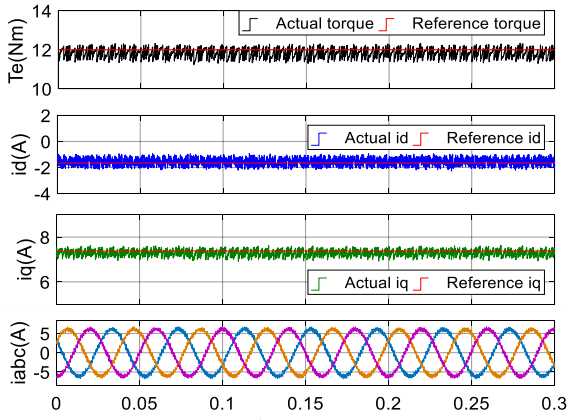

(a) With nominal motor parameters

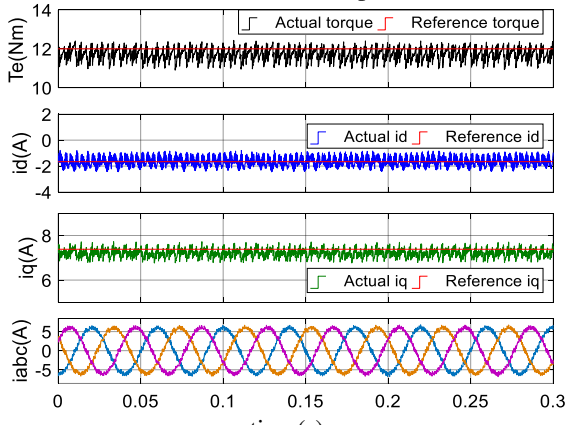

(b) With $0.5L_d$

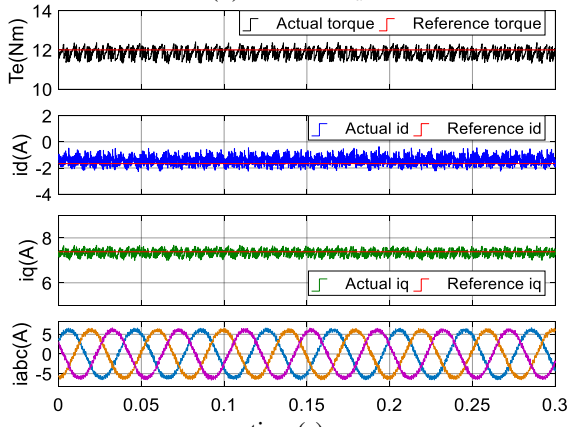

(c) With $0.5L_q$

Figure 6.9: Experimental results of torque, dq-axis current and phase current under the conventional MPCC at 500 r/min.

The results when the d-axis and q-axis inductance are set at 50% of their nominal values are shown in Figure 6.9(b) and Figure 6.9(c), respectively. It is evident that the MPCC is influenced by parameter uncertainties with the parameter mismatches creating current ripples and affecting the steady-state performance.

Although the test presented in Figure 6.9(a) is conducted based on the nominal inductance values as listed in Table 4.3, such nominal values may still be inaccurate due to measurement error. Moreover, the actual inductances may vary due to the variable magnetic state of the machine and frequency effects. As a result, even though the nominal inductance values are used in the test shown in Figure 6.9(a), they are still not well matched with the actual values, as current deviations from the reference can be observed, especially in the waveform of q-axis current. This further reveals the high parameter sensitivity of the conventional MPCC.

The experimental results of the CDSPCC-I and the proposed CDSPCC are shown in Figure 6.10. In these strategies, the system model is abandoned. Instead, current differences are used to predict future currents without involving any system parameters, thereby eliminating the influence of parameter mismatches. Nevertheless, as illustrated in Figure 6.7, the CDSPCC-I strategy suffers the current difference updating stagnation, which leads to unreliable current predictions, even though a minimum updating frequency is guaranteed.

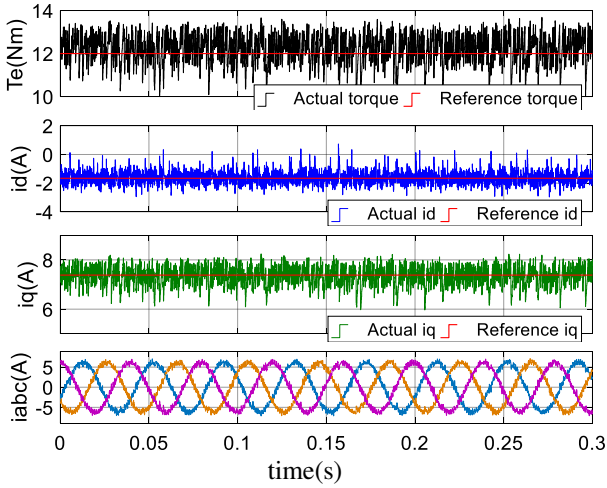

(a) CDSPCC-I

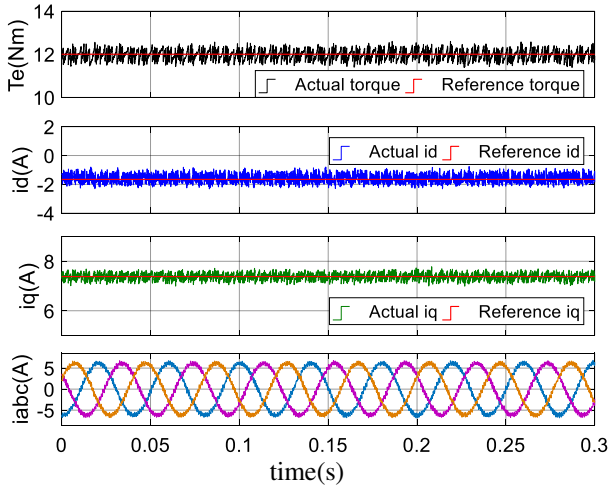

(b) Proposed CDSPCC

Figure 6.10: Experimental results of torque, dq-axis current and phase current under CDSPCC strategies at 500 r/min.

Moreover, as mentioned in Section 6.4.1, the minimum updating frequency mechanism applied in CDSPCC-I imposes a non-optimal voltage vector frequently, which can deteriorate the steady-state performance. The CDSPCC-I therefore results in higher current ripples than the conventional MPCC, which can be seen in Figure 6.10(a).

On the other hand, the proposed CDSPCC obtains current differences for each of the voltage vectors in one control period. The stagnation existing in the CDSPCC-I is then effectively reduced, and more accurate current predictions are achieved. The current deviations in the conventional MPCC are therefore eliminated here, and much better steady-state performance is achieved, as shown in Figure 6.10(b). In addition, the quantitative results of the three strategies are summarised in Table 6.2, which includes the average torque ripples, d-q axis current ripples, total harmonic distortions (THD) of the phase current and average switching frequencies. The average switching frequency f_{av} is obtained by collecting the total switching jumps N of the six VSI switches over a test period t_N and then calculating $f_{av}=N/6/t_N$. From the quantitative results, it is evident that the steady-state performance of the conventional MPCC is sensitive to parameter mismatches. The proposed CDSPCC performs better than the conventional MPCC with nominal parameters in terms of torque ripple, q-axis current ripple and THD rate at a similar average switching frequency.

Table 6.2: Comparison of steady-state performance at 500 r/min

Method	T_e^{rip} (Nm)	I_d^{rip} (A)	I_q^{rip} (A)	THD (%)	f_{av} (kHz)
MPCC	0.277	0.282	0.162	7.53	2.81
MPCC with $0.5L_d$	0.409	0.332	0.246	7.76	2.87
MPCC with $0.5L_q$	0.267	0.415	0.137	7.46	2.78
CDSPCC-I	0.690	0.438	0.390	9.83	2.93
Proposed CDSPCC	0.223	0.293	0.132	7.27	2.89

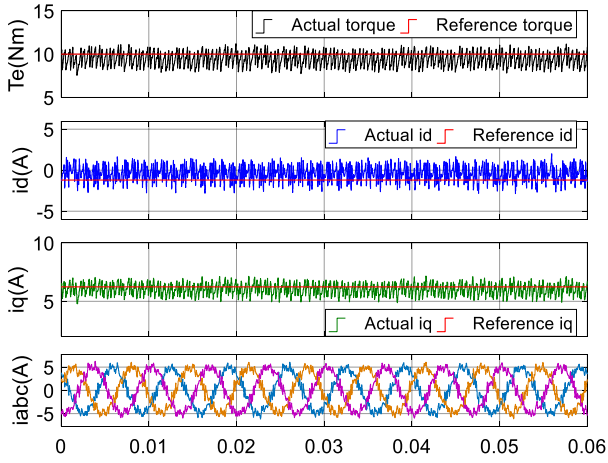

(a) MPCC with nominal motor parameters

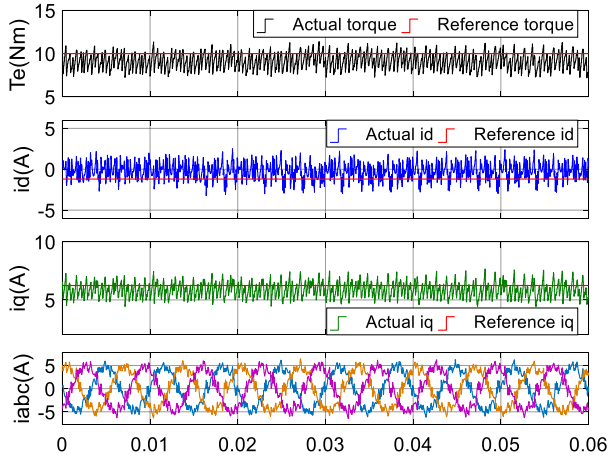

(b) MPCC with $0.5L_d$

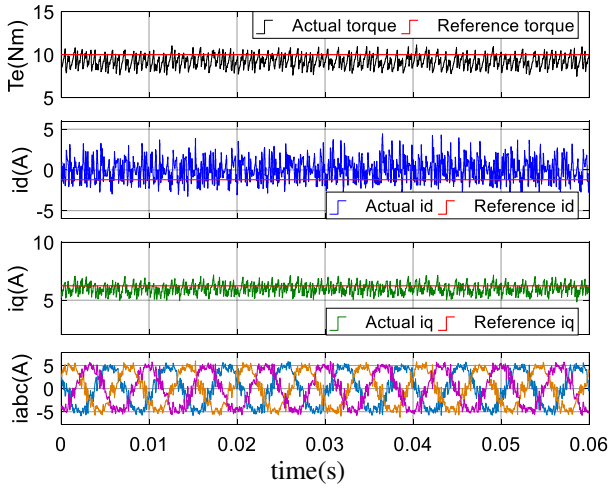

(c) MPCC with $0.5L_q$

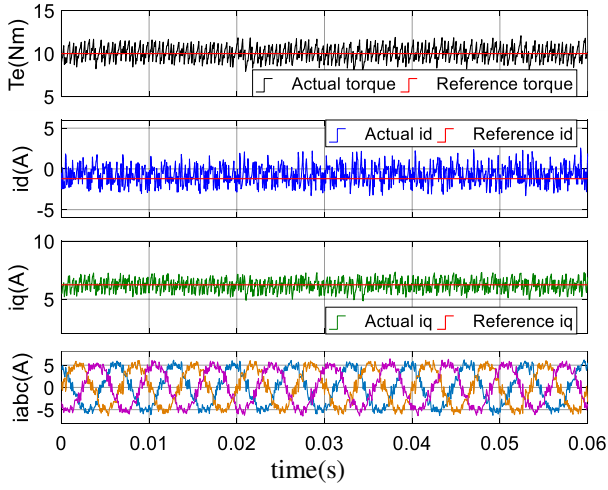

(d) Proposed CDSPCC

Figure 6.11: Experimental results of torque, dq-axis current and phase current at 3000 r/min.

The proposed CDSPCC is further compared to the conventional MPCC with different inductance values at 3000 r/min with a 10 Nm load. The results are shown in Figure 6.11 and Table 6.3 lists the corresponding quantitative results. As with the previous testing, the conventional MPCC is sensitive to inductance parameters. Because inductance mismatches exist, ripples and deviations from the reference can be seen with the conventional MPCC, whereas the proposed

CDSPCC is not affected by motor parameters and achieves better steady-state performance even at a higher operating speed.

Table 6.3: Comparison of steady-state performance at 3000 r/min

Method	T_e^{rip} (Nm)	I_d^{rip} (A)	I_q^{rip} (A)	THD (%)	f_{av} (kHz)
MPCC	0.910	1.011	0.542	18.16	4.57
MPCC with $0.5L_d$	1.270	1.400	0.738	19.57	4.41
MPCC with $0.5L_q$	1.069	1.886	0.513	23.53	4.31
Proposed CDSPCC	0.813	1.187	0.512	18.05	4.48

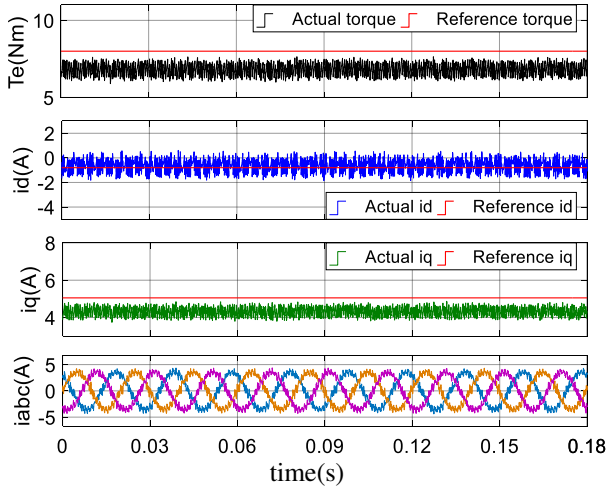

(a) MPCC with $0.5\psi_f$

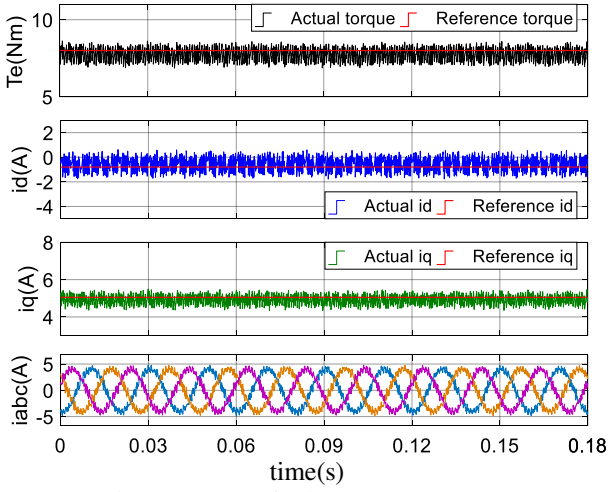

(b) MPCC nominal motor parameters

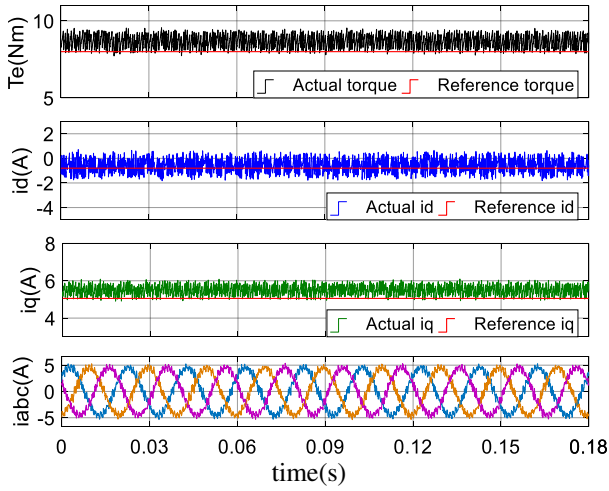

(c) MPCC with $1.5\psi_f$

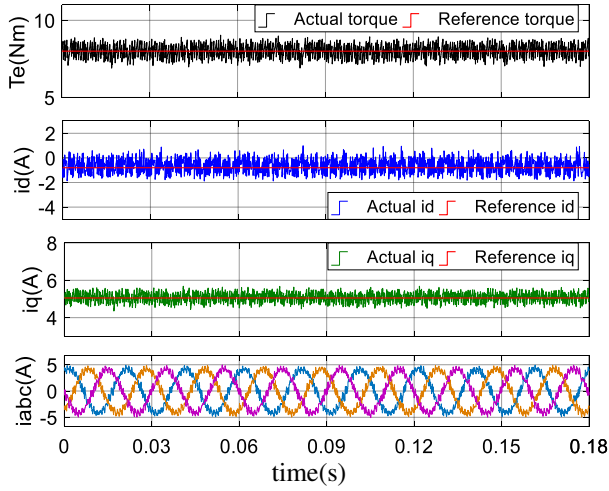

(d) Proposed CDSPCC

Figure 6.12: Experimental results of torque, dq-axis current and phase current at 1000 r/min.

In addition, Figure 6.12 reports the performance comparisons of the conventional MPCC with different PM flux linkage values and the proposed CDSPCC at 1000 r/min with an 8 Nm load. In Figure 6.12(a), (b), (c), the PM flux linkage in the conventional MPCC is set as 50%, 100% and 150% of the nominal value, respectively. It can be seen that obvious deviations are aroused in the q-axis current and torque by the PM flux linkage mismatches, deteriorating the steady-state performance. In contrast, the proposed CDSPCC is not affected by such

parameter uncertainty and still obtains good steady-state performance, as can be seen from the statistic results summarized in Table 6.4.

Table 6.4: Comparison of steady-state performance at 1000 r/min

Method	T_e^{rip} (Nm)	I_d^{rip} (A)	I_q^{rip} (A)	THD (%)	f_{av} (kHz)
MPCC with $0.5\psi_f$	1.238	0.506	0.762	15.49	4.67
MPCC	0.448	0.537	0.268	13.46	4.50
MPCC with $1.5\psi_f$	0.775	0.554	0.522	12.91	4.43
Proposed CDSPCC	0.389	0.539	0.243	13.42	4.55

6.4.3 Low Load Test

Additionally, a low load test is conducted in which the conventional MPCC with nominal parameters and the proposed CDSPCC are compared at 500 r/min with a 0.1 Nm load. Figure 6.13 shows the results in terms of torque and dq-axis current. In this case, even though the reference currents are almost zero, the proposed CDSPCC can still obtain enough information from the current variations to operate normally. The quantitative results of the torque ripple, current ripple and average switching frequency under the two strategies are summarised in Table 6.5. Compared to the conventional MPCC, the proposed CDSPCC performs better in terms of torque ripple and q-axis current ripple at a similar average switching frequency.

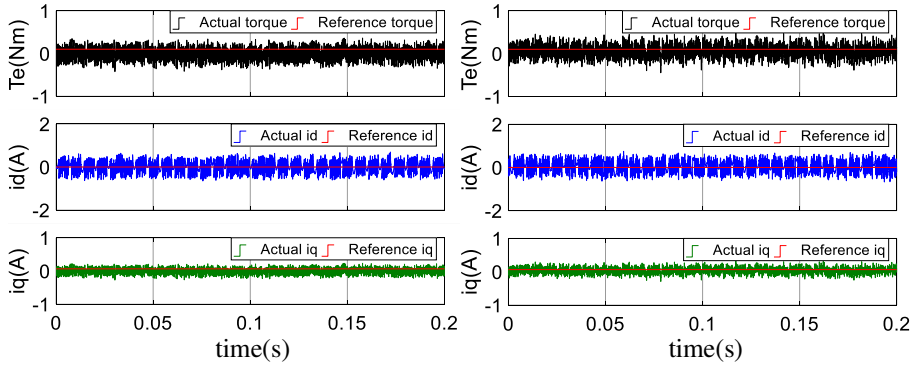

(a) Conventional MPCC (b) Proposed CDSPCC

Figure 6.13: Experimental results of torque and dq-axis current at 500 r/min, 0.1 Nm load.

Table 6.5: Quantitative results of low load test

Method	T_e^{rip} (Nm)	I_d^{rip} (A)	I_q^{rip} (A)	f_{av} (kHz)
Conventional MPCC	0.180	0.258	0.117	5.57
Proposed CDSPCC	0.161	0.270	0.105	5.46

6.4.4 Torque Step Test

To show the dynamic performance of the three strategies, comparative tests are carried out where the load suddenly changed from 4 Nm to 12 Nm. Figure 6.14(a) shows the transient torque and d-q axis currents under the conventional MPCC. The blue lines are the results with nominal motor parameters, whereas the green and purple lines are the results under inductance mismatches. The comparative results under the two CDSPCC strategies are shown in Figure 6.14(b). There are overshoots in the waveforms of the d-axis currents under the conventional MPCC when the reference changes. Conversely, the two CDSPCC strategies complete this transition and enter the steady state without overshoots.

It is noted that the information about current differences with the CDSPCC-I can be unreliable due to the stagnation problem. Such unreliable information can lead the objective function to make a bad and incorrect decision when determining a voltage vector to be applied. This phenomenon could occur in both steady state and dynamic state, thus affecting both steady-state performance and dynamic response. In contrast, the current differences with the proposed CDSPCC are up to date and reliable due to the proposed updating mechanism. This guarantees the objective function to make a good decision in steady state as well as dynamic state. As a result, it can be seen in Figure 6.14(b) that the proposed CDSPCC achieves a faster response in the torque and the q-axis current step compared to the CDSPCC-I, demonstrating the good dynamic performance of the proposed CDSPCC strategy.

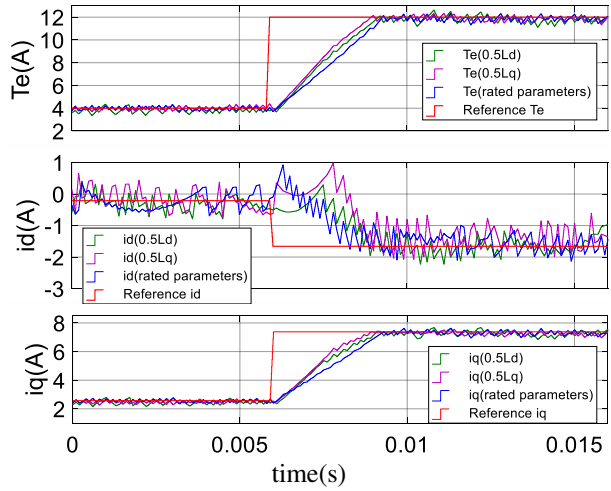

(a) Conventional MPCC

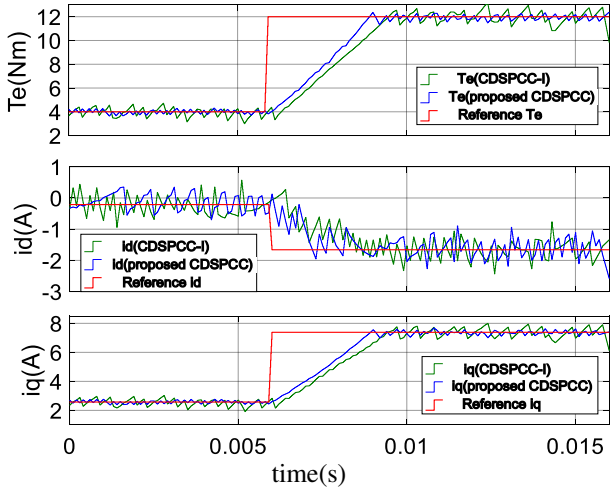

(b) CDSPCC-I and proposed CDSPCC

Figure 6.14: Dynamic performance comparison when load changing.

6.4.5 Speed Reversal Test

To further confirm the dynamic performance of the proposed CDSPCC, a speed reversal test is carried out in which the rotor speed reversed from –3000 r/min to 3000 r/min with a 10 Nm load. Figure 6.15 shows the waveforms of rotor speed, dq-axis currents and phase current. It should be noted that the speed and torque are set separately. The reference torque is set externally, whereas the speed of the PMSM is controlled by the load machine, a servo motor driven by the Siemens SINAMICS

drive system. During the speed changing process, the reference torque and reference dq-axis currents are therefore not affected and are kept constant, as shown in Figure 6.15. The results reveal that the proposed CDSPCC performs well across the entire speed range.

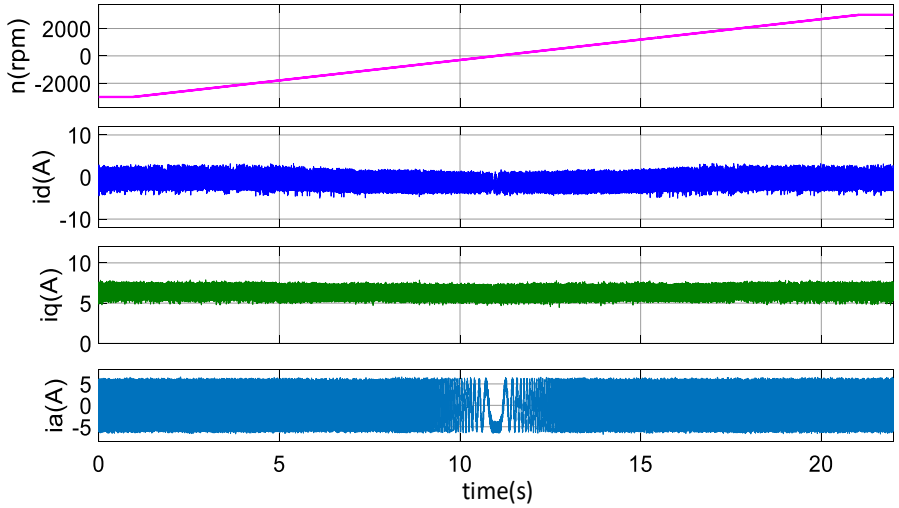

Figure 6.15: Speed reversal test of the proposed CDSPCC.

6.4.6 Computational Time

The computational time is compared for the conventional MPCC, the CDSPCC-I and the proposed CDSPCC. The results for the three strategies are shown in Table 6.6. In the conventional MPCC, the currents need to be predicted under seven voltage vectors, an algorithm that takes 19.2 μs to conduct. In the CDSPCC-I, except for the current predictions and objective function evaluations, the current differences due to the applied voltage vector are measured and used to update one of the corresponding LUT elements, and the computational time slightly increases to 20.1 μs. In the proposed CDSPCC, all the LUT elements are updated based on a simple equation (6.18), and the computational time of the algorithm is 23.8 μs. Generally, the increased computational time of the proposed CDSPCC is caused by the additional LUT update operation. However, considering the improved control performance, such slight increase in computational time is quite acceptable for the proposed CDSPCC.

Table 6.6: Computation burden comparison

Task	Conventional MPCC	CDSPCC-I	Proposed CDSPCC
LUT update	0 μs	1.4 μs	5.1 μs
Prediction	11.7 μs	11.2 μs	11.2 μs
Evaluation	7.5 μs	7.5 μs	7.5 μs
Total time	19.2 μs	20.1 μs	23.8 μs

6.4.7 Simulation Results of Stability Test

In the proposed CDSPCC, the current differences are obtained based on current measurements. Thus, the measurement noise in current can be inevitably involved. To confirm the stability of the proposed CDSPCC against current noise, a simulation considering different levels of current noise is carried out. Here, white noise is added to the dq-axis currents that are further used in the proposed CDSPCC.

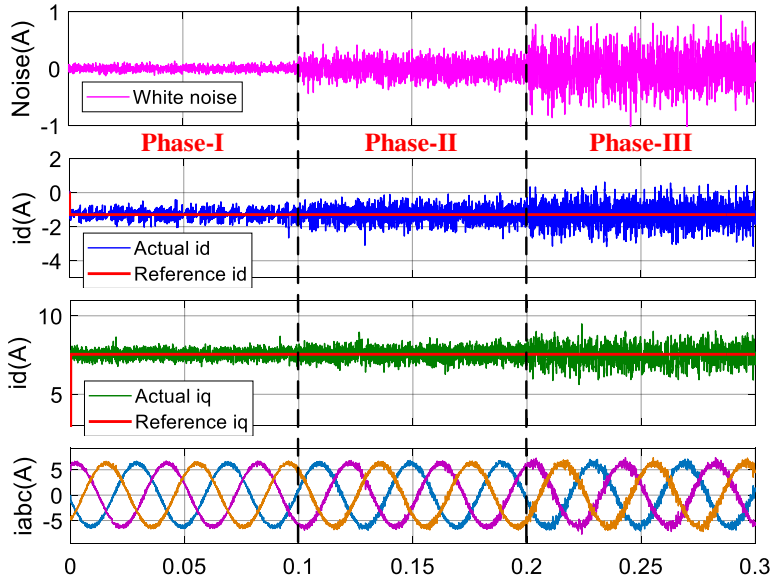

Figure 6.16: Simulation results of steady-state performance considering current noise.

Figure 6.16 shows the steady-state performance considering the white noise. From top to bottom, the waveforms are the white noise

added to the dq-axis currents, d-axis current, q-axis current and phase currents. To clearly show how current noise can influence the proposed CDSPCC, the variance of the white noise in the Phase-I, Phase-II and Phase-III is set as 0.002 A and 0.02 A and 0.1 A, respectively. In the Phase-III, the amplitude of the peak noise is up to 1 A. It can be seen that even though the current noise increases, the proposed CDSPCC still performs stably, although the steady-state performance is influenced by the increased noise. The stability of the proposed CDSPCC is then further confirmed. Moreover, the effect of current noise could be limited by a more accurate current sensing.

6.5 Conclusions

The goal of this chapter is the adaption to counter the parameter dependence problem with predictive control. For this purpose, an improved current-difference sample based predictive current control is proposed. In contrast to the model-based predictive current control, which uses the system model to predict future currents, the proposed CDSPCC realizes current predictions based on online sampled current difference information without involving any motor parameters, therefore avoiding the influence of parameter uncertainties. To obtain reliable current difference information, the relationship between two succeeding applied voltage vectors and the resulting current differences is exploited to deduce the current differences for all the possible voltage vectors within one control period. The main benefit is that such high frequency updating of the LUTs provides a reliable foundation for the current estimations and predictions.

The main flow and the benefits of the proposed CDSPCC are presented in Figure 6.17. The proposed CDSPCC strategy, with simple structure, does not involve any complicated operating mechanisms. All the current differences are obtained within one control period by basic operators. This behaviour also means the reliability of the current difference information is guaranteed. Due to the feature of parameter independence, the proposed CDSPCC could be useful in cases where motor knowledge is not adequately provided.

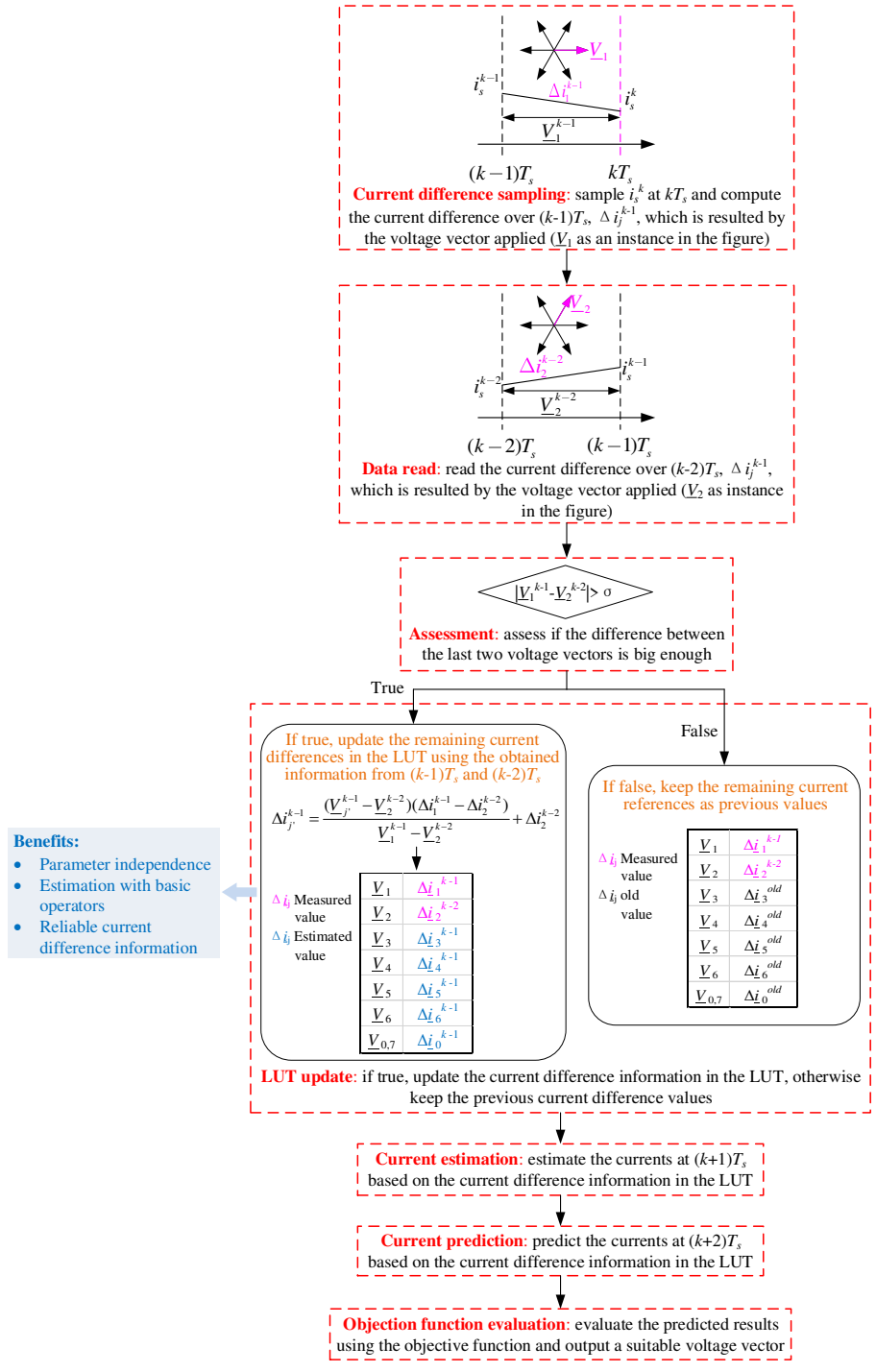

Figure 6.17: The main flow and the benefits of the proposed CDSPCC.

The validity of the proposed strategy has been demonstrated by experiments with comparisons to the conventional MPCC and the conventional CDSPCC. The results show that the current difference updating stagnation of the conventional CDSPCC is significant, while the proposed CDSPCC effectively solves this problem by updating all the current differences within one control period, guaranteeing their reliability. The influence of parameter uncertainties on the conventional MPCC has been revealed by the experimental results. For example, when the MPCC performs with nominal parameters, the average d-axis current ripple is 1.011 A at 3000 r/min, while it increases to 1.886 A when the q-axis inductance is set as 50% of its nominal value. In contrast, due to the feature of parameter independence, the proposed CDSPCC is not affected by parameter uncertainties and can obtain similar performance in comparison with the MPCC incorporating nominal parameters. This is the third goal shown in Figure 1.4 (the third block of Level 5). The results at 3000 r/min indicate that the torque ripple and q-axis current ripple under the proposed CDSPCC (0.813 Nm and 0.512 A) are even lower than those under the MPCC with nominal parameters (0.910 Nm and 0.542 A).

The low load test has confirmed that the proposed CDSPCC can still obtain enough current difference information to operate normally when the reference currents are almost zero. The torque step test demonstrates that the proposed CDSPCC can achieve faster dynamic response than the conventional CDSPCC due to the reliable current difference information. The performance of the proposed CDSPCC over the entire speed range has been verified by the speed reversal test. In addition, the stability of the proposed CDSPCC under different levels of current noise is also confirmed by a simulation study.

Chapter 7
Concluding Remarks and Future Research

7.1 Conclusions

PMSM is widely used in various industrial applications, especially in new energy vehicles due to the pressure of energy shortage and environmental crisis. MPC with an intuitive concept has received more and more attention in academia and is considered a promising control scheme to replace the conventional ones in PMSM drives. MPC shows the benefits of simple structure, fast dynamic response, excellent ability to handle system constraints, etc. However, there are still some aspects need to be improved for MPC, e.g. the steady-state performance, the simplification with high control flexibility and the parameter robustness. Thus, developing adaptive solutions with predictive control addressing these three problems is of importance, which is the focus of this thesis.

In this thesis, a two-level three-phase VSI-fed salient-pole PMSM is studied. In Chapter 2, the PMSM model and the conventional control strategies, FOC and DTC, are presented. As a promising alternative to the conventional strategies, MPC is introduced in Chapter 3. First, the classifications and the basic principles of MPCs are given. For PMSM drive systems, FCS-MPC is the most widely investigated MPC scheme. Thus, all the steps of a MPTC for PMSM are elaborated.

The improvement of steady-state performance of MPC based PMSM system is the focus of Chapter 4. In a conventional MPTC, one voltage

vector is activated over a fixed control period, hence resulting in high torque ripples. Aiming at solving this problem, two-vectors MPC scheme is introduced. Such a scheme applies two voltage vectors during a control period and considers a duty ratio (or switching moment) to be optimized. Its performance is compared with that of the conventional MPC by simulations. The results show that an improved steady-state performance can be achieved with the presented two-vectors MPTCs compared to the conventional MPTC. Different duty ratio optimization solutions are analysed for two-vectors MPTC. In contrast to the deadbeat solution, the RMS solution is more useful to reduce the mean torque ripple, however increasing the computational complexity. In addition, the weighting factor that remains within the objective function is required to be eliminated. Therefore, an adaptive solution with an improved torque boundary based MPTC is proposed. The proposed MPTC is a two-vectors scheme that can restrict the torque ripple within the predefined boundaries during the whole control period. This scheme optimizes the boundary setting by an online adjustment mechanism, which seeks to minimize the torque ripple while avoiding the manual torque boundary design. The experimental results show that the proposed boundary based MPTC can achieve a better steady-state performance compared to a two-vectors MPTC with a deadbeat duty ratio optimization at a similar switching frequency. In addition, as the proposed scheme includes a candidate preselection mechanism, a lower computational burden is obtained. Moreover, due to the introduction of the torque boundaries, the weighting factor is eliminated with the proposed MPTC, avoiding the corresponding tuning work.

The balance between the computational burden and the control performance of FCS-MPC is studied in Chapter 5. In a standard FCS-MPC, all voltage vectors (switching states) need to be evaluated in each control period, resulting in a low computational efficiency, as most of the voltage vectors are far from optimal. In order to obtain the optimal solution in a straightforward way, the RVV-MPC is introduced. Such a strategy generates a reference voltage vector, according to which the optimal solution can be determined without considering all the candidates. Even though the computational burden can be reduced, a disadvantage can be identified with this RVV-MPC. As limited candidate solutions are provided with the RVV-MPC, additional system constraints are less likely to be upheld, which impacts the control flexibility of FCS-MPC and influences the further improvement on the system performance. Therefore, a reference-variant-MPC is proposed.

In the proposed scheme, the first step is to obtain an original reference. Then, a reference region is set up in the neighbourhood of this original point, and a finite set of adaptive reference variants is sampled, resulting in more optimal candidate solutions. A trade-off is then made between the computational burden and the control performance. These optimal solutions allow the inclusion of additional system constraints within the objective function under the premise of guaranteeing the main control objectives. In addition, the reference region can be automatically adjusted to comply truly with the constraints, achieving a flexible control structure. In this study, current boundaries are considered as constraints with the proposed strategy. Simulated and experimental results are given. The results show that improved steady-state performance and dynamic performance are achieved with the proposed reference-variant-MPC compared to the RVV-MPC. Moreover, due to the flexible structure of the proposed MPC, additional efforts could be made to achieve a further development on system performance.

Chapter 6 focuses on the parameter dependence issue, which is another well-known disadvantage of MPC. As the discrete-time model of PMSM is used to predict the motor behaviours, MPC is then sensitive to motor parameter uncertainties. The parameter sensitivity of a MPCC is analysed. It is concluded that inductance and PM flux uncertainties can lead to non-neglectable current prediction errors, whereas the influence of resistance uncertainties on current predictions is relatively weak. To solve the parameter dependence problem, a current-difference sample based predictive current control is introduced. The PMSM model is abandoned with this strategy, instead online measured current differences are used to predict future current. In this strategy, the current differences need to be obtained for all the possible voltage vectors. However, in each control period, the current differences can be obtained for only one voltage vector by measurement. Thus, an advanced current-difference updating mechanism is proposed, in which the current differences due to the remaining voltage vectors can be obtained in each control period by simple calculations. Reliable current difference information can be then guaranteed. The performance of the proposed CDSPCC and that of the MPCC are compared by experiments. The results show that the steady-state performance of the MPCC is largely influenced by inductance uncertainties and PM flux uncertainties. In contrast, as no parameters are involved within the proposed CDSPCC, the influence of parameter uncertainties can be totally eliminated. In addition, the proposed CDSPCC can achieve as

similar performance as the MPCC with nominal parameters does, which means the control performance is not impacted under the premise of parameter robustness improvement. As the proposed CDSPCC strategy does not need PMSM parameters, it is useful in the conditions where motor parameters cannot be properly given.

7.2 Future Research

The objective of this thesis is to develop adaptive solutions with predictive control for PMSM addressing the well-known disadvantages of MPC. Based on the obtained results, some research questions could be further considered in the future.

- A reference-variant-MPC scheme is proposed in this thesis. This scheme sets up an adjustable reference region, resulting in a flexible structure. In this work, a circle region is considered and the reference variant points are randomly selected. The proposed reference-variant-MPC could be further extended by considering better the distribution of reference variant points, the shape of reference variant region or the optimal reference point selection mechanism.

- In this thesis, a current-difference sample based predictive current control (CDSPCC) is developed. As this scheme performs based on online measured currents, measurement noises are inevitably involved. In this work, resistors are used to measure currents. It can be expected that more advanced current sensors can make a positive difference to the performance of this sample-based scheme. Thus, the influences of different current sensing techniques on the control performance could be studied.

- The proposed CDSPCC is a one-vector approach that applies one voltage vector over a control period. Thus, the resulting current differences can be measured at the start of each period. It has been discussed that a two-vectors predictive control scheme can achieve an improved steady-state performance. However, with a two-vectors scheme, two different voltage vectors with variable time durations are activated within a control period, and the vector selection criterion is also

different. Considering the different operating principles, the application of the CDSPCC to a two-vectors scheme could be studied in the future.

Bibliography

[1] "Global EV Outlook 2020," International Energy Agency, 2020.

[2] R. Jose and C. Patricio, *Predictive Control of Power Converters and Electrical Drives*. Wiley, 2012.

[3] C. Xia, S. Wang, Z. Wang, and T. Shi, "Direct Torque Control for VSI–PMSMs Using Four-Dimensional Switching-Table," *IEEE Transactions on Power Electronics,* vol. 31, no. 8, pp. 5774-5785, 2016.

[4] Y. Zhang, J. Jiao, D. Xu, D. Jiang, Z. Wang, and C. Tong, "Model Predictive Direct Power Control of Doubly Fed Induction Generators Under Balanced and Unbalanced Network Conditions," *IEEE Transactions on Industry Applications,* vol. 56, no. 1, pp. 771-786, 2020.

[5] J. H. Chang and B. K. Kim, "Minimum-time minimum-loss speed control of induction motors under field-oriented control," *IEEE Transactions on Industrial Electronics,* vol. 44, no. 6, pp. 809-815, 1997.

[6] Z. Wang, J. Chen, M. Cheng, and K. T. Chau, "Field-Oriented Control and Direct Torque Control for Paralleled VSIs Fed PMSM Drives With Variable Switching Frequencies," *IEEE Transactions on Power Electronics,* vol. 31, no. 3, pp. 2417-2428, 2016.

[7] J. Lara, J. Xu, and A. Chandra, "Effects of Rotor Position Error in the Performance of Field-Oriented-Controlled PMSM Drives for Electric Vehicle Traction Applications," *IEEE Transactions on Industrial Electronics,* vol. 63, no. 8, pp. 4738-4751, 2016.

[8] Z. Tang and B. Akin, "A New LMS Algorithm Based Deadtime Compensation Method for PMSM FOC Drives," *IEEE*

Transactions on Industry Applications, vol. 54, no. 6, pp. 6472-6484, 2018.

[9] C. Xiong, T. Guan, P. Zhou, and H. Xu, "A Fault-Tolerant FOC Strategy for Five-Phase SPMSM With Minimum Torque Ripples in the Full Torque Operation Range Under Double-Phase Open-Circuit Fault," *IEEE Transactions on Industrial Electronics,* vol. 67, no. 11, pp. 9059-9072, 2020.

[10] D. Mohan, X. Zhang, and G. H. B. Foo, "A Simple Duty Cycle Control Strategy to Reduce Torque Ripples and Improve Low-Speed Performance of a Three-Level Inverter Fed DTC IPMSM Drive," *IEEE Transactions on Industrial Electronics,* vol. 64, no. 4, pp. 2709-2721, 2017.

[11] F. Niu, K. Li, and Y. Wang, "Direct Torque Control for Permanent-Magnet Synchronous Machines Based on Duty Ratio Modulation," *IEEE Transactions on Industrial Electronics,* vol. 62, no. 10, pp. 6160-6170, 2015.

[12] A. Shinohara, Y. Inoue, S. Morimoto, and M. Sanada, "Direct Calculation Method of Reference Flux Linkage for Maximum Torque per Ampere Control in DTC-Based IPMSM Drives," *IEEE Transactions on Power Electronics,* vol. 32, no. 3, pp. 2114-2122, 2017.

[13] D. Wang, T. Yuan, X. Wang, X. Wang, and W. Li, "A Composite Vectors Modulation Strategy for PMSM DTC Systems," *Energies,* vol. 11, no. 10, 2018.

[14] X. Wang, Z. Wang, M. Cheng, and Y. Hu, "Remedial Strategies of T-NPC Three-Level Asymmetric Six-Phase PMSM Drives Based on SVM-DTC," *IEEE Transactions on Industrial Electronics,* vol. 64, no. 9, pp. 6841-6853, 2017.

[15] Y. Wang, L. Geng, W. Hao, and W. Xiao, "Control Method for Optimal Dynamic Performance of DTC-Based PMSM Drives," *IEEE Transactions on Energy Conversion,* vol. 33, no. 3, pp. 1285-1296, 2018.

[16] C. Xia, S. Wang, X. Gu, Y. Yan, and T. Shi, "Direct Torque Control for VSI-PMSM Using Vector Evaluation Factor Table," *IEEE Transactions on Industrial Electronics,* vol. 63, no. 7, pp. 4571-4583, 2016.

[17] C. Xia, J. Zhao, Y. Yan, and T. Shi, "A Novel Direct Torque Control of Matrix Converter-Fed PMSM Drives Using Duty Cycle Control for Torque Ripple Reduction," *IEEE Transactions on Industrial Electronics,* vol. 61, no. 6, pp. 2700-2713, 2014.

[18] Z. Yongchang and Z. Jianguo, "Direct Torque Control of Permanent Magnet Synchronous Motor With Reduced Torque Ripple and Commutation Frequency," *IEEE Transactions on Power Electronics,* vol. 26, no. 1, pp. 235-248, 2011.

[19] Z. Yongchang and Z. Jianguo, "A Novel Duty Cycle Control Strategy to Reduce Both Torque and Flux Ripples for DTC of Permanent Magnet Synchronous Motor Drives With Switching Frequency Reduction," *IEEE Transactions on Power Electronics,* vol. 26, no. 10, pp. 3055-3067, 2011.

[20] R. Yuan, Z. Q. Zhu, and L. Jiaming, "Direct Torque Control of Permanent-Magnet Synchronous Machine Drives With a Simple Duty Ratio Regulator," *IEEE Transactions on Industrial Electronics,* vol. 61, no. 10, pp. 5249-5258, 2014.

[21] T. Yuan and D. Wang, "Performance Improvement for PMSM DTC System through Composite Active Vectors Modulation," *Electronics,* vol. 7, no. 10, 2018.

[22] A. Shinohara, Y. Inoue, S. Morimoto, and M. Sanada, "Correction of reference flux for MTPA control in direct torque controlled interior permanent magnet synchronous motor drives," in *2014 International Power Electronics Conference (IPEC-Hiroshima 2014 - ECCE ASIA)*, 2014, pp. 324-329.

[23] G. Tobias, *Model Predictive Control of High Power Converters and Industrial Drives*. Wiley, 2016.

[24] J. Rodriguez, B. Wu, M. Rivera, C. Rojas, and A. Wilson, "Predictive current control of three-phase two-level four-leg inverter," in *Power Electronics and Motion Control Conference (EPE/PEMC), 2010 14th International*, 2010, pp. T3-106-T3-110.

[25] S. J. Qin and T. A. Badgwell, "A survey of industrial model predictive control technology," *Control Engineering Practice,* vol. 11, no. 7, pp. 733-764, 2003.

[26] J. Holtz and S. Stadtfeld, "A predictive controller for the stator current vector of AC machines fed from a switched voltage source," in *Proceedings of IEEE International Power Electronics Conference (Tokyo, Japan)*, 1983, pp. 1665–1675.

[27] J. Holtz and S. Stadtfeld, "Field-Oriented Control by Forced Motor Currents in a Voltage Fed Inverter Drive," in *Proceedings of IFAC Symposium (Lausanne, Switzerland)*, 1983, pp. 103-110.

[28] J. Rodriguez *et al.*, "State of the Art of Finite Control Set Model Predictive Control in Power Electronics," *IEEE Transactions on Industrial Informatics,* vol. 9, no. 2, pp. 1003-1016, 2013.

[29] S. Vazquez, J. Rodriguez, M. Rivera, L. G. Franquelo, and M. Norambuena, "Model Predictive Control for Power Converters and Drives: Advances and Trends," *IEEE Transactions on Industrial Electronics,* vol. 64, no. 2, pp. 935-947, 2017.

[30] H. A. Young, M. A. Perez, and J. Rodriguez, "Analysis of Finite-Control-Set Model Predictive Current Control With Model Parameter Mismatch in a Three-Phase Inverter," *IEEE Transactions on Industrial Electronics,* vol. 63, no. 5, pp. 3100-3107, 2016.

[31] T. Turker, U. Buyukkeles, and A. F. Bakan, "A Robust Predictive Current Controller for PMSM Drives," *IEEE Transactions on Industrial Electronics,* vol. 63, no. 6, pp. 3906-3914, 2016.

[32] Y. Zhang and H. Yang, "Model Predictive Torque Control of Induction Motor Drives With Optimal Duty Cycle Control," *IEEE Transactions on Power Electronics,* vol. 29, no. 12, pp. 6593-6603, 2014.

[33] Y. Zhang and H. Yang, "Generalized Two-Vector-Based Model-Predictive Torque Control of Induction Motor Drives," *IEEE Transactions on Power Electronics,* vol. 30, no. 7, pp. 3818-3829, 2015.

[34] Y. Zhang and H. Yang, "Two-Vector-Based Model Predictive Torque Control Without Weighting Factors for Induction Motor Drives," *IEEE Transactions on Power Electronics,* vol. 31, no. 2, pp. 1381-1390, 2016.

[35] S. A. Davari, D. A. Khaburi, and R. Kennel, "Using a Weighting Factor Table for FCS-MPC of Induction Motors with Extended Prediction Horizon," in *IECON 2012 - 38th Annual Conference on IEEE Industrial Electronics Society*, 2012, pp. 2086-2091.

[36] S. A. Davari, D. A. Khaburi, and R. Kennel, "An Improved FCS–MPC Algorithm for an Induction Motor With an Imposed Optimized Weighting Factor," *IEEE Transactions on Power Electronics,* vol. 27, no. 3, pp. 1540-1551, 2012.

[37] M. Xiao, T. Shi, Y. Yan, W. Xu, and C. Xia, "Predictive Torque Control of Permanent Magnet Synchronous Motors Using Flux Vector," *IEEE Transactions on Industry Applications,* vol. 54, no. 5, pp. 4437-4446, 2018.

[38] X. Zhang and B. Hou, "Double Vectors Model Predictive Torque Control Without Weighting Factor Based on Voltage Tracking Error," *IEEE Transactions on Power Electronics,* vol. 33, no. 3, pp. 2368-2380, 2018.

[39] R. Yang, M.-Y. Wang, L.-Y. Li, C.-M. Zhang, and J.-L. Jiang, "Robust Predictive Current Control With Variable-Gain Adaptive Disturbance Observer for PMLSM," *IEEE Access,* vol. 6, pp. 13158-13169, 2018.

[40] X. Zhang, L. Zhang, and Y. Zhang, "Model Predictive Current Control for PMSM Drives With Parameter Robustness Improvement," *IEEE Transactions on Power Electronics,* vol. 34, no. 2, pp. 1645-1657, 2019.

[41] Z. Chen, J. Qiu, and M. Jin, "Adaptive finite‐control‐set model predictive current control for IPMSM drives with inductance variation," *IET Electric Power Applications,* vol. 11, no. 5, pp. 874-884, 2017.

[42] M. Yang, X. Lang, J. Long, and D. Xu, "Flux Immunity Robust Predictive Current Control With Incremental Model and Extended State Observer for PMSM Drive," *IEEE Transactions on Power Electronics,* vol. 32, no. 12, pp. 9267-9279, 2017.

[43] I. Takahashi and T. Noguchi, "A New Quick-Response and High-Efficiency Control Strategy of an Induction Motor," *IEEE Transactions on Industry Applications,* vol. IA-22, no. 5, pp. 820-827, 1986.

[44] I. Takahashi and Y. Ohmori, "High-performance direct torque control of an induction motor," *IEEE Transactions on Industry Applications,* vol. 25, no. 2, pp. 257-264, 1989.

[45] G. S. Buja and M. P. Kazmierkowski, "Direct Torque Control of PWM Inverter-Fed AC Motors—A Survey," *IEEE Transactions on Industrial Electronics,* vol. 51, no. 4, pp. 744-757, 2004.

[46] Y. Zhang, J. Zhu, W. Xu, and Y. Guo, "A Simple Method to Reduce Torque Ripple in Direct Torque-Controlled Permanent-Magnet Synchronous Motor by Using Vectors With Variable Amplitude and Angle," *IEEE Transactions on Industrial Electronics,* vol. 58, no. 7, pp. 2848-2859, 2011.

[47] J. W. Kang and S. K. Sul, "Analysis and prediction of inverter switching frequency in direct torque control of induction machine based on hysteresis bands and machine parameters," *IEEE Transactions on Industrial Electronics,* vol. 48, no. 3, pp. 545-553, 2001.

[48] D. Casadei, F. Profumo, G. Serra, and A. Tani, "FOC and DTC: two viable schemes for induction motors torque control," *IEEE Transactions on Power Electronics,* vol. 17, no. 5, pp. 779-787, 2002.

[49] C. A. Martins, X. Roboam, T. A. Meynard, and A. S. Carvalho, "Switching frequency imposition and ripple reduction in DTC drives by using a multilevel converter," *IEEE Transactions on Power Electronics,* vol. 17, no. 2, pp. 286-297, 2002.

[50] J. H. Lee, "Model predictive control: Review of the three decades of development," *International Journal of Control, Automation and Systems,* vol. 9, no. 3, pp. 415-424, 2011.

[51] S. Kouro, P. Cortes, R. Vargas, U. Ammann, and J. Rodriguez, "Model Predictive Control—A Simple and Powerful Method to Control Power Converters," *IEEE Transactions on Industrial Electronics,* vol. 56, no. 6, pp. 1826-1838, 2009.

[52] P. Cortes, M. P. Kazmierkowski, R. M. Kennel, D. E. Quevedo, and J. Rodriguez, "Predictive Control in Power Electronics and Drives," *IEEE Transactions on Industrial Electronics,* vol. 55, no. 12, pp. 4312-4324, 2008.

[53] T. Kawabata, T. Miyashita, and Y. Yamamoto, "Dead beat control of three phase PWM inverter," *IEEE Transactions on Power Electronics,* vol. 5, no. 1, pp. 21-28, 1990.

[54] O. Kukrer, "Discrete-time current control of voltage-fed three-phase PWM inverters," *IEEE Transactions on Power Electronics,* vol. 11, no. 2, pp. 260-269, 1996.

[55] J. Holtz and S. Stadtfeld, "A predictive controller for the stator current vector of AC machines fed from a switched voltage source," in *Proc. of IEE of Japan IPEC-Tokyo'83*, 1983, pp. 1665–1675.

[56] P. Mutschler, "A new speed-control method for induction motors," in *PCIM*, 1998, pp. 131–136.

[57] P. Karamanakos, K. Pavlou, and S. Manias, "An Enumeration-Based Model Predictive Control Strategy for the Cascaded H-Bridge Multilevel Rectifier," *IEEE Transactions on Industrial Electronics,* vol. 61, no. 7, pp. 3480-3489, 2014.

[58] J. I. Leon, S. Kouro, L. G. Franquelo, J. Rodriguez, and B. Wu, "The Essential Role and the Continuous Evolution of Modulation Techniques for Voltage-Source Inverters in the Past, Present, and Future Power Electronics," *IEEE Transactions on Industrial Electronics,* vol. 63, no. 5, pp. 2688-2701, 2016.

[59] C. Bordons and C. Montero, "Basic Principles of MPC for Power Converters: Bridging the Gap Between Theory and Practice," *IEEE Industrial Electronics Magazine,* vol. 9, no. 3, pp. 31-43, 2015.

[60] Y. Zhang, Y. Bai, and H. Yang, "A Universal Multiple-Vector-Based Model Predictive Control of Induction Motor Drives," *IEEE Transactions on Power Electronics,* vol. 33, no. 8, pp. 6957-6969, 2018.

[61] J. Rodriguez, R. M. Kennel, J. R. Espinoza, M. Trincado, C. A. Silva, and C. A. Rojas, "High-Performance Control Strategies for Electrical Drives: An Experimental Assessment," *IEEE Transactions on Industrial Electronics,* vol. 59, no. 2, pp. 812-820, 2012.

[62] C. Ma, X. Yao, H. Li, and F. D. Belie, "Reference Voltage Vector Based Model Predictive Torque Control with RMS Solution for PMSM," in *2019 IEEE 28th International Symposium on Industrial Electronics (ISIE)*, 2019, pp. 384-389.

[63] Q. Tang, A. Shen, P. Luo, H. Shen, W. Li, and X. He, "IPMSMs Sensorless MTPA Control Based on Virtual q-Axis Inductance by Using Virtual High-Frequency Signal Injection," *IEEE Transactions on Industrial Electronics,* vol. 67, no. 1, pp. 136-146, 2020.

[64] R. Rajendran and D. N.Devarajan, "A Comparative Performance Analysis of Torque Control Schemes for Induction Motor Drives," *International Journal of Power Electronics and Drive Systems (IJPEDS),* vol. 2, no. 2, pp. 159-168, 2012.

[65] L. He, F. Wang, J. Wang, and J. Rodriguez, "Zynq Implemented Luenberger Disturbance Observer Based Predictive Control Scheme for PMSM Drives," *IEEE Transactions on Power Electronics,* vol. 35, no. 2, pp. 1770-1778, 2020.

[66] M. Liu, K. W. Chan, J. Hu, W. Xu, and J. Rodriguez, "Model Predictive Direct Speed Control With Torque Oscillation Reduction for PMSM Drives," *IEEE Transactions on Industrial Informatics,* vol. 15, no. 9, pp. 4944-4956, 2019.

[67] R. P. Aguilera, P. Lezana, and D. E. Quevedo, "Finite-Control-Set Model Predictive Control With Improved Steady-State Performance," *IEEE Transactions on Industrial Informatics,* vol. 9, no. 2, pp. 658-667, 2013.

[68] H. Zhu, X. Xiao, and Y. Li, "Torque Ripple Reduction of the Torque Predictive Control Scheme for Permanent-Magnet Synchronous Motors," *IEEE Transactions on Industrial Electronics,* vol. 59, no. 2, pp. 871-877, 2012.

[69] W. Xie *et al.*, "Finite-Control-Set Model Predictive Torque Control With a Deadbeat Solution for PMSM Drives," *IEEE Transactions on Industrial Electronics,* vol. 62, no. 9, pp. 5402-5410, 2015.

[70] P. Karamanakos and T. Geyer, "Guidelines for the Design of Finite Control Set Model Predictive Controllers," *IEEE Transactions on Power Electronics,* vol. 35, no. 7, pp. 7434-7450, 2020.

[71] Y. Xu, Q. Zhou, and B. Zhang, "A model predictive torque control strategy of PMSM with torque deadbeat duty cycle control," in *2016 IEEE 8th International Power Electronics and Motion Control Conference (IPEMC-ECCE Asia)*, 2016, pp. 782-785.

[72] Y. Zhang and H. Yang, "Torque ripple reduction of model predictive torque control of induction motor drives," in *2013 IEEE Energy Conversion Congress and Exposition (ECCE)* 2013, pp. 1176-1183.

[73] Y. Zhang and H. Yang, "Performance evaluation of two-vector-based model predictive current control of PMSM drives," *Chinese Journal of Electrical Engineering,* vol. 4, no. 2, pp. 65-81, 2018.

[74] H. Miranda, P. Cortes, J. I. Yuz, and J. Rodriguez, "Predictive Torque Control of Induction Machines Based on State-Space Models," *IEEE Transactions on Industrial Electronics,* vol. 56, no. 6, pp. 1916-1924, 2009.

[75] S.-W. Kang, J.-H. Soh, and R.-Y. Kim, "Symmetrical Three-Vector-Based Model Predictive Control With Deadbeat Solution for IPMSM in Rotating Reference Frame," *IEEE Transactions on Industrial Electronics,* vol. 67, no. 1, pp. 159-168, 2020.

[76] Z. Zhou, C. Xia, Y. Yan, Z. Wang, and T. Shi, "Torque Ripple Minimization of Predictive Torque Control for PMSM With Extended Control Set," *IEEE Transactions on Industrial Electronics,* vol. 64, no. 9, pp. 6930-6939, 2017.

[77] C. Ma, X. Yao, H. Li, and F. D. Belie, "An Improved Two-Vector Model Predictive Torque Control Based on RMS Duty Ratio Optimization for PMSM," in *2019 IEEE International Electric Machines & Drives Conference (IEMDC)*, 2019, pp. 1674-1679.

[78] Y. Zhang, B. Zhang, H. Yang, M. Norambuena, and J. Rodriguez, "Generalized Sequential Model Predictive Control of IM Drives With Field-Weakening Ability," *IEEE Transactions on Power Electronics,* vol. 34, no. 9, pp. 8944-8955, 2019.

[79] C. A. Rojas, J. R. Rodriguez, S. Kouro, and F. Villarroel, "Multiobjective Fuzzy-Decision-Making Predictive Torque Control for an Induction Motor Drive," *IEEE Transactions on Power Electronics,* vol. 32, no. 8, pp. 6245-6260, 2017.

[80] F. Wang, H. Xie, Q. Chen, S. A. Davari, J. Rodriguez, and R. Kennel, "Parallel Predictive Torque Control for Induction Machines Without Weighting Factors," *IEEE Transactions on Power Electronics,* vol. 35, no. 2, pp. 1779-1788, 2020.

[81] M. Pacas and J. Weber, "Predictive Direct Torque Control for the PM Synchronous Machine," *IEEE Transactions on Industrial Electronics,* vol. 52, no. 5, pp. 1350-1356, 2005.

[82] Y. Xue *et al.*, "Vector-Based Model Predictive Hysteresis Current Control for Asynchronous Motor," *IEEE Transactions on Industrial Electronics,* vol. 66, no. 11, pp. 8703-8712, 2019.

[83] C. Ma, X. Yao, H. Li, and F. D. Belie, "Current Boundary Based Model Predictive torque control of PMSM," in *2019 22nd International Conference on Electrical Machines and Systems (ICEMS)*, 2019, pp. 2447-2452.

[84] W. Xu, J. Zou, Y. Liu, and J. Zhu, "Weighting Factorless Model Predictive Thrust Control for Linear Induction Machine," *IEEE Transactions on Power Electronics,* vol. 34, no. 10, pp. 9916-9928, 2019.

[85] A. Andersson and T. Thiringer, "Assessment of an Improved Finite Control Set Model Predictive Current Controller for Automotive Propulsion Applications," *IEEE Transactions on Industrial Electronics,* vol. 67, no. 1, pp. 91-100, 2020.

[86] C. F. Garcia, C. A. Silva, J. R. Rodriguez, P. Zanchetta, and S. A. Odhano, "Modulated Model-Predictive Control With Optimized Overmodulation," *IEEE Journal of Emerging and Selected Topics in Power Electronics,* vol. 7, no. 1, pp. 404-413, 2019.

[87] M. Morari and J. H. Lee, "Model predictive control: past, present and future," *Computers & Chemical Engineering,* vol. 23, no. 4-5, pp. 667-682, 1999.

[88] E. F. Camacho and C. Bordons, *Model Predictive Control*. Springer London, 2007.

[89] S. Mariethoz and M. Morari, "Explicit Model-Predictive Control of a PWM Inverter With an LCL Filter," *IEEE Transactions on Industrial Electronics,* vol. 56, no. 2, pp. 389-399, 2009.

[90] A. G. Beccuti, M. Kvasnica, G. Papafotiou, and M. Morari, "A Decentralized Explicit Predictive Control Paradigm for Parallelized DC-DC Circuits," *IEEE Transactions on Control Systems Technology,* vol. 21, no. 1, pp. 136-148, 2013.

[91] R. Errouissi and M. Ouhrouche, "Robust continuous generalized predictive control of a permanent magnet synchronous motor drive," in *2009 IEEE Electrical Power & Energy Conference (EPEC)*, 2009, pp. 1-7.

[92] S. Vazquez, C. Montero, C. Bordons, and L. G. Franquelo, "Design and experimental validation of a Model Predictive Control strategy for a VSI with long prediction horizon," in *IECON 2013 - 39th Annual Conference of the IEEE Industrial Electronics Society*, 2013, pp. 5788-5793.

[93] J. Rodriguez *et al.*, "Predictive Current Control of a Voltage Source Inverter," *IEEE Transactions on Industrial Electronics,* vol. 54, no. 1, pp. 495-503, 2007.

[94] P. Cortes, J. Rodriguez, C. Silva, and A. Flores, "Delay Compensation in Model Predictive Current Control of a Three-Phase Inverter," *IEEE Transactions on Industrial Electronics,* vol. 59, no. 2, pp. 1323-1325, 2012.

[95] R. Vargas, P. Cortes, U. Ammann, J. Rodriguez, and J. Pontt, "Predictive Control of a Three-Phase Neutral-Point-Clamped Inverter," *IEEE Transactions on Industrial Electronics,* vol. 54, no. 5, pp. 2697-2705, 2007.

[96] S. Kouro *et al.*, "Recent Advances and Industrial Applications of Multilevel Converters," *IEEE Transactions on Industrial Electronics,* vol. 57, no. 8, pp. 2553-2580, 2010.

[97] J.-W. Moon, J.-S. Gwon, J.-W. Park, D.-W. Kang, and J.-M. Kim, "Model Predictive Control With a Reduced Number of Considered States in a Modular Multilevel Converter for HVDC System," *IEEE Transactions on Power Delivery,* vol. 30, no. 2, pp. 608-617, 2015.

[98] F. Kieferndorf, P. Karamanakos, P. Bader, N. Oikonomou, and T. Geyer, "Model predictive control of the internal voltages of a five-level active neutral point clamped converter," in *2012 IEEE Energy Conversion Congress and Exposition (ECCE)*, 2012, pp. 1676-1683.

[99] M. Vatani, B. Bahrani, M. Saeedifard, and M. Hovd, "Indirect Finite Control Set Model Predictive Control of Modular Multilevel Converters," *IEEE Transactions on Smart Grid,* vol. 6, no. 3, pp. 1520-1529, 2015.

[100] M. Norambuena, S. Dieckerhoff, S. Kouro, and J. Rodriguez, "Finite control set model predictive control of a stacked multicell converter with reduced computational cost," in *IECON 2015 - 41st Annual Conference of the IEEE Industrial Electronics Society*, 2016, pp. 001819-001824.

[101] Y. Zhang and H. Lin, "Simplified model predictive current control method of voltage-source inverter," in *8th International Conference on Power Electronics - ECCE Asia*, 2011, pp. 1726-1733.

[102] P. Cortés, A. Wilson, S. Kouro, J. Rodriguez, and H. Abu-Rub, "Model Predictive Control of Multilevel Cascaded H-Bridge Inverters," *IEEE Transactions on Industrial Electronics,* vol. 57, no. 8, pp. 2691-2699, 2010.

[103] T. Benslimane, K. Aliouane, and B. Chetate, "Implementation of SVPWM based on hysteresis control strategy applied on autonomous parallel active filter," in *7th International Conference on Automatic Control, Modeling and Simulation*, 2005, pp. 309-313.

[104] D. Casadei, G. Serra, and K. Tani, "Implementation of a direct control algorithm for induction motors based on discrete space vector modulation," *IEEE Transactions on Power Electronics,* vol. 15, no. 4, pp. 769-777, 2000.

[105] B. Singh and D. Goyal, "Improved DSVM-DTC Based Current Sensorless Permanent Magnet Synchronous Motor Drive," in *7th International Conference on Power Electronics and Drive Systems*, 2007, pp. 1354-1360.

[106] X. Changliang, L. Tao, S. Tingna, and S. Zhanfeng, "A Simplified Finite-Control-Set Model-Predictive Control for

Power Converters," *IEEE Transactions on Industrial Informatics,* vol. 10, no. 2, pp. 991-1002, 2014.

[107] S. Kwak and J.-C. Park, "Switching Strategy Based on Model Predictive Control of VSI to Obtain High Efficiency and Balanced Loss Distribution," *IEEE Transactions on Power Electronics,* vol. 29, no. 9, pp. 4551-4567, 2014.

[108] M. Xiao, T. Shi, X. Gu, and C. Xia, "Simplified predictive torque control for permanent magnet synchronous motor with discrete duty cycle control," *IET Electric Power Applications,* vol. 13, no. 3, pp. 294-301, 2019.

[109] O. Wallscheid, W. Peters, and J. Bcker, "A Precise Open-Loop Torque Control for an Interior Permanent Magnet Synchronous Motor (IPMSM) Considering Iron Losses," in *IECON 2012 - 38th Annual Conference on IEEE Industrial Electronics Society*, 2012, pp. 2877-2882.

[110] S. Morimoto, M. Sanada, and Y. Takeda, "Wide-speed operation of interior permanent magnet synchronous motors with high-performance current regulator," *IEEE Transactions on Industry Applications,* vol. 30, no. 4, pp. 920-926, 1994.

[111] I. Boldea, M. C. Paicu, and G.-D. Andreescu, "Active Flux Concept for Motion-Sensorless Unified AC Drives," *IEEE Transactions on Power Electronics,* vol. 23, no. 5, pp. 2612-2618, 2008.

[112] F. D. Belie, T. Vyncke, J. Melkebeek, K. Geldhof, and R. Boel, "On the Influence of Saturation and Mutual Coupling of both Orthogonal Magnetic Axes on a MTPA Controlled Interior PMSM Drive," in *17th International Conference on Electrical Machines (ICEM 2006)*, 2006, pp. OTM2-5.

[113] F. M. L. L. De Belie, J. A. A. Melkebeek, L. Vandevelde, R. K. Boel, K. R. Geldhof, and T. J. Vyncke, "A nonlinear model for synchronous machines to describe high-frequency signal based position estimators," in *IEEE International Conference on Electric Machines and Drives*, 2005, pp. 696-703.

[114] T. Lefebvre, "Approximate numerical solution strategies for dynamic optimization and optimal control problems," PhD dissertation, Ghent University, 2019.

[115] F. D. Belie, E. D. Brabandere, J. Druant, P. Sergeant, and J. Melkebeek, "Model based predictive torque control of an electric variable transmission for hybrid electric vehicles," in *2016 International Symposium on Power Electronics, Electrical Drives, Automation and Motion (SPEEDAM)*, 2016, pp. 1203-1207.

[116] S. Hanke, O. Wallscheid, and J. Bocker, "Continuous-Control-Set Model Predictive Control with Integrated Modulator in Permanent Magnet Synchronous Motor Applications," in *2019 IEEE International Electric Machines & Drives Conference (IEMDC)*, 2019, pp. 2210-2216.

[117] M. H. Vafaie, "Approach for classifying continuous control set - predictive controllers applied in AC motor drives," *IET Power Electronics,* vol. 13, no. 8, pp. 1500-1513, 2020.

[118] A. A. Ahmed, B. K. Koh, and Y. I. Lee, "Continuous Control Set-Model Predictive Control for Torque Control of Induction Motors in a Wide Speed Range," *Electric Power Components and Systems,* vol. 46, no. 19-20, pp. 2142-2158, 2018.

[119] A. A. Ahmed, B. K. Koh, and Y. I. Lee, "A Comparison of Finite Control Set and Continuous Control Set Model Predictive Control Schemes for Speed Control of Induction Motors," *IEEE Transactions on Industrial Informatics,* vol. 14, no. 4, pp. 1334-1346, 2018.

[120] A. G. Bartsch, D. M. Cavalcanti, M. S. M. Cavalca, and A. Nied, "A comparison among different Finite Control Set approaches and Convex Control Set Model-based Predictive Control applied in a Three-Phase Inverter with RL load," in *2019 IEEE 15th Brazilian Power Electronics Conference and 5th IEEE Southern Power Electronics Conference (COBEP/SPEC)*, 2019, pp. 1-6.

[121] F. Morel, L.-S. Xuefang, J. M. Retif, B. Allard, and C. Buttay, "A Comparative Study of Predictive Current Control Schemes for a Permanent-Magnet Synchronous Machine Drive," *IEEE Transactions on Industrial Electronics,* vol. 56, no. 7, pp. 2715-2728, 2009.

[122] X. Liu, L. Zhou, J. Wang, X. Gao, Z. Li, and Z. Zhang, "Robust Predictive Current Control of Permanent-Magnet Synchronous

Motors With Newly Designed Cost Function," *IEEE Transactions on Power Electronics,* vol. 35, no. 10, pp. 10778-10788, 2020.

[123] C.-K. Lin, T.-H. Liu, J.-t. Yu, L.-C. Fu, and C.-F. Hsiao, "Model-Free Predictive Current Control for Interior Permanent-Magnet Synchronous Motor Drives Based on Current Difference Detection Technique," *IEEE Transactions on Industrial Electronics,* vol. 61, no. 2, pp. 667-681, 2014.

[124] N. Chaovalit and S. Yamamoto, "Model-Free Predictive Control and Its Relation to Parameter Estimation Based Predictive Control," in *2019 SICE International Symposium on Control Systems (SICE ISCS)*, 2019, pp. 84-89.

[125] M. Siami, D. A. Khaburi, A. Abbaszadeh, and J. Rodriguez, "Robustness Improvement of Predictive Current Control Using Prediction Error Correction for Permanent-Magnet Synchronous Machines," *IEEE Transactions on Industrial Electronics,* vol. 63, no. 6, pp. 3458-3466, 2016.

[126] C.-K. Lin, J.-t. Yu, Y.-S. Lai, and H.-C. Yu, "Improved Model-Free Predictive Current Control for Synchronous Reluctance Motor Drives," *IEEE Transactions on Industrial Electronics,* vol. 63, no. 6, pp. 3942-3953, 2016.

[127] D. D. Ru, M. Polato, and S. Bolognani, "Model-free predictive current control for a SynRM drive based on an effective update of measured current responses," in *2017 IEEE International Symposium on Predictive Control of Electrical Drives and Power Electronics (PRECEDE)*, 2017, pp. 119-124.

[128] P. G. Carlet, F. Tinazzi, S. Bolognani, and M. Zigliotto, "An Effective Model-Free Predictive Current Control for Synchronous Reluctance Motor Drives," *IEEE Transactions on Industry Applications,* vol. 55, no. 4, pp. 3781-3790, 2019.

[129] F. M. L. De Belie, P. Sergeant, and J. A. Melkebeek, "A Sensorless Drive by Applying Test Pulses Without Affecting the Average-Current Samples," *IEEE Transactions on Power Electronics,* vol. 25, no. 4, pp. 875-888, 2010.

Permanent Magnet Synchronous Machine.